



Structural Applications of Ferritic Stainless Steels (SAFSS)

RFSR-CT-2010-00026 (July 01, 2010 - June 30, 2013)

Work package 2: Structural performance of steel members
Deliverable 2.2: Report on preliminary finite element study

Petr Hradil, Asko Tajla

VTT, Technical Research Centre of Finland

Itsaso Arrayago, Marina Bock, Esther Real, Enrique Mirambell

Departament d'Enginyeria de la Construcció,
Universitat Politècnica de Catalunya

Table of contents

Overall buckling

HRADIL, P., VTT-R-04891-12: Preliminary finite element study, VTT research report

Local buckling

BOCK, M., REAL, E., MIRAMBELL, E., Report on preliminary FEM study: Local buckling

Web-crippling

ARRAYAGO, I., REAL, E., BOCK, M., MIRAMBELL, E., Preliminary FEM study: Web-crippling

Appendix

HRADIL, P., Abaqus plug-in user manual, VTT technical note

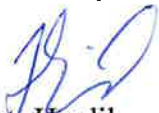


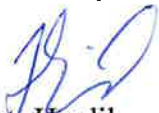


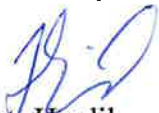




Structural Applications of Ferritic Stainless Steels (SAFSS)
WP2: Structural performance of steel members

Preliminary finite element study

Authors: Petr Hradil

Confidentiality: Confidential until May 2014

Report's title SAFSS WP2: Report on preliminary finite element study											
Customer, contact person, address Commission of the European Communities		Order reference RFSR-CT-2010-00026									
Project name Structural Applications of Ferritic Stainless Steels		Project number/Short name 39594/SAFSS									
Author(s) Petr Hradil		Pages 37 p. + app. 17 p.									
Keywords stainless steel, ferritic, finite element, parametric study		Report identification code VTT-R-04891-12									
<p>Summary</p> <p>The report discusses the specific phenomena of global stability of members from metallic non-linear materials with a special focus on ferritic stainless steel. The numerical study presented in this report supports the theoretical assumptions for the buckling behaviour of thin-walled members with different material properties, especially hardening parameters and yield points.</p> <p>Flexural, torsional-flexural and lateral-torsional buckling modes are studied on hollow sections, lipped channels and I-sections. The finite element models are calculated using the Abaqus plug-in for virtual testing of thin-walled structural members, developed in VTT.</p> <p>The scope of the report is defined in the work package description of WP2: Structural performance of steel members, Task 2.2: Preliminary FEM study (preliminary parametric study on overall buckling behaviour) and Task 2.4: Parametric study and recommendations (validation of design approaches).</p> <p>Additional studies were carried out in this task to verify the suitability of modified Ayrton-Perry strength curve approximation model that takes into account the material gradual yielding in form of tangent modulus.</p> <p>The effect of bending residual stresses was also investigated in order to prepare parameters for the future full parametric study with complex numerical models.</p>											
Confidentiality	Confidential until May 2014										
<p>Espoo 12.7.2012</p> <table border="0"> <tr> <td>Written by</td> <td>Reviewed by</td> <td>Accepted by</td> </tr> <tr> <td></td> <td></td> <td></td> </tr> <tr> <td>Petr Hradil Research Scientist</td> <td>Asko Talja Senior Scientist</td> <td>Eila Lehmus Technology Manager</td> </tr> </table>			Written by	Reviewed by	Accepted by				Petr Hradil Research Scientist	Asko Talja Senior Scientist	Eila Lehmus Technology Manager
Written by	Reviewed by	Accepted by									
											
Petr Hradil Research Scientist	Asko Talja Senior Scientist	Eila Lehmus Technology Manager									
VTT's contact address P.O. Box 1000, FI-02044 VTT, Finland											
<p>Distribution (customer and VTT)</p> <table border="0"> <tr> <td>Project group</td> <td>1 pdf copy in project workspace</td> </tr> <tr> <td>VTT/Register Office</td> <td>1 copy</td> </tr> </table>			Project group	1 pdf copy in project workspace	VTT/Register Office	1 copy					
Project group	1 pdf copy in project workspace										
VTT/Register Office	1 copy										
<p><i>The use of the name of the VTT Technical Research Centre of Finland (VTT) in advertising or publication in part of this report is only permissible with written authorisation from the VTT Technical Research Centre of Finland.</i></p>											

Preface

The report summarizes the findings from the preliminary finite element study. Its aim is to identify clearly the parameters and their ranges that affect the overall buckling of stainless steel members. The calculations were carried out using plugin for Abaqus that is also described herein. The scope of presented calculations is beam and column buckling of thin-walled members, particularly flexural and torsional-flexural stability of columns and lateral-torsional buckling of beams. Local and distortional stability is not addressed in this part of WP2 since it was studied independently by UPC.

Additional studies were carried out in this task to verify the suitability of modified Ayrton-Perry strength curve approximation model that takes into account the material gradual yielding in form of tangent modulus.

The effect of bending residual stresses was also investigated in order to prepare parameters for the future full parametric study with complex numerical models.

Espoo 12.7.2012

Authors

Contents

Preface	2
Abbreviations	4
1 Introduction	5
2 Material models	6
3 Cross-sections	8
4 Simplified numerical model	9
4.1 Loading and supports	9
4.2 Imperfection modelling and elastic buckling analysis	9
4.3 Model simplification	10
5 Advanced numerical model	11
6 Strength curve approximation models	12
6.1 Existing models	12
6.2 Transformed Ayrton-Perry model	16
7 Flexural buckling tests	17
8 Torsional-flexural buckling tests	19
9 Lateral torsional buckling tests	21
10 Tension tests	23
11 Results of parametric study	24
11.1 The effect of material nonlinearity	24
11.2 The effect of material yield strength	26
11.3 The effect of bending residual stresses	28
12 Regression analysis of proposed strength curve	32
13 Conclusions	35
References	36

Appendices

Appendix A: Austenitic steel

Appendix B: Duplex steel

Appendix C: Ferritic steel 1

Appendix D: Ferritic steel 2

Appendix E: Carbon steel

Appendix F: Material models comparison

Appendix G: Methods for transformed Ayrton-Perry curve calculation

Abbreviations

AS/NZS	Australian Standard/New Zealand Standard
CRF	Circle-to-Rectangle Forming
EN	European Standards
FB	Flexural buckling
FE, FEA	Finite Element, Finite Element Analysis
FEM	Finite Element Method
GMNIA	Geometrically and Materially Non-linear Analysis with Imperfections
LEA (LBA)	Linear Eigenvalue (Buckling) Analysis
LTB	Lateral-torsional buckling
NLR	Nonlinear regression analysis
RHS	Rectangular Hollow Section
Riks	Arc-length method used e.g. in Abaqus FE solver
SEI/ASCE	Structural Engineering Institute/American Society of Civil Engineers
SHS	Square Hollow Section
TB, TFB	Torsional buckling, Torsional-flexural buckling

1 Introduction

The report discusses the specific phenomena of global stability of members from metallic non-linear materials with a special focus on ferritic stainless steel. The numerical study presented in this report supports the theoretical assumptions for the buckling behaviour of thin-walled members with different material properties [1], especially hardening parameters. Flexural, torsional-flexural and lateral-torsional buckling modes are studied on hollow sections, lipped channels and I-sections. The finite element models are calculated using the Abaqus plug-in for virtual testing of thin-walled structural members, developed in VTT.

The scope of the report is defined in the work package description of WP2: Structural performance of steel members, Task 2.2: Preliminary FEM study (*preliminary parametric study on overall buckling behaviour*) and Task 2.4: Parametric study and recommendations (*validation of design approaches*). The other parts of Task 2.2 are covered in the Profiler – Abaqus plug-in: User manual [2] (*Abaqus plug-in development*) and WP2 Model calibration test report [3] (*classification of mechanical properties of base materials*).

2 Material models

The stress-strain relationship in Eqs. (1) to (3) used in the presented study is based on Rasmussen's modification of the Mirambell-Real model [4, 5]. This is also included in the existing design rules, e.g. in Annex C of Eurocode 3, Part 1-4 [6].

$$\varepsilon = \begin{cases} \frac{\sigma}{E_0} + 0,002 \left(\frac{\sigma}{\sigma_{0,2}} \right)^n & \text{for } \sigma \leq \sigma_{0,2} \\ \frac{\sigma - \sigma_{0,2}}{E_{0,2}} + \varepsilon_{pu} \left(\frac{\sigma - \sigma_{0,2}}{\sigma_u - \sigma_{0,2}} \right)^m + \varepsilon_{0,2} & \text{for } \sigma > \sigma_{0,2} \end{cases}, \quad (1)$$

where E_0 is the initial modulus of elasticity, $\sigma_{0,2}$ and σ_u stands for the 0.2% offset yield strength and ultimate strength respectively, n and m are the nonlinear parameters of each segment, and the tangent modulus at 0.2% stress $E_{0,2}$ can be calculated using the following equation:

$$E_{0,2} = \frac{E_0}{1 + 0.002n(E_0/\sigma_{0,2})} \quad (2)$$

The total strain corresponding to 0.2% proof stress $\varepsilon_{0,2}$ and the plastic strain difference ε_{pu} of the second stage are described here:

$$\varepsilon_{0,2} = \frac{\sigma_{0,2}}{E_0} + 0.002 \quad \text{and} \quad \varepsilon_{pu} = \varepsilon_u - \varepsilon_{0,2} - \frac{\sigma_u - \sigma_{0,2}}{E_{0,2}} \quad (3)$$

A group of materials with different 0.2% proof stress, ultimate strength, initial modulus of elasticity and non-linear parameter n was studied. The material stress-strain behaviour was described according to Rasmussen's modification of the model, where the parameter of non-linearity of the second stage m is presented by Eq. (4)

$$m = 1 + 3.5 \frac{\sigma_{0,2}}{\sigma_u} \quad (4)$$

and the ultimate strain by Eq. (5).

$$\varepsilon_u = 1 - \frac{\sigma_{0,2}}{\sigma_u} \quad (5)$$

Material was then transformed to true stress and plastic logarithmic strain according to the Eq. (6).

$$\begin{aligned} \sigma_{true} &= \sigma_{nom} (1 + \varepsilon_{nom}) \\ \varepsilon_{true} &= \ln(1 + \varepsilon_{nom}) - \frac{\sigma_{true}}{E} \end{aligned} \quad (6)$$

Table 1. Basic material models.

	E_0	σ_{02}	n	σ_u	m	ε_u
A: Austenitic	200 GPa	300 MPa	5	600 MPa	2.75	0.50
B: Duplex	200 GPa	500 MPa	5	700 MPa	3.50	0.29
C: Ferritic 1	200 GPa	300 MPa	10	600 MPa	2.75	0.50
D: Ferritic 2	200 GPa	300 MPa	10	420 MPa	3.50	0.29
E: Carbon	200 GPa	355 MPa	25	500 MPa	3.49	0.29

Table 2. Additional material models (for preliminary parametric study).

	E_0	σ_{02}	n	σ_u	m	ε_u
F: $n = 25$	200 GPa	300 MPa	25	600 MPa	2.75	0.50
G: $f_y = 400$ MPa	200 GPa	400 MPa	10	560 MPa	3.50	0.29
H: $f_y = 500$ MPa	200 GPa	500 MPa	10	700 MPa	3.50	0.29

3 Cross-sections

For each buckling mode analysis we selected a different cross-section to demonstrate that the studied phenomena are common to hollow sections as well as open double-symmetrical and single-symmetrical cross-sectional shapes.

- a) **square hollow section (SHS)** with centre-to-centre side length 72 mm, wall thickness 5 mm and no corners

The doubly symmetric cross-section was used for the flexural buckling tests (FB) because the radius of gyration is the same in all directions and the member global failure is always in flexural buckling. Additionally, the same cross-section with thicknesses 3.0 mm and 1.0 mm was used to study the effect of changing A/W ratio.

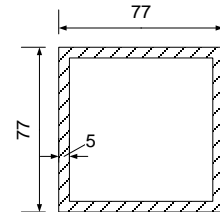


Figure 1. SHS section for FB tests.

- b) **lipped channel** with centre-to-centre side length 72 mm, lip end-to-centre length 18 mm, wall thickness 5 mm and no corners

The open section was forced to fail in flexural-torsional buckling (TFB) by fixing the end-supports in rotation in the vertical direction.

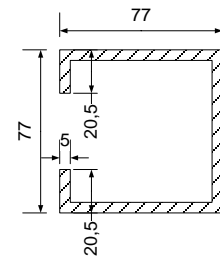


Figure 2. Lipped channel for TFB tests.

- c) **I section** 100 x 200 mm with flange thickness 8.5 mm and web thickness 5.6 mm

Even though the cross-sectional parameters are the common dimensions of IPE 200 profile, this cross-section doesn't represent any hot-rolled member because no residual stresses were used in FE calculation. Unlike the previous cases, the members with I section were loaded with end-moments to obtain lateral-torsional buckling (LTB) failure.

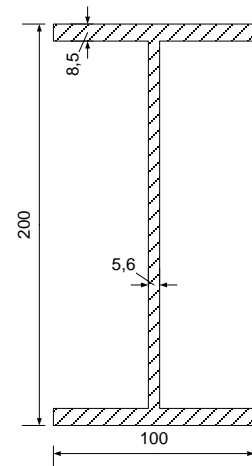


Figure 3. I-section for LTB tests.

4 Simplified numerical model

In order to evaluate the effect of nonlinear stress-strain behaviour on member buckling strength, multiple series of numerical models have been created with variable length and material parameters. The suitability of linear and quadratic shell elements was tested, as well as different shell thicknesses. Because element types and thicknesses did not significantly affect the calculation results, we selected nine-node shells with reduced integration (S9R5), and higher material thickness to limit the effect of local buckling in shorter members.

4.1 Loading and supports

Pinned-pinned supports and concentric axial loading were applied in the flexural buckling (FB) study. The single-symmetric members were forced to fail in torsional-flexural buckling (TFB), fixing both ends in y axis bending, torsion and warping. In the case of lateral-torsional buckling (LTB), members were simply supported and loaded with end-moments (see Figure 4). Both ends were additionally restrained against torsion and warping. These conditions were also considered in calculation of nondimensional slenderness.

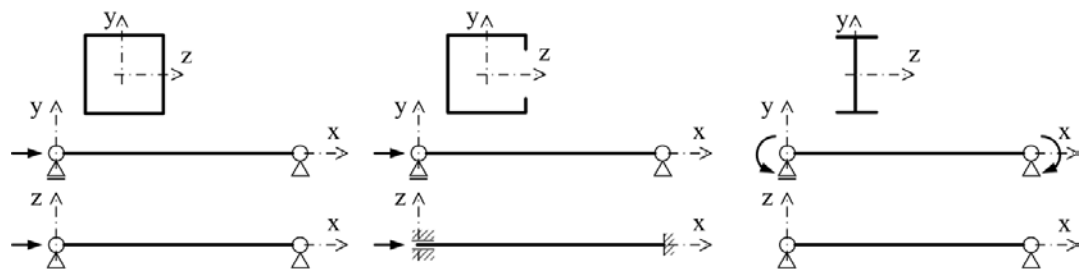


Figure 4. Loading and supports in FB tests (left), TFB tests (middle) and LTB tests (right).

4.2 Imperfection modelling and elastic buckling analysis

The distribution of initial imperfections was obtained from linear eigenvalue analysis as the first overall buckling shape with positive critical load. In order to suppress local and distortional buckling modes in shorter members, each cross-section was stiffened with membrane elements in eigenvalue analysis. This method was verified successfully in lateral-torsional buckling [7], and our numerical results also showed a good agreement with analytically predicted critical loads for flexural and torsional-flexural cases. The selection of imperfection amplitude usually corresponds to the mean geometrical imperfections and ranges from $L/1000$ to $L/2000$. For instance, European buckling curves were defined with imperfections $L/1000$. Since our numerical models excluded the effect of residual stresses and strains in the material, a higher amplitude of initial imperfection ($L/750$) was chosen to compensate for these effects. It should be noted that $L/750$ corresponds to the fabrication tolerances in EN 1090-2 [8], where the additional deformation caused by residual stresses is expected. The lengths of tested members were selected as an approximate match for a nondimensional slenderness sequence of 0.125, 0.25, 0.5, 0.7, 1.0, 1.4, 2.0, 2.8 and 4.0. In a few cases it was impossible to obtain ultimate loads for the shortest columns and longest beams due to the geometrical and material limits. Some of the calculations were also affected by local and distortional buckling and

were excluded from the further study. All the strength curves, therefore, are based on seven to nine calculated points.

4.3 Model simplification

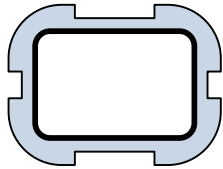
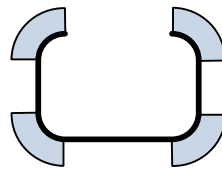
As it was not the goal of our numerical study to simulate any particular member behaviour, several simplifications were used to increase computational efficiency and to highlight the differences in specific material parameters clearly, without additional disturbing effects. Each of the following assumptions was carefully studied before application:

- Enhanced material properties in corners were included in the average values of the entire cross-section. This method is also accepted by the Eurocode [9].
- Residual stresses from cold-forming were not used due to their small effect on the member behaviour, as concluded by Gardner and Cruise [10].
- Residual stresses from fabrication and press-braking were also assumed to be included in the material model and initial imperfections.
- An isotropic material model was used with nonlinear hardening. This provides sufficient accuracy compared to other possible isotropic and anisotropic models, according to Rasmussen et al. [11].
- Rounded corners were ignored, giving greater flexibility for reasonable aspect ratios of flat part shell elements.

5 Advanced numerical model

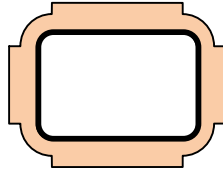
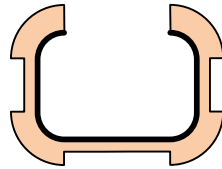
To compare simplified numerical model with the expected behaviour of real structural members we created advanced numerical models with real corners (centre radius equal to the sheet thickness) and enhanced material properties in the corner area [12, 13]. Enhanced material properties in flats (f) and corners (c) were calculated from the virgin material (v) according to the equations in Table 3.

Table 3. Enhanced material properties.

	Cold-rolled (CRF) hollow section (flexural buckling test)	Press-braked lipped channel (flexural-torsional buckling test)
		
	(corner extension 2t)	(only corners)
$\sigma_{02,f}$	$\frac{0.85 \sigma_{02,v}}{-0.19 + \frac{1}{12.42 \left[\pi t / 2 (b + d) \right] + 0.83}} \quad [12]$	no change
$\sigma_{u,f}$	$\sigma_{u,v} \left[0.19 \left(\frac{\sigma_{02,f}}{\sigma_{02,v}} \right) + 0.85 \right] \quad [12]$	no change
$\sigma_{02,c}$	$0.83 \sigma_{u,f} \quad [12]$	$\frac{1.673 \sigma_{02,v}}{(r_i/t)^{0.126}} \quad [12]$
$\sigma_{u,c}$	$0.75 \sigma_{02,c} \left(\frac{\sigma_{u,v}}{\sigma_{02,v}} \right) \quad [13]$	$0.75 \sigma_{02,c} \left(\frac{\sigma_{u,v}}{\sigma_{02,v}} \right) \quad [13]$

The residual stresses and corresponding plastic strains were also inserted in the numerical model as its initial conditions according the assumed fabrication process (CRF or press-braking). Their calculation is in the Table 4.

Table 4. Residual stress models.

	Cold-rolled (CRF) hollow section (flexural buckling test)	Press-braked lipped channel (flexural-torsional buckling test)
		
corners	$0.37 \sigma_{02,v} \quad [10]$	$0.36 \sigma_{02,v} \quad [10]$
flats	$0.63 \sigma_{02,v} \quad [10]$	$0.15 \sigma_{02,v} \quad [10]$

6 Strength curve approximation models

6.1 Existing models

The well-established Ayrton-Perry formula for buckling of columns with initial imperfections in Eq. (7) has been used in calculations of carbon steel members for many years, also being adapted for stainless steel in European and Australian standards [14, 15]. However, the calculation has a physical meaning only for compressed members from linear elastic-plastic material with sinusoidal initial shape, and therefore its parameters, – imperfection factor α and the initial slenderness λ_0 – are usually selected to match the experimental results. Many analogies of more complex phenomena to this model (such as lateral-torsional buckling, instability of tubes) have been developed later on.

$$\chi = \frac{1}{\phi + \sqrt{\phi^2 - \lambda^2}}, \text{ where } \phi = 0.5(1 + \eta + \lambda^2) \text{ and } \eta = \alpha(\lambda - \lambda_0) \quad (7)$$

In such models, the limiting factor for the plastic collapse is usually the yield strength, which is convenient for materials with a sharp yield point. As Holmquist and Nadai noted as long ago as 1939, in materials without a well-defined yield point the yield strength becomes an arbitrary value, and must be substituted by a different approach, for example by using reduced modulus (or so called “double modulus”) theory. Holmquist and Nadai also laid the basis for the well-known Ramberg-Osgood constitutive model by establishing the nonlinear factor n that defines the relation between stress and strain beyond the proportionality limit. An alternative to reduced modulus theory could be use of the tangent modulus of material directly, as proposed by Engesser; this is the current design procedure in SEI/ASCE specification for stainless steels and in the Australian and New Zealand standard. Shanley showed that the true resistance is somewhere between these models, meaning that the tangent modulus provides a lower bound and reduced modulus gives higher resistances.

It should be noted that both theories were established for geometrically perfect columns (see Figure 5), and were in most cases replaced by the Ayrton-Perry formula that takes into account initial imperfections but leaves out the influence of material nonlinearity.

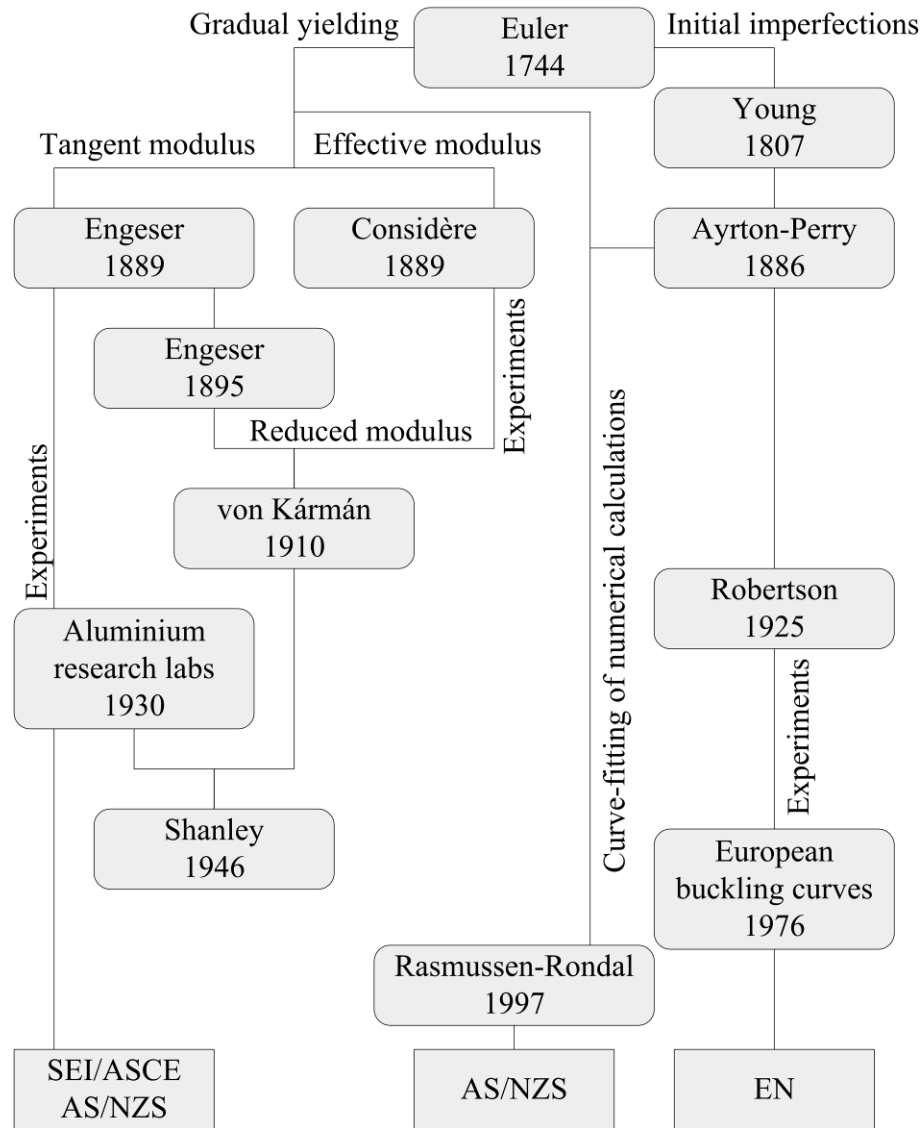


Figure 5. The development of theories for assessment of member buckling strength that formed a background of today's design codes for stainless steel.

The problem of implementing material nonlinearity in evaluation of geometrically imperfect columns was addressed in 1997 by Rasmussen and Rondal [16], who modified the imperfection factor formula (Eq. (8)) and parameters using Eqs. (9) to (12) as functions of the nonlinear n factor and with parameter e as the ratio of $\sigma_{0.2}$ and E_0 .

The curves were fitted to match finite element calculations of compressed rectangular hollow sections with initial geometrical imperfections of $L/1500$. Enhanced material properties and residual stresses were included in their numerical calculations in the material model in the same way as in the presented study.

$$\eta = \alpha \left[(\lambda - \lambda_1)^\beta - \lambda_0 \right] \geq 0 \quad (8)$$

$$\alpha = \frac{1.5}{(e^{0.6} + 0.03) \left(n^{(0.0048/e^{0.55})+1.4} + 13 \right)} + \frac{0.002}{e^{0.6}} \quad (9)$$

$$\beta = \frac{0.36 \exp(-n)}{e^{0.45} + 0.007} + \tanh \left(\frac{n}{180} + \frac{6 \cdot 10^{-6}}{e^{1.4}} + 0.04 \right) \quad (10)$$

$$\lambda_0 = 0.82 \left(\frac{e}{e + 0.0004} - 0.01n \right) \geq 0.2 \quad (11)$$

$$\lambda_1 = 0.8 \frac{e}{e + 0.0018} \left[1 - \left(\frac{n - 5.5}{n + \frac{6e - 0.0054}{e + 0.0015}} \right)^{1.2} \right] \quad (12)$$

The calculation published by Rasmussen and Rondal describes accurately the buckling behaviour of concentrically loaded members not subjected to torsional or torsional-flexural buckling. A set of recommended parameters for 8 basic stainless steel grades is given in the AS/NZS standard for the designer's convenience. The example comparison in Fig. 6 shows the close agreement of Rasmussen and Rondal's model with the flexural buckling behaviour of rectangular hollow sections. However, the model would require recalibrating constants for torsional or lateral-torsional buckling strength prediction.

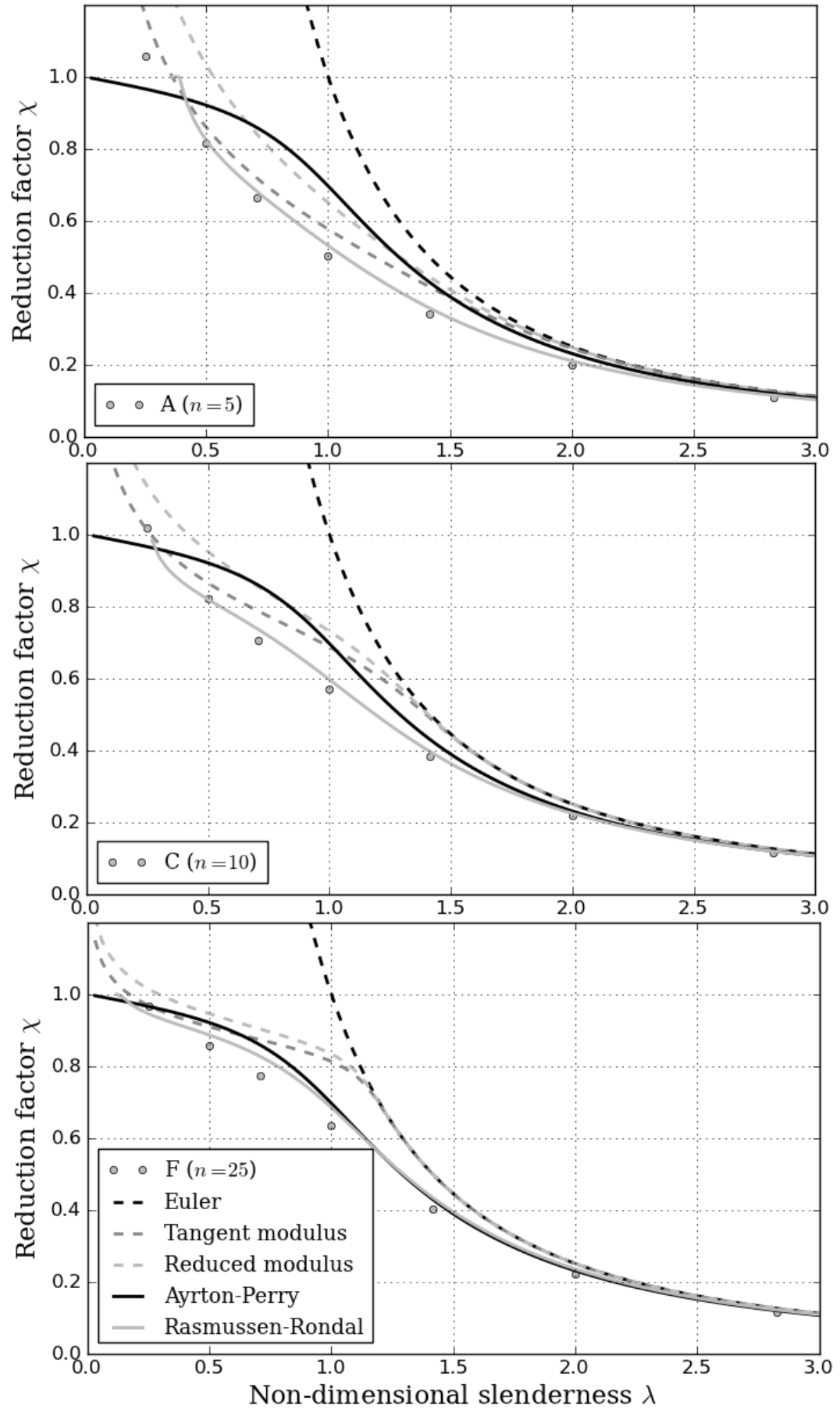


Figure 6. Example of comparison with existing theories in flexural buckling.

6.2 Transformed Ayrton-Perry model

We propose using a similar approach to the SEI/ASCE and AS/NZS standards [15, 18], where the buckling curve is calculated with tangent modulus E_t of the Ramberg-Osgood stress-strain relationship in Eq. (13) instead of initial elastic modulus E_0 .

$$E_t = \frac{df}{d\varepsilon} = \frac{E_0 \sigma_{02}}{\sigma_{02} + 0,002nE_0 (\sigma/\sigma_{02})^{n-1}} \quad (13)$$

Although these design codes are based on transformed Euler's law without initial imperfections, it is possible to extend this idea to the Ayrton-Perry curve. As a result we obtain a simple recursive model in Eqs. (14) to (16), which can be solved numerically.

$$\chi = \frac{1}{\phi + \sqrt{\phi^2 - \lambda^{*2}}}, \text{ where } \phi = 0.5(1 + \eta + \lambda^{*2}) \text{ and } \eta = \alpha(\lambda^* - \lambda_0^*) \quad (14)$$

$$\lambda^* = \lambda \cdot \sqrt{1 + 0.002n \frac{E_0}{\sigma_{02}} \chi^{n-1}} \quad (15)$$

with the following limitation of the transformed initial slenderness λ_0^* :

$$\lambda_0^* < 1.0, \text{ and therefore } \lambda_0 < \frac{1}{\sqrt{1 + 0.002n E_0 / \sigma_{0.2}}} \quad (16)$$

Such equations are easy to solve using the personal computer with spreadsheet editor or any other technical computing environment. In our case, the iteration script was developed in the Python programming language and integrated directly in Abaqus finite element simulations.

The proposed model excludes several important factors of nonlinear material behaviour: it neglects the nonlinear distribution of stresses and strains over the member cross-section; the initial imperfection shape is assumed to be sinusoidal; and the material stiffness reduction is constant in the entire member. The model is therefore unable to produce reduction factors directly without adjustment of its parameters to fit the real observed buckling behaviour. However, the possibility of including the Ramberg-Osgood nonlinear factor n in strength curves offers a significant advantage compared to the standard Ayrton-Perry model, while the model can still be used for TFB and LTB analyses if properly calibrated parameters are provided.

7 Flexural buckling tests

Square hollow sections with the centre-line dimension of $a = 72$ mm, wall thickness $t = 5$ mm and sharp corners were tested in member buckling test experimental setup. The length of the member was calculated to achieve relative slenderness from 0.0625 to 2.8 according to the following Eq. (17), where the radius of gyration $i = 29.4$ mm in all directions and $f_y = \sigma_{02}$.

$$L = \lambda \cdot \pi \sqrt{\frac{E_0}{f_y}} \cdot i \quad (17)$$

Table 5. Member lengths (mm).

Case	Non-dimensional slenderness	A, C, D, F	B, H	E	G	Mesh size (mm)
1	0.125	298.2	231.0	274.1	129.1	5
2	0.25	596.4	462.0	548.3	258.3	10
3	0.5	1192.9	924.0	1096.6	516.5	15
3B	0.7	1687.0	1306.7	1550.8	1033.1	15
4	1	2385.7	1848.0	2193.2	1460.9	20
4B	1.4	3373.9	2613.4	3101.6	2066.1	20
5	2	4771.5	3696.0	4386.3	2921.9	25
5B	2.8	6747.8	5226.8	6203.1	4132.2	25

The critical force was compared with the theoretical Euler's critical force for pinned-pinned column (Eq. (1)), where the second moment of area $I = 1245660$ mm⁴ in all directions.

$$N_{cr,E} = \frac{\pi^2 E_0 I}{L^2} \quad (18)$$

Table 6. Critical loads (kN) from LEA.

Case	A, C, D, F	B,H	E	G
1	20261	n/a	n/a	n/a
2	6621	10312	7695	4972
3	1661	2697	1950	2207
3B	847	1393	998.5	1124
4	427.7	708.3	505.4	562.3
4B	215	357.2	254.1	282.4
5	107.7	179.3	127.5	141.5
5B	53.95	89.83	63.83	70.84

The load distribution was then inserted into the FEM model and amplified to maximum imperfection $e_0 = L/750$.

Table 7. Ultimate loads (kN) from GMNIA.

Case	A	B	C	D	E	F	G	H
1	568.9	n/a	561.8	493.8	n/a	548.6	n/a	n/a
2	457.3	764.1	440.1	430.1	499.8	417.8	589.8	752.56
3	352.7	645	354.7	352.1	441.9	370.3	490.98	631.6
3B	286	533.48	305.4	305.6	401.7	333.6	425.91	549
4	217.1	398.2	246.7	247.1	331.4	274.2	341.51	439.5
4B	146.7	264	165.4	165.5	212.5	173.2	225.37	288
5	86.4	151.8	93.49	93.52	115.8	95.02	125.64	158.6
5B	46.54	80.83	49.07	49.08	59.53	49.75	65.63	82.85

The reduction factor for member buckling comes from the calculated ultimate load and characteristic elastic cross-sectional resistance (Eq. (19)), where the cross-sectional area $A = 1440 \text{ mm}^2$.

$$\chi = \frac{N_{ult}}{f_y A} \quad (19)$$

Table 8. Reduction factors.

Case	A	B	C	D	E	F	G	H
1	1.317	n/a	1.300	1.143	n/a	1.270	n/a	n/a
2	1.059	1.061	1.019	0.996	0.978	0.967	1.024	1.045
3	0.816	0.896	0.821	0.815	0.864	0.857	0.852	0.877
3B	0.662	0.741	0.707	0.707	0.786	0.772	0.739	0.763
4	0.503	0.553	0.571	0.572	0.648	0.635	0.593	0.610
4B	0.340	0.367	0.383	0.383	0.416	0.401	0.391	0.400
5	0.200	0.211	0.216	0.216	0.227	0.220	0.218	0.220
5B	0.108	0.112	0.114	0.114	0.116	0.115	0.114	0.115

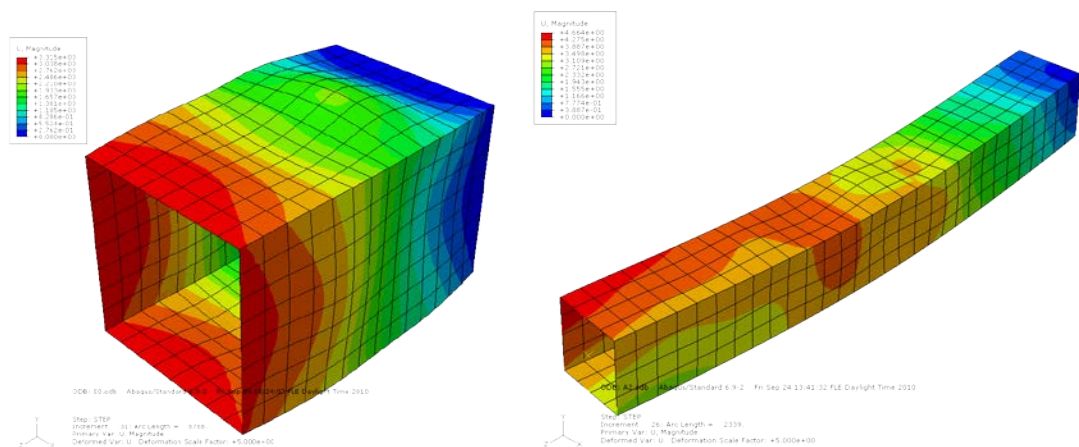


Figure 7. Local and global failure of SHS members.

8 Torsional-flexural buckling tests

Lipped channels centre-line dimension $a = 72$ mm, wall thickness $t = 5$ mm, lips length $c = 18$ mm and sharp corners were tested in member buckling test experimental setup. The length of the member was from 150 to 6788 mm.

The theoretical torsional-flexural buckling force was calculated as Eq. (20)

$$N_{cr,TF} = \frac{N_{cr,FB}}{2 \left[1 - (y_0/i_0)^2 \right]} \left[1 + \frac{N_{cr,T}}{N_{cr,FB}} - \sqrt{\left(1 - \frac{N_{cr,T}}{N_{cr,FB}} \right)^2 + 4 \left(y_0/i_0 \right)^2 \frac{N_{cr,T}}{N_{cr,FB}}} \right] \quad (20)$$

where the distance from centre of gravity to the shear centre is $y_0 = 70.86$ mm, polar radius of gyration with respect to the shear centre is $i_0 = 82.45$ mm, critical forces from flexural and torsional buckling are in Eqs. (21) and (22):

$$N_{cr,EB} = \frac{\pi^2 E_0 I}{L^2} \quad (21)$$

$$N_{cr,T} = \frac{1}{i_0^2} \left[GI_t + \frac{\pi^2 E_0 I_w}{(0.5L)^2} \right] \quad (22)$$

(fixed in torsion and warping in both ends) torsional constant is 10500 mm^4 and warping constant is 1567640000 mm^6 . The respective slenderness was calculated from the theoretical buckling load:

Table 9. Non-dimensional slenderness.

Case	Member length (mm)	A, C, D, F	B, H	E	G	Mesh size (mm)
0	150	0.0873	0.1127	0.0949	0.1008	5
1	300	0.174	0.225	0.190	0.201	5
2	600	0.347	0.448	0.377	0.401	10
3	1200	0.681	0.879	0.741	0.786	15
3B	1697	0.941	1.215	1.024	1.087	15
4	2400	1.28	1.66	1.39	1.48	20
4B	3394	1.72	2.22	1.87	1.98	20
5	4800	2.27	2.93	2.47	2.62	25
5B	6788	3.01	3.89	3.28	3.48	25

Table 10. Critical loads from LEA and ultimate loads (kN) from GMNIA.

Case	Critical loads (kN)	Ultimate loads (kN)							
		A	B	C	D	E	F	G	H
0	4791	460.7	705.9	455.2	424.6	495.1	439	564	701.6
1	3308	419.5	660.3	410	396.1	453	392.3	524	649.5
2	2222	387.3	644.7	367	367	424	359.4	490.9	601
3	830.8	271.7	412.4	285.7	285.9	361	309.1	368	442.8
3B	447.3	214.4	301.7	240.5	240.6	300.9	267.4	294.8	334.6
4	243.1	157.9	198.6	179	179.1	204.3	193	200.6	213.9
4B	135.4	105.8	122.2	116	116	124.7	120.6	123.4	128.8
5	76.62	65.79	72.15	70.1	70.11	73.69	72.24	73.09	75.06
5B	42.88	38.36	40.49	40.12	40.13	41.33	40.86	41.04	41.6

Table 11. Reduction factors.

Case	Ultimate loads (kN)							
	A	B	C	D	E	F	G	H
0	1.219	1.120	1.204	1.123	1.107	1.161	1.119	1.114
1	1.110	1.048	1.085	1.048	1.013	1.038	1.040	1.031
2	1.025	1.023	0.971	0.971	0.948	0.951	0.974	0.954
3	0.719	0.655	0.756	0.756	0.807	0.818	0.730	0.703
3B	0.567	0.479	0.636	0.637	0.673	0.707	0.585	0.531
4	0.418	0.315	0.474	0.474	0.457	0.511	0.398	0.340
4B	0.280	0.194	0.307	0.307	0.279	0.319	0.245	0.204
5	0.174	0.115	0.185	0.185	0.165	0.191	0.145	0.119
5B	0.101	0.064	0.106	0.106	0.092	0.108	0.081	0.066

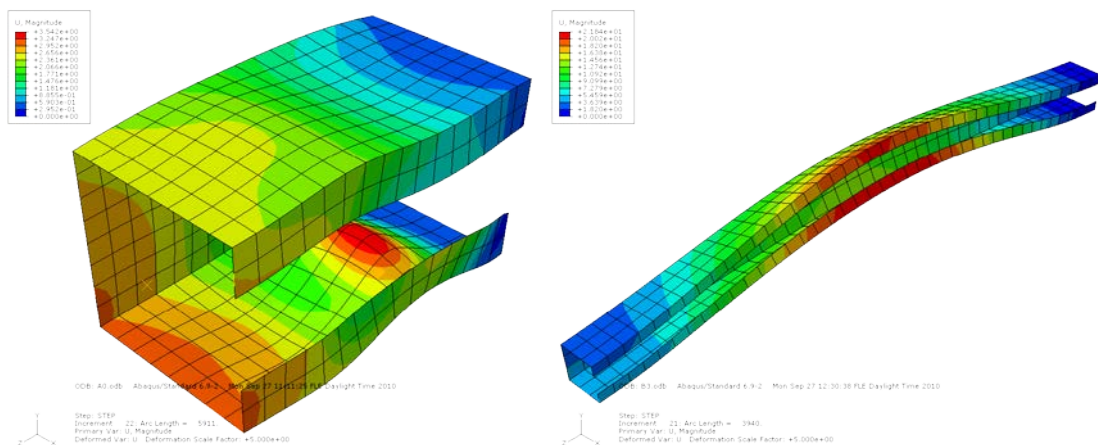


Figure 8. Local and global failure of lipped channels.

9 Lateral torsional buckling tests

Members with double-symmetrical I-section with basic dimensions of IPE200 (flange centre-to-centre distance 191.5 mm, flange width 100 mm and thickness 8.5 mm, web thickness 5.6 mm) were subjected to uniform major-axis bending by applying bending moment to their end sections.

The theoretical lateral-torsional buckling load was calculated as Eq. (23).

$$M_{cr} = C_1 \frac{\pi^2 EI_z}{(k_z L)^2} \sqrt{\left(\frac{k_z}{k_w}\right)^2 \frac{I_w}{I_z} + \frac{(k_z L)^2 GI_t}{\pi^2 EI_z}} \quad (23)$$

where $C_1 = 1.0$ based on the uniform moment diagram, $k_z = 1.0$ and $k_w = 0.5$ according to the support conditions (free to rotate, fixed in torsion and warping) and cross-sectional properties are $I_z = 1.419 \cdot 10^6 \text{ mm}^4$, $I_t = 52152 \text{ mm}^4$, $I_w = 12.9881 \cdot 10^9 \text{ mm}^6$. The respective slenderness was calculated from the theoretical buckling load.

Table 12. Non-dimensional slenderness.

Case	Member length (mm)	A, C, D, F	B, H	E	G	Mesh size (mm)
0	200	0.0664	0.0857	0.0722	0.0767	5
1	400	0.133	0.171	0.144	0.153	5
2	800	0.264	0.341	0.287	0.305	10
2B	1131	0.371	0.479	0.404	0.428	10
3	1600	0.519	0.670	0.564	0.599	15
3B	2263	0.718	0.927	0.781	0.829	15
4	3200	0.977	1.26	1.06	1.13	20
4B	4525	1.30	1.67	1.41	1.50	20
5	6400	1.67	2.16	1.82	1.93	25
5B	9051	2.10	2.71	2.28	2.42	25

Critical loads from LEA and ultimate loads from GMNIA were also compared to the theoretical curves.

It was impossible to reach the peak load in two extremely slender cases (material B and E, case 5B) because it was smaller than minor axis bending resistance and members failed in minor axis bending already turned 90 degrees prior to reaching elastic buckling load.

The reduction factor for member buckling comes from the calculated ultimate load and characteristic elastic cross-sectional resistance (Eq. (24)), where the section modulus $W_{y,el} = 197 \cdot 10^3 \text{ mm}^3$ and $W_{y,pl} = 221 \cdot 10^3 \text{ mm}^3$

$$\chi = \frac{M_{ult}}{f_y W_y} \quad (24)$$

Table 13. Critical loads from LEA and ultimate loads (kNm) from GMNIA.

Case	Critical loads (kNm)	Ultimate loads (kNm)							
		A	B	C	D	E	F	G	H
0	706.6	92.21	132.4	91.66	80.44	94.73	89.85	106.7	132.24
1	592.6	80.4	122.1	79.55	78.73	85.95	76.26	97.64	121.39
2	560.3	77.13	118.2	76.05	71.41	83.04	72.84	94.79	117.45
2B	452.4	63.27	99.42	61.6	60.76	70.06	59.82	79.53	97.62
3	237.8	55.11	84.76	54.67	54.52	64.29	55.13	70.37	85.24
3B	125.6	45.6	67	47.19	47.22	57.7	49.87	59.53	70.65
4	68.12	35.77	48.73	39.04	39.07	47.78	42.55	47.11	53.24
4B	38.53	26.68	33.06	29.69	29.71	33.53	31.73	33.18	35.23
5	22.27	18.57	21.48	20.14	20.14	22.57	20.88	21.5	22.77
5B	14.07	13.03	n/a	14.04	14.04	n/a	14.66	n/a	n/a

Table 14. Reduction factors (using elastic section modulus).

Case	A	B	C	D	E	F	G	H
0	1.559	1.343	1.550	1.360	1.354	1.519	1.353	1.342
1	1.360	1.239	1.345	1.331	1.228	1.290	1.238	1.232
2	1.304	1.199	1.286	1.208	1.187	1.232	1.202	1.192
2B	1.070	1.009	1.042	1.028	1.001	1.012	1.009	0.991
3	0.932	0.860	0.925	0.922	0.919	0.932	0.893	0.865
3B	0.771	0.680	0.798	0.799	0.825	0.843	0.755	0.717
4	0.605	0.494	0.660	0.661	0.683	0.720	0.598	0.540
4B	0.451	0.335	0.502	0.502	0.479	0.537	0.421	0.357
5	0.314	0.218	0.341	0.341	0.323	0.353	0.273	0.231
5B	0.220	n/a	0.237	0.237	n/a	0.248	n/a	n/a

Table 15. Reduction factors (using plastic section modulus).

Case	A	B	C	D	E	F	G	H
0	1.391	1.198	1.383	1.213	1.207	1.355	1.207	1.197
1	1.213	1.105	1.200	1.187	1.096	1.150	1.105	1.099
2	1.163	1.070	1.147	1.077	1.058	1.099	1.072	1.063
2B	0.954	0.900	0.929	0.916	0.893	0.902	0.900	0.883
3	0.831	0.767	0.825	0.822	0.819	0.832	0.796	0.771
3B	0.688	0.606	0.712	0.712	0.735	0.752	0.673	0.639
4	0.540	0.441	0.589	0.589	0.609	0.642	0.533	0.482
4B	0.402	0.299	0.448	0.448	0.427	0.479	0.375	0.319
5	0.280	0.194	0.304	0.304	0.288	0.315	0.243	0.206
5B	0.197	n/a	0.212	0.212	n/a	0.221	n/a	n/a

10 Tension tests

In order to study the average material model of the complex cold-formed cross sections with enhanced material properties and residual stresses, we created several series of numerical models for the tensile tests of the whole members and coupons from their flat faces. Member cross-sectional shape was fixed at both ends and the member was loaded with increasing deformation up to 150% of its original length.

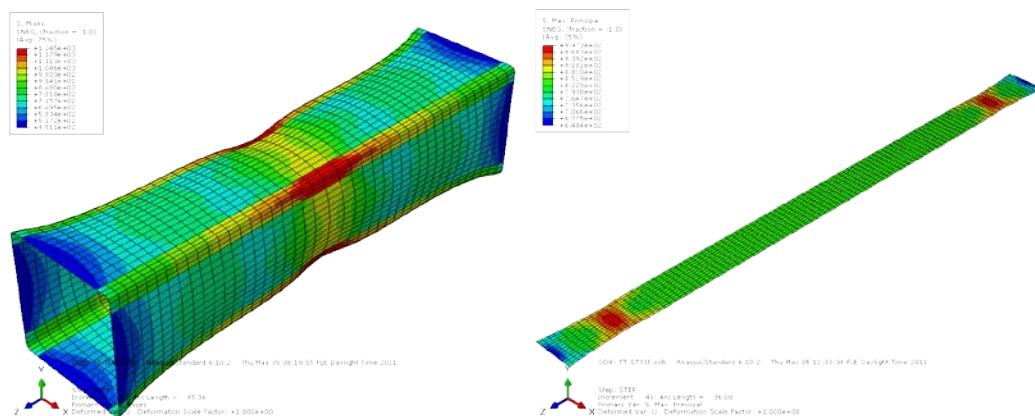


Figure 9. Tension tests.

11 Results of parametric study

From the collected buckling resistances of 8 materials, we selected two most important parameters that affect the shape of strength curve, nonlinear factor n and the yield point f_y (σ_{02}). In the following parametric study, those effects are investigated with three materials for each of the variable parameters for flexural buckling, torsional-flexural buckling and lateral-torsional buckling. Reduction factors χ were calculated as ratios of member loading capacities obtained by finite element calculations and characteristic compression or bending resistances according to Eurocode 3. Maximum differences between reduction factors obtained at the same nondimensional slenderness λ were observed and reported in the following chapters.

11.1 The effect of material nonlinearity

Three material models were used in this study with variable n factor (see Figure 10).

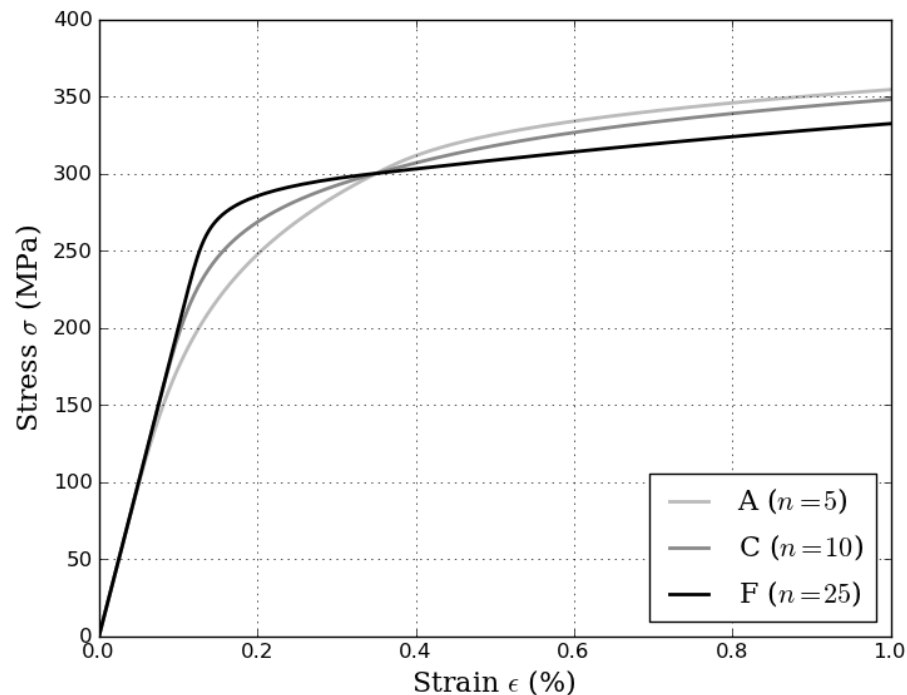


Figure 10. Stress-strain relationship of studied materials.

The examples of typical strength curves are plotted in Figure 11 where the curve “Difference” shows the quantity $\chi_{N3} - \chi_{N1}$, reaching its maximum value at slenderness approximately equal to 1.

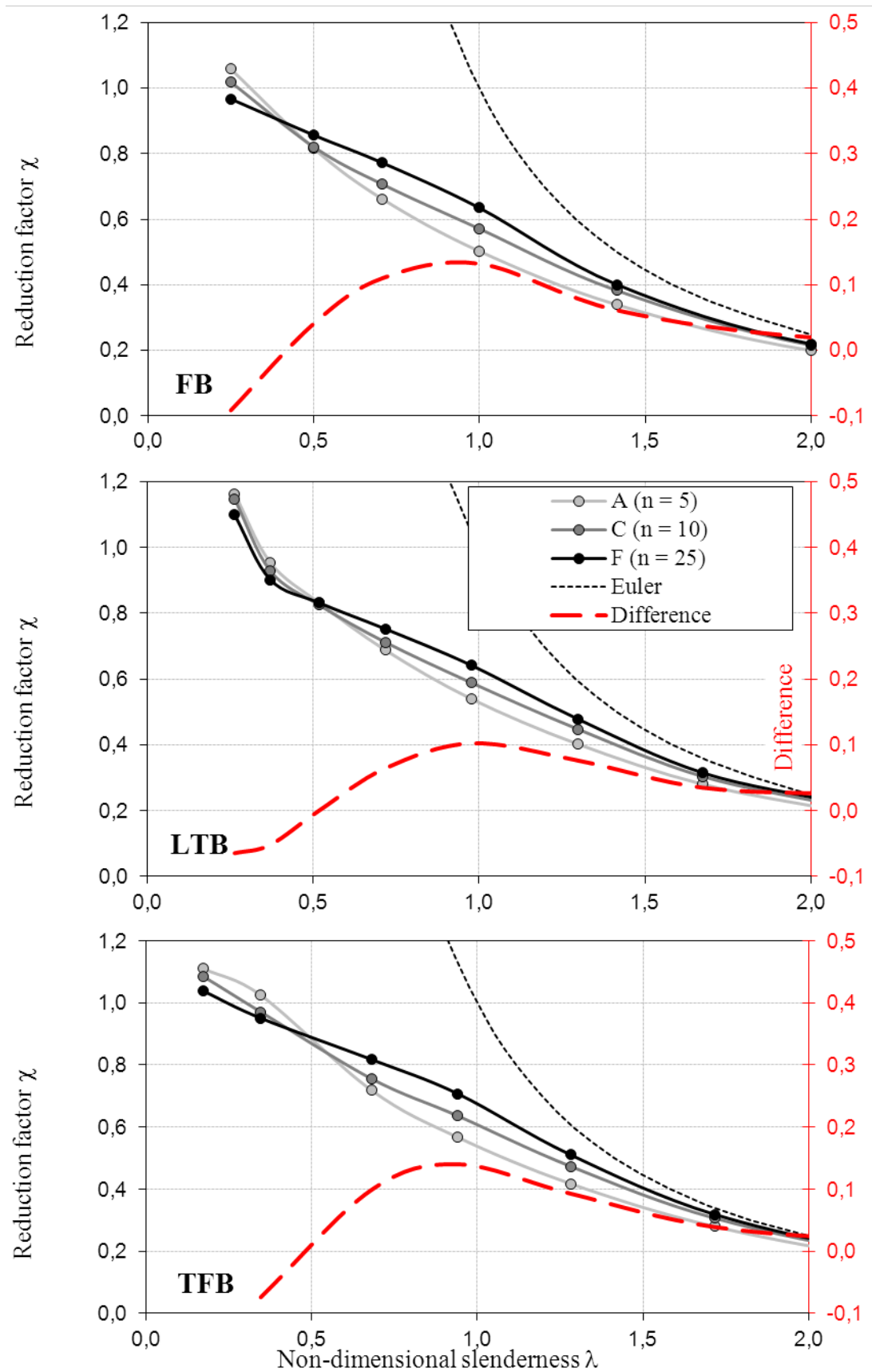


Figure 11. Comparison of FEM results with variable n .

Although, the numerical studies were carried out with the complex two-stage material model, it was more convenient to use the simple Ramberg-Osgood

equation for the evaluation of strength curve approximations. In the studied range of material strains the difference in both material models is insignificant.

11.2 The effect of material yield strength

The same study was carried out on three materials with different yield point (see Figure 12).

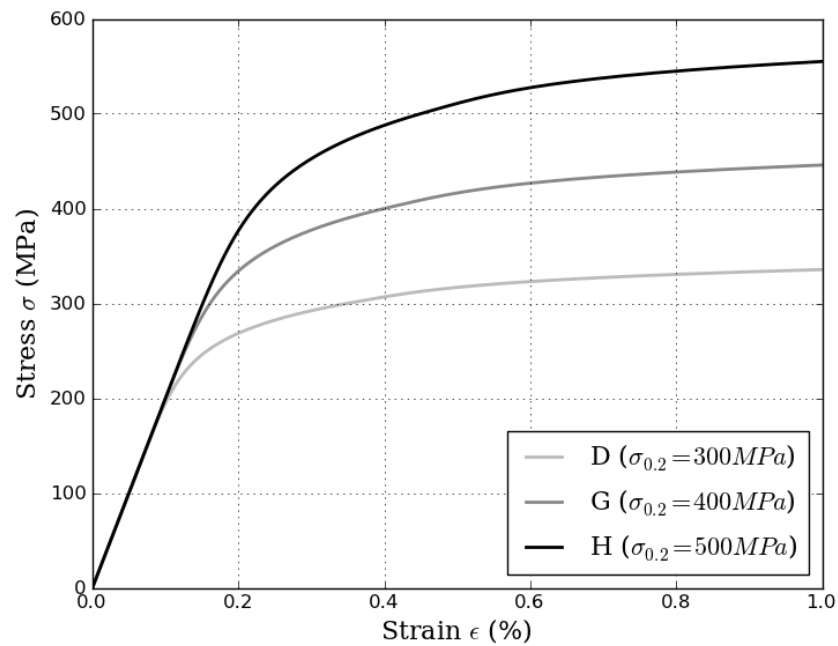


Figure 12. Stress-strain relationship of studied materials.

The strength curves formed from the ultimate member resistances are plotted in Figure 13. Even though the big differences in stress-strain relationships indicate that the effect on strength curves may be higher, the degradation of tangent modulus governs the shape of non-dimensional strength curve rather than the yield point.

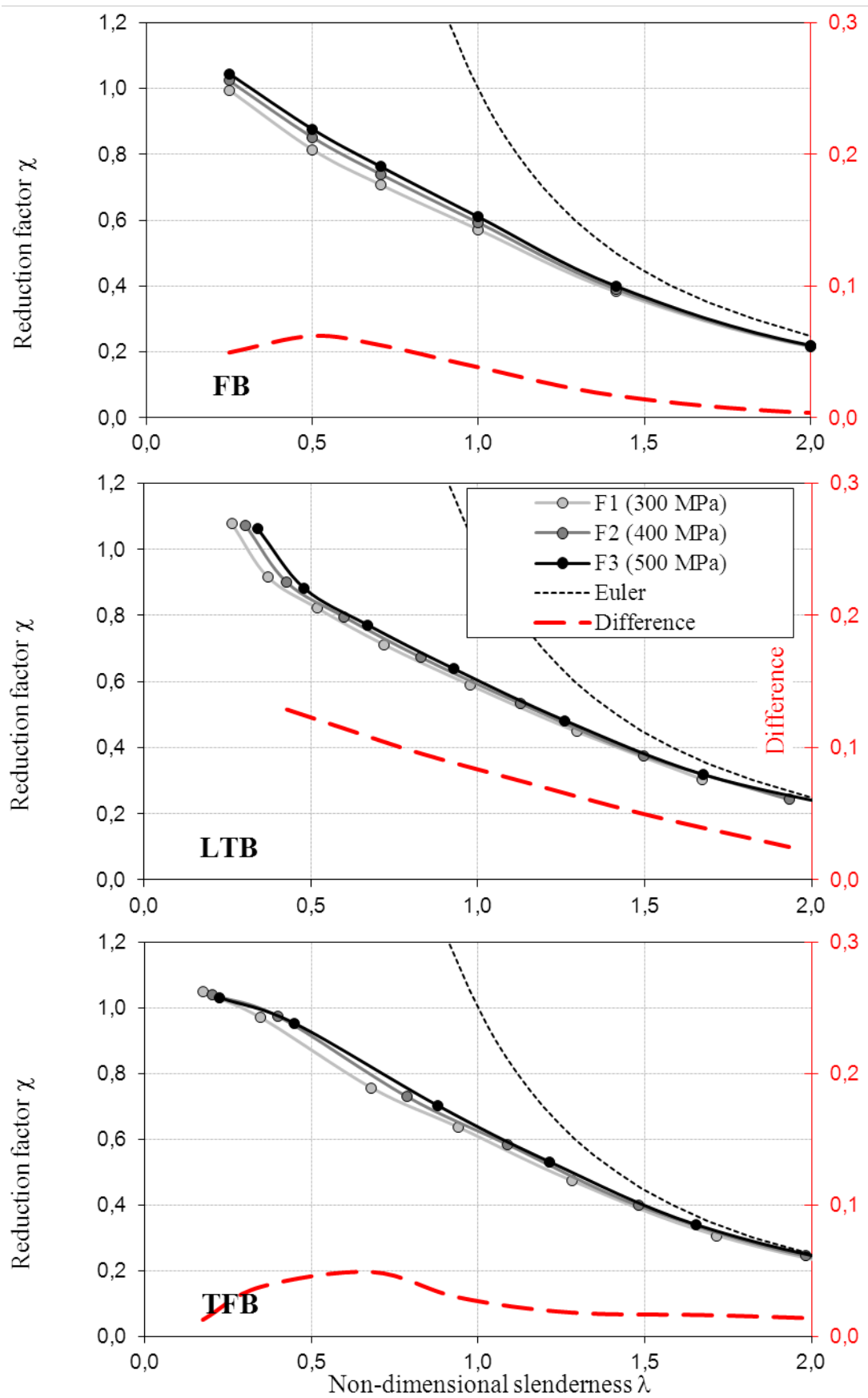


Figure 13. Comparison of FEM results with variable yield strength.

11.3 The effect of bending residual stresses

Additional study was carried on to evaluate the effect of residual stresses on the load-displacement relationship of work-hardened materials. The load-displacement curve of the full member tension test is usually the basis of stress-strain model of the average material of the cross-section. Because of the complex non-linear material behavior is different in corners and flat parts of the cross-section, it is difficult to calculate the material model parameters analytically and therefore either experimental or numerical analysis has to be performed (see Chapter 10).

In this study, we chose the material C (ferritic steel 1 with $n = 10$) as a virgin material that is usually given by mill certificate and we assumed that the square hollow section (side 72 mm, thickness 3 mm, corner radius 3 mm) was cold formed by circle-to-rectangle forming process, where bending residual stresses are too high to be neglected. Material properties of corners and flats were calculated according the theory in Chapters 2 and 5 and are presented in the Table 16.

Table 16. Material parameters used for the residual bending stress study.

	E_0 GPa	σ_{02} MPa	n	σ_u MPa	m	ε_u
Virgin material	200	300.0	10	600.0	2.75	0.500
Flats	200	412.1	10	666.6	3.16	0.382
Corners	200	553.3	10	829.9	3.33	0.333

We assumed the fully plastic through-thickness stress distribution according to [19] and the uniform maximum value in the whole cross-section that was changing up to 150% of virgin material yield strength which corresponds to 89% of average material proof stress (that is reported in the figures and tables).

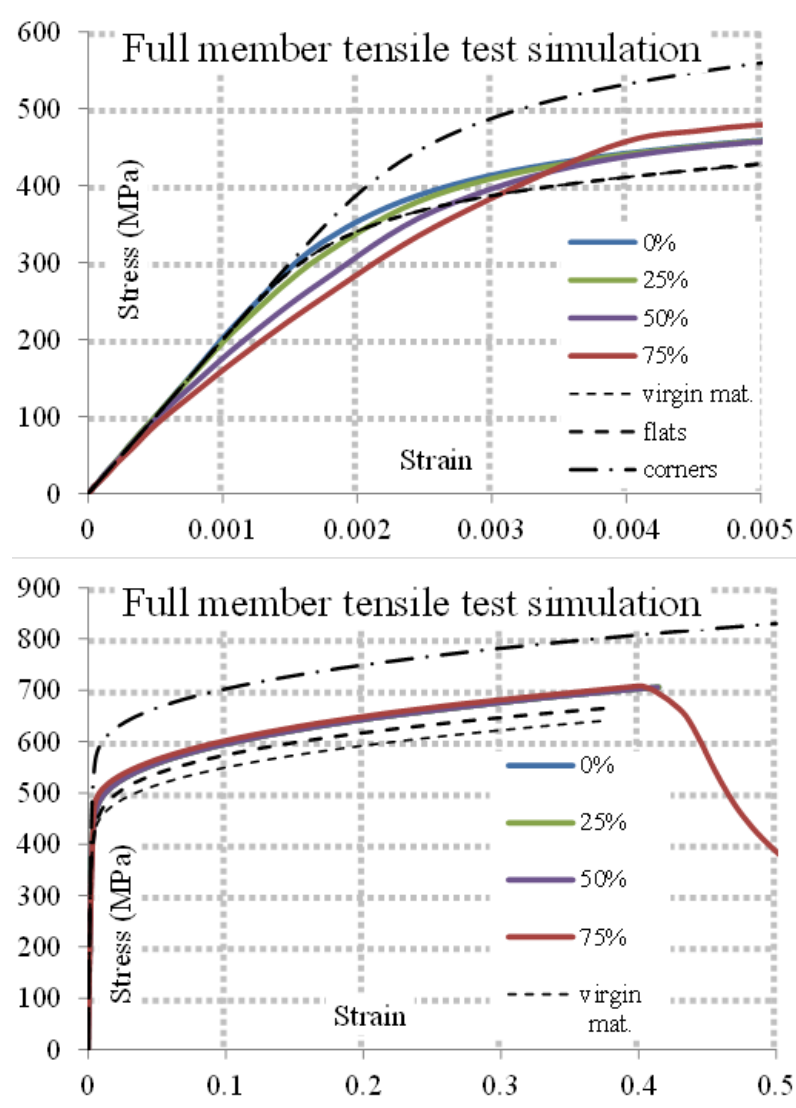


Figure 14. Stress-strain diagrams from the tensile test simulations of full members.

As a reference calculation, we simulated also coupons with the material properties of the flat faces. In those simulations, the level of residual bending stress maximum was changing from 0% to 100% of the flats yield strength that was assumed to be the reference average material yield strength as well.

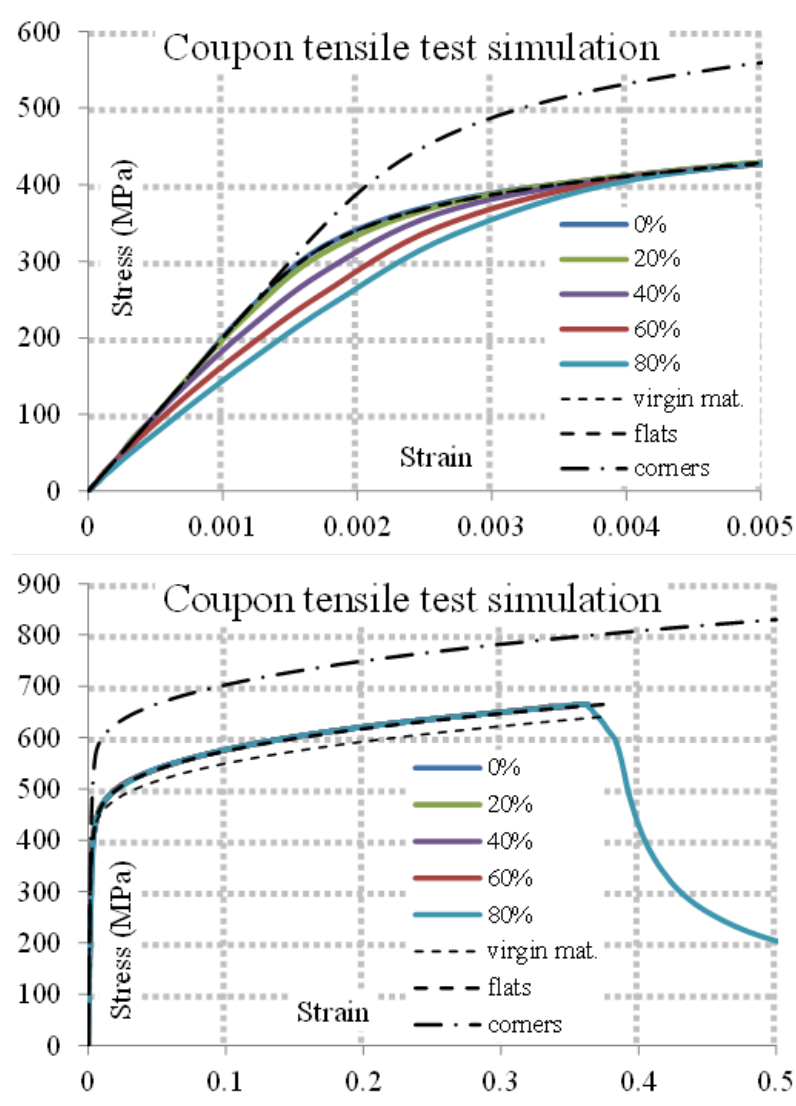


Figure 15. Stress-strain diagrams from the tensile tests of coupons.

Using the load-displacement data converted to the stress-strain format (Figure 14 and Figure 15), we were able to calculate material parameters of the average material, where the residual stresses are already included in the material properties. We applied the advanced optimization algorithm reported in [3] to obtain the accurate material parameters for the selected two-stage material model.

We observed a decreasing initial elastic modulus with increasing residual stress which is the clear effect of material non-linearity, where half of the sheet thickness has initial stiffness equal to the tangent modulus corresponding to the level of residual stress. The same effect was expected to alter also the value of non-linear n factor.

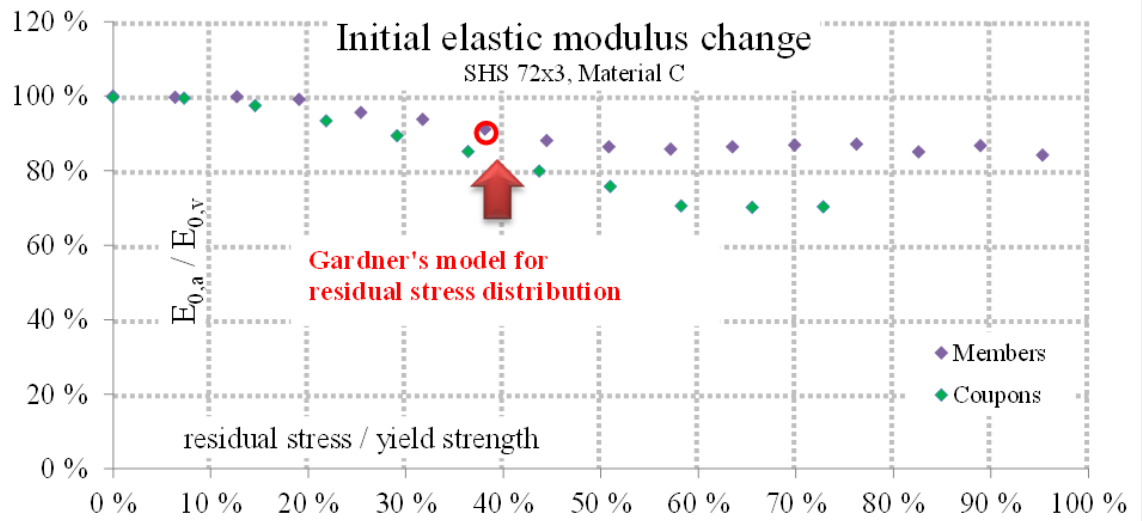


Figure 16. Initial elastic modulus change.

As it is demonstrated on the Figure 16, the ratio between the initial elastic modulus of the average material and the virgin material is decreasing more significantly from 20% residual stress level. The residual stress distribution proposed by Gardner and Cruise [10] is plotted for comparison and it well corresponds with the observed trends using the uniform level of residual stress over the whole cross-section.

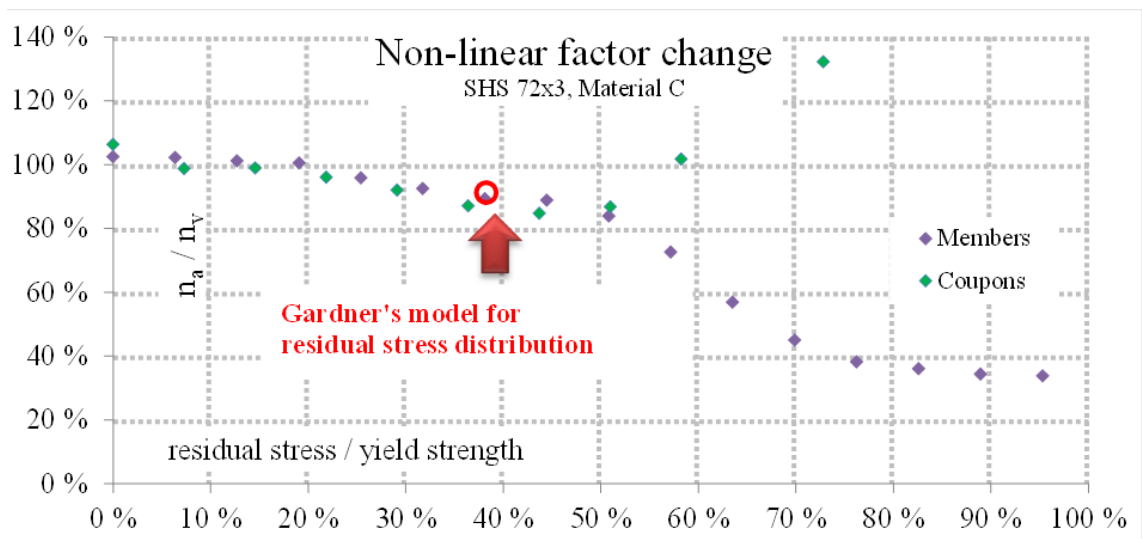


Figure 17. Non-linear factor change.

The non-linear factor n is also dependent on the residual stress level, however, its behaviour is more complex and it can have also higher values than the original virgin material non-linear factor (see Figure 17).

12 Regression analysis of proposed strength curve

In order to compare the suitability of the transformed Ayrton-Perry law to be used as strength curve approximation formula, we used non-linear regression analysis to fit the Eq. (14) to the finite element results and compared it with the same regression on the original Ayrton-Perry curve from Eq. (7).

The outputs of non-linear regression analysis are the unknown parameters α and λ_0 and the average absolute error of the best-fitted curve to the numerical results R (Table 17 to Table 19). The results are also compared to the Rasmussen and Rondal strength curves [16], even though they are based on the numerical analysis with lower initial imperfection amplitude ($L/1500$) showing higher reduction factors with almost constant offset to the transformed Ayrton-Perry calculation (see Figure 18). The parameters of Rasmussen and Rondal imperfection factor α , β , λ_0 and λ_1 are included in the Table 17 to Table 19 for comparison.

The transformed Ayrton-Perry curve (TAP) has the lowest error value R in 17 of 18 cases showing that the proposed law can describe the shape of strength curve of non-linear materials very well taking into account the Ramberg-Osgood hardening parameter n .

With the increasing non-linear factor n , the initial slenderness λ_0 was decreasing which is the most visible effect in the transformed Ayrton-Perry results (0.36→0.27→0.18 in flexural buckling, 0.35→0.27→0.18 in torsional-flexural buckling and 0.36→0.27→0.16 in lateral-torsional buckling study).

Table 17. Comparison of approximations of flexural buckling (FB) strength curves.

N1 ($n = 5$)			N2 ($n = 10$)			N3 ($n = 25$)		
AP	TAP	R97	AP	TAP	R97	AP	TAP	R97
0.88	0.31	1.27	0.64	0.35	0.69	0.25	0.26	0.27
		0.16			0.15			0.23
0.31	0.36	0.61	0.28	0.27	0.57	0.12	0.18	0.44
		0.35			0.24			0.11
0.030	0.016	0.059	0.046	0.010	0.051	0.044	0.011	0.061
F1 ($f_y = 300$ MPa)			F2 ($f_y = 400$ MPa)			F3 ($f_y = 500$ MPa)		
AP	TAP	R97	AP	TAP	R97	AP	TAP	R97
0.60	0.35	0.69	0.29	0.31	0.66	0.28	0.29	0.63
		0.15			0.13			0.12
0.25	0.27	0.57	0.03	0.27	0.60	0.11	0.32	0.63
		0.24			0.29			0.33
0.029	0.007	0.030	0.018	0.011	0.017	0.018	0.010	0.020

Table 18. Comparison of approximations of torsional-flexural buckling (TFB) strength curves.

N1 ($n = 5$)			N2 ($n = 10$)			N3 ($n = 25$)		
AP	TAP	R97	AP	TAP	R97	AP	TAP	R97
0.65	0.15	1.27	0.43	0.15	0.69	0.25	0.14	0.27
		0.16			0.15			0.23
0.36	0.35	0.61	0.35	0.27	0.57	0.32	0.18	0.44
		0.35			0.24			0.11
0.021	0.011	0.046	0.032	0.018	0.047	0.031	0.022	0.034
F1 ($f_y = 300$ MPa)			F2 ($f_y = 400$ MPa)			F3 ($f_y = 500$ MPa)		
AP	TAP	R97	AP	TAP	R97	AP	TAP	R97
0.38	0.15	0.69	0.29	0.17	0.66	0.31	0.18	0.63
		0.15			0.13			0.12
0.29	0.27	0.57	0.33	0.31	0.60	0.32	0.34	0.63
		0.24			0.29			0.33
0.023	0.018	0.034	0.021	0.017	0.033	0.020	0.017	0.029

Table 19. Comparison of approximations of lateral-torsional buckling (LTB) strength curves.

N1 ($n = 5$)			N2 ($n = 10$)			N3 ($n = 25$)		
AP	TAP	R97	AP	TAP	R97	AP	TAP	R97
0.79	0.22	1.27	0.72	0.28	0.69	0.56	0.26	0.27
		0.16			0.15			0.23
0.35	0.36	0.61	0.36	0.27	0.57	0.36	0.16	0.44
		0.35			0.24			0.11
0.039	0.016	0.086	0.053	0.035	0.084	0.060	0.040	0.089
F1 ($f_y = 300$ MPa)			F2 ($f_y = 400$ MPa)			F3 ($f_y = 500$ MPa)		
AP	TAP	R97	AP	TAP	R97	AP	TAP	R97
0.64	0.28	0.69	0.52	0.22	0.66	0.46	0.26	0.63
		0.15			0.13			0.12
0.34	0.27	0.57	0.33	0.31	0.60	0.37	0.33	0.63
		0.24			0.29			0.33
0.038	0.024	0.057	0.037	0.027	0.052	0.036	0.024	0.050

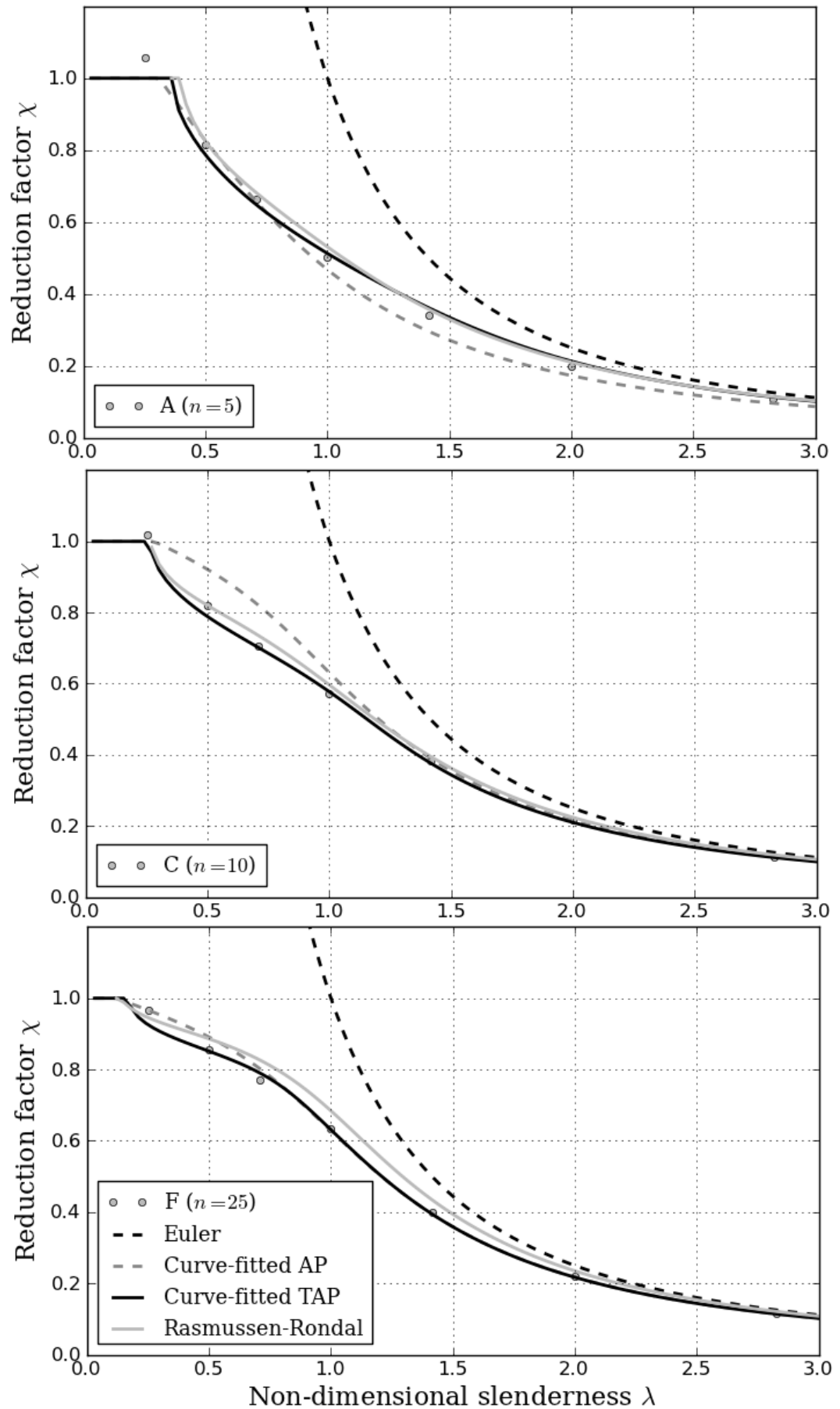


Figure 18. Example comparison of models with curve-fitted parameters in flexural buckling.

13 Conclusions

With increasing non-linear n parameter, initial slenderness λ_0 decreases. This effect implies that while initial slenderness 0.4 in Eurocode (derived from mainly austenitic steel experimental results) can be used for materials with low n parameter, it may be unconservative to use it in combination with ferritic grades that have generally higher n values.

The transformed Ayrton-Perry curve describes more precisely the behaviour of ferritic stainless-steel members subjected to buckling loads than the formulas used in present codes. However it does not account on many uncertainties such as non-linear stress distribution in the cross-section, and therefore it would be necessary to adjust its parameters to the real experimental results. The rule can be easily extended to all metallic alloys and materials following Ramberg-Osgood law.

The effect of variation of yield strength confirms the results of Rasmussen and Rondal [16] also in torsional-flexural and lateral-torsional buckling showing that the biggest difference in studied cases occurs when the non-dimensional slenderness λ ranges from 0.5 to 1.0.

Bending residual stresses due to cold-working are one of the reasons for the different load-displacement behaviour of the virgin material and the whole member or coupons originating from the flat and curved member parts. However, their prediction is very complex and therefore it is usually recommended to perform full-section tests to obtain these values experimentally.

References

- [1] Hradil, P., Talja, A., Real, E. & Mirambell, E. SAFSS Work Package 2: Review of available data. VTT Technical Research Centre of Finland, 2010.
- [2] Hradil, P. SAFSS Work Package 2: Profiler – Abaqus plug-in manual. VTT Technical Research Centre of Finland, 2011.
- [3] Talja, A. & Hradil, P. SAFSS Work Package 2: Model calibration test report. VTT Technical Research Centre of Finland, 2011.
- [4] Rasmussen, K.J.R. Full-range stress-strain curves for stainless steel alloys. *Journal of Constructional Steel Research* 2003, 1, Vol. 59, No. 1, pp. 47–61. ISSN 0143-974X. doi: DOI: 10.1016/S0143-974X(02)00018-4.
- [5] Mirambell, E. & Real, E. On the calculation of deflections in structural stainless steel beams: an experimental and numerical investigation. *Journal of Constructional Steel Research* 2000, 4, Vol. 54, No. 1, pp. 109–133. ISSN 0143-974X. doi: DOI: 10.1016/S0143-974X(99)00051-6.
- [6] European Committee for Standardization Eurocode 3. Design of steel structures. Part 1-4: General rules. Supplementary rules for stainless steels. Brussels, Belgium: 2006.
- [7] Zhang, L. & Tong, G.S. Lateral buckling of web-tapered I-beams: A new theory. *Journal of Constructional Steel Research* 2008, 12, Vol. 64, No. 12, pp. 1379–1393. ISSN 0143-974X. doi: DOI: 10.1016/j.jcsr.2008.01.014.
- [8] European Committee for Standardization EN 10088-2: Stainless steels. Part 2: Technical delivery conditions for sheet/plate and strip of corrosion resisting steels for general purposes. Brussels, Belgium: 2005.
- [9] European Committee for Standardization Eurocode 3. Design of steel structures. Part 1-3: General rules. Supplementary rules for coldformed members and sheeting. Brussels, Belgium: 2006.
- [10] Gardner, L. & Cruise, R.B. Modeling of Residual Stresses in Structural Stainless Steel Sections. *Journal of Structural Engineering* 2009, 01, Vol. 135, No. 1, pp. 42–53. ISSN 07339445. doi: 10.1061/(ASCE)0733-9445(2009)135:1(42).
- [11] Rasmussen, K.J.R., Burns, T., Bezkorovainy, P. & Bambach, M.R. Numerical modelling of stainless steel plates in compression. *Journal of Constructional Steel Research* 2003, 11, Vol. 59, No. 11, pp. 1345–1362. ISSN 0143-974X. doi: DOI: 10.1016/S0143-974X(03)00086-5.
- [12] Cruise, R.B. & Gardner, L. Strength enhancements induced during cold forming of stainless steel sections. *Journal of Constructional Steel Research* 2008, 11, Vol. 64, No. 11, pp. 1310–1316. ISSN 0143-974X. doi: DOI: 10.1016/j.jcsr.2008.04.014.
- [13] Ashraf, M., Gardner, L. & Nethercot, D.A. Strength enhancement of the corner regions of stainless steel cross-sections. *Journal of Constructional*

Steel Research 2005, 1, Vol. 61, No. 1, pp. 37–52. ISSN 0143-974X. doi: DOI: 10.1016/j.jcsr.2004.06.001.

- [14] European Committee for Standardization Eurocode 3: Design of steel structures. Part 1-1: General rules and rules for buildings. Brussels, Belgium: 2005.
- [15] Standards Australia & Standards New Zealand Australian/New Zealand Standard: Cold-formed stainless steel structures. Sydney Australia: 2001. ISBN 0 7337 3979 2.
- [16] Rasmussen, K.J.R. & Rondal, J. Strength curves for metal columns. Journal of Structural Engineering 1997, 06, Vol. 123, No. 6, pp. 721. ISSN 07339445.
- [17] Report No. 22. European Convention for Constructional Steelwork Manual on Stability of Steel Structures, Second edition. ECCS Committee 8 – Stability, 1976.
- [18] American Society of Civil Engineers & Structural Engineering Institute Specification for the Design of Cold-Formed Stainless Steel Structural Members. Reston, Virginia: 2002. ISBN 0-7844-0556-5.
- [19] Jandera, M., Gardner, L. & Machacek, J. Residual stresses in cold-rolled stainless steel hollow sections. Journal of Constructional Steel Research 2008, 11, Vol. 64, No. 11, pp. 1255-1263. ISSN 0143-974X. doi: DOI: 10.1016/j.jcsr.2008.07.022.

Appendix A: Austenitic steel

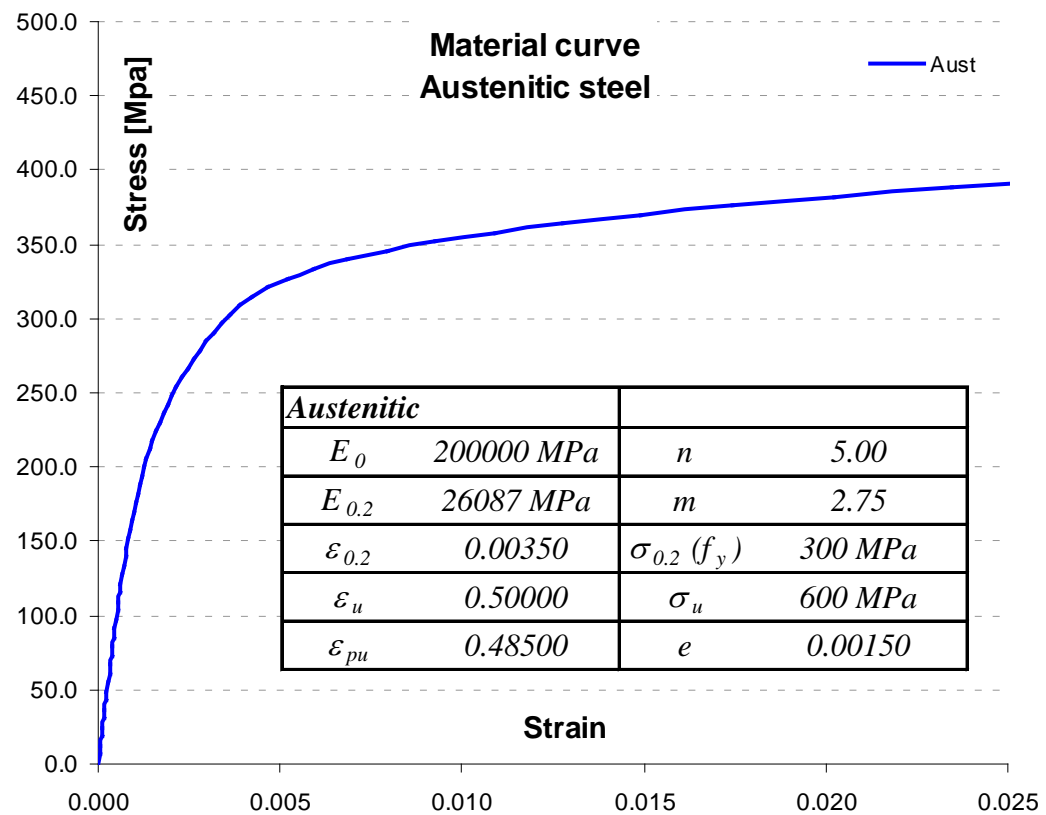


Figure 19. Material model.

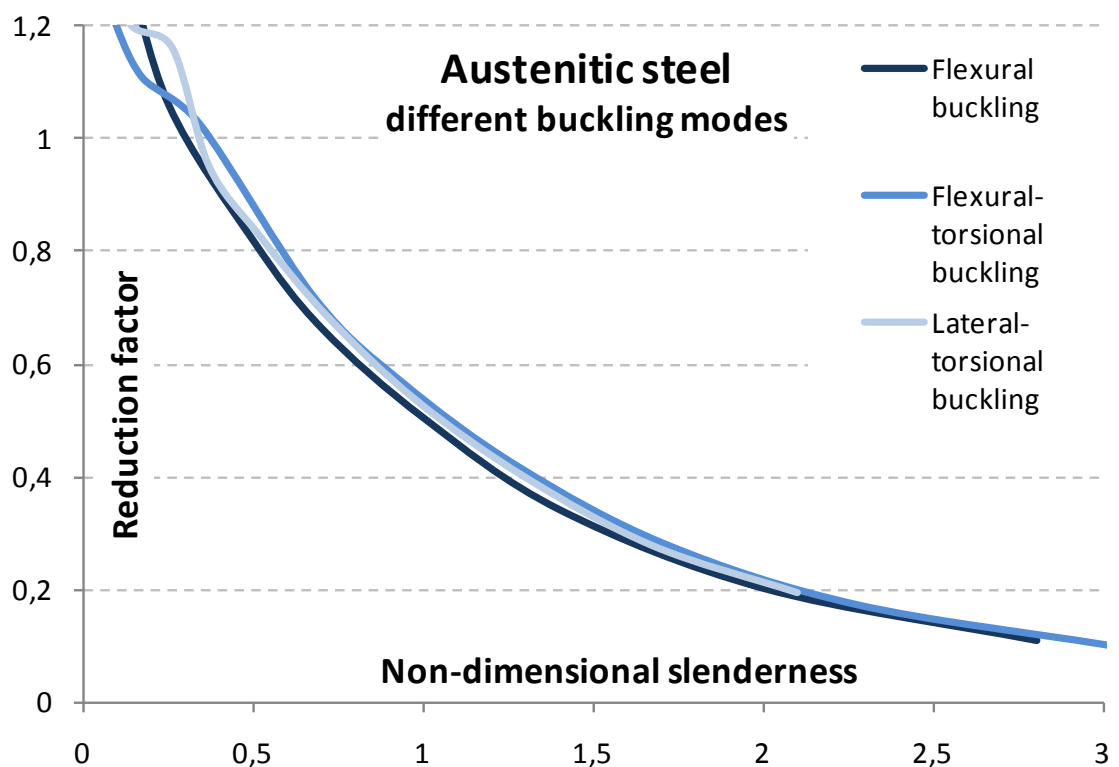
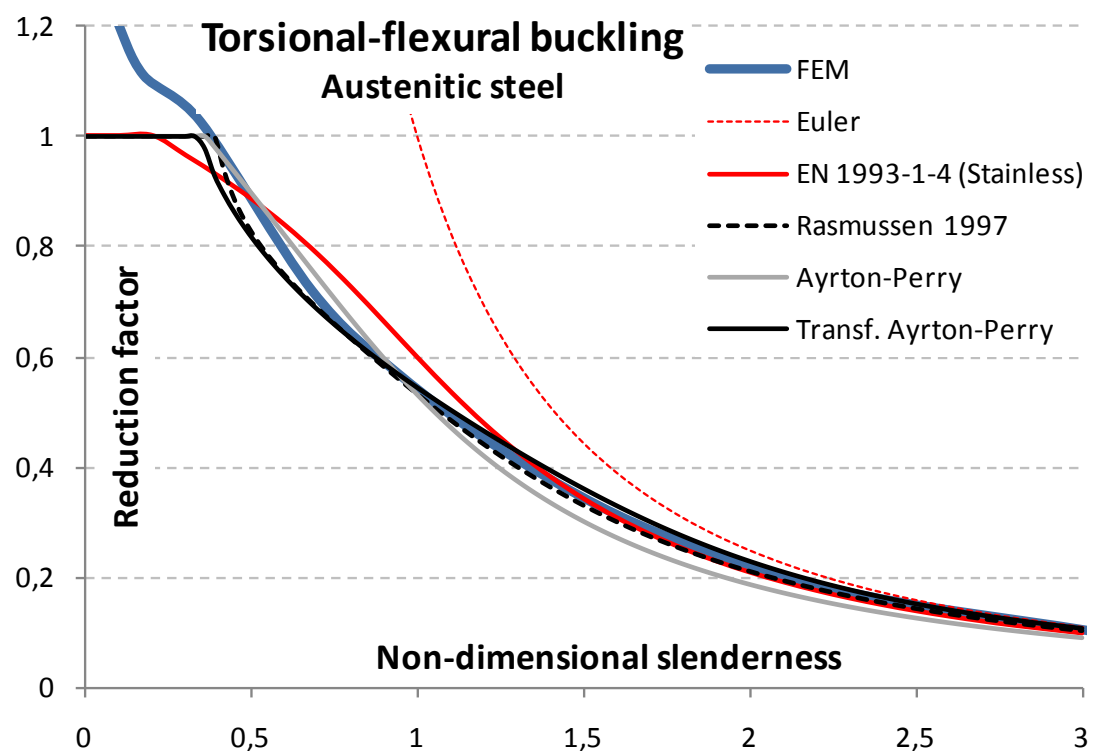
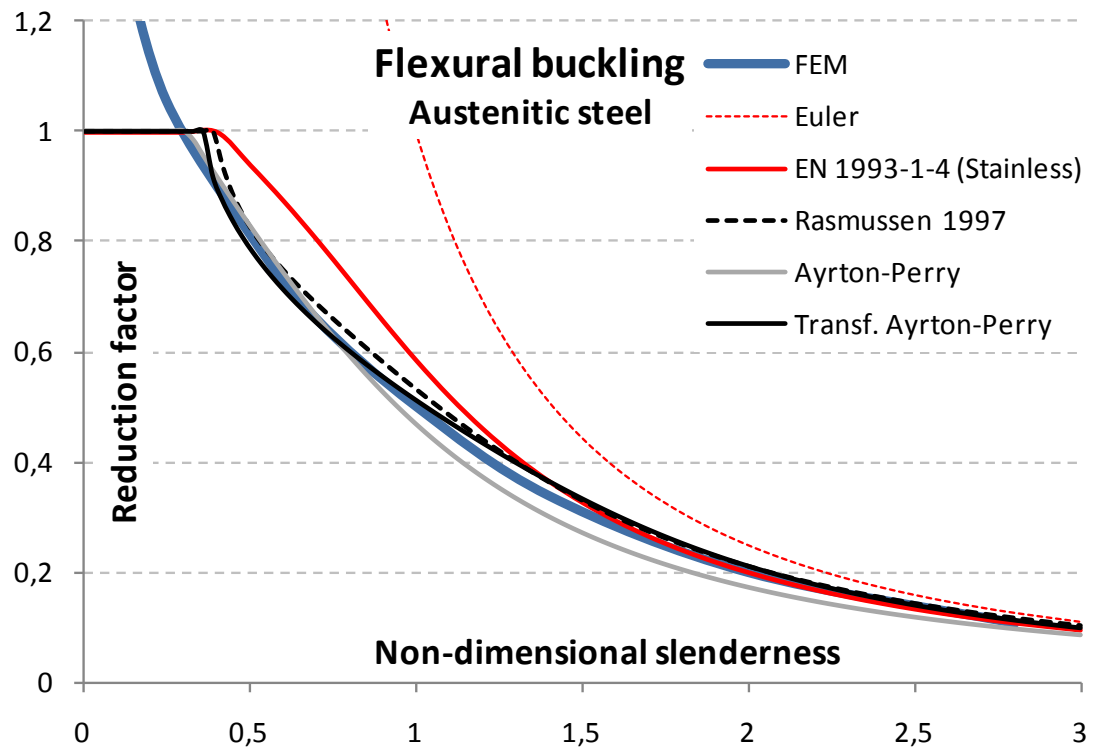
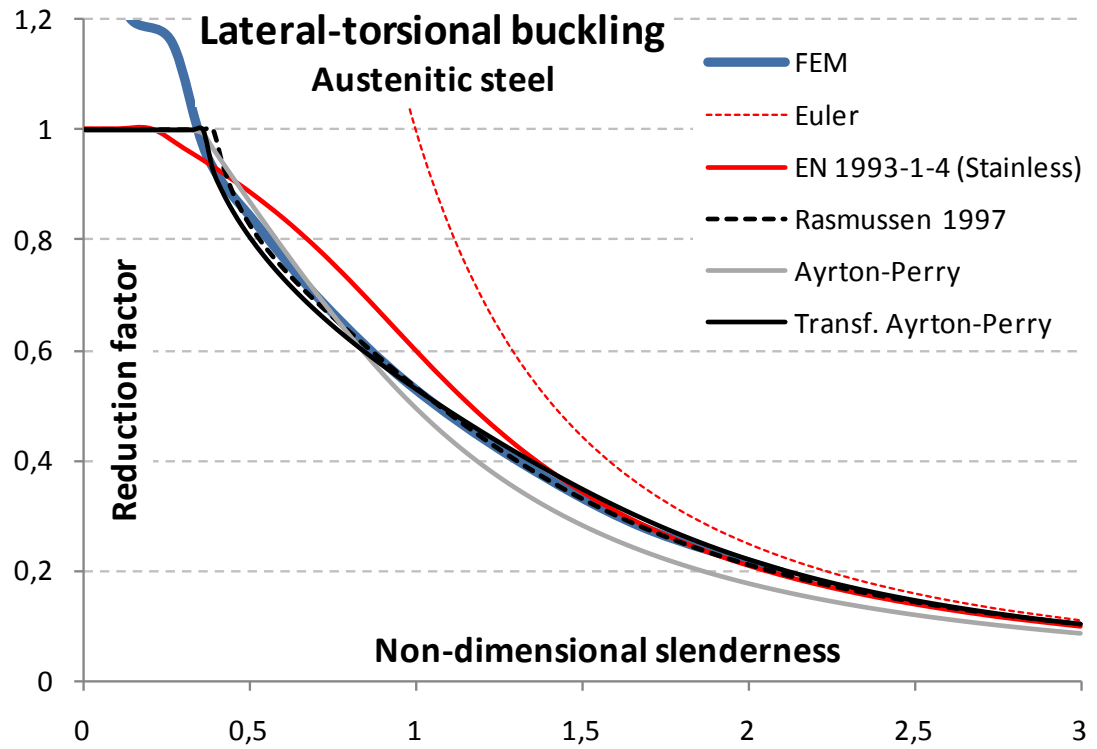


Figure 20. FE results: Strength curves for different buckling modes.





Appendix B: Duplex steel

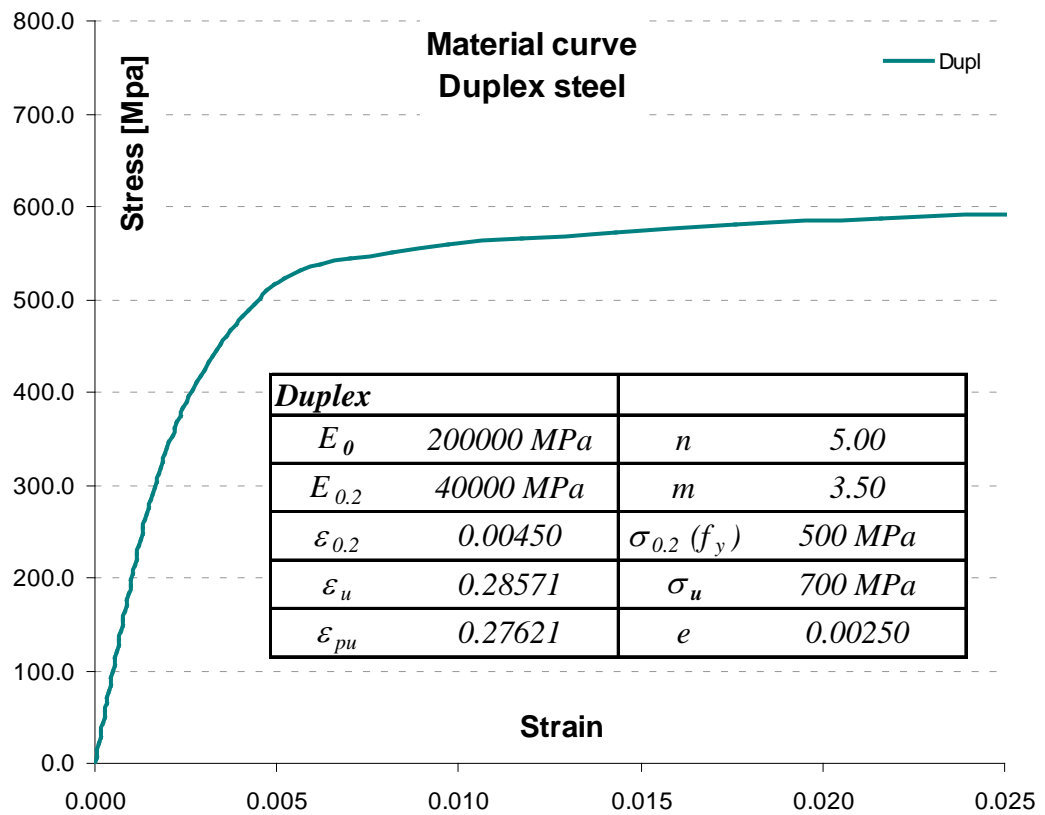


Figure 21. Material model.

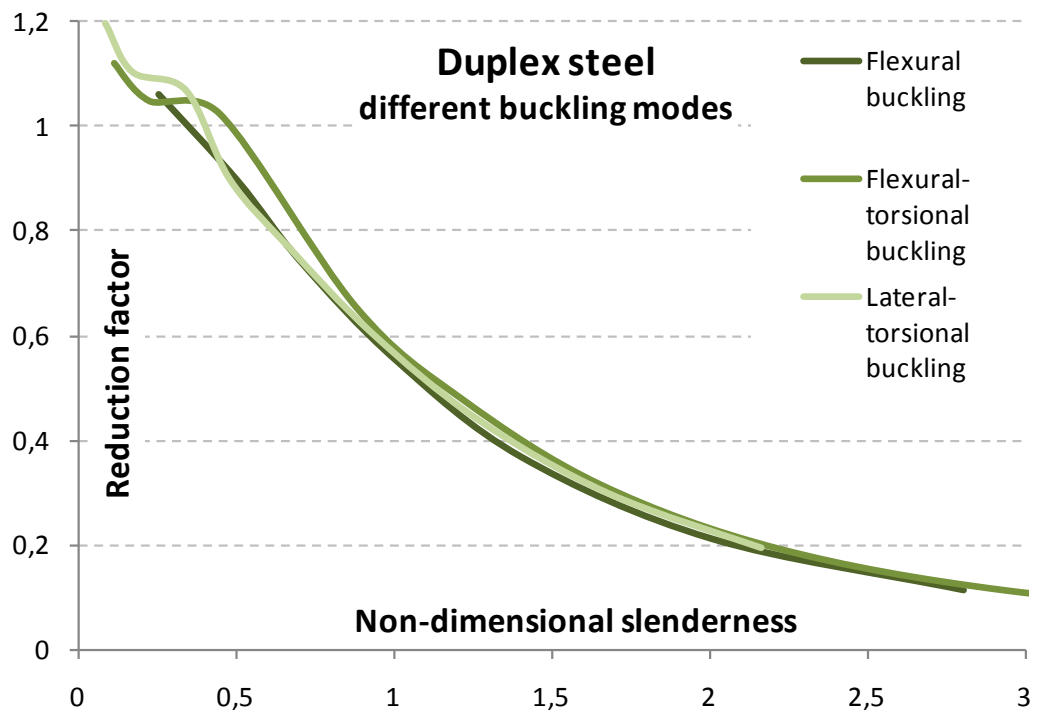
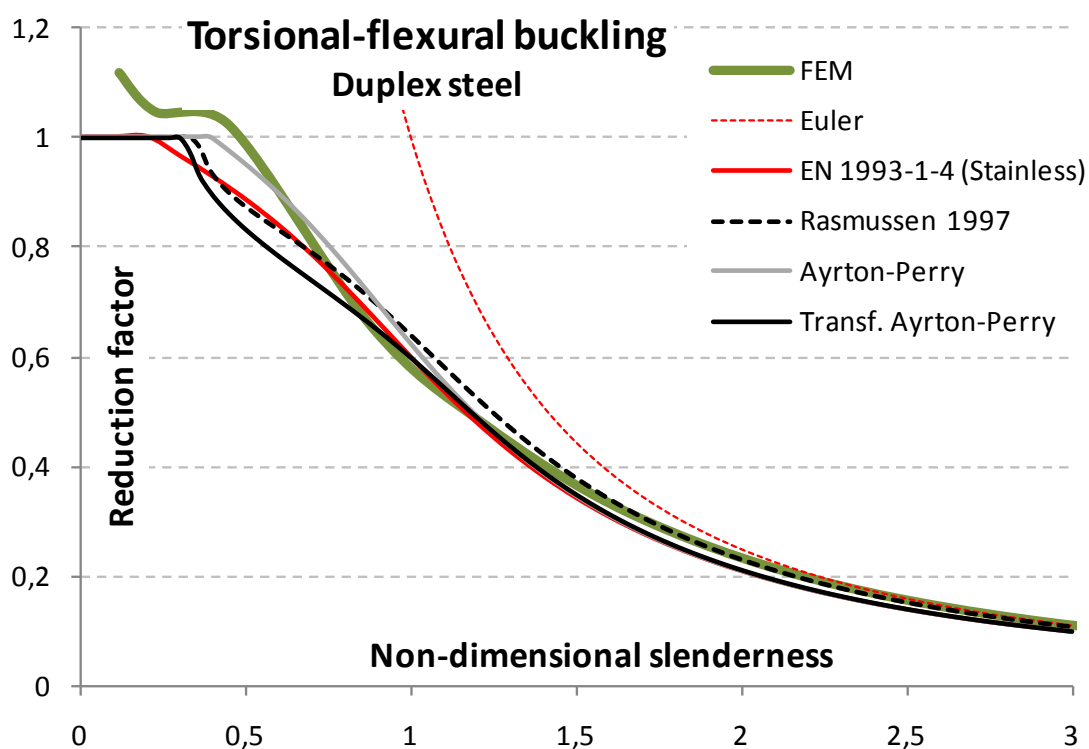
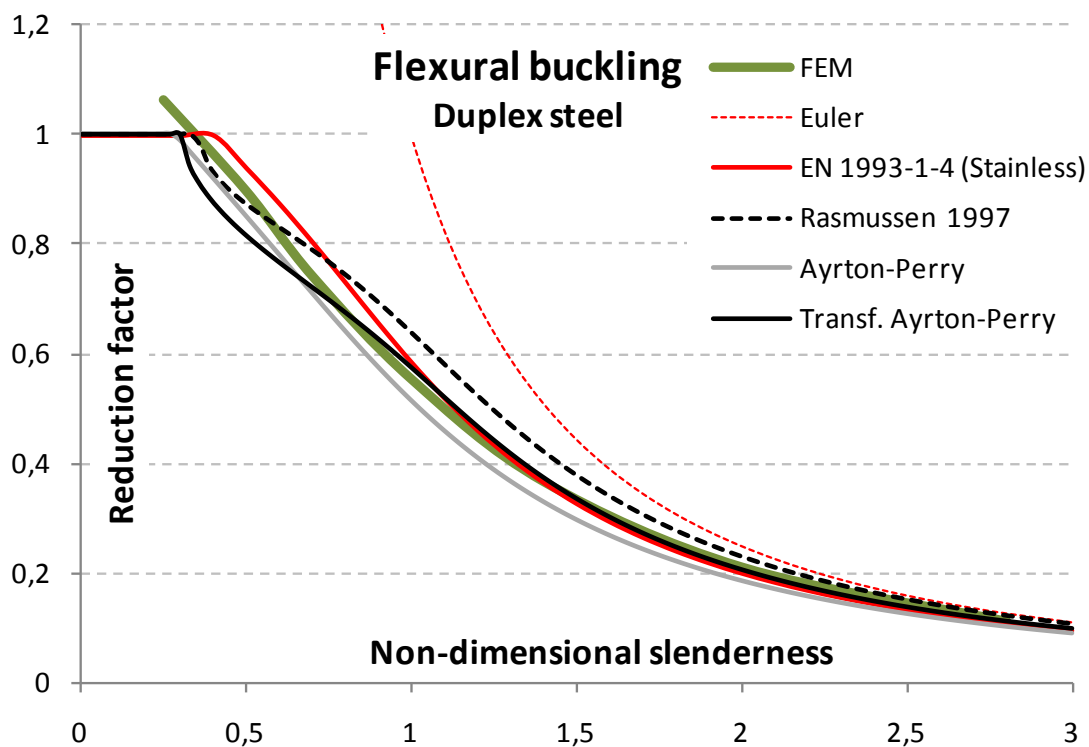
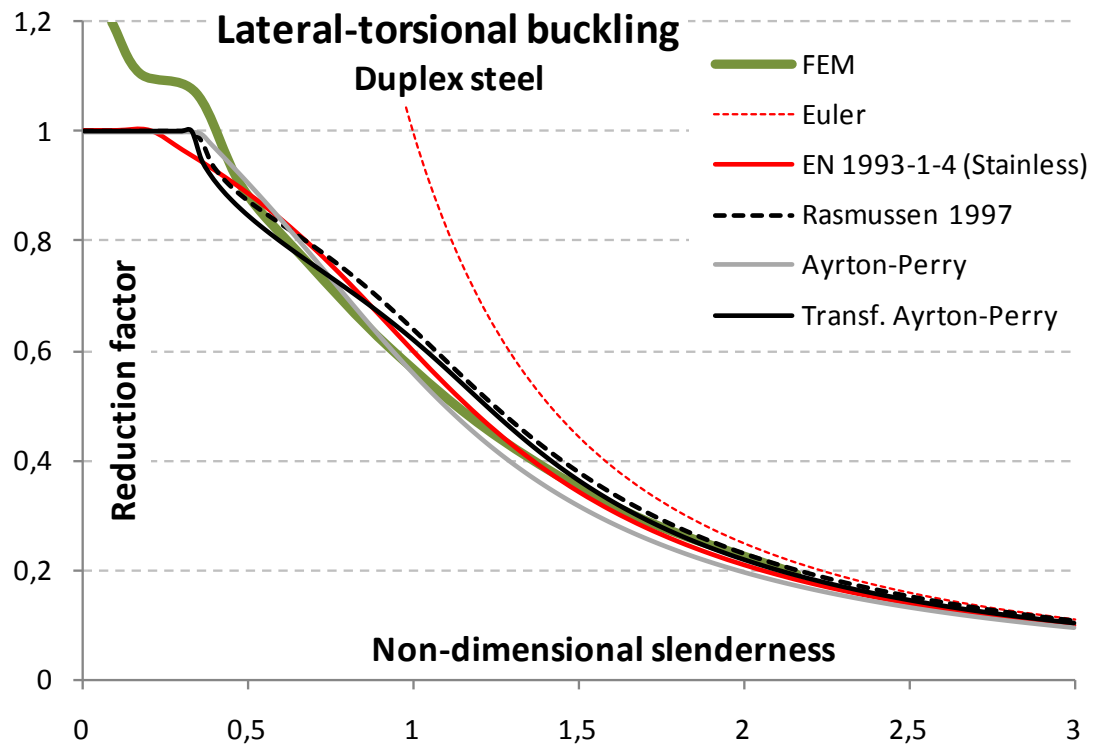


Figure 22. FE results: Strength curves for different buckling modes.





Appendix C: Ferritic steel 1

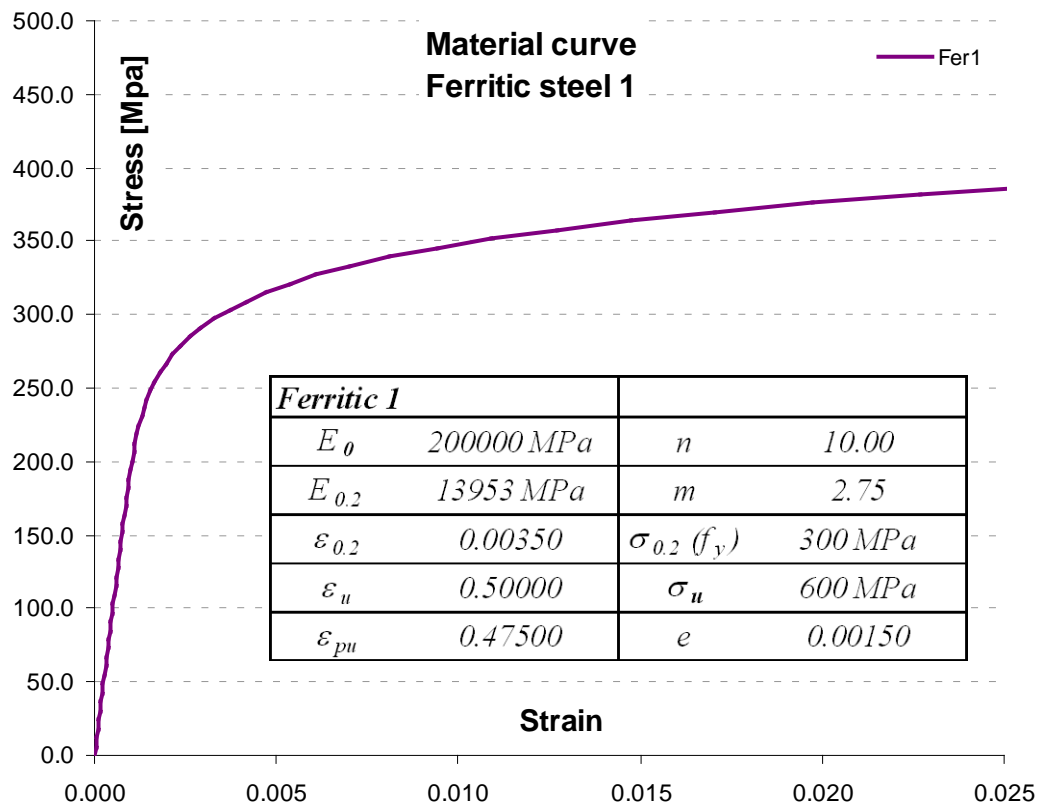


Figure 23. Material model.

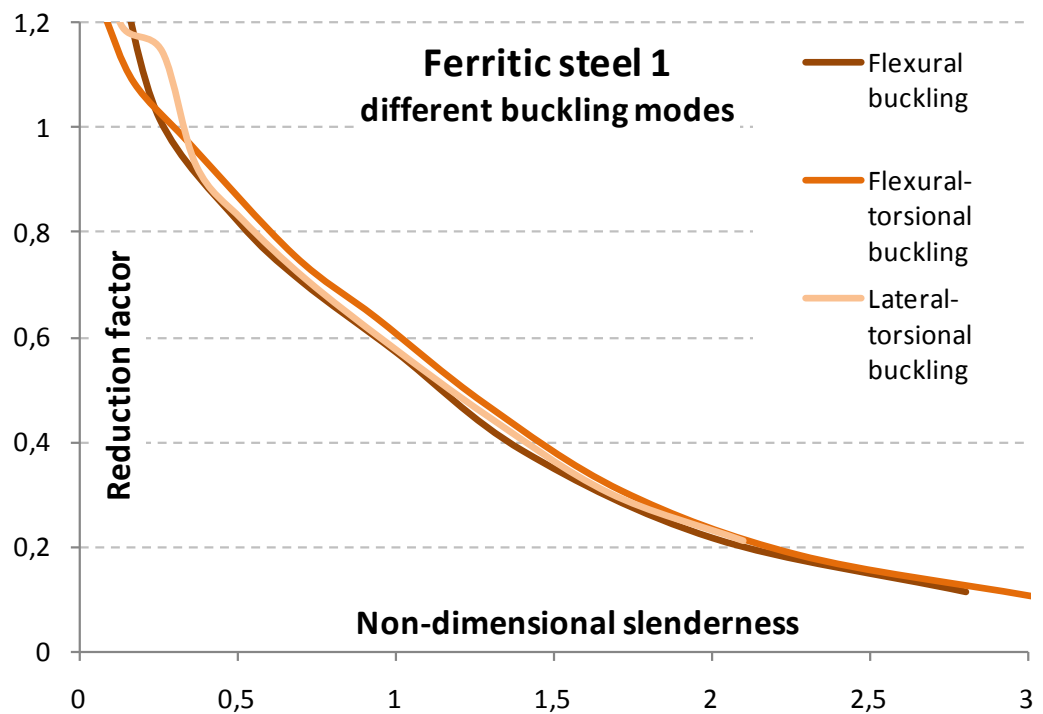


Figure 24. FE results: Strength curves for different buckling modes.

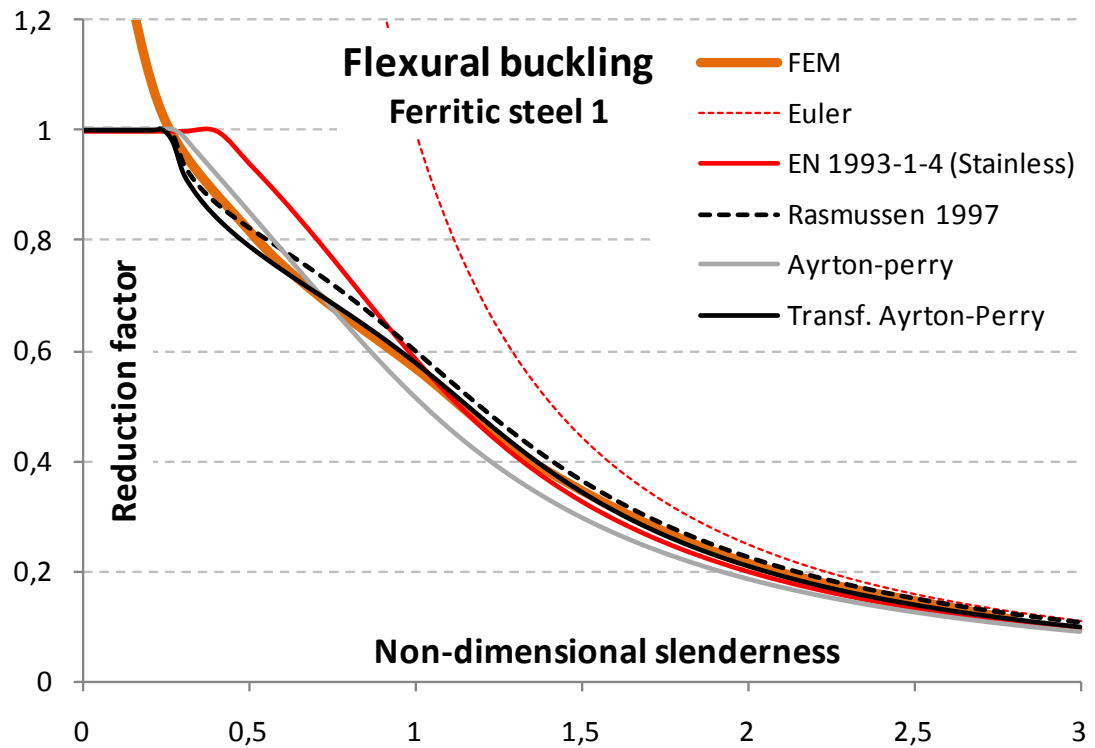


Figure 25. NLR results: The best-fitted approximation curves (Ayrton-Perry and Transformed Ayrton-Perry) compared to Rasmussen and Rondal model.

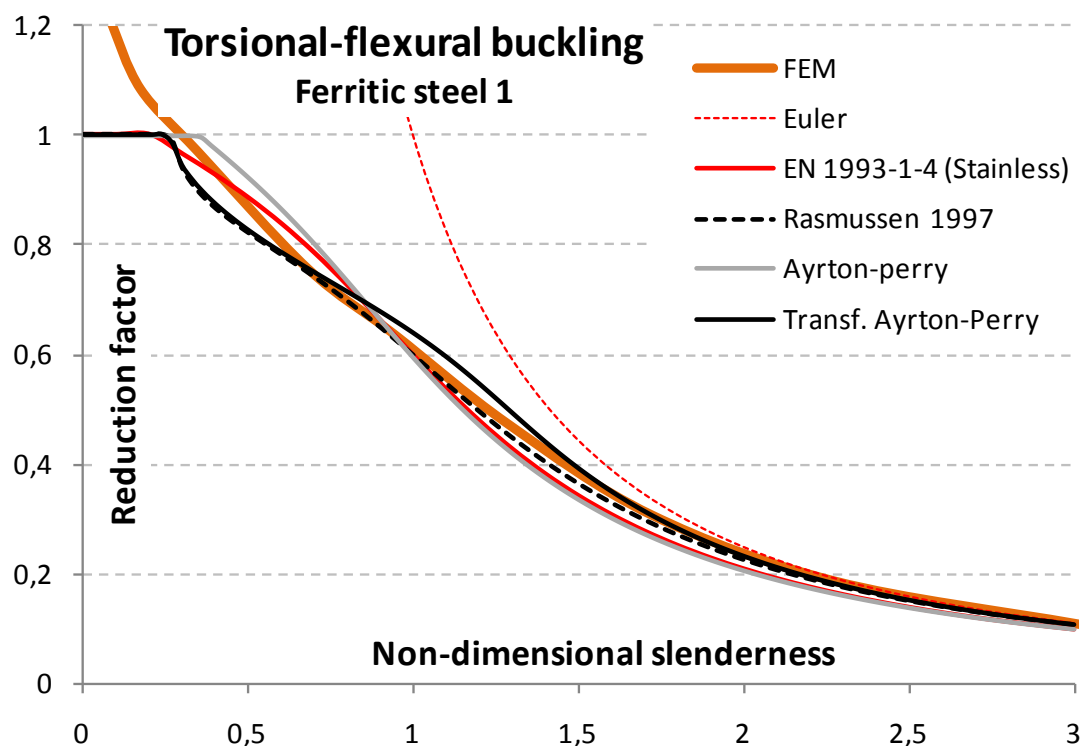


Figure 26. NLR results: The best-fitted approximation curves (Ayrton-Perry and Transformed Ayrton-Perry) compared to Rasmussen and Rondal model.

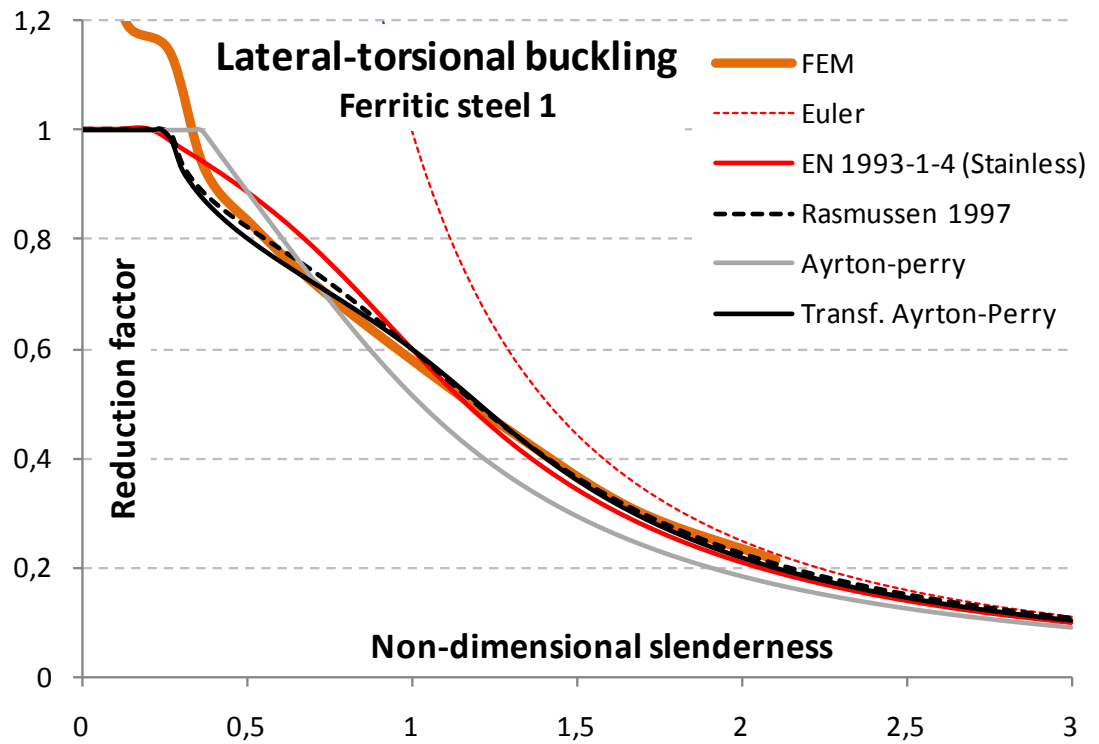


Figure 27. NLR results: The best-fitted approximation curves (Ayrton-Perry and Transformed Ayrton-Perry) compared to Rasmussen and Rondal model.

Appendix D: Ferritic steel 2

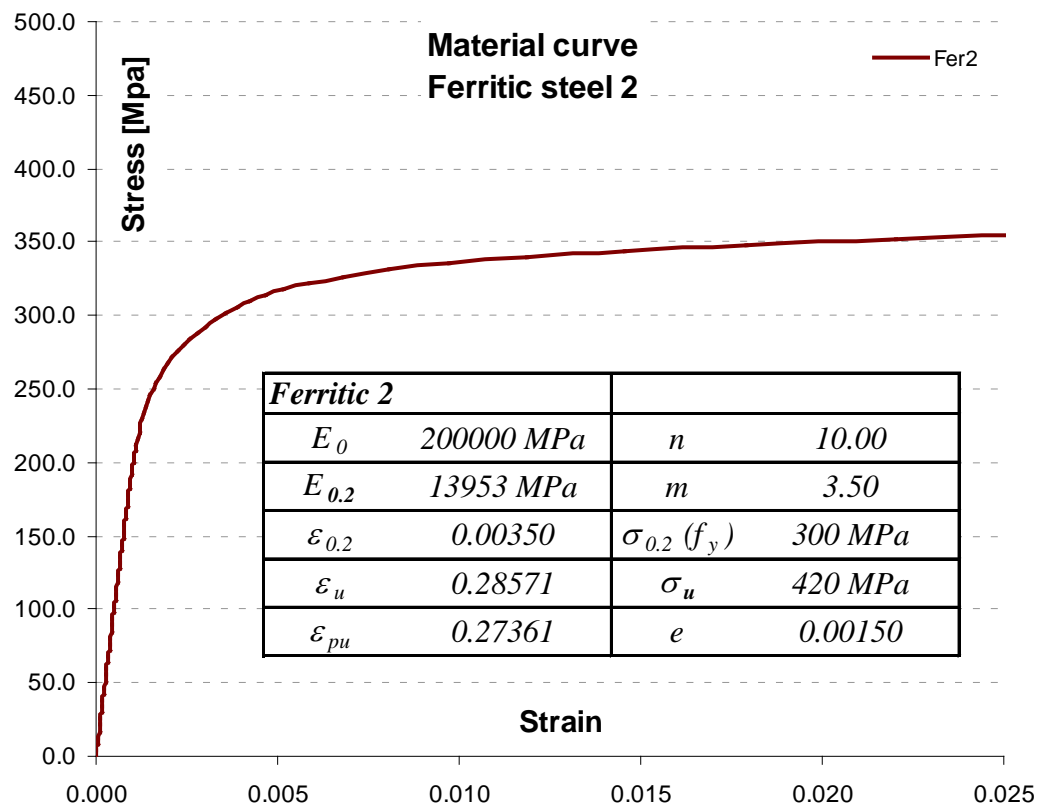


Figure 28. Material model.

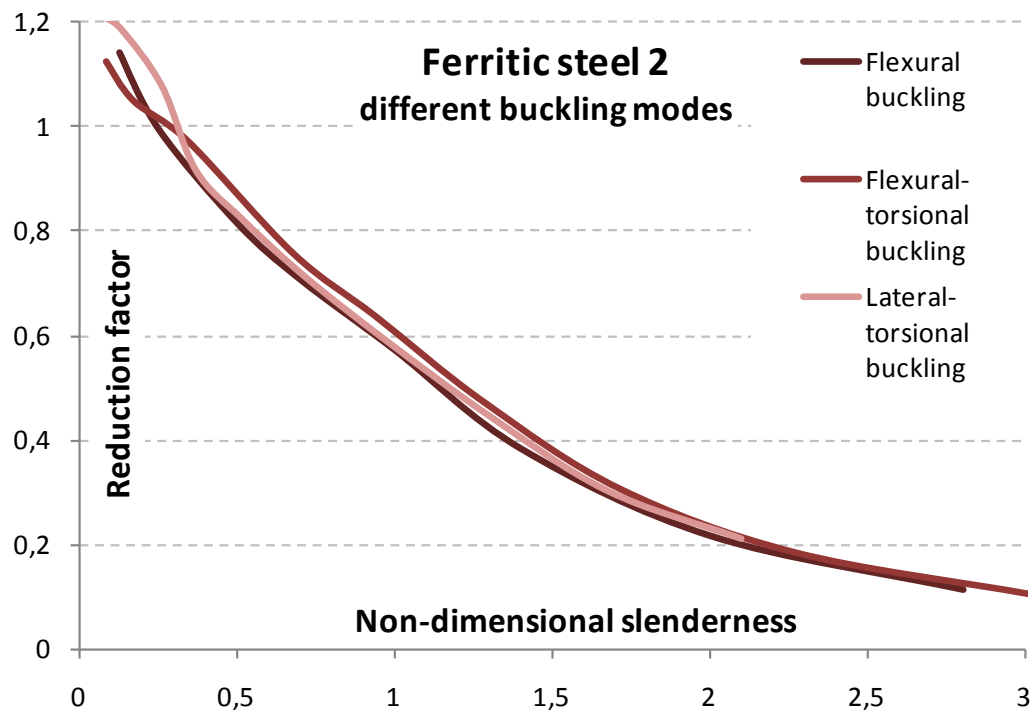


Figure 29. FE results: Strength curves for different buckling modes.

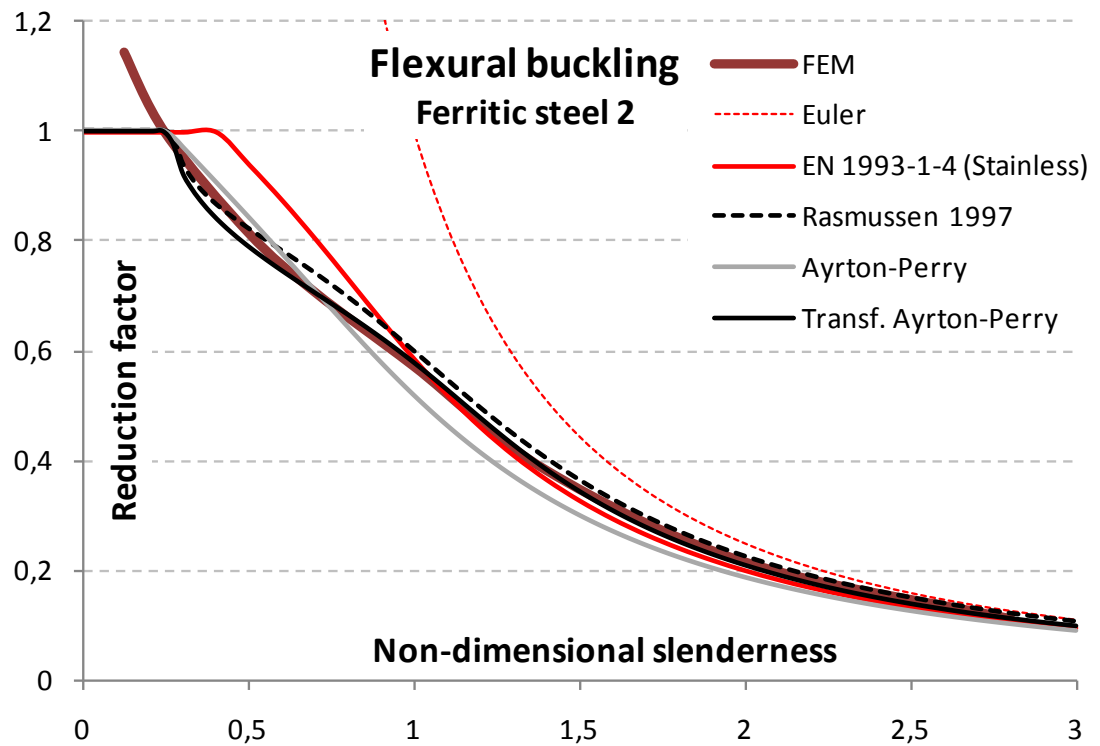


Figure 30. NLR results: The best-fitted approximation curves (Ayrton-Perry and Transformed Ayrton-Perry) compared to Rasmussen and Rondal model.

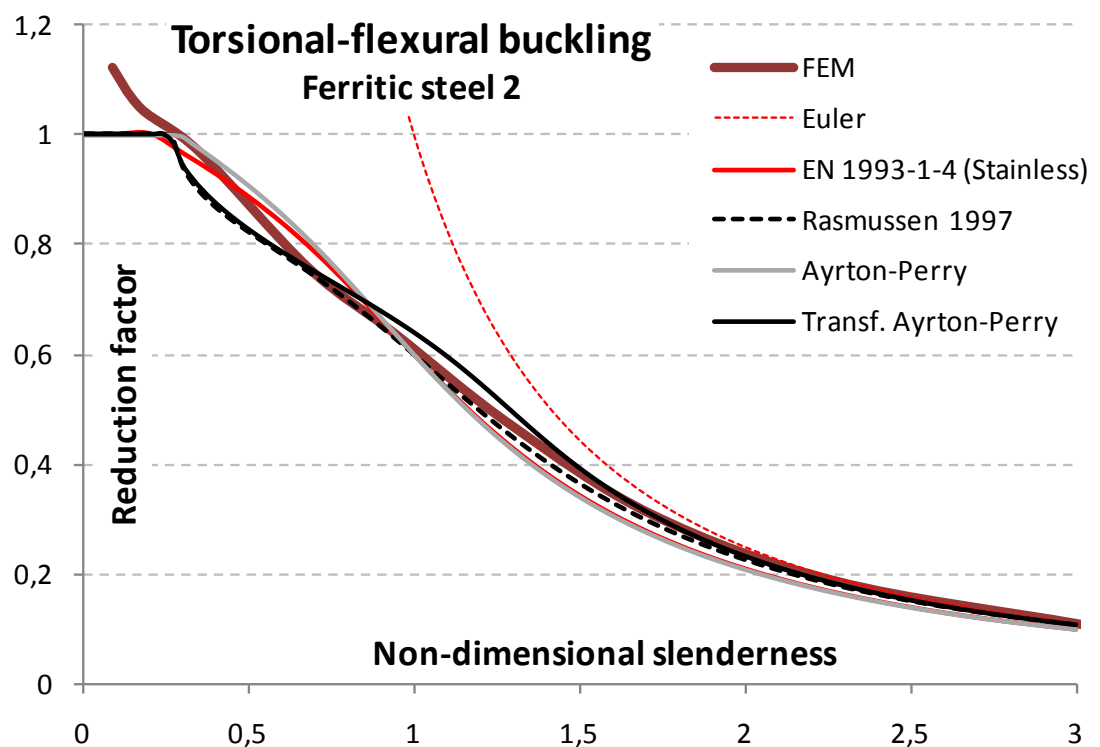


Figure 31. NLR results: The best-fitted approximation curves (Ayrton-Perry and Transformed Ayrton-Perry) compared to Rasmussen and Rondal model.

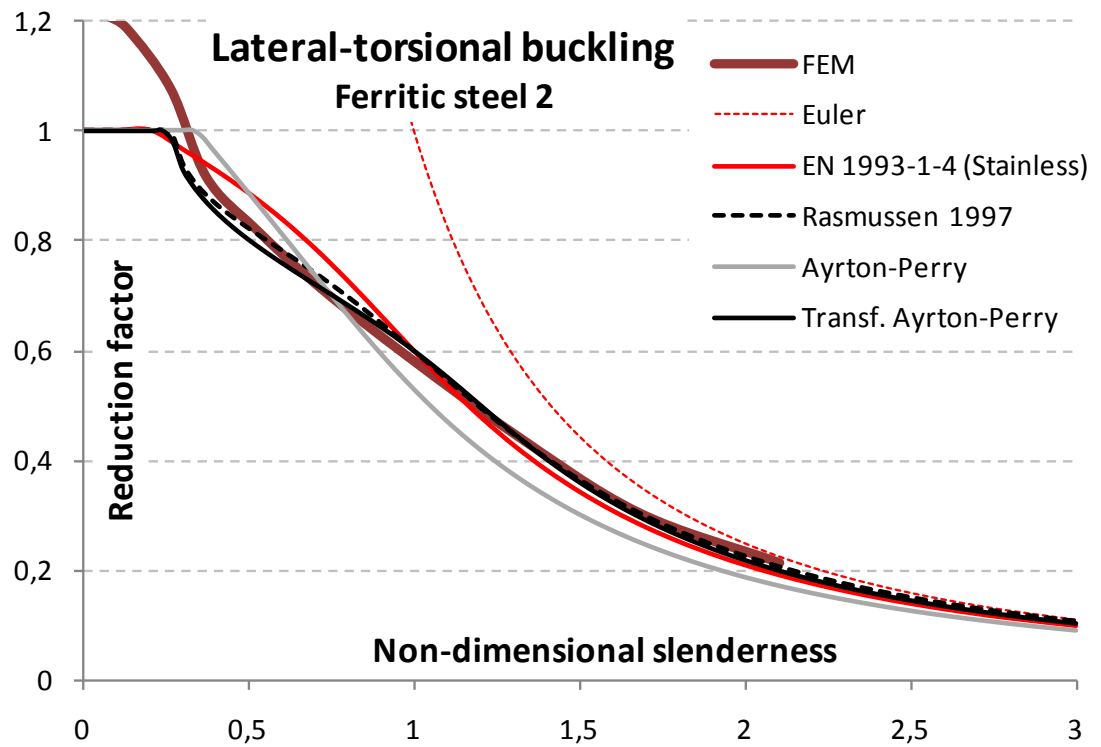


Figure 32. NLR results: The best-fitted approximation curves (Ayrton-Perry and Transformed Ayrton-Perry) compared to Rasmussen and Rondal model.

Appendix E: Carbon steel

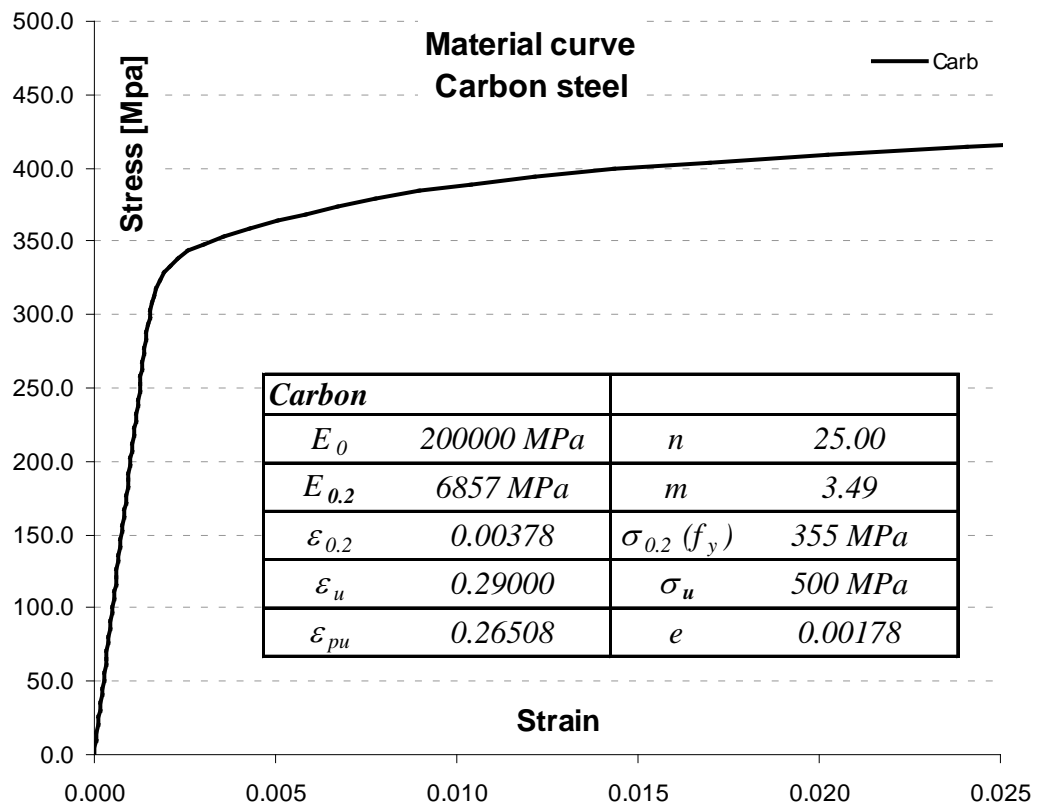


Figure 33. Material model.

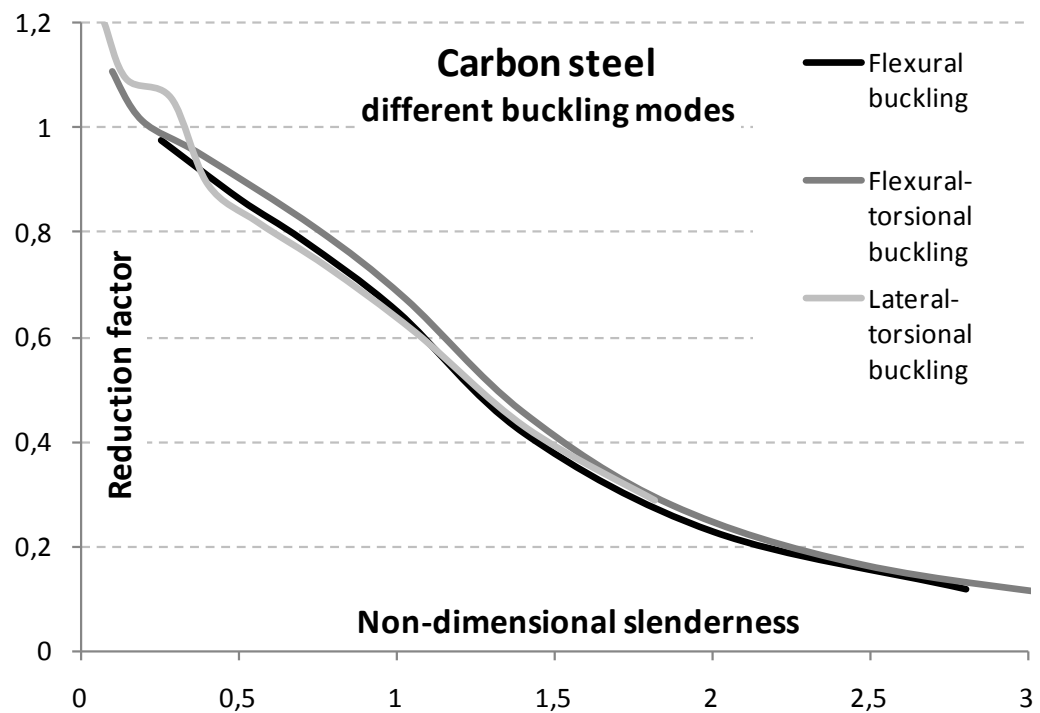


Figure 34. FE results: Strength curves for different buckling modes.

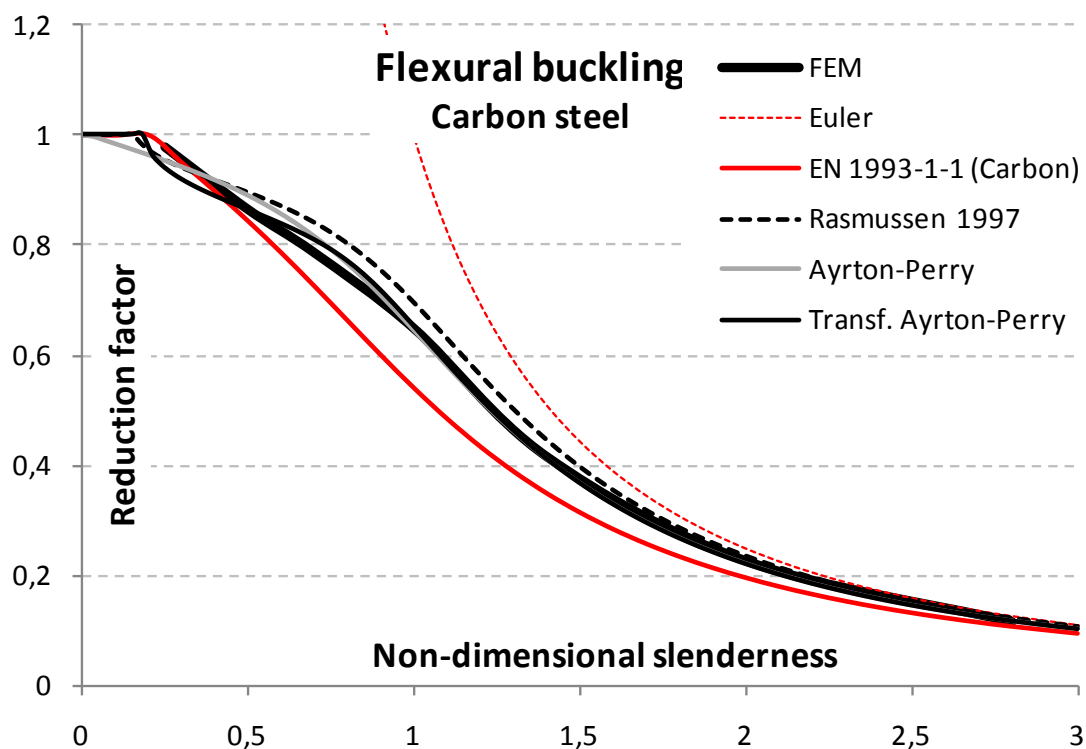


Figure 35. NLR results: The best-fitted approximation curves (Ayrton-Perry and Transformed Ayrton-Perry) compared to Rasmussen and Rondal model.

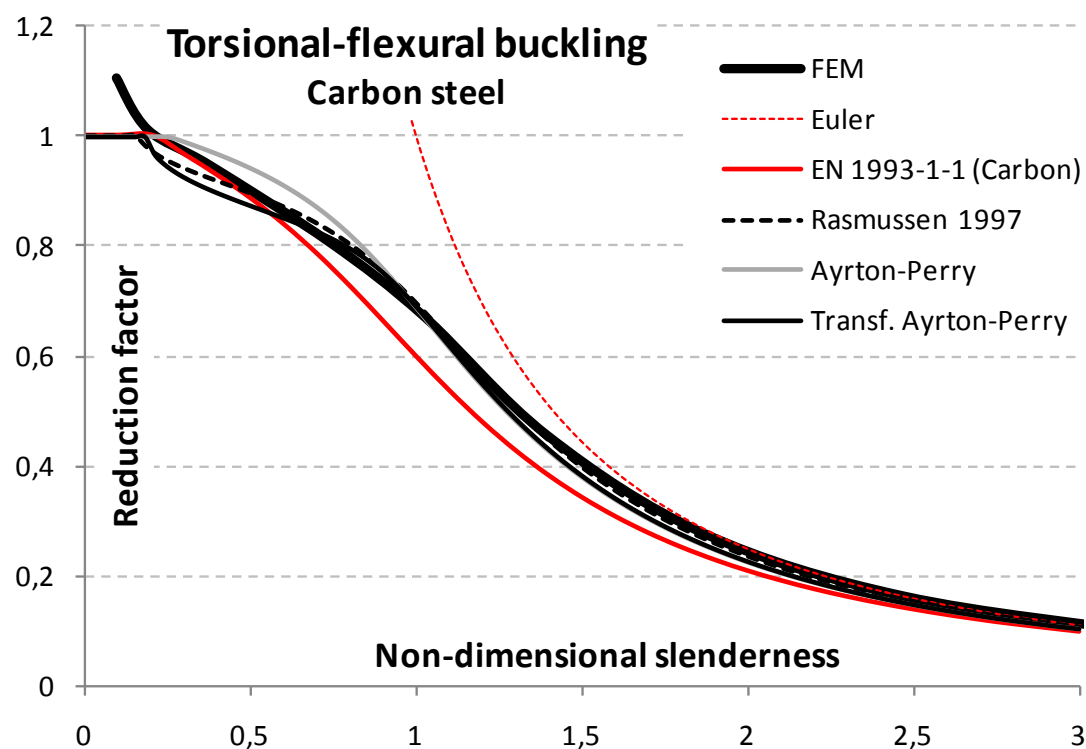


Figure 36. NLR results: The best-fitted approximation curves (Ayrton-Perry and Transformed Ayrton-Perry) compared to Rasmussen and Rondal model.

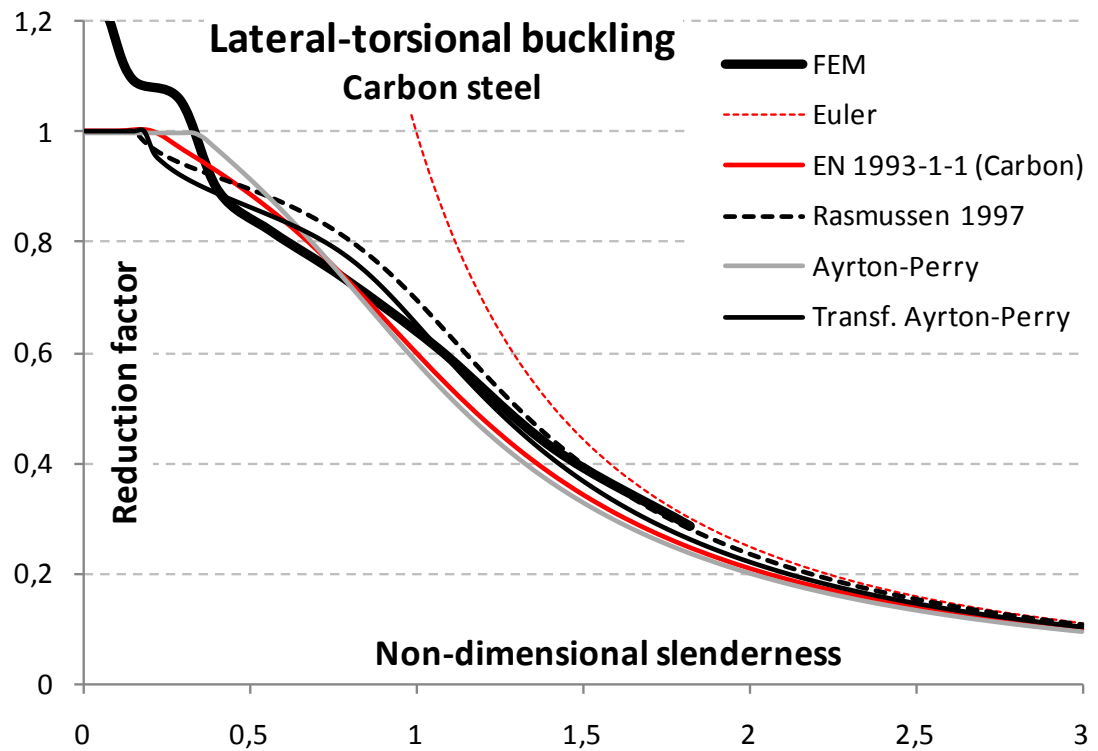


Figure 37. NLR results: The best-fitted approximation curves (Ayrton-Perry and Transformed Ayrton-Perry) compared to Rasmussen and Rondal model.

Appendix F: Material models comparison

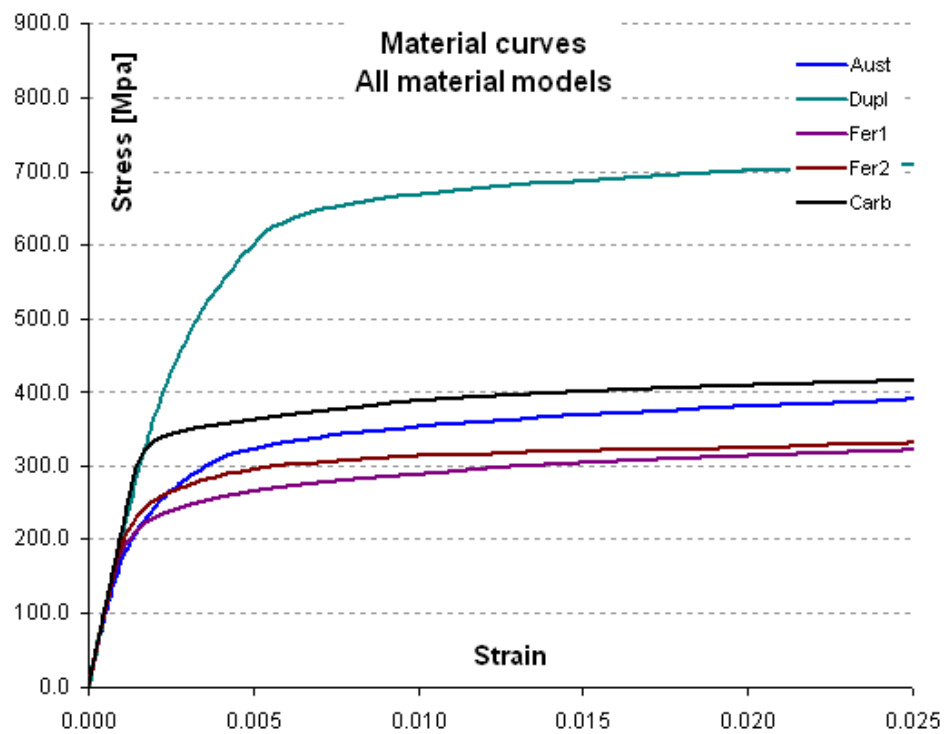


Figure 38. Comparison of the basic material models.

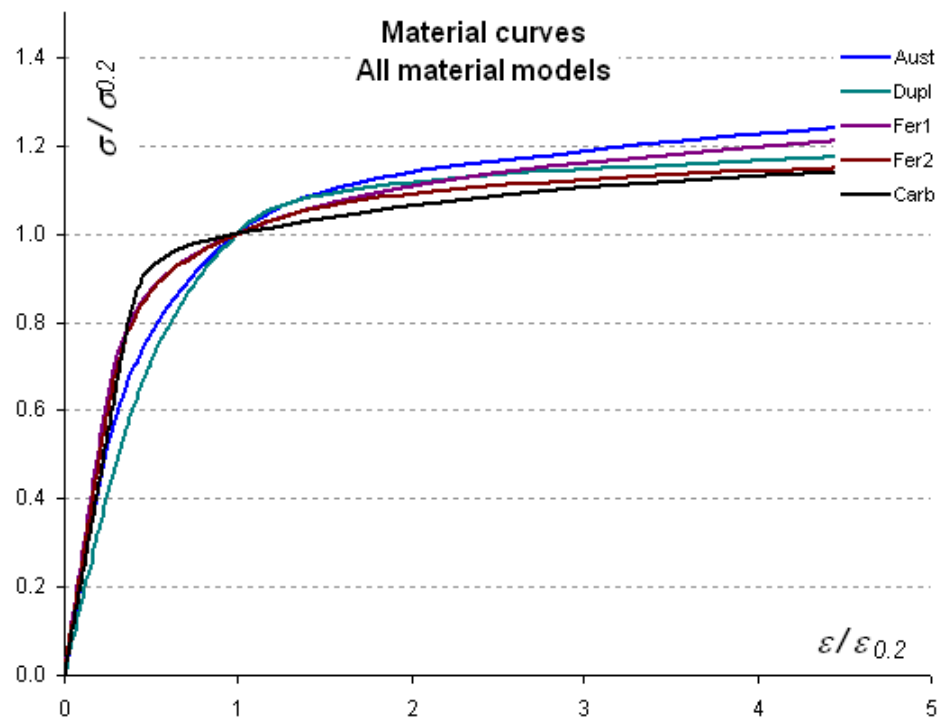


Figure 39. Comparison of the basic material models with normalized stress and strain.

Appendix G: Methods for transformed Ayrton-Perry curve calculation

The following calculation script is coded in Python in order to easily construct strength curves with transformed slenderness using the iterative approach.

```
class matClass:
    """ Definition of material parameters """
    def __init__(self):
        self.n=5.
        self.E0=200000.
        self.s02=300.

def lamNL(lam,chi,mat):
    """ Calculation of transformed slenderness """
    return lam*(1+0.002*mat.n*(mat.E0/mat.s02)*chi**(mat.n-1))**0.5

def fi(lam,lam0,alp):
    """ Calculation fi factor """
    return 0.5*(1+alp*(lam-lam0)+lam**2)

def chi(lam,lam0,alp):
    """ Calculation of reduction factor """
    if fi(lam,lam0,alp)>lam:
        return min(1.,1./(fi(lam,lam0,alp)+(fi(lam,lam0,alp)**2-
lam**2)**0.5))
    else: return 1.

def getTransformedAP(mat=matClass(), alp=0., lam0=0., maxLam=3.,
maxSteps=50):
    """ Calculation of strength curve """
    n,E0,s02 = mat.n,mat.E0,mat.s02
    lam0=min(lam0,1/(1+0.002*n*(E0/s02))**0.5)
    minDif=0.00001
    maxIter=500
    curve=[['lam','chi(Transformed_AP)'],]
    for i in range(maxSteps+1):
        lam=i*maxLam/maxSteps
        chiMax=1.
        chiMin=0.
        chiAct=1.
        iter=0
        while abs(chiAct-chi(lamNL(lam, chiAct, mat),lamNL(lam0, chiAct,
mat),alp))>minDif and iter<maxIter:
            if chiAct-chi(lamNL(lam, chiAct, mat),lamNL(lam0, chiAct,
mat),alp)>0:
                chiMax=chiAct
            else: chiMin=chiAct
            chiAct=0.5*(chiMax+chiMin)
            iter=iter+1
        if iter<maxIter:curve.append([lam,chiAct])
    return curve
```




Structural Applications of Ferritic Stainless Steels (SAFSS)

Work package 2.2a. Report on preliminary FEM study: Local Buckling

Marina Bock

Esther Real

Enrique Mirambell

Departament d'Enginyeria de la Construcció,
Universitat Politècnica de Catalunya



**UNIVERSITAT POLITÈCNICA
DE CATALUNYA**

Project name:
Project's short
name:

Structural Applications of Ferritic Stainless Steels
SAFSS

Change log:

Version	Date	Status (draft/proposal/updated /to be reviewed /approved)	Author(s)	Remarks
0.1	15.11.2011	Final	Bock , Real & Mirambell	

Distribution:

Project group

EUROPEAN COMMISSION

Research Programme of
The Research Fund for Coal and Steel-Steel RTD

Title of Research Project:	Structural Application of Ferritic Stainless Steels (SAFSS)
Executive Committee:	TGS8
Contract:	RFSR-CT-2010-00026
Commencement Date:	July 01, 201
Completion Date:	June 30, 2013
Beneficiary:	Universitat Politècnica de Catalunya (UPC)
Research Location:	Univeristat Poltècnica de Catalunya C/ Jordi Girona, 31 08034-Barcelona Espana
Project leader:	Esther Real
Report authors:	Bock, M., Real, E., Mirambell, E.

Contents

Contents	3
1. Introduction	4
2. Literature Review	4
2.1 Yielding	4
2.2 Elastic buckling	4
2.3 Inelastic buckling	6
2.4 Post-buckling strength and effective design width	7
2.5 Classification of cross-section and slender limits	12
3. Numerical model	16
3.1 Validation	16
3.2 Model simplification	17
3.3 Material model	17
3.4 Cross sections	18
4 Local buckling tests. Results	21
4.1 Introduction	21
4.2 Class limits assessment	21
4.3 Numerical results vs EN1993-1-4	24
5 Sectional stress distribution	30
5.1 SHSN11	30
5.2 SHSN31	32
5.3 Comparison between SHSN11 and SHSN31	34
5.4 RHSN11	35
5.5 RHSN31	39
5.6 Comparison between RHSN11 and RHSN31	41
5.7 Summary of the results	42
References	43
Annex A	45
A. Numerical database extension	45

1. Introduction

This report discusses the specific phenomena of local buckling of members from metallic non-linear materials with a special focus on ferritic stainless steel. The goal of this parametric study is to assess the class 3 for fully compressed elements proposed in EN1993-1-4.

2. Literature Review

This chapter is focused on local buckling, a local instability which appears in structural members subjected to compression. The chapter presents theoretical background and how this phenomenon is tackled in the current European specifications for stainless steel (Eurocode and Euro Inox).

Stocky sections fail by means of yielding and inelastic local buckling, however, slender sections fail due to elastic local buckling. These failure modes are described in following sections.

2.1 Yielding

The strength of a stiffened compression element such as the compression flange of a hat section is governed by yielding if its width-to-thickness ratio is relatively small. It may be governed by local buckling at a stress level less than the yielding point if its width-to-thickness ratio is relatively large.

2.2 Elastic buckling

Considering a simply supported square plate subjected to a uniform compression stress in one direction, it will buckle in a single curvature in both directions. However, for individual elements of a cross-section, the length of the element is usually much larger than the width (rectangular plate). In this case, the plate buckles in one single curve in the short direction (width) and in a multiple curve along the large dimension (length) according to figure 2.1. The critical buckling stress of a plate can be determined by solving Bryan's differential equation, which was established in 1891, based on small deflection theory.

$$\frac{\partial^4 \omega}{\partial x^4} + 2 \frac{\partial^4 \omega}{\partial x^2 \partial y^2} + \frac{\partial^4 \omega}{\partial y^4} + \frac{\sigma_x t}{D} \frac{\partial^2 \omega}{\partial x^2} = 0 \quad D = \frac{E}{12(1 - \nu^2)} \quad (1)$$

If m and n are the number of half sine waves in the x and y directions, respectively, the deflected shape of the rectangular may be represented by a double series:

$$\omega = \sum_{m=1}^{\infty} \sum_{n=1}^{\infty} A_{mn} \sin \frac{m\pi x}{a} \sin \frac{n\pi y}{b} \quad (2)$$

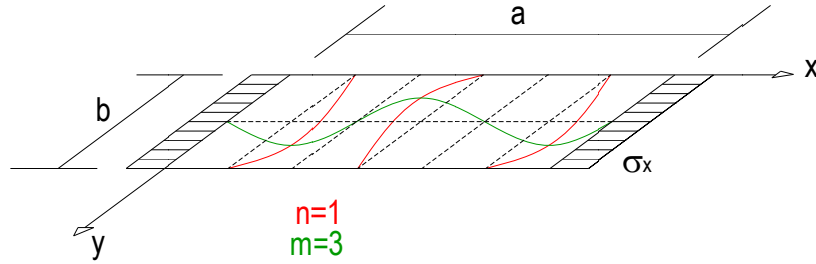


Figure 2.1 Buckling of an individual element of a section in compression

Where a is the length and b is the width. This equation is satisfied for a simply supported plate ($x=0, y=0$). Using ω to solve the first equation, one can then obtain the following equation:

$$\sum_{m=1}^{\infty} \sum_{n=1}^{\infty} A_{mn} \left[\pi^4 \left(\frac{m^2}{a^2} + \frac{n^2}{b^2} \right) - \frac{\sigma_x t}{D} \frac{m^2 \pi^2}{a^2} \right] \sin \frac{m\pi x}{a} \sin \frac{n\pi y}{b} = 0 \quad (3)$$

It is obvious that the solution can be obtained if either $A_{mn}=0$ or the quantity in square brackets equals zero. The former condition means that no buckling will occur, which is not applicable to this particular case. By solving:

$$\pi^4 \left(\frac{m^2}{a^2} + \frac{n^2}{b^2} \right) - \frac{\sigma_x t}{D} \frac{m^2 \pi^2}{a^2} = 0 \quad (4)$$

One can obtain an expression for critical local buckling stress as follows:

$$\sigma_{cr} = \sigma_x = \frac{D\pi^2}{tb^2} \left[m \left(\frac{b}{a} \right) + \frac{n^2}{m} \left(\frac{a}{b} \right) \right]^2 \quad (5)$$

The minimum value in square brackets is $n=1$, that is, only one half sine wave occurs in the y direction:

$$\sigma_x = \frac{k_{\sigma} D \pi^2}{tb^2} \quad k_{\sigma} = \left[m \left(\frac{b}{a} \right) + \frac{1}{m} \left(\frac{a}{b} \right) \right]^2 \quad (6)$$

Substituting the value of D , the general equation for critical buckling stress for a rectangular plate subjected to compression stress in one direction can be obtained:

$$\sigma_{cr} = \frac{k_{\sigma} \pi^2 E}{12(1 - \nu^2)} \left(\frac{t}{b} \right)^2 \quad (7)$$

It should be noted that when the ratio a/b is an integer, the value of k_{σ} equals 4. The value of the aspect ratio a/b will determine the number of half sine waves in the x direction as shown in the figure 2.2. For a long plate, the length of the half sine waves equals approximately the width of the plate, and therefore square waves are formed.

The k_σ coefficient depends on the boundary conditions and the type of stress. The values of k_σ for a long rectangular plate subjected to different types of stress and under different boundary conditions are tabulated (see figure 2.3).

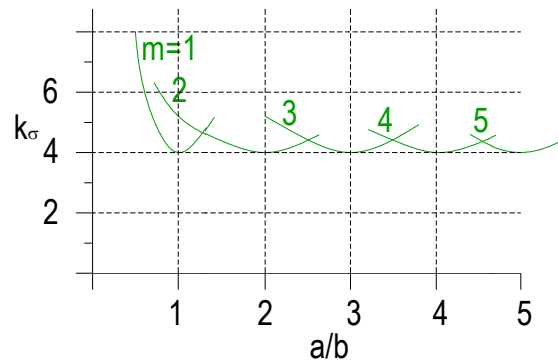


Figure 2.2 Number of half sine waves as a function of the aspect ratio in a simply supported plate

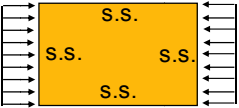
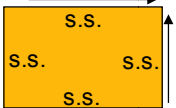
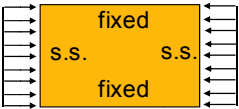
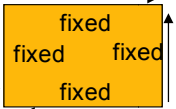

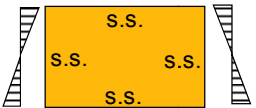
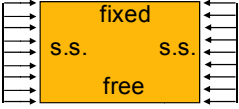
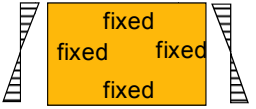
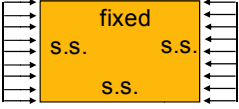
Boundary condition	Types of stress	k_σ	Boundary condition	Types of stress	k_σ
	Comp.	4.0		Shear	5.34
	Comp.	6.97		Shear	8.98
	Comp.	0.425		Bending	23.9
	Comp.	1.277		Bending	41.8
	Comp.	5.42			

Figure 2.3 values of k_σ for a long rectangular plate subjected to different types of stress. Lee (2000)

2.3 Inelastic buckling

Buckling of plates in the inelastic range: when $\sigma_x > f_y$ the plate becomes anisotropic which has different properties in different directions of the plate. Bleich (1924) proposed the following differential equation for inelastic buckling:

$$\tau \frac{\partial^4 \omega}{\partial x^4} + 2\sqrt{\tau} \frac{\partial^4 \omega}{\partial x^2 \partial y^2} + \frac{\partial^4 \omega}{\partial y^4} + \frac{\sigma_x t}{D} \frac{\partial^2 \omega}{\partial x^2} = 0 \quad \tau = \frac{E_t}{E} \quad (8)$$

where E_t is the tangent modulus. Applying the modified boundary conditions, one can obtain the following critical buckling stress for plastic buckling of the plate:

$$\sigma_{cr} = \frac{k_{\sigma}\pi^2 E \sqrt{\tau}}{12(1-\nu^2)} \left(\frac{t}{b}\right)^2 = \frac{k_{\sigma}\pi^2 \sqrt{E E_t}}{12(1-\nu^2)} \left(\frac{t}{b}\right)^2 \quad (9)$$

The wavelength for a long plate is $\lambda = \sqrt[4]{\tau} b$. On the other hand, $\sqrt{\tau}$ is the plasticity reduction factor for a simply supported plate subjected to a uniform compression stress in one direction. This factor varies with the type of loading and boundary conditions.

2.4 Post-buckling strength and effective design width

When $\sigma_x > \sigma_{cr}$ the plate will not collapse because an additional load can be carried out by the element after buckling by means of a redistribution of stress. This phenomenon is known as postbuckling strength and is most pronounced for elements with large b/t ratios. The figure 2.4 shows the evolution of the stress distribution in a plate subjected to a uniform compression stress. As it shows, the stress distribution is uniform prior to its buckling but after that a portion of the prebuckling load of the centre strip is transferred to the edge portion of the plate. The result is a nonuniform stress distribution. The redistribution continues until the stress at the edge reaches the yield point of the steel and then the plate begins to fail.

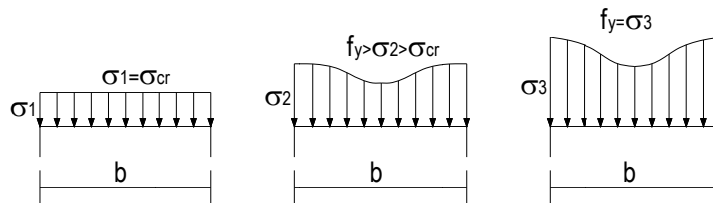


Figure 2.4 Evolution of stress distribution in a compressed plate. Post-buckling strength

The postbuckling behaviour of a plate can be analyzed by using large deflection theory. In 1910 Von Kármán (1910) proposed the following differential equation:

$$\frac{\partial^4 \omega}{\partial x^4} + 2 \frac{\partial^4 \omega}{\partial x^2 \partial y^2} + \frac{\partial^4 \omega}{\partial y^4} = \frac{t}{D} \left(\frac{\partial^2 F}{\partial y^2} \frac{\partial^2 \omega}{\partial x^2} - 2 \frac{\partial^2 F}{\partial x \partial y} \frac{\partial^2 \omega}{\partial x \partial y} + \frac{\partial^2 F}{\partial x^2} \frac{\partial^2 \omega}{\partial y^2} \right) \quad (10)$$

where F is a stress function defining the median fiber stress of the plate:

$$\sigma_x = \frac{\partial^2 F}{\partial y^2} \quad \sigma_y = \frac{\partial^2 F}{\partial x^2} \quad \tau_{xy} = -\frac{\partial^2 F}{\partial x \partial y}$$

The solution of the differential equation for large deflection theory is very complex. For this reason, a concept of “effective width” was introduced by Von Kármán et al. (1932). In this approach, it is assumed that the total load is carried by a fictitious width b_{eff} subjected to a uniformly distributed stress equal to the edge stress σ_{max} (see figure 2.5). The width b_{eff} is selected so that the area under the curve of the actual non uniform stress distribution is equal to the sum of the two parts of the equivalent rectangular distribution with a total width b_{eff} and a stress equal to σ_{max} :

$$\int_0^b \sigma dx = b_{eff} \cdot \sigma_{max} \quad (11)$$

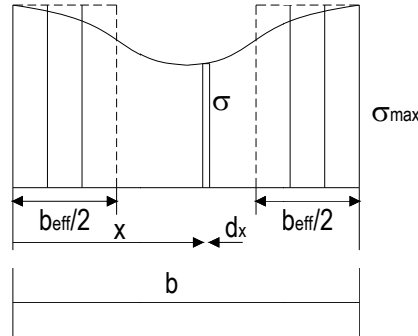


Figure 2.5 Typical effective width model of a compressed plate

It may be considered that the effective width b_{eff} represents a particular width of the plate which just buckles when the compressive stress reaches the yield point of steel:

$$\sigma_{cr,f} = \frac{k_\sigma \pi^2 E}{12(1 - \nu^2)} \left(\frac{t}{b_{eff}} \right)^2 = f_y \quad (12)$$

Operating this expression, the following relationship of b_{eff} and b can be obtained:

$$\begin{aligned} \sigma_{cr,f} &= \frac{k_\sigma \pi^2 E}{12(1 - \nu^2)} \left(\frac{t}{b} \right)^2 \frac{b^2}{b_{eff}^2} = \sigma_{cr,b} \frac{b^2}{b_{eff}^2} = f_y \\ \frac{b}{b_{eff}} &= \sqrt{\frac{f_y}{\sigma_{cr,b}}} \\ \frac{b}{b_{eff}} &= \bar{\lambda}_p \end{aligned} \quad (13)$$

Von Kármán also proposed other different expressions for the effective width according to the boundary conditions. Theories from Von Kármán had an outstanding consideration but unfortunately, experimental results not validate these. The main reason was that initial imperfections were not taken into account and equation was only applicable to perfect plates.

In 1947 Winter (1947) developed an experimental research on cold formed plates and suggested a new reduction function to determine the effective width for stiffened elements in compression

$$\frac{b_{eff}}{b} = \sqrt{\frac{\sigma_{cr}}{f_y}} \left(1 - 0.22 \sqrt{\frac{\sigma_{cr}}{f_y}} \right) \quad (14)$$

Which can be rewritten as

$$\frac{b_{eff}}{b} = \frac{\bar{\lambda}_p - 0.22}{\bar{\lambda}_p^2} \quad \text{for} \quad \bar{\lambda}_p \geq 0.673 \quad (15)$$

Other researchers proposed other expressions of the initial Von Kármán's formula i.e. Gerard (1957), Faulkner (1965), Dubas and Gehri (1986).

Even though a lot of effort has been put into this research field, the Winter function, based on the cold formed members survived and was set as the function used in the experimental version of Eurocode, the ENV 1993-1-5 as follows:

$$\begin{aligned}\frac{b_{eff}}{b} &= \rho \\ \rho &= \frac{\bar{\lambda}_p - 0.22}{\bar{\lambda}_p^2} \\ \varepsilon &= \sqrt{\frac{235}{f_y}}\end{aligned}\tag{16}$$

$$\bar{\lambda}_p = \sqrt{\frac{f_y}{\sigma_{cr,b}}} = \frac{b/t}{28.4\varepsilon\sqrt{k_\sigma}}\tag{17}$$

However, a new reduction factor has been proposed in EN1993-1-5 (2006) in order to enhance the prediction of the effective width of a plate. This improvement has been possible due to adding the coefficient which takes into account a non uniform stress distribution:

$$\begin{aligned}\rho &= \frac{\bar{\lambda}_p - 0.055(3 + \psi)}{\bar{\lambda}_p^2} && \text{For internal compression parts} \\ \rho &= \frac{\bar{\lambda}_p - 0.188}{\bar{\lambda}_p^2} && \text{For outstand flanges}\end{aligned}\tag{18}$$

In this new formulation, the buckling coefficient should be calculated according to figure 2.6 for internal plates and figure 2.7 for outstand flanges.

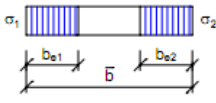
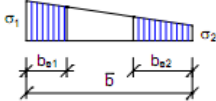
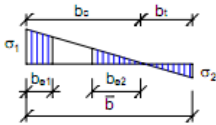
Stress distribution (compression positive)				Effective ^p width b_{eff}		
				$\underline{\psi = 1:}$ $b_{eff} = \rho \bar{b}$ $b_{e1} = 0,5 b_{eff} \quad b_{e2} = 0,5 b_{eff}$		
				$\underline{1 > \psi \geq 0:}$ $b_{eff} = \rho \bar{b}$ $b_{e1} = \frac{2}{5 - \psi} b_{eff} \quad b_{e2} = b_{eff} - b_{e1}$		
				$\underline{\psi < 0:}$ $b_{eff} = \rho b_c = \rho \bar{b} / (1 - \psi)$ $b_{e1} = 0,4 b_{eff} \quad b_{e2} = 0,6 b_{eff}$		
$\psi = \sigma_2 / \sigma_1$	1	$1 > \psi > 0$	0	$0 > \psi > -1$	-1	$-1 > \psi > -3$
Buckling factor k_σ	4,0	$8,2 / (1,05 + \psi)$	7,81	$7,81 - 6,29\psi + 9,78\psi^2$	23,9	$5,98 (1 - \psi)^2$

Figure 2.6 k_σ coefficient for internal plates

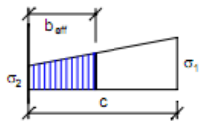
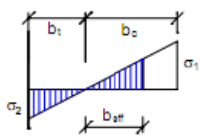
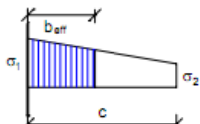
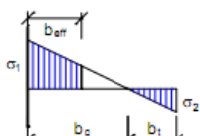
Stress distribution (compression positive)				Effective ^p width b_{eff}		
				$\underline{1 > \psi \geq 0:}$ $b_{eff} = \rho c$		
				$\underline{\psi < 0:}$ $b_{eff} = \rho b_c = \rho c / (1 - \psi)$		
$\psi = \sigma_2 / \sigma_1$	1	0	-1	$1 \geq \psi \geq -3$		
Buckling factor k_σ	0,43	0,57	0,85	$0,57 - 0,21\psi + 0,07\psi^2$		
				$\underline{1 > \psi \geq 0:}$ $b_{eff} = \rho c$		
				$\underline{\psi < 0:}$ $b_{eff} = \rho b_c = \rho c / (1 - \psi)$		
$\psi = \sigma_2 / \sigma_1$	1	$1 > \psi > 0$	0	$0 > \psi > -1$	-1	
Buckling factor k_σ	0,43	$0,578 / (\psi + 0,34)$	1,70	$1,7 - 5\psi + 17,1\psi^2$	23,8	

Figure 2.7 k_σ coefficient for outstand flanges

Figure 2.8 shows the historical evolution of the aforementioned expressions of the effective width against slenderness parameter.

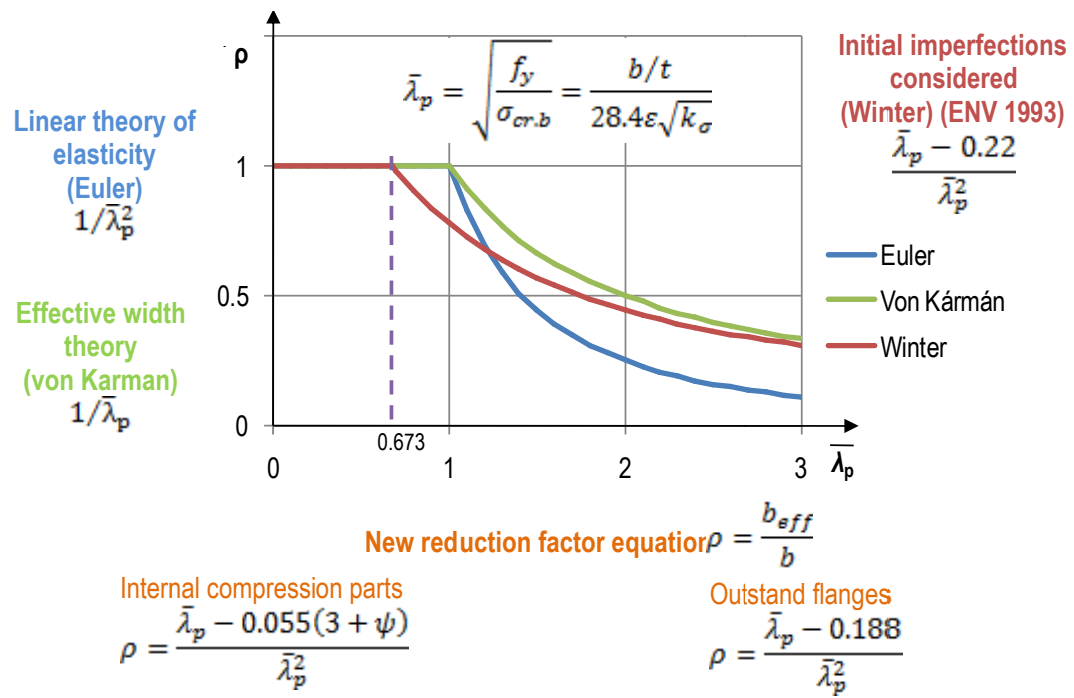


Figure 2.8 Historical evolution of effective width formulae

2.5 Classification of cross-section and slender limits

Eurocode 3 classifies compressed (or partially compressed) elements of cross-sections in four discrete groups, Class 1, 2, 3 or 4, by comparing its width-to-thickness ratio with slenderness limits that depend on the element boundary conditions, the stress distribution and the manufacturing process. The whole cross-section is classified according to its most slender element. The main drawback of this procedure is that does not consider interaction between the different constituent plates and junctions are always assumed to be simply supported.

Stocky cross-sections (Class 1-3) subjected to pure compression fail by means of material yielding and inelastic local buckling at stresses above the yield stress whereas slender cross-sections (Class 4) fail by elastic local buckling at stresses below the yield stress. However, the cross section is able to resist a higher load due to the redistribution of stresses which is a phenomenon called postbuckling strength. Unfortunately, the equations to describe postbuckling strength exhibit high complexity and the concept of “effective width” was introduced by Von Kármán to overcome this complication.

Although material response of stainless steel differs from carbon steel, the treatment of local buckling for both materials is similar and the non-linear response of stainless steels is not taken into account. This supposition does not have consequence for very slender elements which fail by stiffness, nevertheless, for the fundamental case of stocky elements, which its failure is governed by material response, may compromise accuracy and design efficiency. Actually, slender limits for stainless steels cross-sections are more conservative than those for carbon steel.

Tables 2.1-2.4 summarizes the effective width formulation of the both EN1993-1-3 (2006), which refers to EN1993-1-5 (2006), and EN1993-1-4 (2006), which is the same as the Euro Inox (2006), as well as the slenderness limits considered and those proposed by Gardner and Theofanous (2008). The element slenderness is defined in Eq. (17)

$$\varepsilon = \sqrt{\frac{235}{\sigma_{0.2}}} \quad \text{For carbon steel}$$

$$\varepsilon = \sqrt{\frac{235}{\sigma_{0.2}} \frac{E}{210000}} \quad \text{For stainless steel}$$

		EN1993-1-4 Euro Inox (Stainless Steel)	EN1993-1-3 refers to EN1993-1-1 (Carbon steel)	Theofanous and Gardner (2008) (Stainless Steel)
Internal parts	1	$c/t \leq 25.7\varepsilon$	$c/t \leq 33\varepsilon$	$c/t \leq 33\varepsilon$
	2	$c/t \leq 26.7\varepsilon$	$c/t \leq 38\varepsilon$	$c/t \leq 35\varepsilon$
	3	$c/t \leq 30.7\varepsilon$	$c/t \leq 42\varepsilon$	$c/t \leq 37\varepsilon$
Outstand flanges	1	Cold formed	$c/t \leq 10\varepsilon$	$c/t \leq 9\varepsilon$
		Welded	$c/t \leq 9\varepsilon$	$c/t \leq 9\varepsilon$
	2	Cold formed	$c/t \leq 10.4\varepsilon$	$c/t \leq 10\varepsilon$
		Welded	$c/t \leq 9.4\varepsilon$	$c/t \leq 10\varepsilon$
	3	Cold formed	$c/t \leq 11.9\varepsilon$	$c/t \leq 14\varepsilon$
		Welded	$c/t \leq 11\varepsilon$	$c/t \leq 14\varepsilon$
Angles	3	h : the longest flange	$h/t \leq 11.9\varepsilon$	$h/t \leq 15\varepsilon$
			$\frac{b+h}{2t} \leq 9.1\varepsilon$	$\frac{b+h}{2t} \leq 11.5\varepsilon$
Tubular sections	1	$d/t \leq 50\varepsilon^2$	$d/t \leq 50\varepsilon^2$	$d/t \leq 50\varepsilon^2$
	2	$d/t \leq 70\varepsilon^2$	$d/t \leq 70\varepsilon^2$	$d/t \leq 70\varepsilon^2$
	3	$d/t \leq 90\varepsilon^2$	$d/t \leq 90\varepsilon^2$	$d/t \leq 90\varepsilon^2$

Table 2.1 slenderness limits for members in compression

		EN1993-1-4 Euro Inox (Stainless Steel)	EN1993-1-3 refers to EN1993-1-1 (Carbon steel)	Theofanous and Gardner (2008) (Stainless Steel)
Internal parts	1	$c/t \leq 56.0\varepsilon$	$c/t \leq 72\varepsilon$	$c/t \leq 72\varepsilon$
	2	$c/t \leq 58.2\varepsilon$	$c/t \leq 83\varepsilon$	$c/t \leq 76\varepsilon$
	3	$c/t \leq 74.8\varepsilon$	$c/t \leq 124\varepsilon$	$c/t \leq 90\varepsilon$
Tubular sections	1	$d/t \leq 50\varepsilon^2$	$d/t \leq 50\varepsilon^2$	$d/t \leq 50\varepsilon^2$
	2	$d/t \leq 70\varepsilon^2$	$d/t \leq 70\varepsilon^2$	$d/t \leq 70\varepsilon^2$
	3	$d/t \leq 280\varepsilon^2$	$d/t \leq 90\varepsilon^2$	$d/t \leq 280\varepsilon^2$

Table 2.2 slenderness limits for members in bending

		EN1993-1-4 Euro Inox (Stainless Steel)	EN1993-1-3 refers to EN1993-1-1 (Carbon steel)	Theofanous and Gardner (2008) (Stainless Steel)
Internal parts	1	$\alpha > 0.5$ $\psi > -1$	$c/t \leq \frac{308\varepsilon}{13\alpha - 1}$	$c/t \leq \frac{396\varepsilon}{13\alpha - 1}$
		$\alpha \leq 0.5$ $\psi \leq -1$	$c/t \leq \frac{28\varepsilon}{\alpha}$	$c/t \leq \frac{36\varepsilon}{\alpha}$
	2	$\alpha > 0.5$ $\psi > -1$	$c/t \leq \frac{320\varepsilon}{13\alpha - 1}$	$c/t \leq \frac{420\varepsilon}{13\alpha - 1}$
		$\alpha \leq 0.5$ $\psi \leq -1$	$c/t \leq \frac{29.1\varepsilon}{\alpha}$	$c/t \leq \frac{38\varepsilon}{\alpha}$
	3	$\alpha > 0.5$ $\psi > -1$	$c/t \leq 15.3\varepsilon\sqrt{k_\sigma}$	$c/t \leq 18.5\varepsilon\sqrt{k_\sigma}$
		$\alpha \leq 0.5$ $\psi \leq -1$	$c/t \leq 15.3\varepsilon\sqrt{k_\sigma}$	$c/t \leq 18.5\varepsilon\sqrt{k_\sigma}$
Outstand flanges (Tip in compression)	1	Cold formed	$c/t \leq \frac{10\varepsilon}{\alpha}$	$c/t \leq \frac{9\varepsilon}{\alpha}$
		Welded	$c/t \leq \frac{9\varepsilon}{\alpha}$	$c/t \leq \frac{9\varepsilon}{\alpha}$
	2	Cold formed	$c/t \leq \frac{10.4\varepsilon}{\alpha}$	$c/t \leq \frac{10\varepsilon}{\alpha}$
		Welded	$c/t \leq \frac{9.4\varepsilon}{\alpha}$	$c/t \leq \frac{10\varepsilon}{\alpha}$
	3	Cold formed	$c/t \leq 18.1\varepsilon\sqrt{k_\sigma}$	$c/t \leq 21\varepsilon\sqrt{k_\sigma}$
		Welded	$c/t \leq 16.7\varepsilon\sqrt{k_\sigma}$	$c/t \leq 21\varepsilon\sqrt{k_\sigma}$
Outstand flanges (Tip in tension)	1	Cold formed	$c/t \leq \frac{10\varepsilon}{\alpha\sqrt{\alpha}}$	$c/t \leq \frac{9\varepsilon}{\alpha\sqrt{\alpha}}$
		Welded	$c/t \leq \frac{9\varepsilon}{\alpha\sqrt{\alpha}}$	$c/t \leq \frac{9\varepsilon}{\alpha\sqrt{\alpha}}$
	2	Cold formed	$c/t \leq \frac{10.4\varepsilon}{\alpha\sqrt{\alpha}}$	$c/t \leq \frac{10\varepsilon}{\alpha\sqrt{\alpha}}$
		Welded	$c/t \leq \frac{9.4\varepsilon}{\alpha\sqrt{\alpha}}$	$c/t \leq \frac{10\varepsilon}{\alpha\sqrt{\alpha}}$
	3	Cold formed	$c/t \leq 18.1\varepsilon\sqrt{k_\sigma}$	$c/t \leq 21\varepsilon\sqrt{k_\sigma}$
		Welded	$c/t \leq 16.7\varepsilon\sqrt{k_\sigma}$	$c/t \leq 21\varepsilon\sqrt{k_\sigma}$

Table 2.3 slenderness limits for members in combined bending and compression

		EN1993-1-4 Euro Inox (Stainless Steel)	EN1993-1-3 refers to EN1993-1-1 (Carbon steel)	Theofanous and Gardner (2008) (Stainless Steel)
Internal		$\rho = \frac{0.772}{\bar{\lambda}_p} - \frac{0.125}{\bar{\lambda}_p^2} \leq 1$	$\rho = \frac{\bar{\lambda}_p - 0.055(3 + \psi)}{\bar{\lambda}_p^2} \leq 1$ $\rho = 1$ for $\bar{\lambda}_p \leq 0.673$	$\rho = \frac{0.772}{\bar{\lambda}_p} - \frac{0.079}{\bar{\lambda}_p^2} \leq 1$
	Cold formed	$\rho = \frac{1}{\bar{\lambda}_p} - \frac{0.231}{\bar{\lambda}_p^2} \leq 1$	$\rho = \frac{\bar{\lambda}_p - 0.188}{\bar{\lambda}_p^2} \leq 1$ $\rho = 1$ for $\bar{\lambda}_p \leq 0.748$	$\rho = \frac{\bar{\lambda}_p - 0.188}{\bar{\lambda}_p^2} \leq 1$
	Welded	$\rho = \frac{1}{\bar{\lambda}_p} - \frac{0.242}{\bar{\lambda}_p^2} \leq 1$	$\rho = \frac{\bar{\lambda}_p - 0.188}{\bar{\lambda}_p^2} \leq 1$	$\rho = \frac{\bar{\lambda}_p - 0.188}{\bar{\lambda}_p^2} \leq 1$

Table 2.4 Reduction factor for local buckling (ρ function)

3. Numerical model

3.1 Validation

The numerical model used in to evaluate the effects of local buckling was the implemented in the Abaqus plug-in developed by VTT Technical Research Centre of Finalnd. The specimens were modelled constraining all degrees of freedom in both ends (fixed ends) excluding the displacement in the longitudinal axis. The load was applied axially by means of an imposed displacement.

The Abaqus plug-in was found to be suitable to model hollow sections, I-sections and channels undergoing axial compression. This was concluded after simulating different experimental tests found in Gardner and Nethercot (2004a) for hollow sections, Gardner and Saliba (2011) for I-sections and Kuwamura (2003) for channels. Some ultimate deformed shapes for these sections are shown in Figure 3.1 and a summary of results is presented in Table 3.1. The element type used was S9R5 for hollow sections and S4R for channels and I-sections. The distance between nodes was set to be one twentieth of the largest cross section element in I-sections and channels whereas one thirtieth in hollow sections. Neither strength corner properties nor residual stresses were considered. The distribution of initial imperfections was obtained from linear eigenvalue analysis as the first local buckling shape with positive critical deformation. Different initial imperfections were considered: $t/10$, $t/100$ and the provided by Dawson and Walker formula and adapted to stainless steel by Gardner and Nethercot (2004b) according to eq. 19. It was found that both $t/100$ and Dawson and Walker formula provide similar magnitudes but for consistency with other studies the latter was used.

$$w_0 = 0.023 \left(\frac{\sigma_{0.2}}{\sigma_{cr}} \right) t \quad (19)$$

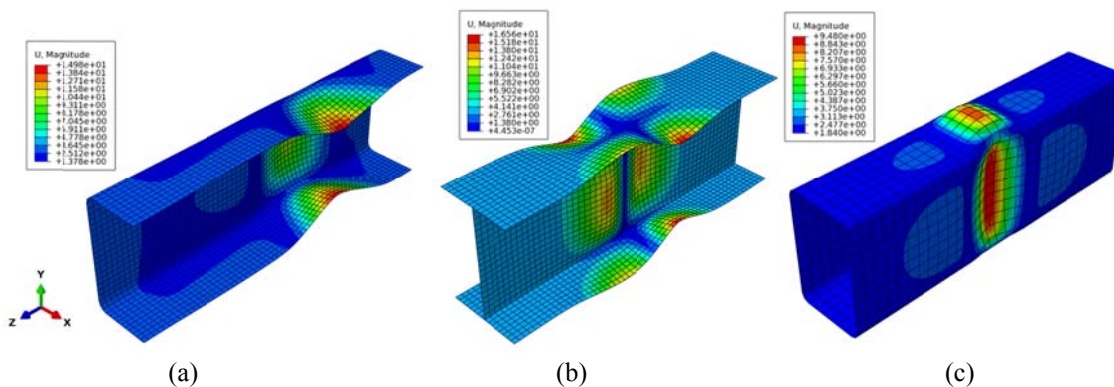


Figure 3.1 Ultimate deformed shapes in (a) Channels, (b) I-sections and (c) hollow sections

Reference		$N_{u,exp}$ (kN)	$N_{u,num}$ (kN)	$N_{u,num}/N_{u,exp}$
RHS100x50x2-SC2	RHS	181	175	0.967
SHS100x100x4-SC2	SHS	774	761	0.983
I-200x140x6x6	I-section	1473	1464	0.994
I-200x140x10x8	I-section	2540	2495	0.982
SC-2C2	Channel	134	127	0.947

Table 3.1 Comparison of ultimate load from numerical model and experimental tests

3.2 Model simplification

The goal of the preliminary FEM study was not to simulate particular member behaviour, and therefore several simplifications were used to increase the computational efficiency of hundreds of simulations and to clearly highlight the differences in specific material parameters without additional effects. Each of the following assumptions was carefully studied before application:

- Enhanced strength properties in corners were neglected using average values in the whole cross-section. This method is also included in EN1993-1-3 (2006).
- Residual stresses from cold-forming were not included due to their small effect on the member behaviour as concluded by Gardner and Cruise (2009).
- Residual stresses from fabrication and press-braking were also neglected in the study to keep the number of input parameters as low as possible.
- Isotropic material model was used with non-linear hardening. This model provides sufficient accuracy compared to other possible isotropic and anisotropic models according to Rasmussen et al. (2003).

Rounded corners were neglected giving greater flexibility for keeping reasonable aspect ratios of flat part shell elements.

3.3 Material model

The selected material model is based on Rasmussen's (2003) modification of Mirambell-Real (2000) model and it is also included in existing design rules, e.g. in Annex C of EN1993-1-4 (2006).

$$\varepsilon = \begin{cases} \frac{\sigma}{E_0} + 0.002 \left(\frac{\sigma}{\sigma_{0.2}} \right)^n & \text{for } \sigma \leq \sigma_{0.2} \\ \frac{\sigma - \sigma_{0.2}}{E_{0.2}} + \varepsilon_{pu} \left(\frac{\sigma - \sigma_{0.2}}{\sigma_u - \sigma_{0.2}} \right)^m + \varepsilon_{0.2} & \text{for } \sigma > \sigma_{0.2} \end{cases}$$

Where

$$E_{0.2} = \frac{E_0}{1 + 0.002n \left(E_0 / \sigma_{0.2} \right)} \quad (20)$$

$$\varepsilon_{0.2} = \frac{\sigma_{0.2}}{E_0} + 0.002$$

$$\varepsilon_{pu} = \varepsilon_u - \varepsilon_{0.2} - \frac{\sigma_u - \sigma_{0.2}}{E_{0.2}}$$

A group of materials with different 0.2% proof stress, ultimate strength, initial modulus of elasticity and non-linear parameter n was studied. The material stress-strain behaviour was described

according to Rasmussen's modification of the model, where the parameter of non-linearity of the second stage m is presented by Eq. (21)

$$m = 1 + 3.5 \frac{\sigma_{0.2}}{\sigma_u} \quad (21)$$

and the ultimate strain by Eq. (22).

$$\varepsilon_u = 1 - \frac{\sigma_{0.2}}{\sigma_u} \quad (22)$$

Material was then transformed to true stress and plastic logarithmic strain according to the Eq.(23).

$$\begin{aligned} \sigma_{true} &= \sigma_{nom}(1 + \varepsilon_{nom}) \\ \varepsilon_{true} &= \ln(1 + \varepsilon_{nom}) - \frac{\sigma_{true}}{E} \end{aligned} \quad (23)$$

Table 3.2 and figure 3.2 show the values of the six studied materials and the stress-strain curve respectively.

	E_0	$\sigma_{0.2}$	n	σ_u	m	ε_u	$\sigma_u / \sigma_{0.2}$
N1	200	300	5	600	2.75	0.5	2
N2	200	300	10	600	2.75	0.5	2
N3	200	300	25	600	2.75	0.5	2
F1	200	300	10	420	3.5	0.29	1.4
F2	200	400	10	560	3.5	0.29	1.4
F3	200	500	10	700	3.5	0.29	1.4

Table 3.2 Material properties

In one hand, group N studies the difference in non-linear parameter n . N1 is close to austenitic steels with low n values whereas N3 is close to carbon steel with high n values.

On the other hand, group F studies the effect of increased strength due to cold-working with lower $\sigma_u / \sigma_{0.2}$ ratio than grup N. In group N this ratio worths 2 but in group F is equal to 1.4 which is a typical value for ferritic stainless steels such as 3Cr12 grade.

3.4 Cross sections

Local buckling tests on two different cross-section types were used in the parametric study.

a) Square hollow section (SHS) with centre-to-centre side length 72mm, wall thickness 5 mm and no corners. Additionally, the same cross-section with thicknesses 3.0 mm and 1.0 mm was used to study the effect of changing slenderness. According to EN1993-1-3 (2006), these SHS should have 216mm length.

b) Rectangular hollow section (RHS) with centre-to-centre long side length 144mm and centre-to-centre short side length 72mm, wall thickness 5 mm and no corners. Additionally, the same cross-section with thicknesses 3.0 mm and 1.0 mm was used to study the effect of changing slenderness. The length of these specimens is 432mm.

The mesh size (distance between nodes) has been chosen as one thirtieth of the largest plate that makes up the cross-section.

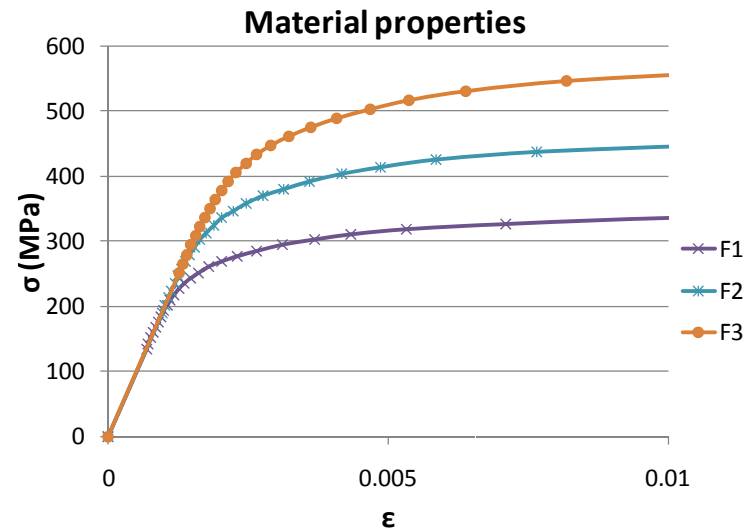
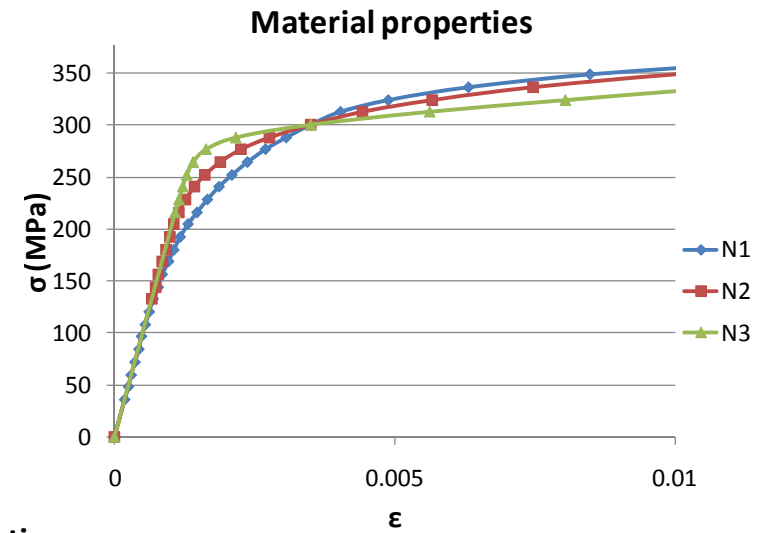
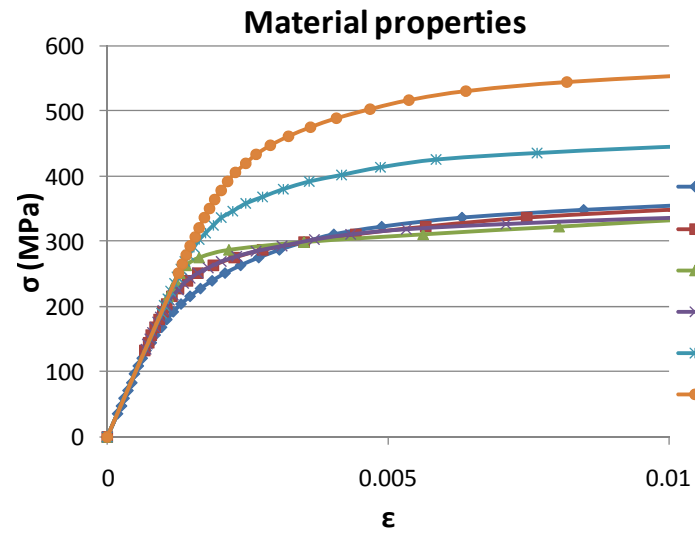


Figure 3.2 Material properties

4 Local buckling tests. Results

4.1 Introduction

The numerical results obtained with ABAQUS plug-in are shown herein, and the sensitivity of the model to the key modeling parameters, particularly the imperfection amplitudes as well as the non-linear parameter 'n' and the effect of cold-working ($\sigma_u/\sigma_{0.2}$ ratio). However, no comparisons with experimental test are presented in this preliminary FEM study.

In order to identify easily the specimens, they have been labeled. The first three letters abridge the cross section type followed by the material and the last number is the thickness of the section (Table 4.1 shows an example). A total of 108 specimens have been simulated.

	Cross section	Material	Thickness
	RHS	N1, N2, N3,	1
	SHS	F1, F2, F3	3
			5
SHSN23 →	SHS	N2	3

Table 4.1 Section labeling

4.2 Class limits assessment

Tables 4.2 and 4.3 summarize the most relevant values obtained from applying the effective width method adopted in EN1993-1-4 used to classify cross sections. The former shows results from RHS and the latter from SHS.

There are mainly three different parameters which have to be deeply studied to take into account the behaviour of stainless steels. They are:

- The non linear parameter 'n', which can be studied analyzing N materials.
- The $\sigma_{0.2}$ value, which can be studied analyzing F materials.
- The σ_u value, which can be studied comparing N2 material with F1 material.

Figure 3.2, where the ratios of the numerical to the squash load ($A\sigma_{0.2}$) against the slenderness of the most slender constituent element in the cross section of all specimens, shows the influence of the non linear parameter. The main conclusions drew from this figure are:

- The ratio $N_{u,num}/A\sigma_{0.2}$ decreases when the non linear parameter raises in stocky sections.
- However, this ratio increases when 'n' raises in slender sections.
- The changeable trend may be at a value of $N_{u,num}/A\sigma_{0.2}$ equal to 1. In one hand, from this point upwards, cross-section failure may occur by yielding at stresses greater than $\sigma_{0.2}$ when the assumed material model shows grater stresses for low values of 'n'. On the other hand, from this point downwards, cross-section failure may occur by local at stresses smaller than $\sigma_{0.2}$ when the assumed material model shows smaller stresses for low values of 'n' (see Figure 4.1).
- The vertical line that defines the change in the trend, which is the ratio $c/t\epsilon$ that defines the limit between class 3 and class 4, cannot be already defined and more realistic numerical simulations are required. However, it seems that class 3 limit proposed in

EN1993-1-4 is more conservative than class 3 limit of EN1993-1-5 as it was concluded in Gardner and Theofanous (2008).

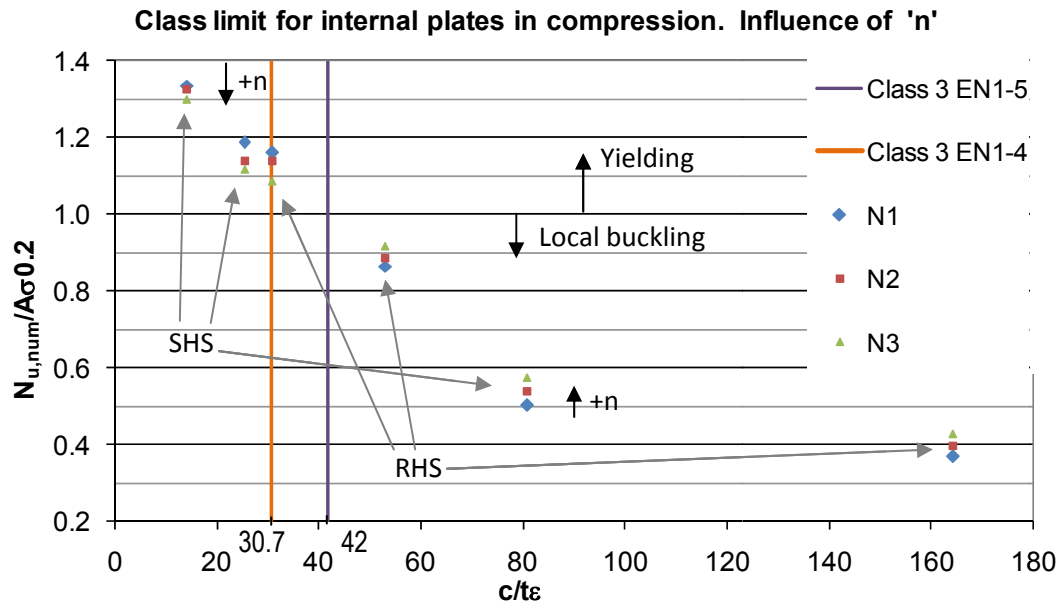


Figure 4.1 Influence of the non linear parameter
Material properties

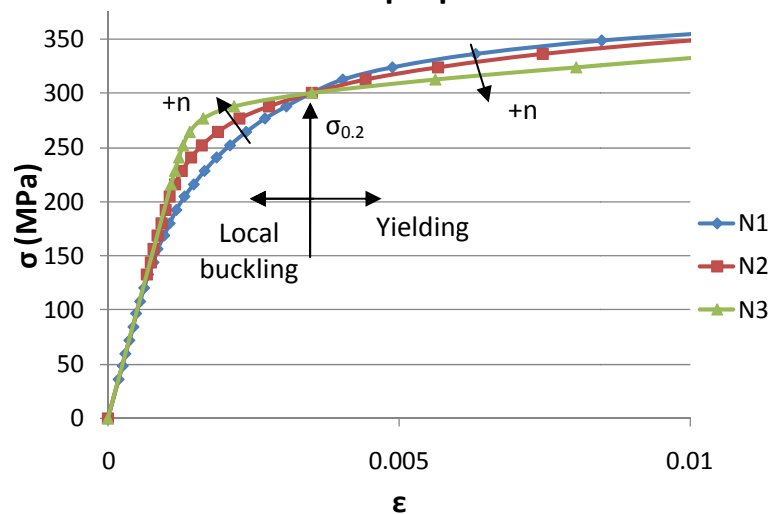


Figure 4.2 Non linear parameter evolution in N materials

The influence of $\sigma_{0.2}$ value is shown in Figure 4.3 where the ratios of the numerical to the squash load ($A\sigma_{0.2}$) against the slenderness of the most slender constituent element in the cross section of all specimens are plotted only for F materials. It can be noticeable:

- Material F3, which has the highest proof stress value, provide higher $c/t\epsilon$ values and lower $N_{u,num}/A\sigma_{0.2}$.
- This means that the higher $\sigma_{0.2}$ value is, the greater section class obtains the plate which is in agreement on theory.

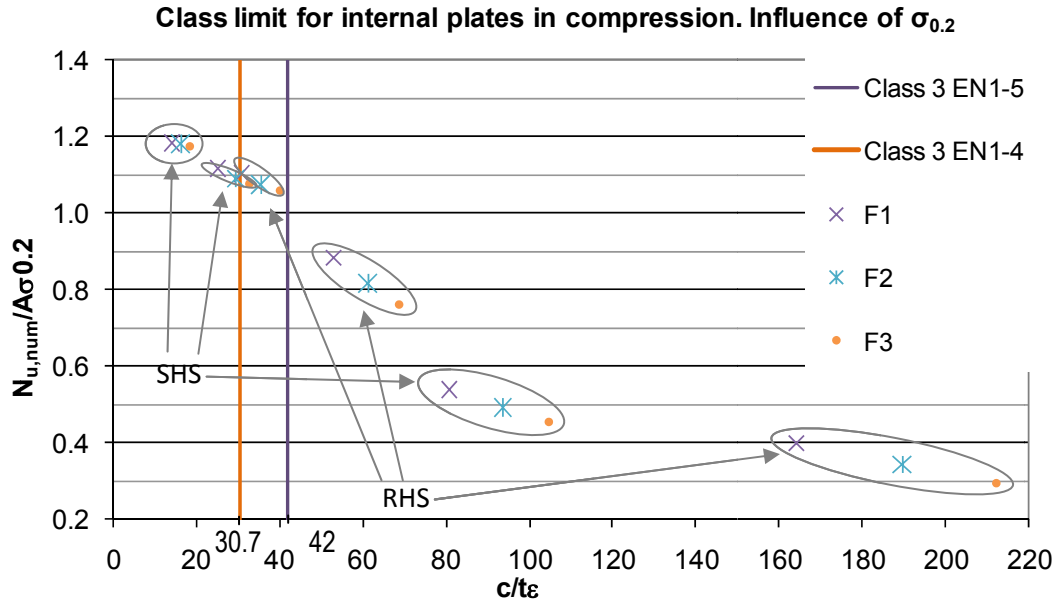


Figure 4.3 Influence of the $\sigma_{0.2}$ value

Finally, in order to assess the influence of σ_u material N2 is compared with material F1 in Figure 4.4. The ratios of the numerical to the squash load ($A\sigma_{0.2}$) against the slenderness of the most slender constituent element in the cross section of all specimens are represented. Following conclusions can be noticed:

- The σ_u value influences only in stocky sections which are capable to reach high stress values above $\sigma_{0.2}$.

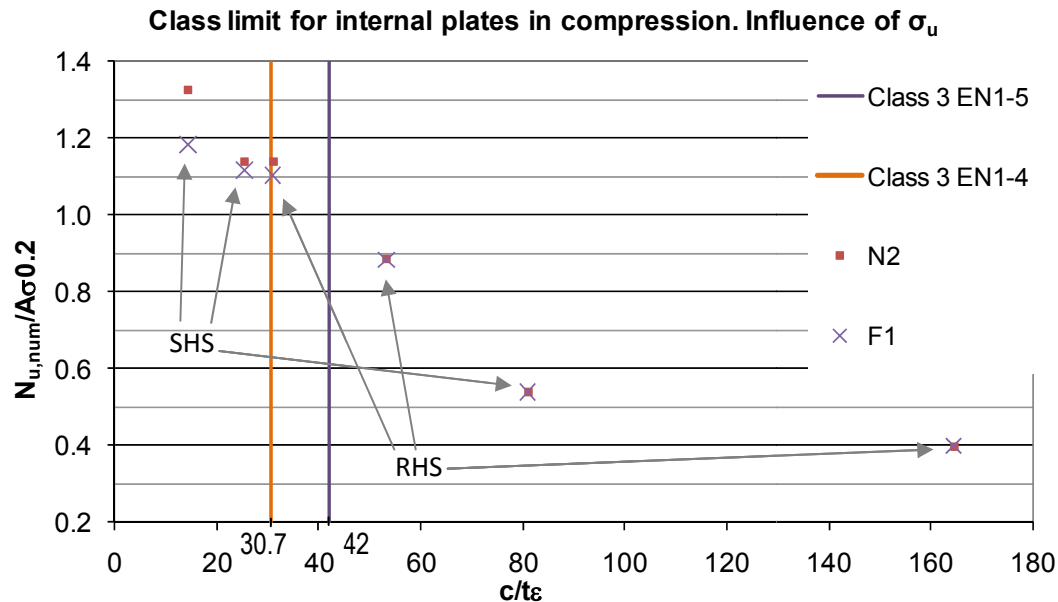


Figure 4.4 Influence of the σ_u value

Once the results have been presented, some conclusions can be extracted:

- The non linear parameter 'n', which is not taken into account in the current formulation, influences on the ultimate load. However, a more thorough investigation of its influence should be carried out to study whether this influence is important or not.
- The ultimate load is also sensitive to $\sigma_{0.2}$, but included in the current formulation.

- Stocky sections are sensitive to σ_u value whereas slender sections are not. It might be considered if parameter σ_u has a relatively important influence.

4.3 Numerical results vs EN1993-1-4

Tables 4.2 and 4.3 summarizes the most relevant results from applying EN1993-1-4 to predict the ultimate load of the simulated sections. The procedure to obtain the ultimate load is described as follows:

1. Calculation of the non dimensional slenderness: $\bar{\lambda}_p = \sqrt{\frac{f_y}{\sigma_{cr,b}}} = \frac{b/t}{28.4\epsilon\sqrt{k_\sigma}}$
2. Calculation of the reduction parameter: $\rho = \frac{0.772}{\bar{\lambda}_p} - \frac{0.125}{\bar{\lambda}_p^2} \leq 1$
3. Calculation of the effective width: $\frac{b_{eff}}{b} = \rho$
4. Calculation of the effective area: $A_{eff} = \sum_i b_{eff,i} t_i$
5. Calculation of the ultimate load: $N_{ult,EN} = A_{eff} \sigma_{0.2}$

Specimen	ε	c/t ε	Section class	A _{tot} (mm ²)	$\sigma_{cr, theo}$ (MPa)	$\lambda_{p,h}$	$\lambda_{p,b}$	ρ_h	ρ_b	A _{eff,tot} (mm ²)	N _{ult,num} (kN)	A $\sigma_{0.2}$ (kN)	N _{ult,EN} (kN)	N _{ult,num} /A $\sigma_{0.2}$	N _{ult,EN} /A $\sigma_{0.2}$	N _{ult,num} /N _{ult,EN}
RHSF11	0.86	164.40	4	432	34.87	2.9332	1.4666	0.2487	0.4683	139.05	51.60	129.60	41.71	0.3981	0.3219	1.2370
RHSF13	0.86	53.26	4	1296	313.82	0.9777	0.4889	0.6588	1.0000	1001.23	343.30	388.80	300.37	0.8830	0.7726	1.1429
RHSF15	0.86	31.03	4	2160	871.73	0.5866	0.2933	0.9528	1.0000	2091.97	713.80	648.00	627.59	1.1015	0.9685	1.1374
RHSF21	0.75	189.84	4	432	34.87	3.3870	1.6935	0.2170	0.4123	121.88	59.60	172.80	48.75	0.3449	0.2821	1.2226
RHSF23	0.75	61.50	4	1296	313.82	1.1290	0.5645	0.5857	0.9753	927.41	422.50	518.40	370.96	0.8150	0.7156	1.1389
RHSF25	0.75	35.83	4	2160	871.73	0.6774	0.3387	0.8673	1.0000	1968.84	926.10	864.00	787.54	1.0719	0.9115	1.1759
RHSF31	0.67	212.24	4	432	34.87	3.7867	1.8934	0.1952	0.3729	109.90	63.80	216.00	54.95	0.2954	0.2544	1.1611
RHSF33	0.67	68.75	4	1296	313.82	1.2622	0.6311	0.5332	0.9094	853.50	494.40	648.00	426.75	0.7630	0.6586	1.1585
RHSF35	0.67	40.06	4	2160	871.73	0.7573	0.3787	0.8014	1.0000	1874.04	1144.60	1080.00	937.02	1.0598	0.8676	1.2215
RHSN11	0.86	164.40	4	432	34.87	2.9332	1.4666	0.2487	0.4683	139.05	48.00	129.60	41.71	0.3704	0.3219	1.1507
RHSN13	0.86	53.26	4	1296	313.82	0.9777	0.4889	0.6588	1.0000	1001.23	336.00	388.80	300.37	0.8642	0.7726	1.1186
RHSN15	0.86	31.03	4	2160	871.73	0.5866	0.2933	0.9528	1.0000	2091.97	751.70	648.00	627.59	1.1600	0.9685	1.1978
RHSN21	0.86	164.40	4	432	34.87	2.9332	1.4666	0.2487	0.4683	139.05	51.50	129.60	41.71	0.3974	0.3219	1.2346
RHSN23	0.86	53.26	4	1296	313.82	0.9777	0.4889	0.6588	1.0000	1001.23	343.80	388.80	300.37	0.8843	0.7726	1.1446
RHSN25	0.86	31.03	4	2160	871.73	0.5866	0.2933	0.9528	1.0000	2091.97	738.80	648.00	627.59	1.1401	0.9685	1.1772
RHSN31	0.86	164.40	4	432	34.87	2.9332	1.4666	0.2487	0.4683	139.05	55.30	129.60	41.71	0.4267	0.3219	1.3257
RHSN33	0.86	53.26	4	1296	313.82	0.9777	0.4889	0.6588	1.0000	1001.23	356.40	388.80	300.37	0.9167	0.7726	1.1865
RHSN35	0.86	31.03	4	2160	871.73	0.5866	0.2933	0.9528	1.0000	2091.97	704.20	648.00	627.59	1.0867	0.9685	1.1221

Table 4.2 Stub column results in RHS. Class limits assessment according to EN1993-1-4

Specimen	ε	c/t _e	Section class	A _{tot} (mm ²)	$\sigma_{cr, theo}$ (MPa)	λ_p	ρ	A _{eff,tot} (mm ²)	N _{ult,num} (kN)	A $\sigma_{0.2}$ (kN)	N _{ult,EN} (kN)	N _{ult,num} /A $\sigma_{0.2}$	N _{ult,EN} /A $\sigma_{0.2}$	N _{ult,num} /N _{ult,EN}
SHSF11	0.86	81.04	4	288	139.48	1.4666	0.4683	134.86	46.40	86.40	40.46	0.5370	0.4683	1.1468
SHSF13	0.86	25.47	1	864	1255.29	0.4889	1.0000	864.00	289.10	259.20	259.20	1.1154	1.0000	1.1154
SHSF15	0.86	14.36	1	1440	3486.92	0.2933	1.0000	1440.00	510.30	432.00	432.00	1.1813	1.0000	1.1813
SHSF21	0.75	93.58	4	288	139.48	1.6935	0.4123	118.74	56.20	115.20	47.49	0.4878	0.4123	1.1833
SHSF23	0.75	29.41	3	864	1255.29	0.5645	0.9753	842.68	377.20	345.60	337.07	1.0914	0.9753	1.1190
SHSF25	0.75	16.58	1	1440	3486.92	0.3387	1.0000	1440.00	678.00	576.00	576.00	1.1771	1.0000	1.1771
SHSF31	0.67	104.63	4	288	139.48	1.8934	0.3729	107.39	65.70	144.00	53.69	0.4563	0.3729	1.2236
SHSF33	0.67	32.88	4	864	1255.29	0.6311	0.9094	785.72	465.20	432.00	392.86	1.0769	0.9094	1.1841
SHSF35	0.67	18.53	1	1440	3486.92	0.3787	1.0000	1440.00	846.20	720.00	720.00	1.1753	1.0000	1.1753
SHSN11	0.86	81.04	4	288	139.48	1.4666	0.4683	134.86	43.50	86.40	40.46	0.5035	0.4683	1.0752
SHSN13	0.86	25.47	1	864	1255.29	0.4889	1.0000	864.00	307.80	259.20	259.20	1.1875	1.0000	1.1875
SHSN15	0.86	14.36	1	1440	3486.92	0.2933	1.0000	1440.00	577.20	432.00	432.00	1.3361	1.0000	1.3361
SHSN21	0.86	81.04	4	288	139.48	1.4666	0.4683	134.86	46.40	86.40	40.46	0.5370	0.4683	1.1468
SHSN23	0.86	25.47	1	864	1255.29	0.4889	1.0000	864.00	295.00	259.20	259.20	1.1381	1.0000	1.1381
SHSN25	0.86	14.36	1	1440	3486.92	0.2933	1.0000	1440.00	573.30	432.00	432.00	1.3271	1.0000	1.3271
SHSN31	0.86	81.04	4	288	139.48	1.4666	0.4683	134.86	49.70	86.40	40.46	0.5752	0.4683	1.2284
SHSN33	0.86	25.47	1	864	1255.29	0.4889	1.0000	864.00	289.30	259.20	259.20	1.1161	1.0000	1.1161
SHSN35	0.86	14.36	1	1440	3486.92	0.2933	1.0000	1440.00	560.80	432.00	432.00	1.2981	1.0000	1.2981

Table 4.3 Stub column results in SHS. Class limits assessment according to EN1993-1-4

For the fundamental case of internal members in compression, Gardner and Theofanous (2008) suggested a new class 3 limit for stainless steel ($37c/t\varepsilon$). For consistency, it was also proposed that the effective width formulae specified in EN1993-1-4 (2006) be modified to Equation (24), which has been statistically validated according to EN 1990.

$$c/t = 30.7\varepsilon \rightarrow c/t = 37\varepsilon$$

$$\rho = \frac{0.772}{\bar{\lambda}_p} - \frac{0.125}{\bar{\lambda}_p^2} \leq 1 \rightarrow \rho = \frac{0.772}{\bar{\lambda}_p} - \frac{0.079}{\bar{\lambda}_p^2} \leq 1 \quad (24)$$

In order to assess if this new proposal formulae is more suitable to predict the ultimate load, all specimens have been recalculated using this new reduction factor. Tables 4.4 and 4.5 summarize the most relevant results. The new obtained values are less conservative which means that a more efficient design can be carried out by applying the new proposal limits by Gardner and Theofanous (2008).

Specimen	ε	c/t ε	Section class EC	New Section class	ρ, h	New ρ, h	ρ, b	New ρ, b	$A_{eff,tot}$ (mm ²)	New $A_{eff,tot}$ (mm ²)	$N_{ult,num}$ (kN)	$N_{ult,EN}$ (kN)	$N_{ult,new}$ (kN)	$N_{ult,num}/$ $N_{ult,EN}$	$N_{ult,num}/$ $N_{ult,new}$
RHSF11	0.86	164.40	4	4	0.2487	0.2540	0.4683	0.4897	139.05	143.67	51.60	41.71	43.10	1.2370	1.1972
RHSF13	0.86	53.26	4	4	0.6588	0.7069	1.0000	1.0000	1001.23	1042.80	343.30	300.37	312.84	1.1429	1.0974
RHSF15	0.86	31.03	4	3	0.9528	1.0000	1.0000	1.0000	2091.97	2160.00	713.80	627.59	648.00	1.1374	1.1015
RHSF21	0.75	189.84	4	4	0.2170	0.2210	0.4123	0.4283	121.88	125.34	59.60	48.75	50.14	1.2226	1.1888
RHSF23	0.75	61.50	4	4	0.5857	0.6218	0.9753	1.0000	927.41	969.25	422.50	370.96	387.70	1.1389	1.0898
RHSF25	0.75	35.83	4	3	0.8673	0.9675	1.0000	1.0000	1968.84	2113.20	926.10	787.54	845.28	1.1759	1.0956
RHSF31	0.67	212.24	4	4	0.1952	0.1984	0.3729	0.3857	109.90	112.67	63.80	54.95	56.33	1.1611	1.1325
RHSF33	0.67	68.75	4	4	0.5332	0.5620	0.9094	1.0000	853.50	917.59	494.40	426.75	458.80	1.1585	1.0776
RHSF35	0.67	40.06	4	4	0.8014	0.8816	1.0000	1.0000	1874.04	1989.53	1144.60	937.02	994.76	1.2215	1.1506
RHSN11	0.86	164.40	4	4	0.2487	0.2540	0.4683	0.4897	139.05	143.67	48.00	41.71	43.10	1.1507	1.1137
RHSN13	0.86	53.26	4	4	0.6588	0.7069	1.0000	1.0000	1001.23	1042.80	336.00	300.37	312.84	1.1186	1.0740
RHSN15	0.86	31.03	4	3	0.9528	1.0000	1.0000	1.0000	2091.97	2160.00	751.70	627.59	648.00	1.1978	1.1600
RHSN21	0.86	164.40	4	4	0.2487	0.2540	0.4683	0.4897	139.05	143.67	51.50	41.71	43.10	1.2346	1.1949
RHSN23	0.86	53.26	4	4	0.6588	0.7069	1.0000	1.0000	1001.23	1042.80	343.80	300.37	312.84	1.1446	1.0990
RHSN25	0.86	31.03	4	3	0.9528	1.0000	1.0000	1.0000	2091.97	2160.00	738.80	627.59	648.00	1.1772	1.1401
RHSN31	0.86	164.40	4	4	0.2487	0.2540	0.4683	0.4897	139.05	143.67	55.30	41.71	43.10	1.3257	1.2831
RHSN33	0.86	53.26	4	4	0.6588	0.7069	1.0000	1.0000	1001.23	1042.80	356.40	300.37	312.84	1.1865	1.1392
RHSN35	0.86	31.03	4	3	0.9528	1.0000	1.0000	1.0000	2091.97	2160.00	704.20	627.59	648.00	1.1221	1.0867

Table 4.4 Stub column results in RHS according to the new proposal formulae by Gardner and Theofanous (2008)

Specimen	ε	$c/t\varepsilon$	Section class	New Section class	ρ	New ρ	$A_{eff,tot}$ (mm ²)	New $A_{eff,tot}$ (mm ²)	$N_{ult,num}$ (kN)	$N_{ult,EN}$ (kN)	$N_{ult,new}$ (kN)	$N_{ult,num}/N_{ult,EN}$	$N_{ult,num}/N_{ult,new}$
SHSF11	0.86	81.04	4	4	0.4683	0.4897	134.86	141.02	46.40	40.46	42.31	1.1468	1.0968
SHSF13	0.86	25.47	1	1	1.0000	1.0000	864.00	864.00	289.10	259.20	259.20	1.1154	1.1154
SHSF15	0.86	14.36	1	1	1.0000	1.0000	1440.00	1440.00	510.30	432.00	432.00	1.1813	1.1813
SHSF21	0.75	93.58	4	4	0.4123	0.4283	118.74	123.36	56.20	47.49	49.34	1.1833	1.1390
SHSF23	0.75	29.41	3	3	0.9753	1.0000	842.68	864.00	377.20	337.07	345.60	1.1190	1.0914
SHSF25	0.75	16.58	1	1	1.0000	1.0000	1440.00	1440.00	678.00	576.00	576.00	1.1771	1.1771
SHSF31	0.67	104.63	4	4	0.3729	0.3857	107.39	111.08	65.70	53.69	55.54	1.2236	1.1829
SHSF33	0.67	32.88	4	4	0.9094	1.0000	785.72	864.00	465.20	392.86	432.00	1.1841	1.0769
SHSF35	0.67	18.53	1	1	1.0000	1.0000	1440.00	1440.00	846.20	720.00	720.00	1.1753	1.1753
SHSN11	0.86	81.04	4	4	0.4683	0.4897	134.86	141.02	43.50	40.46	42.31	1.0752	1.0282
SHSN13	0.86	25.47	1	1	1.0000	1.0000	864.00	864.00	307.80	259.20	259.20	1.1875	1.1875
SHSN15	0.86	14.36	1	1	1.0000	1.0000	1440.00	1440.00	577.20	432.00	432.00	1.3361	1.3361
SHSN21	0.86	81.04	4	4	0.4683	0.4897	134.86	141.02	46.40	40.46	42.31	1.1468	1.0968
SHSN23	0.86	25.47	1	1	1.0000	1.0000	864.00	864.00	295.00	259.20	259.20	1.1381	1.1381
SHSN25	0.86	14.36	1	1	1.0000	1.0000	1440.00	1440.00	573.30	432.00	432.00	1.3271	1.3271
SHSN31	0.86	81.04	4	4	0.4683	0.4897	134.86	141.02	49.70	40.46	42.31	1.2284	1.1748
SHSN33	0.86	25.47	1	1	1.0000	1.0000	864.00	864.00	289.30	259.20	259.20	1.1161	1.1161
SHSN35	0.86	14.36	1	1	1.0000	1.0000	1440.00	1440.00	560.80	432.00	432.00	1.2981	1.2981

Table 4.5 Stub column results in SHS according to the new proposal formulae by Gardner and Theofanous (2008)

5 Sectional stress distribution

The goal herein is to carry out a detailed study of the stress distribution in some sections made up of different materials. The sections have been chosen in order to study the influence of the non linear parameter 'n' in slender sections. Three topics will be presented to study the sectional stress distribution: the cross-section stress evolution in mid span, the stress-displacement of the point perched on the centre of the plate that sets of the whole section and the stress evolution of this point against the applied external stresses.

Furthermore, the real effective width obtained from the numerical model will be compared with those calculated by applying current EN1993-1-4 formulae and proposed by Gardner and Theofanous (2008).

5.1 SHSN11

The first section chosen was a square hollow section with centre-to-centre side length 72mm and wall thickness 1 mm made up of material N1. Due to its double symmetry, only results from one plate will be presented so the other three plates have also the same response.

Figure 5.1 shows the evolution of the compression stress distribution along the width when load (step) increases. The most relevant conclusions from this chart are:

- The onset of local buckling begins at step 8 when the stress distribution loses linearity.
- The stress distribution at high steps resembles the effective width theory.

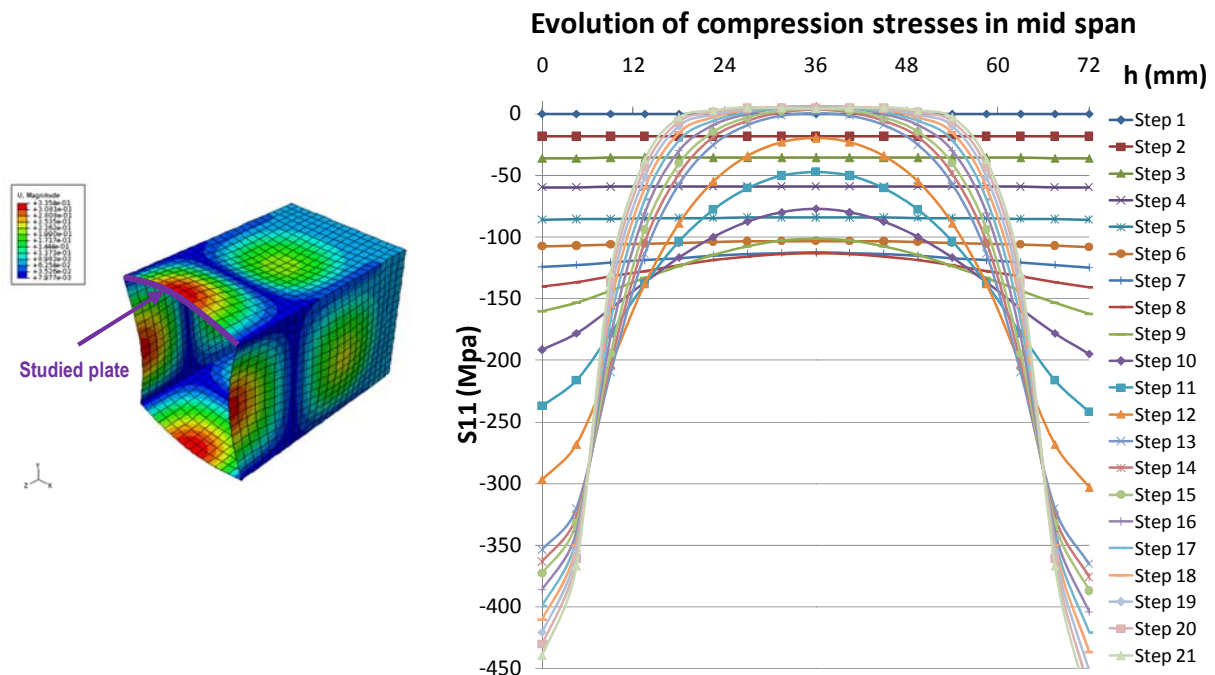


Figure 5.1 Compression stress evolution along the plate width in SHSN11 section

The stress-displacement of the point perched on the centre of the plate is plotted in figure 5.2. The chart shows how when the point reaches the critical stress at step 8 ($\sigma_{cr}=113.59\text{MPa}$ when the external load is equal to $N_{cr}=36.8\text{kN}$) is incapable of carrying more load which means that plate buckling has started.

In order to prove the post-buckling strength of the specimen, Figure 5.3 shows the stress evolution of the central point and the applied stresses. When the evolution of both stresses split up, local buckling begins. It is important to highlight that both curves differ at critical stress.

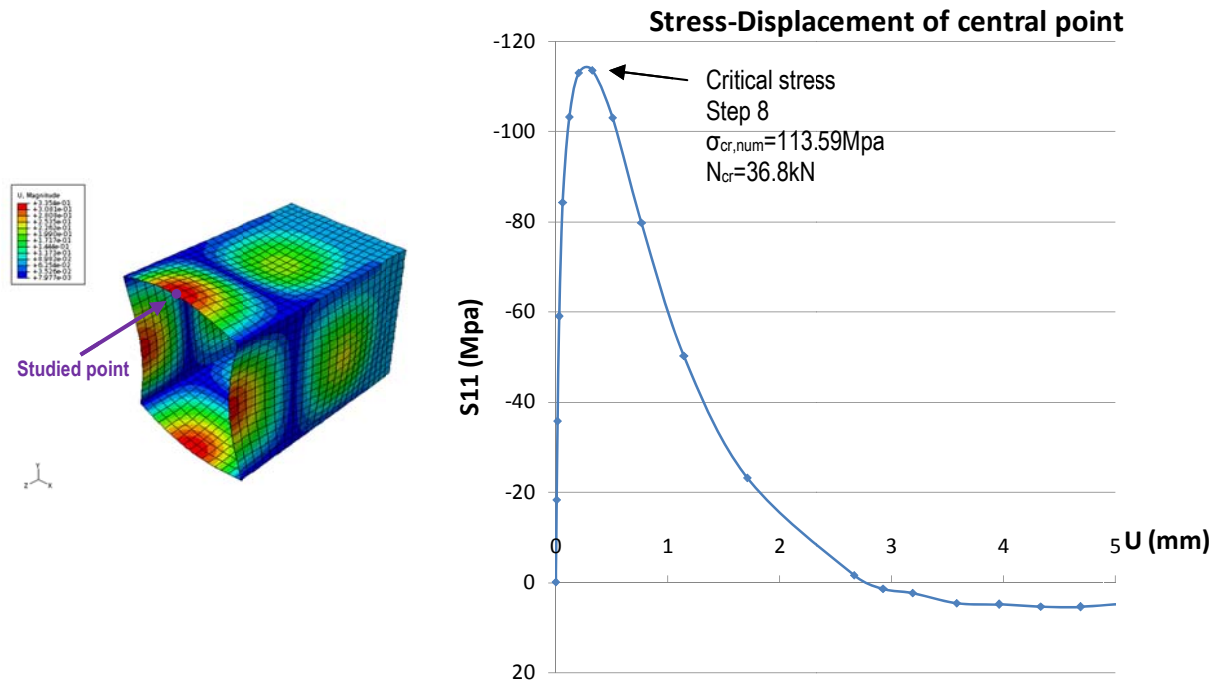


Figure 5.2 Evolution of stress-displacement of central point in SHSN11 section

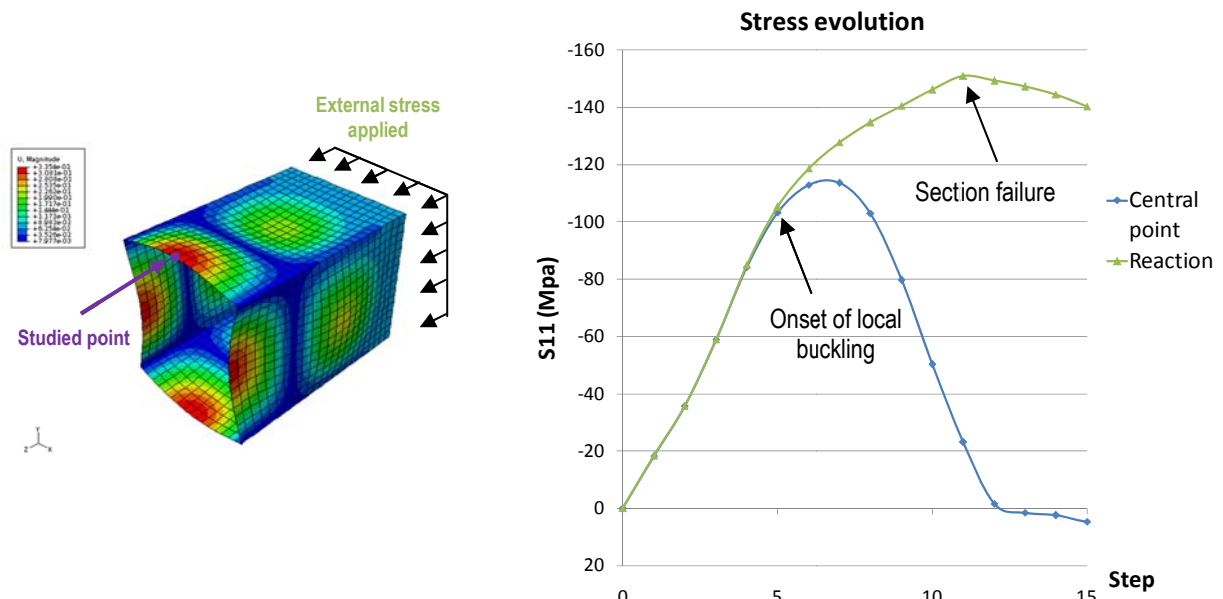


Figure 5.3 Evolution of stress-displacement of central point in SHSN11 section

Finally, the followed procedure to calculate the real effective width is presented. Figure 5.4 shows the development of the effective cross section in double symmetric cross-sections and table 5.1 presents all the parameters necessary to calculate the real effective width (negative symbol means compression).

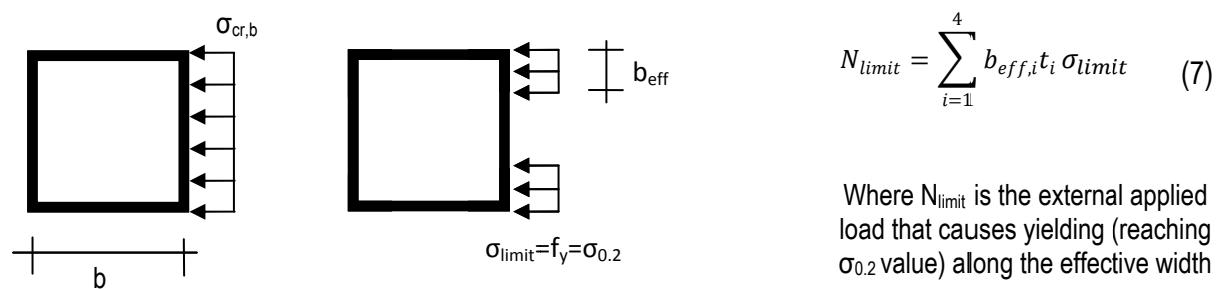


Figure 5.4 development of the effective width in double symmetric cross-sections

Load step (see Figure 4.1)	Compression stress S11 (MPa)	External load (kN)	External stress (A=288mm ²)
11	-237.244	-42.1	-146.18
12	-296.865 $\approx\sigma_{0.2}=\sigma_{limit}$	-43.5=N _{limit}	-151.04
13	-354.034	-43	-149.31
14	-363.773	-42.4	-147.22

Table 5.1 Compression stresses and external applied load in SHSN11

$$b_{eff,real} = \frac{N_{limit}}{4 \cdot t \cdot \sigma_{limit}} = \frac{43500}{4 \cdot 1 \cdot 296.865} = 36.633mm$$

Table 5.2 compares the real effective width and the real effective area with those obtained from applying current EN1993-1-4 and Gardner and Theofanous (2008) proposal. Again, the new proposal formulae provide less conservative values.

	b_{eff} (mm)	A_{eff} (mm ²)
Numerical ("real")	36.63	146.53
EN1993-1-4	33.72	134.86
Theofanous and Gardner (2008)	35.25	141.02

Table 5.2 comparison between effective widths and effective areas

5.2 SHSN31

Similar results are presented for the same section but made up of N3 material which differs from N1 by having a greater non linear parameter. N3 is close to carbon steel whereas N1 is close to austenitic stainless steel. Figure 5.5, 5.6 and 5.7 as well as table 5.3 and 5.4 present equivalent results from above but for SHSN31.

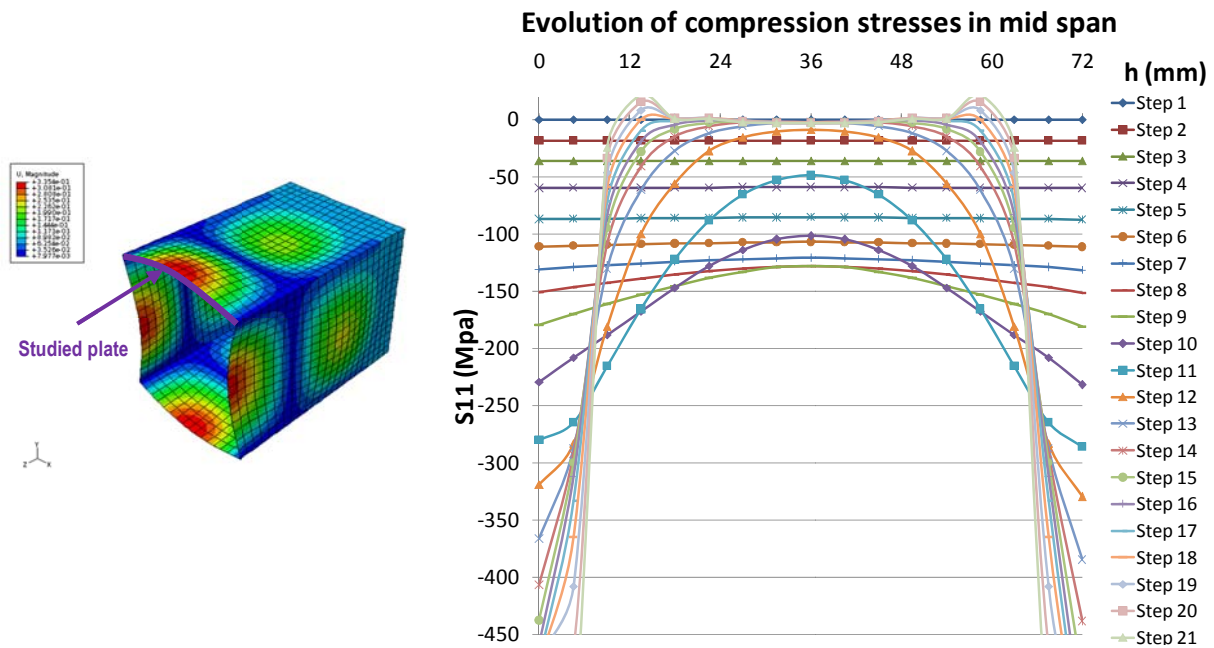


Figure 5.5 Compression stress evolution along the plate width in SHSN31 section

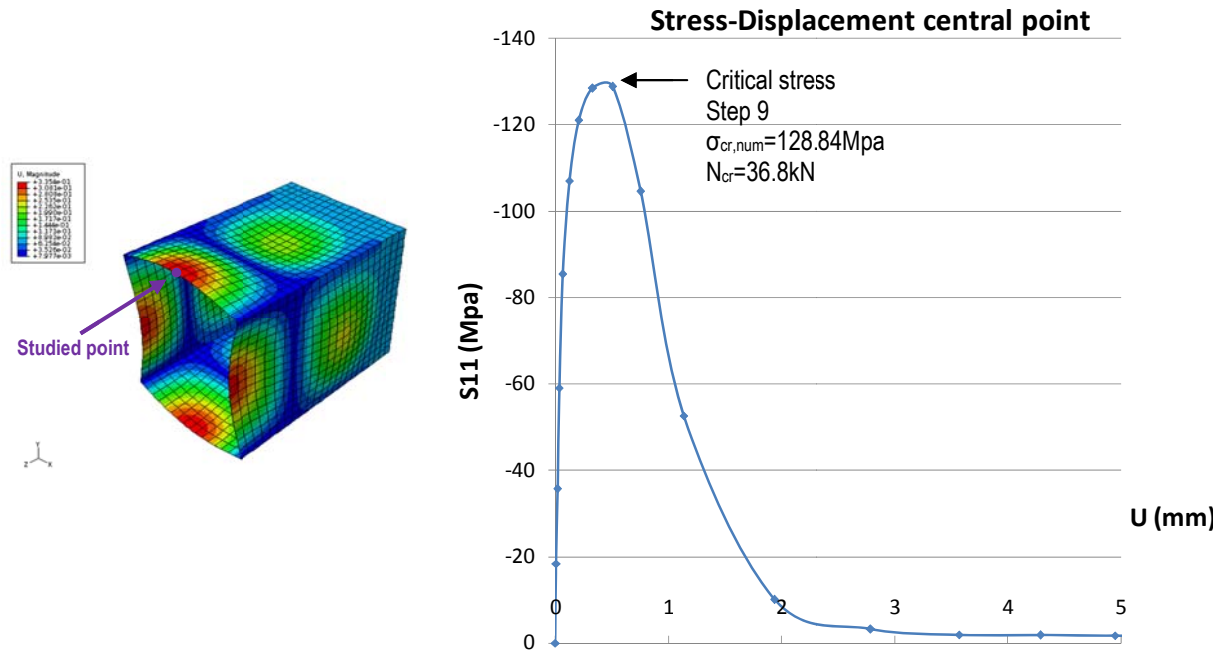


Figure 5.6 Evolution of stress-displacement of central point in SHSN31 section

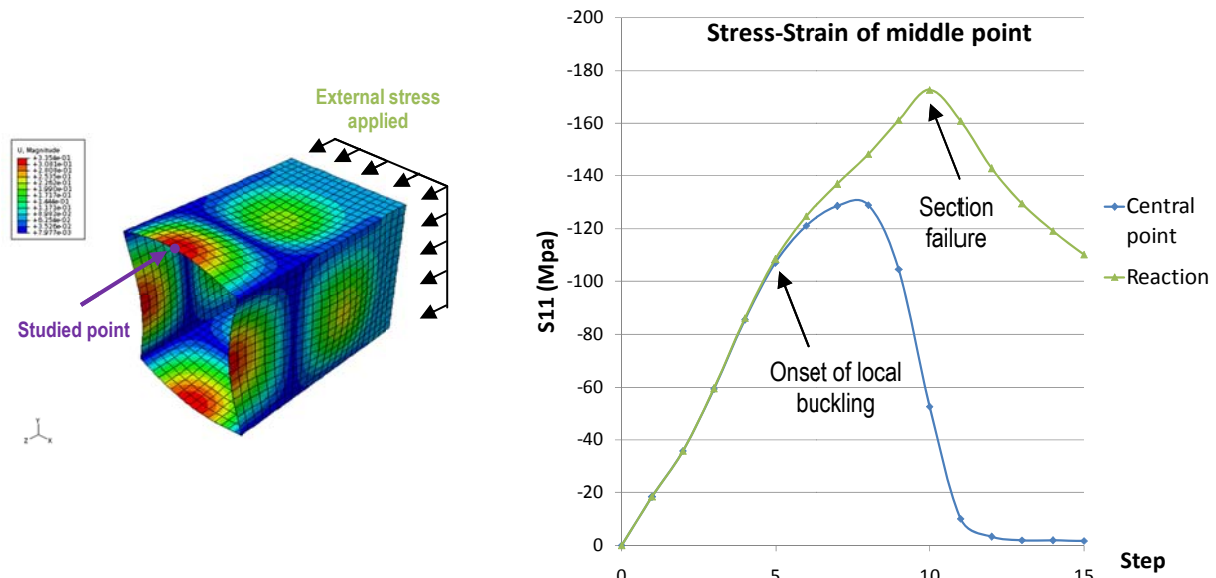


Figure 5.7 Evolution of stress-displacement of central point in SHSN31 section

Load step (see Figure 4.5)	Compression stress S11 (MPa)	External load (kN)	External stress (A=288mm ²)
10	-229.073	-46.4	-161.11
11	-280.063 ≈ $\sigma_{0.2} = \sigma_{limit}$	-49.7 = N_{limit}	-172.57
12	-319.068	-46.3	-160.76
13	-366.322	-41.1	-142.71

Table 5.3 Compression stresses and external applied load in SHSN31

	b_{eff} (mm)	A_{eff} (mm ²)
Numerical ("real")	44.36	177.46
EN1993-1-4	33.72	134.86
Theofanous and Gardner (2008)	35.25	141.02

Table 5.4 comparison between effective widths and effective areas

5.3 Comparison between SHSN11 and SHSN31

Results from both sections are presented herein. Table 5.5 summarizes the critical stress obtained from LEA analysis ($\sigma_{cr,LEA}$), the critical stress from theory assuming that the SHS is made up of four simply supported plates ($\sigma_{cr,theo}$) and the stress of the central point at the onset of local buckling from non-linear analysis ($\sigma_{cr,num}$). Moreover, three effective widths (just one plate) are presented. The first one is the result from applying the current EN1993-1-4 ($b_{eff,EN}$). The second one gives the effective width after considering Gardner and Theofanous (2008) modification. And the last one is the value obtained from equation (7).

	SHSN11	SHSN31
$\sigma_{cr,LEA}$ (MPa)	151	151
$\sigma_{cr,theo}$ (MPa)	139.48	139.48
$\sigma_{cr,num}$ (MPa)	113.59	128.84
$b_{eff,EN}$ (mm)	33.72	33.72→(41.73*)
$b_{eff,T\&G}$ (mm)	35.25	35.25
$b_{eff,num}$ (mm)	36.63	44.36

Table 5.5 comparison between both specimens

*Value obtained from applying EN1993-1-5

It is important to remark that the current specification does not take into account the non linear parameter. Numerical effective width ($b_{eff,num}$) of specimen SHSN11, which is close to austenitic stainless steel, fits well with both predicted by EN1993-1-4 and Gardner and Theofanous modification. Concerning Specimen SHSN31, which is close to carbon steel ($n=25$), its $b_{eff,num}$ is quite different and it may be calculated using reduction factor from EN1993-1-5.

5.4 RHSN11

Similar results are presented for RHSN11. Figure 5.8, 5.9 and 5.10 as well as table 5.6 and 5.7 present equivalent results from above.

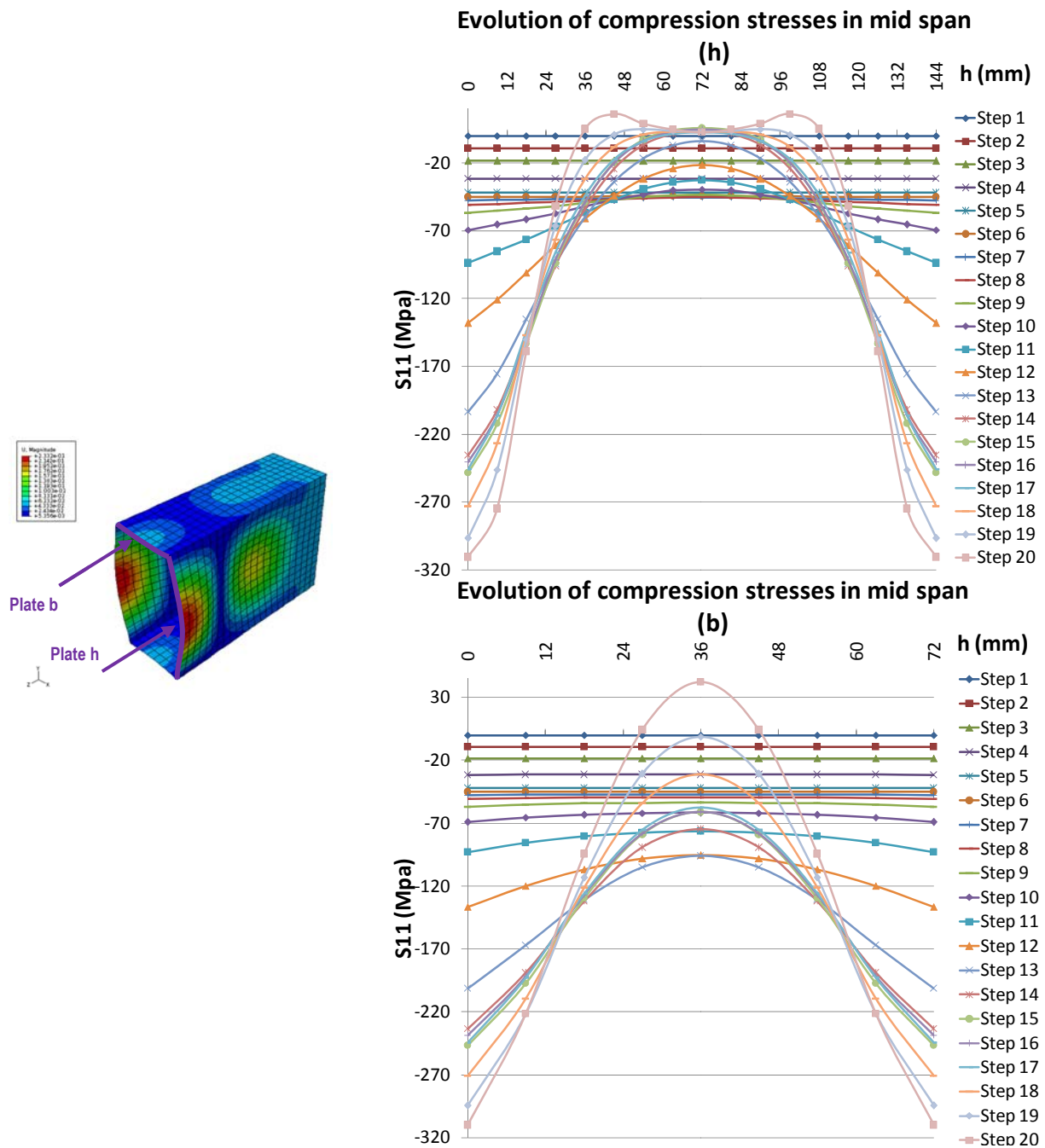


Figure 5.8 Compression stress evolution along both plates in RHSN11 section

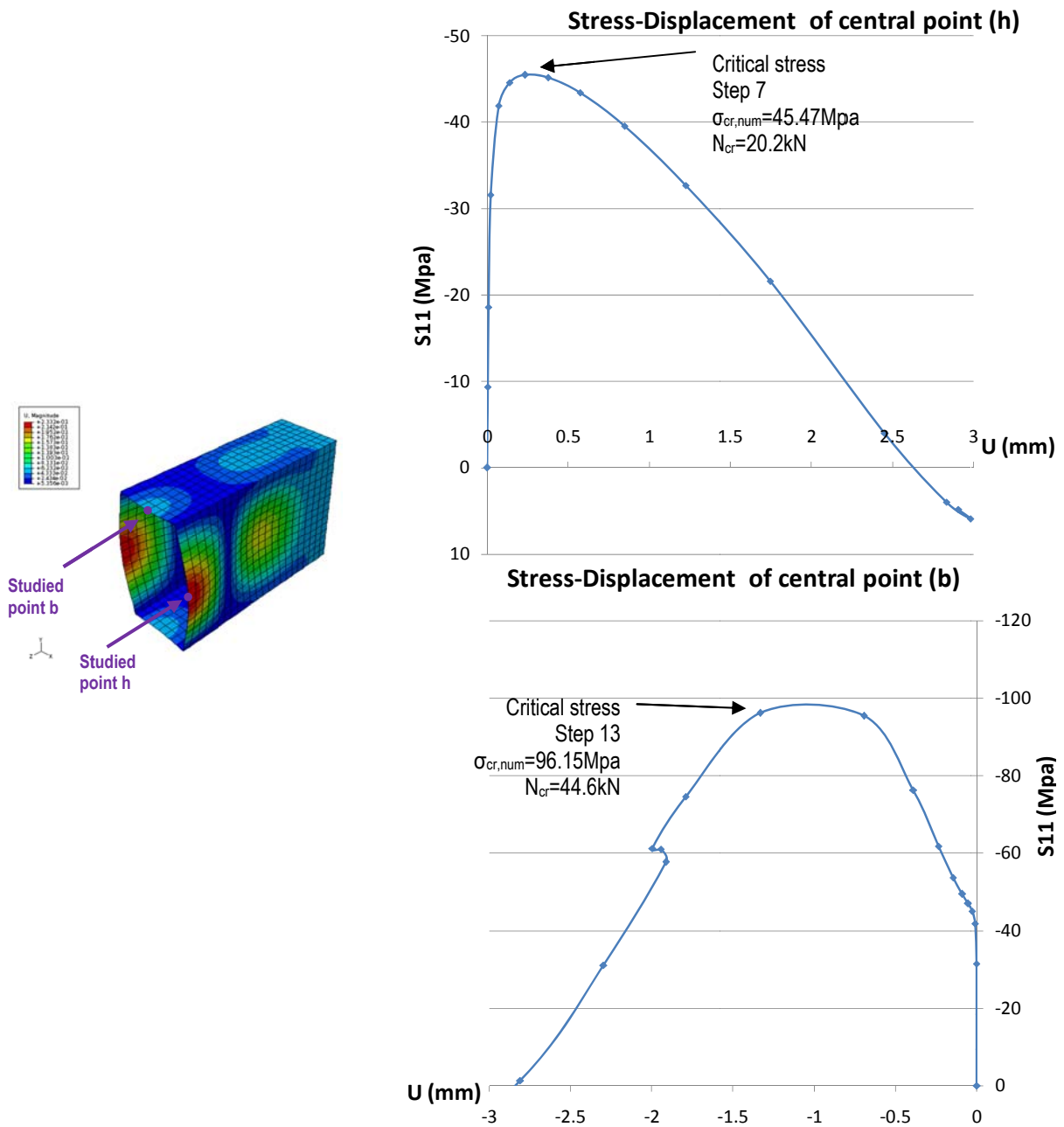


Figure 5.9 Evolution of stress-displacement of central points in RHSN11 section

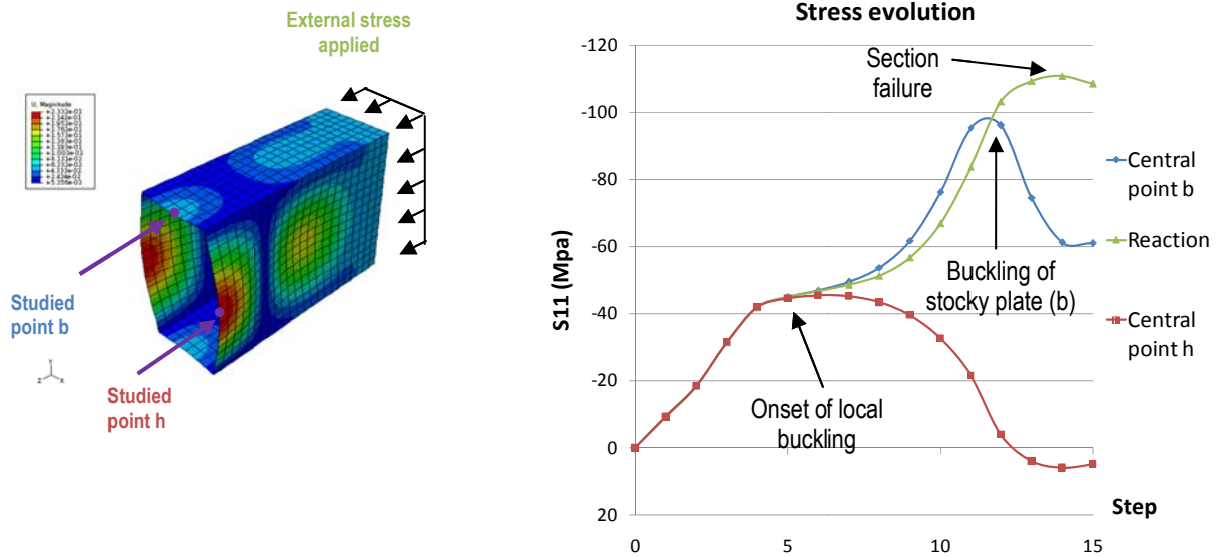


Figure 5.10 Evolution of stress-displacement of central points in RHSN11 section

The calculation process to obtain the effective width is slightly different in case of simply symmetric sections. Figure 5.11 shows the development of the effective cross section in double symmetric cross-sections and table 5.6 presents all the parameters necessary to calculate the real effective width (negative symbol means compression).

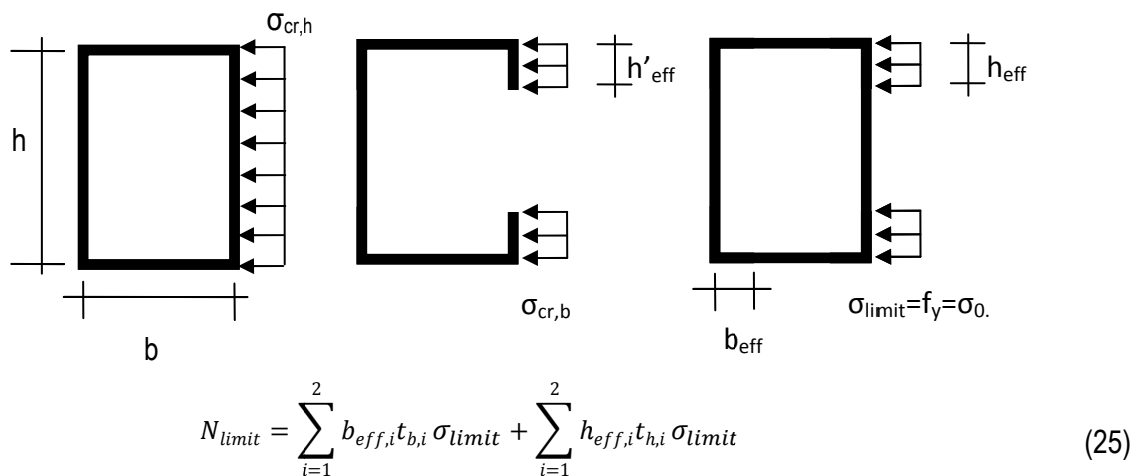


Figure 5.11 development of the effective width in simply symmetric cross-sections

The problem in simply symmetric cross-sections is that there are two unknown effective widths (h_{eff} and b_{eff}) but only one equation. However, the total effective area can be easily obtained:

$$A_{eff} = \frac{N_{limit}}{\sigma_{limit}} = \frac{48300}{296.811} = 162.73 \text{ mm}^2$$

Load step (see Figure 4.9)	Compression stress S11 (MPa)	External load (kN)	External stress (A=432mm ²)
17	-246.044	-46.8	-108.3
18	-273.25	-47.9	-110.88
19	-296.811 $\approx \sigma_{0.2} = \sigma_{limit}$	-48.3 = N_{limit}	-111.81
20	-310.79	-45.8	-106.02

Table 5.6 Compression stresses and external applied load in SHSN31

Table 5.7 compares the real effective area with those obtained from applying current EN1993-1-4 and Gardner and Theofanous (2008) proposal. Again, the new proposal formulae provide less conservative values.

In order to calculate both h_{eff} (effective height) and b_{eff} (effective width) of this RHS 72x144 it is proposed to simulate a SHS 72x72 with the same material, that it has already done, and use the obtained effective width to calculate the effective height according to equation 26.

$$h_{eff,RHS(bxh)} = A_{eff,RHS(bxh)} - 2 \cdot b_{eff,SHS(bxb)} \quad (26)$$

$$h_{eff,RHS(bxh)} = 44.735mm$$

This assumption can be checked by simulating a SHS 144x144 to obtain its effective width. It is expected to obtain a similar value (see table 5.7). However, this procedure does not take into account the greater restraint of the two longer faces.

	$A_{eff} (mm^2)$	b_{eff}	h_{eff}	$b_{eff} SHSN11$ (72x72)	h_{eff} (using eq.26)	$h_{eff} SHSN11$ (144x144)
Numerical ("real")	162.73	-	-	36.63	44.735	45.49
EN1993-1-4	139.05	33.72	35.81	-	-	-
Theofanous and Gardner (2008)	143.67	35.26	36.58	-	-	-

Table 5.7 comparison between effective areas

5.5 RHSN31

Similar results are presented for RHSN31. Figure 5.12, 5.13 and 5.14 as well as table 5.9 and 5.10 present equivalent results from above.

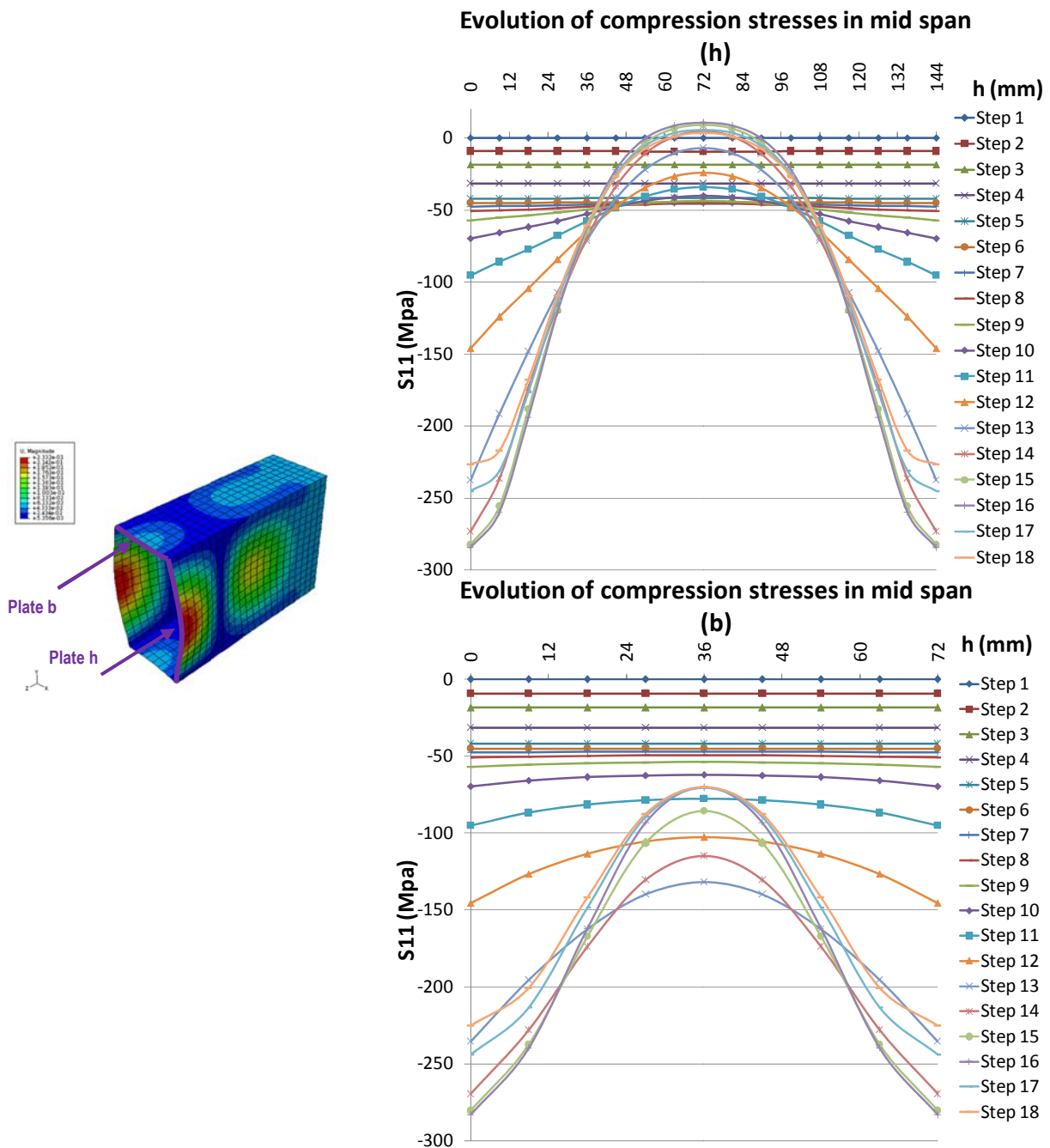


Figure 5.12 Compression stress evolution along both plates in RHSN31 section

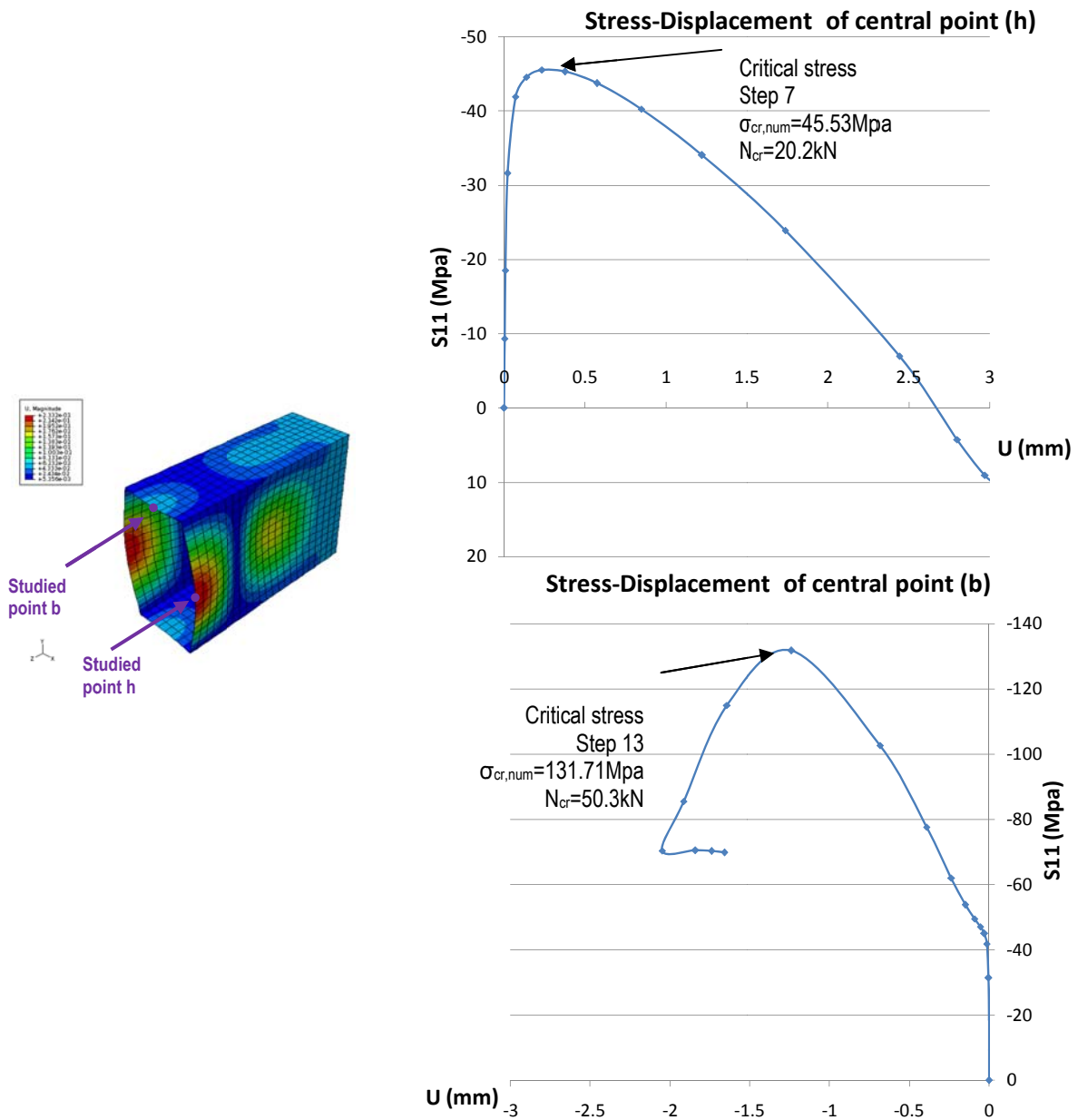


Figure 5.13 Evolution of stress-displacement of central points in RHSN31 section

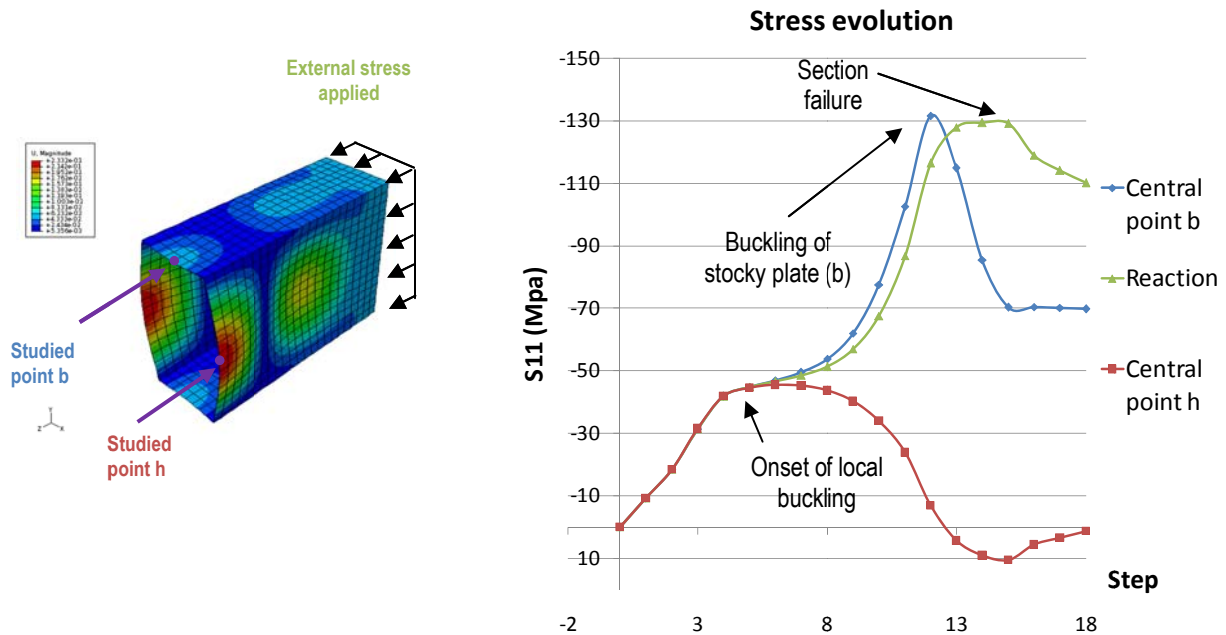


Figure 5.14 Evolution of stress-displacement of central points in RHSN31 section

Load step (see Figure 5.18)	Compression stress S11 (MPa)	External load (kN)	External stress (A=432mm ²)
13	237.75	-50.3	-116.44
14	-273.32	-55.3	-128.01
15	-282.74	-55.9	-129.39
16	-284.73 $\approx\sigma_{0.2}=\sigma_{limit}$	-55.8=N _{limit}	-129.16
17	-245.47	-51.4	-118.98

Table 5.9 Compression stresses and external applied load in SHSN31

	A _{eff} (mm ²)	b _{eff}	h _{eff}	b _{eff} SHSN31 (72x72)	h _{eff} (using eq.26)	h _{eff} SHSN31 (144x144)
Numerical ("real")	195.98	-	-	44.36	53.63	54.54
EN1993-1-4	139.05	33.72	35.81	-	-	-
Theofanous and Gardner (2008)	143.67	35.26	36.58	-	-	-

Table 5.10 comparison between effective areas

5.6 Comparison between RHSN11 and RHSN31

Results from both sections are presented herein. Table 5.11 summarizes the critical stress obtained from LEA analysis ($\sigma_{cr,LEA}$), the critical stress from theory assuming that the SHS is made up of four simply supported plates ($\sigma_{cr,theo}$) and the stress of the central point at the onset of local buckling from non-linear analysis ($\sigma_{cr,num}$). Moreover, three effective areas are presented. The first one is the result from applying the current EN1993-1-4 ($b_{eff,EN}$). The second one gives the effective area after considering Gardner and Theofanous (2008) modification. And the last one is the value obtained from equation (25).

	RHSN11	RHSN31
$\sigma_{cr,LEA}$ (MPa)	47.624	47.624
$\sigma_{cr,theo}$ (MPa)	34.87	34.87
$\sigma_{cr,num}$ (MPa)	45.47	45.53
A _{eff,EN} (mm)	139.05	139.05 \rightarrow (174.25*)
A _{eff,T&G} (mm)	143.67	143.67
A _{eff,num} (mm)	162.73	195.97

Table 5.11 comparison between both specimens

*Value obtained from applying EN1993-1-5

5.7 Summary of the results

Table 5.12 summarizes all the results from the four sections studied.

	$\sigma_{cr,LEA}$ (MPa)	$\sigma_{cr,num}$ (MPa)	$N_{cr,num}$ (kN)	$N_{u,num}$ (kN)	$N_{u,EN}$ (kN)	$N_{u,T\&G}$ (kN)	$b_{eff,num}$ (mm)	$A_{eff,num}$ (mm ²)	A_g (mm ²)
SHSN11	151	113.59	36.8	43.5	40.46	42.31	36.73	146.53	288
SHSN31	151	128.84	42.7	49.7	40.46	42.31	44.36	177.46	288
RHSN11	47.624	45.47	20.2	48.3	41.71	43.1	44.73*	162.73	432
RHSN31	47.624	45.53	20.2	55.9	41.71	43.1	53.615*	195.95	432

Table 4.12 Summary of the results

*Value obtained from applying Eq.27

Analyzing the results can be concluded:

- Current specification does not take into account the non linear parameter.
- The effective width is sensitive to the non-linear parameter.
- Effective widths of N1 sections (n=5; close to austenitic) are better predicted by EN1993-1-4 and Gardner and Theofanous (2008) proposal.
- Effective widths of N3 sections (n=25; close to carbon) are better predicted by EN1993-1-5.
- Gardner and Theofanous (2008) proposal fits better (less conservative) to numerical results than current specifications

References

EN 1990 (2004)

Eurocode 0 (2004): Basis of structural design.

EN 1993-1-1 (2006)

EN 1993-1-1. Eurocode 3 (2006): Design of steel structures - Part 1.3: General rules and rules for buildings.

EN 1993-1-3 (2006)

EN 1993-1-3. Eurocode 3 (2006): Design of steel structures - Part 1.3: General rules - Supplementary rules for cold-formed members and sheeting.

EN 1993-1-4 (2006)

EN 1993-1-4. Eurocode 3 (2006): Design of steel structures - Part 1.4: General rules - Supplementary rules for stainless steel. CEN.

EN 1993-1-5 (2006)

EN 1993-1-5. Eurocode 3 (2006): Design of steel structures - Part 1.5: General rules – Plated structural elements. CEN.

Euro Inox (2006)

Euro Inox (2006). Design Manual for Structural Stainless Steel. 3rd Edition.

Gardner and Cruise (2009)

Gardner L and Cruise RB. Modeling of Residual Stresses in Structural Stainless Steel Sections. Journal of Structural Engineering 2009; 135(1):42-53.

Gardner and Nethercot (2004a)

Gardner L, Nethercot DA. Experiments on stainless steel hollow sections—Part 2: Member behaviour of columns and beams. Journal of Constructional Steel Research 2004; 60(9): 1319-1332.

Gardner and Nethercot (2004b)

Gardner L, Nethercot DA. Numerical modeling of stainless steel structural components—A consistent approach. J Struct Eng, ASCE 2004; 130(10): 1586–601.

Gardner and Theofanous (2008)

Gardner, L. & Teofanous, M. Discrete and continuous treatment of local buckling in stainless steel elements. Journal of Constructional Steel Research 2008; 64: 1207-1216.

Gardner and Saliba (2011)

Gardner, L. and Saliba, N. (2011). Experimental study of lean duplex stainless steel. Eurosteel 2011. Budapest, Hungary.

Kuwamura (2003)

Kuwamura, H. (2003). Local buckling of thin-walled stainless steel members. Steel Structures (2003). Vol. 3(3), 191–201.

Rasmussen et al. (2003)

Rasmussen KJR, Burns T, Bezkorovainy P and Bambach MR. Numerical modelling of stainless steel plates in compression. Journal of Constructional Steel Research (2003); 59(11):1345-1362.

Theofanous and Gardner (2009)

Theofanous, M. & Gardner, L. Testing and numerical modelling of lean duplex stainless steel hollow section columns. *Engineering Structures* 2009; 31(12) 3047-3058.

Theofanous (2010)

Theofanous, M. Studies of the Nonlinear Response of Stainless Steel Structures. PhD Thesis. Imperial College London

Yu (2000)

Yu WW. Cold-formed steel design. 3rd ed. New York: Wiley.

Annex A

A. Numerical database extension

Once the results have been analyzed, it seems that more numerical specimens should be simulated in order to cover more slender ratios specially those situated between the EN1993-1-4 class 3 limit (30.7ϵ) and the EN1993-1-5 (42ϵ).

Four new cross sections made up with the same materials have been calculated using ABAQUS plug-in which means that 24 members have been added to the first numerical database. All those new specimens were square hollow sections and their dimensions were 30x30x1, 40x40x1, 80x80x3 and 100x100x3. The amplitude of the initial geometric imperfection was predicted using equation 1.

Again, they have been labelled in order to be identified easily, see Table A1. The first letter, which is always an S, is an abridged version of SHS to make a distinction from the first square hollow sections followed by the type of material. The last digits are the width and thickness of the section.

	Cross section	Material	Width and thickness
	S	N1, N2, N3, F1, F2, F3	301 401 803 1003
SN2803 →	S	N2	803

Table A1 Labelling of new sections

Figures A14.7 to A34.9 show the influence of the non-linear parameter, the $\sigma_{0.2}$ value and the σ_u value and Tables A24.9, A34.10 and A44.11 summarize the most relevant values from LEA analysis, from applying EN1993-1-4 and from new proposal formulae by Gardner and Theofanous respectively.

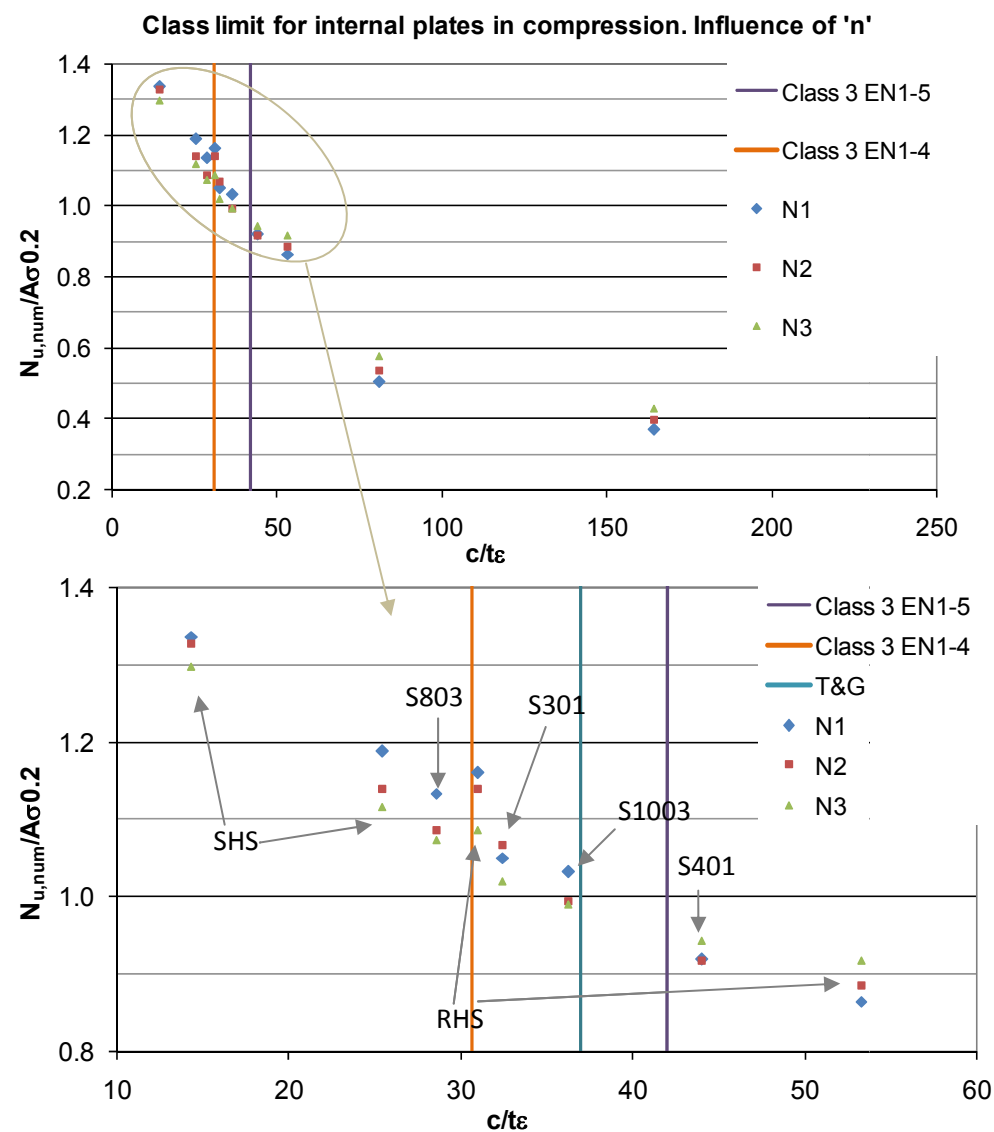
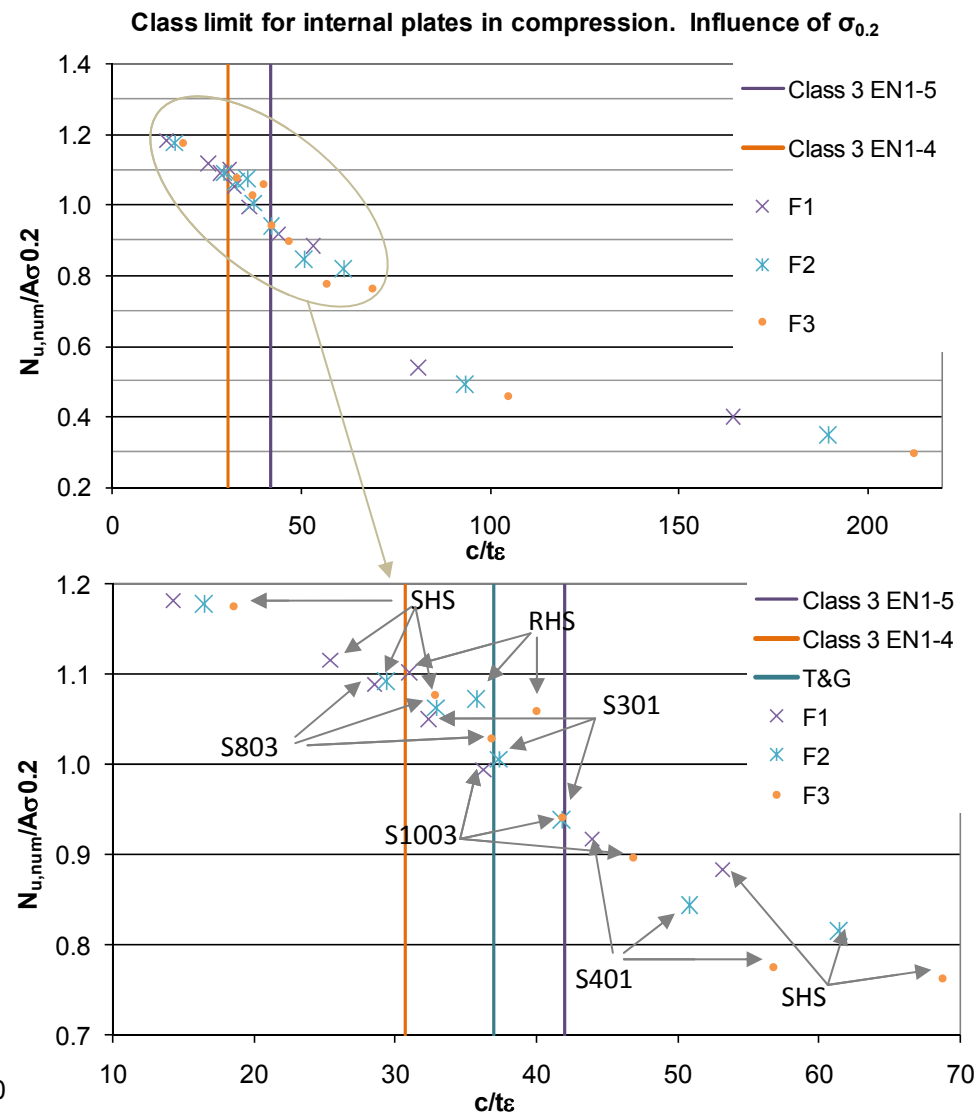


Figure 4.7 Influence of the non linear parameter


Figure 4.8 Influence of the $\sigma_{0.2}$ value

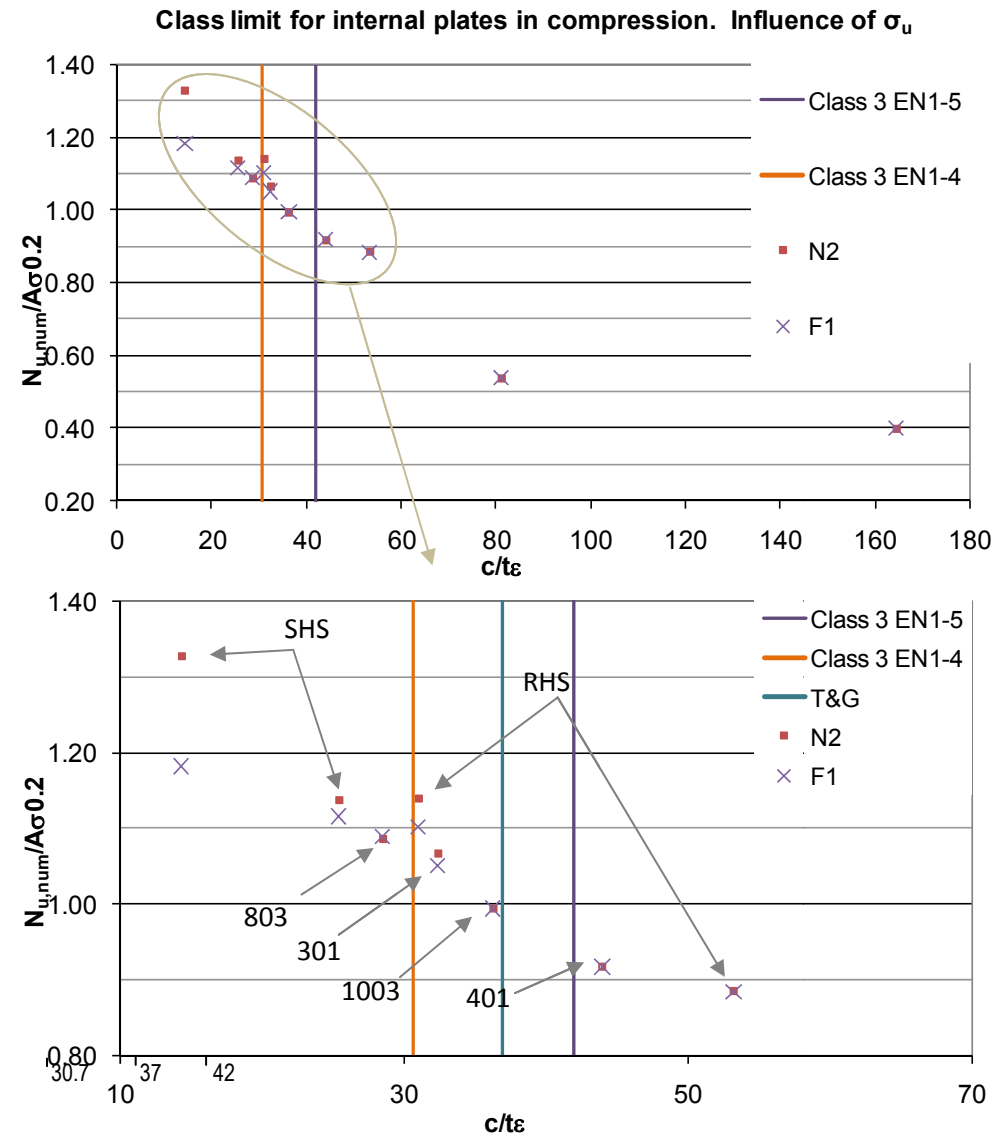


Figure 4.9 Influence of the σ_u value

Specimen	ε	c/t ε	D&W	$\sigma_{cr,LEA}$ (MPa)	$N_{cr,LEA}$ (kN)	Section class	D&W $N_{ult,num}$ (kN)	$A\sigma_{0.2}$ (kN)	D&W $N_{ult,num}/A\sigma_{0.2}$
SN1301	0.86	32.42	0.009	854.66	102.56	4	37.80	36.0	1.0500
SN2301	0.86	32.42	0.009	854.66	102.56	4	38.40	36.0	1.0667
SN3301	0.86	32.42	0.009	854.66	102.56	4	36.70	36.0	1.0194
SF1301	0.86	32.42	0.009	854.66	102.56	4	37.80	36.0	1.0500
SF2301	0.75	37.43	0.011	854.66	102.56	4	48.30	48.0	1.0063
SF3301	0.67	41.85	0.014	854.66	102.56	4	56.50	60.0	0.9417
SN1401	0.86	44.00	0.015	484.93	77.59	4	44.10	48.0	0.9188
SN2401	0.86	44.00	0.015	484.93	77.59	4	44.00	48.0	0.9167
SN3401	0.86	44.00	0.015	484.93	77.59	4	45.20	48.0	0.9417
SF1401	0.86	44.00	0.015	484.93	77.59	4	44.00	48.0	0.9167
SF2401	0.75	50.80	0.020	484.93	77.59	4	54.00	64.0	0.8438
SF3401	0.67	56.80	0.025	484.93	77.59	4	62.10	80.0	0.7763
SN1803	0.86	28.56	0.020	1076.43	1033.38	3	326.40	288.0	1.1333
SN2803	0.86	28.56	0.020	1076.43	1033.38	3	312.50	288.0	1.0851
SN3803	0.86	28.56	0.020	1076.43	1033.38	3	309.30	288.0	1.0740
SF1803	0.86	28.56	0.020	1076.43	1033.38	3	313.50	288.0	1.0885
SF2803	0.75	32.98	0.027	1076.43	1033.38	4	408.30	384.0	1.0633
SF3803	0.67	36.87	0.034	1076.43	1033.38	4	494.10	480.0	1.0294
SN11003	0.86	36.28	0.032	694.84	833.81	4	371.60	360.0	1.0322
SN21003	0.86	36.28	0.032	694.84	833.81	4	357.60	360.0	0.9933
SN31003	0.86	36.28	0.032	694.84	833.81	4	356.60	360.0	0.9906
SF11003	0.86	36.28	0.032	694.84	833.81	4	357.70	360.0	0.9936
SF21003	0.75	41.89	0.042	694.84	833.81	4	449.90	480.0	0.9373
SF31003	0.67	46.83	0.053	694.84	833.81	4	537.80	600.0	0.8963

Table 4.9 Results from LEA analysis

Specimen	ε	$c/t\varepsilon$	Section class	A_{tot} (mm ²)	$\sigma_{cr, theo}$ (MPa)	λ	ρ	$A_{eff, tot}$ (mm ²)	$N_{ult, num}$ (kN)	$A\sigma_{0.2}$ (kN)	$N_{ult, EN}$ (kN)	$N_{ult, num}/A\sigma_{0.2}$	$N_{ult, EN}/A\sigma_{0.2}$	$N_{ult, num}/N_{ult, EN}$
SF11003	0.86	32.42	4	1200	694.840	0.6790	0.8659	1039.03	37.80	36.0	311.71	0.9936	0.8659	1.1475
SF1301	0.86	32.42	4	120	854.667	0.6111	0.9286	111.43	38.40	36.0	33.43	1.0500	0.9286	1.1307
SF1401	0.86	32.42	4	160	484.933	0.8148	0.7592	121.47	36.70	36.0	36.44	0.9167	0.7592	1.2074
SF1803	0.86	32.42	3	960	1076.433	0.5432	0.9976	957.69	37.80	36.0	287.31	1.0885	0.9976	1.0912
SF21003	0.75	37.43	4	1200	694.840	0.7840	0.7813	937.58	48.30	48.0	375.03	0.9373	0.7813	1.1996
SF2301	0.67	41.85	4	120	854.667	0.7056	0.8430	101.16	56.50	60.0	40.47	1.0063	0.8430	1.1936
SF2401	0.86	44.00	4	160	484.933	0.9408	0.6793	108.69	44.10	48.0	43.48	0.8438	0.6793	1.2420
SF2803	0.86	44.00	4	960	1076.433	0.6272	0.9131	876.57	44.00	48.0	350.63	1.0633	0.9131	1.1645
SF31003	0.86	44.00	4	1200	694.840	0.8766	0.7180	861.64	45.20	48.0	430.82	0.8963	0.7180	1.2483
SF3301	0.86	44.00	4	120	854.667	0.7889	0.7777	93.33	44.00	48.0	46.66	0.9417	0.7777	1.2108
SF3401	0.75	50.80	4	160	484.933	1.0519	0.6210	99.35	54.00	64.0	49.68	0.7763	0.6210	1.2501
SF3803	0.67	56.80	4	960	1076.433	0.7012	0.8467	812.83	62.10	80.0	406.42	1.0294	0.8467	1.2157
SN11003	0.86	28.56	4	1200	694.840	0.6790	0.8659	1039.03	326.40	288.0	311.71	1.0322	0.8659	1.1921
SN1301	0.86	28.56	4	120	854.667	0.6111	0.9286	111.43	312.50	288.0	33.43	1.0500	0.9286	1.1307
SN1401	0.86	28.56	4	160	484.933	0.8148	0.7592	121.47	309.30	288.0	36.44	0.9188	0.7592	1.2101
SN1803	0.86	28.56	3	960	1076.433	0.5432	0.9976	957.69	313.50	288.0	287.31	1.1333	0.9976	1.1361
SN21003	0.75	32.98	4	1200	694.840	0.6790	0.8659	1039.03	408.30	384.0	311.71	0.9933	0.8659	1.1472
SN2301	0.67	36.87	4	120	854.667	0.6111	0.9286	111.43	494.10	480.0	33.43	1.0667	0.9286	1.1487
SN2401	0.86	36.28	4	160	484.933	0.8148	0.7592	121.47	371.60	360.0	36.44	0.9167	0.7592	1.2074
SN2803	0.86	36.28	3	960	1076.433	0.5432	0.9976	957.69	357.60	360.0	287.31	1.0851	0.9976	1.0877
SN31003	0.86	36.28	4	1200	694.840	0.6790	0.8659	1039.03	356.60	360.0	311.71	0.9906	0.8659	1.1440
SN3301	0.86	36.28	4	120	854.667	0.6111	0.9286	111.43	357.70	360.0	33.43	1.0194	0.9286	1.0978
SN3401	0.75	41.89	4	160	484.933	0.8148	0.7592	121.47	449.90	480.0	36.44	0.9417	0.7592	1.2403

Table 4.10 Stub column results in new database extension. Class limits assessment according to EN1993-1-4

Specimen	ε	c/t ε	Section class	New Section class	ρ	New ρ	$A_{eff,tot}$ (mm ²)	New $A_{eff,tot}$ (mm ²)	$N_{ult,num}$ (kN)	$N_{ult,EN}$ (kN)	$N_{ult,new}$ (kN)	$N_{ult,num}/N_{ult,EN}$	$N_{ult,num}/N_{ult,new}$
SF11003	0.86	32.42	4	3	0.8659	0.9656	1039.03	1158.77	357.70	311.71	347.63	1.1475	1.0290
SF1301	0.86	32.42	4	1	0.9286	1.0000	111.43	120.00	37.80	33.43	36.00	1.1307	1.0500
SF1401	0.86	32.42	4	4	0.7592	0.8285	121.47	132.56	44.00	36.44	39.77	1.2074	1.1064
SF1803	0.86	32.42	3	1	0.9976	1.0000	957.69	960.00	313.50	287.31	288.00	1.0912	1.0885
SF21003	0.75	37.43	4	4	0.7813	0.8562	937.58	1027.38	449.90	375.03	410.95	1.1996	1.0948
SF2301	0.67	41.85	4	4	0.8430	0.9354	101.16	112.25	48.30	40.47	44.90	1.1936	1.0757
SF2401	0.86	44.00	4	4	0.6793	0.7313	108.69	117.01	54.00	43.48	46.80	1.2420	1.1538
SF2803	0.86	44.00	4	1	0.9131	1.0000	876.57	960.00	408.30	350.63	384.00	1.1645	1.0633
SF31003	0.86	44.00	4	4	0.7180	0.7779	861.64	933.48	537.80	430.82	466.74	1.2483	1.1522
SF3301	0.86	44.00	4	4	0.7777	0.8516	93.33	102.20	56.50	46.66	51.10	1.2108	1.1057
SF3401	0.75	50.80	4	4	0.6210	0.6625	99.35	106.00	62.10	49.68	53.00	1.2501	1.1716
SF3803	0.67	56.80	4	3	0.8467	0.9402	812.83	902.64	494.10	406.42	451.32	1.2157	1.0948
SN11003	0.86	28.56	4	3	0.8659	0.9656	1039.03	1158.77	371.60	311.71	347.63	1.1921	1.0690
SN1301	0.86	28.56	4	1	0.9286	1.0000	111.43	120.00	37.80	33.43	36.00	1.1307	1.0500
SN1401	0.86	28.56	4	4	0.7592	0.8285	121.47	132.56	44.10	36.44	39.77	1.2101	1.1089
SN1803	0.86	28.56	3	1	0.9976	1.0000	957.69	960.00	326.40	287.31	288.00	1.1361	1.1333
SN21003	0.75	32.98	4	3	0.8659	0.9656	1039.03	1158.77	357.60	311.71	347.63	1.1472	1.0287
SN2301	0.67	36.87	4	1	0.9286	1.0000	111.43	120.00	38.40	33.43	36.00	1.1487	1.0667
SN2401	0.86	36.28	4	4	0.7592	0.8285	121.47	132.56	44.00	36.44	39.77	1.2074	1.1064
SN2803	0.86	36.28	3	1	0.9976	1.0000	957.69	960.00	312.50	287.31	288.00	1.0877	1.0851
SN31003	0.86	36.28	4	3	0.8659	0.9656	1039.03	1158.77	356.60	311.71	347.63	1.1440	1.0258
SN3301	0.86	36.28	4	1	0.9286	1.0000	111.43	120.00	36.70	33.43	36.00	1.0978	1.0194
SN3401	0.75	41.89	4	4	0.7592	0.8285	121.47	132.56	45.20	36.44	39.77	1.2403	1.1366

Table 4.11 Stub column results in SHS according to the new proposal formulae by Theofanous and Gardner (2008)



Structural Applications of Ferritic Stainless Steels (SAFSS)

Work package 2.2b. Preliminary FEM study: Web crippling

Itsaso Arrayago

Esther Real

Marina Bock

Enrique Mirambell

Departament d'Enginyeria de la Construcció,
Universitat Politècnica de Catalunya



**UNIVERSITAT POLITÈCNICA
DE CATALUNYA**

Project name: Structural Applications of Ferritic Stainless Steels
Project's short name: SAFSS

Change log:

Version	Date	Status (draft/proposal/updated/ to be reviewed /approved)	Author(s)	Remarks
0.1	25.08.11	Final	Itsaso Arrayago et al.	

Distribution: Project group

EUROPEAN COMMISSION

Research Programme of The Research Fund for Coal and Steel-Steel RTD

Title of Research Project:	Structural Application of Ferritic Stainless Steels (SAFSS)
Executive Committee:	TGS8
Contract:	RFSR-CT-2010-00026
Commencement Date:	July 01, 201
Completion Date:	June 30, 2013
Beneficiary:	Universitat Politècnica de Catalunya (UPC)
Research Location:	Universitat Politècnica de Catalunya C/ Jordi Girona, 31 08034-Barcelona España
Project leader:	Esther Real
Report authors:	Arrayago, I., Real, E., Bock, M., Mirambell, E.

Contents

1. Introduction	4
2. Literature review.....	4
3. Numerical model	5
3.1. Material models.....	6
3.2. Transformation for Abaqus solver	7
3.3. Element type	7
3.4. Mesh size.....	7
3.5. Initial geometric imperfections	8
3.6. Numerical model simplification.....	8
3.7. Numerical model calibration.....	9
3.7.1 General.....	9
3.7.2 Eurocode 3-1-3.....	10
3.7.3 FE assessment and results	11
4. Parametric study	14
4.1. Cross sections	14
4.2. Materials	14
4.3. Initial geometrical imperfections.....	15
4.4. Numerical results	15
4.4.1 Internal support test.....	15
4.4.2 End support test	20
5. Comparative analysis	25
5.1. Initial imperfection magnitude analysis	25
5.2. Stainless-steel: material analysis	26
5.3. Internal bend radius analysis	27
5.4. Effective bearing length analysis.....	28
6. Conclusions.....	28
7. References.....	29

1. Introduction

Cold-formed steel members are widely used due to their high resistance/weight ratio compared with other structural materials. They usually show high height-to-thickness and width-to-thickness ratio values, so a special care has to be taken in the local instability phenomena. Web crippling is one of these instabilities, where the web buckles due to concentrated transverse forces.

On the other hand, stainless steels show, in addition to good mechanical properties, an excellent corrosion resistance in most environments. The price of ferritic stainless steel is stable due to its low nickel content whilst still maintaining good mechanical properties. Consequently, ferritic stainless steel cold formed members have a promising future as an alternative to the austenitic ones. As the existing design standards for cold formed members are based on carbon steel and do not cover ferritic stainless steel, new projects are being carried out to develop new design guidance taking into account stainless steel non-linear behavior, in order to achieve efficient design techniques.

This work is part of one of these projects, in which web crippling is studied for stainless steel members in general, and for ferritic ones in particular. The applicability of existing guidance has been checked for stainless steel members, and a new expression has been proposed for this type of materials.

The new European research project "*Structural Applications in Ferritic Stainless Steel*" in progress, is intended to provide the necessary information to develop new design guidelines for the ferritic stainless steel involving both aspects of the complex material behavior, as well as the cold formed element's aspects. The Universitat Politècnica de Catalunya (UPC) and the VTT Technical Research Centre of Finland are the partners responsible for work on WP2, *Structural performance of steel members*. The tasks that are being developed at UPC focus mainly on cross section stability (plate buckling and web crippling).

2. Literature review

The theoretical analysis of web crippling under concentrated loading condition is very complex because it involves a large number of factors. Due to these difficulties, most of the research carried out mainly in carbon steel and therefore predictions, as well as recommendations, have been based on experimental results. Hence, the web crippling design equations are empiric.

The web crippling design rules in specifications for stainless steel structures are adopted from the specifications for carbon steel structures. The web crippling design rules for stainless steel can be found in EN 1993-1-4 [1] for stainless steel members, referred to the EN 1993-1-3 [2] for steel cold formed members.

Other specifications for the design of cold-formed stainless steel structural members are the American Society of Civil Engineers Specification [3] and the Australian/New Zealand Standard [4].

Because of the many factors influencing the ultimate web crippling strength of cold-formed steel sections, the majority of research has been experimental, but also finite element modeling has been used to model web crippling behavior. Some authors have also created so-called mechanical models that could be used to produce more accurate and descriptive design methods for web crippling [5, 6]. Although promising results have been achieved, especially at the University of Eindhoven in the Netherlands [5, 6], these methods have not yet been incorporated in design practice [7].

The current design methods are based on curve-fitting of experimental results, which has been criticized for two main reasons [8]: "(i) the rules are strictly confined to the range for which they have been proven, and (ii) it is often difficult to ascertain the engineering reasoning behind the different parts of the rather complex equations".

A great amount studies involving web crippling strength of carbon steel have been carried out. The first research on web crippling was conducted in Cornell University by Winter and Pian in 1946. Since then, several researchers have carried out comprehensive experimental studies on different sections and types of loading [9–17].

A lack of studies involving web crippling strength of stainless steel comparing with carbon steel can be noticed. The first web crippling studies carried out in stainless steel found in the literature were performed by Korvink et al. [18] in the Rand Afrikaans University.

Other experimental investigations were carried out by Talja and Salmi [19] and Talja and Zilli [20] for cold worked austenitic stainless steel members analyzing the behavior of different cross sections and comparing experimental and numerical simulations with EN 1993-1-4 [1].

Since 2006, Zhou and Young have been carrying out amount of tests on cold formed stainless steel members subjected to web crippling [21, 24]. Using the tests, Zhou and Young [25] proposed a new design procedure derived through a combination of theoretical and empirical analysis for cold formed stainless steel RHS, SHS sections under web crippling.

A review of all studies dealing with web crippling of cold-formed stainless steel tubular sections performed by Zhou and Young can be founded in Zhou and Young [26].

3. Numerical model

The Finite Element Method (FEM) is presented as a powerful tool for analyzing complex phenomena of instability as web crippling, in which is important to conduct experiments to gather information. The use of numerical models allows the realization of numerous modeling of these experimental tests with a far lower cost than actual ones. In this study, numerical models have been carried out using Abaqus finite element analysis program [27], with the help of a plug-in developed at VTT Technical Research Centre of Finland. The plug-in generates the model and allows an easy definition of all the needed parameters.

The implemented web crippling tests are the end one flange loading (EOF) and the interior one flange loading (IOF) conditions. The parameters involved in these tests are: the element length, the bearing length of (either the length of the metal plate that enters the load in the case of internal loading, or the length of the support in the end loading condition), and the dimensions of the studied cross section. Schemes of these tests are shown in Figure 1. Figures 2 and 3 show the real configuration and model simplification for the two web crippling tests on the most important sections: under the load and at the support.

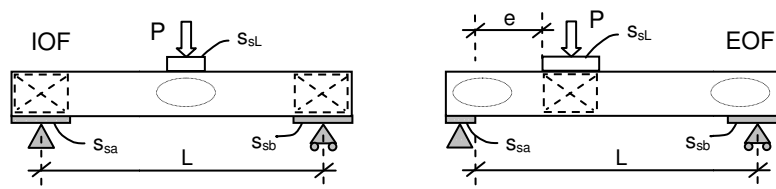


Figure 1. Web crippling IOF and EOF tests analyzed

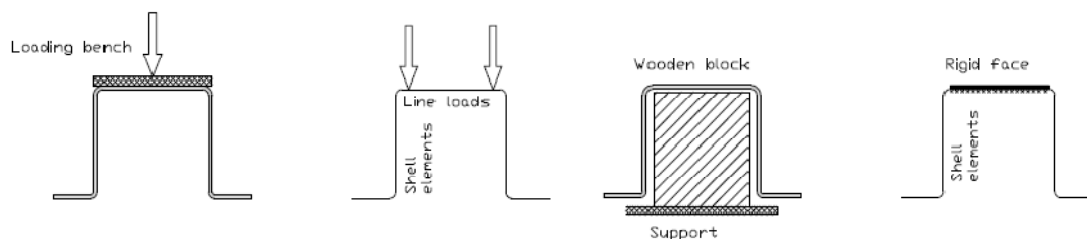


Figure 2. Real configuration and model simplification under the load and at the support for IOF tests

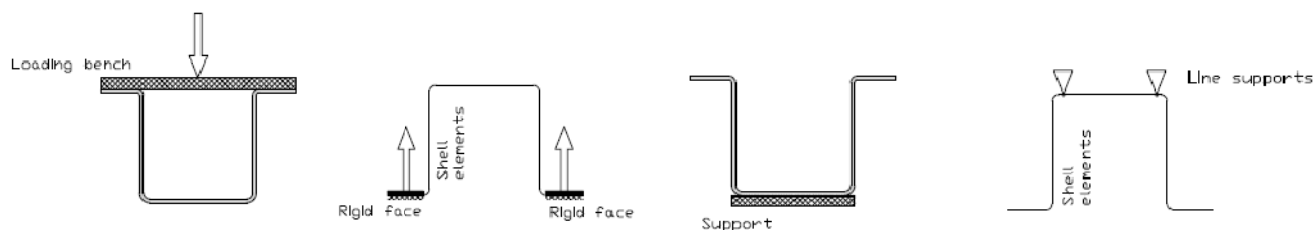


Figure 3. Real configuration and model simplification under the load and at the support for EOF tests

In the case of internal support tests, interaction between the local transverse force and the bending moment has to be considered and for this comparison the M_R moment resistance value is needed. This M_R value is taken as the measured moment resistance of the 4-point-bending test moment. The configuration of the bending moment test is shown on Figure 4.

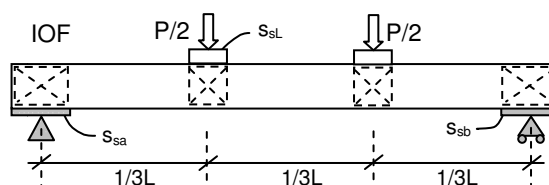


Figure 4. Bending moment test configuration

3.1. Material models

Several material models have been developed during the last decades mostly originated from Ramberg-Osgood [28] law. Mirambell and Real [29] model was developed from Ramberg-Osgood formulation, including strain hardening effect and is able to describe the material behaviour more precisely for strains larger than 0,2%. Rasmussen's study [20] extends Mirambell & Real model reducing its original six parameters to three. Gardner [31] proposed another modification of Mirambell & Real material model, where the second part of Ramberg-Osgood curve passes through 1,0% proof stress instead of ultimate stress. This approach can also include compressive behaviour.

The material model used in the present study is based on Rasmussen's modification [30] of Mirambell and Real model [29], which is also included in EN 1993-1-4, Annex C.

$$\varepsilon = \begin{cases} \frac{\sigma}{E_0} + 0,002 \left(\frac{\sigma}{\sigma_{0,2}} \right)^n & \text{for } \sigma \leq \sigma_{0,2} \\ \frac{\sigma - \sigma_{0,2}}{E_{0,2}} + \varepsilon_u \left(\frac{\sigma - \sigma_{0,2}}{\sigma_u - \sigma_{0,2}} \right)^m + \varepsilon_{0,2} & \text{for } \sigma > \sigma_{0,2} \end{cases} \quad (\text{Eq. 1})$$

Where $\varepsilon_u = 1 - \frac{\sigma_{0,2}}{\sigma_u}$, $m = 1 + 3,5 \frac{\sigma_{0,2}}{\sigma_u}$

3.2. Transformation for Abaqus solver

According to the Abaqus documentation, nominal (engineering) stress is recalculated to true stress and nominal (engineering) strain to logarithmic (true) strain using following equations:

$$\sigma_{true} = \sigma_{nom} (1 + \varepsilon_{nom}) \quad (\text{Eq. 2})$$

$$\varepsilon_{true} = \ln(1 + \varepsilon_{nom}) - \frac{\sigma_{true}}{E} \quad (\text{Eq. 3})$$

3.3. Element type

Linear S4R and quadratic S9R5 elements are provided by Abaqus for cold-formed steel numerical simulations. The former ones are used in Rasmussen et al. [32] and Ellobody and Young [33] for their simple application and because they are also included in Abaqus/GUI interface, while the latter ones are preferred in recent studies such as Jandera et al. [34], Rossi et al. [35] and Ashraf et al. [36] as slightly more accurate and much more robust. Quadratic elements also offer more flexibility when modeling rounded corners avoiding large aspect ratios, so they have been chosen in this study.

3.4. Mesh size

For the definition of the number of elements to be used when modeling each of the elements, it should be noted that the greater number of elements employed, the better results are obtained. However, the computational cost that this implies (memory and computing time required) conducts to a study on the optimal mesh, reaching a compromise between the accuracy of the results and resources spent in obtaining it. The method of obtaining the proper mesh goes through a convergence analysis, shown in Figure 2, from which it follows that the optimal mesh is one containing about 40 elements.

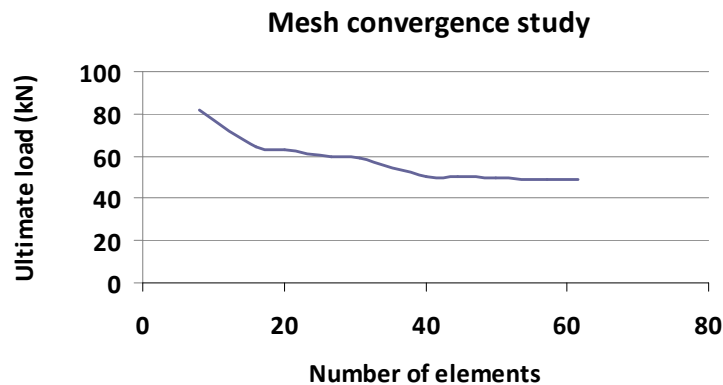


Figure 5. Mesh convergence study

3.5. Initial geometric imperfections

Geometric imperfections are present in all structural members, so they must be included in the numerical models. Local imperfections dominate the element behavior for members with small length, as shown in Figure 5. Therefore, as the elements to be analyzed are relatively short, and due to the local nature of the studied phenomenon, global imperfections have been neglected, focusing the study on the influence of the local ones.

There are several ways of modeling geometrical imperfections. In case of simulating the experiment, usually the real initial imperfection data are inserted into a model either in form of the whole deformed geometry or as an amplification of an idealized imperfect shape. For the modeling of a cold-formed member, the idealized imperfection distribution is usually obtained from linear elastic analysis (LEA). In this case the geometric imperfections are simulated using the first buckling mode, as shown in Figure 6.

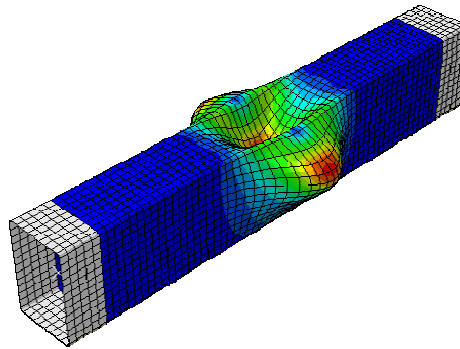


Figure 6. First buckling mode for a RHS

As proposed in Theofanous and Gardner [37] three values of local imperfection amplitude were considered in the non-linear analyses: 1/10 and 1/100 of the cross sectional thickness and the imperfection amplitude obtained from the model of Dawson and Walker [38] as adapted by Gardner and Nethercot [39] for stainless steels, which is defined by equation 4.

$$w_0 / t = 0,023 \cdot (\sigma_{0,2} / \sigma_{cr}) \quad (\text{Eq. 4})$$

where w_0 is the initial imperfection amplitude; t the plate thickness; $\sigma_{0,2}$ the material 0.2% proof stress and σ_{cr} the elastic buckling stress of the plated elements, assuming simply supported conditions.

3.6. Numerical model simplification

Several simplifications have been made in the numerical model in order to increase the computational efficiency. These simplifications are:

- Residual stresses from cold-working and press-braking are not included.
- Enhanced corner properties are neglected.
- Rounded corners are neglected.

3.7. Numerical model calibration

3.7.1 General

To ensure that the numerical results are representative, the model should be calibrated by comparing the experimental test results on certain elements and the ultimate loads predicted by the numerical models.

As there have been no experimental tests, results have been extracted from published tests carried out by other authors. The calibration was based on the work of Gardner et al. [40] for RHS and SHS sections of austenitic stainless steel and interior loading condition and on the results of an experimental campaign carried out by VTT [41] for ferritic stainless steel top hat sections, under interior and end loading conditions.

The studied sections in the calibration of the numerical model are shown in Table 1 and Figure 6, and Table 2 shows the mechanical properties of these elements.

Test	Specimen	b (mm)	h (mm)	c (mm)	R (mm)	r (mm)	r _m (mm)	t (mm)	L (mm)	Source
External support	SHS_ES	80.04	80	-	5.2	2.9	4.03	1.97	400	[41]
	TH_10_ES	72.85	71.05	24.15	2.5	0.8	1.65	0.99	399	[41]
	TH_15_ES	70.47	70.84	24.03	3	0.8	1.9	1.53	399	[41]
	TH_20_ES	69.65	70.52	23.98	4	0.8	2.4	1.99	399	[41]
	TH_30_ES	68.86	69.39	23.74	6.5	2	4.25	2.94	399	[41]
Internal support	SHS_IS	79.64	80.1	-	5.2	2.9	4.09	1.95	401	[41]
	TH_10_IS	72.89	71.09	24.17	2.5	0.8	1.65	0.99	399	[41]
	TH_15_IS	70.56	70.73	24.11	3	0.8	1.9	1.53	399	[41]
	TH_20_IS	69.72	70.08	24.02	4	0.8	2.4	1.99	399	[41]
	TH_30_IS	68.86	69.95	23.82	6.5	2	4.25	2.94	399	[41]
	SHS 100x100x3	100.1	100	-	5.57	2.5	4.04	3.07	800	[40]
	RHS 120x80x3	79.8	120	-	7.07	4	5.54	3.07	800	[40]
	RHS 140x60x3	60.4	139.9	-	7.58	4.5	6.04	3.08	800	[40]

Table 1. Geometrical dimensions used in FE calibration

Test	Specimen	E (Mpa)	$\sigma_{0.2}$ (Mpa)	n	σ_u	m	ϵ_u	Type
External support	SHS_ES	195592	502	6.1	527	4.07	0.0123	Ferritic
	TH_10_ES	199968	359	23.1	479	1.46	0.017	Ferritic
	TH_15_ES	191226	322	26.1	475	1.21	0.016	Ferritic
	TH_20_ES	192780	372	23	489	1.3	0.0164	Ferritic
	TH_30_ES	180369	297	23.5	445	1.22	0.016	Ferritic
Internal support	SHS_IS	195592	502	6.1	527	4.07	0.0123	Ferritic
	TH_10_IS	199968	359	23.1	479	1.46	0.017	Ferritic
	TH_15_IS	191226	322	26.1	475	1.21	0.016	Ferritic
	TH_20_IS	192780	372	23	489	1.3	0.0164	Ferritic
	TH_30_IS	180369	297	23.5	445	1.22	0.016	Ferritic
	SHS 100x100x3							Austenitic
	RHS 120x80x3							Austenitic
	RHS 140x60x3							Austenitic

Table 2. Mechanical properties used in FE calibration

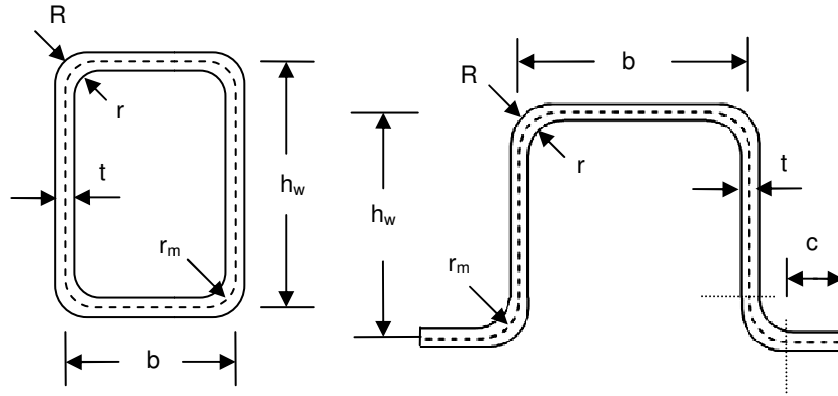


Figure 6. Hollow and hat sections.

3.7.2 Eurocode 3-1-3

EN 1993-1-3 [2] does not have specific expressions for rectangular hollow sections, so following the Talja and Salmi [42] proposal; parameters defined for sheeting have been used in these cases. Thus, the web crippling resistance for web, for cross sections with two or more webs, is given by:

$$R_{w,Rd} = \alpha t^2 \sqrt{f_{yb} E} \cdot (1 - 0,1\sqrt{r/t}) (0,5 + \sqrt{0,02 l_a / t}) (2,4 + (\phi / 90)^2) / \gamma_{M1} \quad (\text{Eq. 5})$$

where α is a constant coefficient, t is the web thickness, r is the internal corner radii, E is the material Young's modulus, f_{yb} is the material 0.2% proof strength, and l_a is the effective bearing length. Both α and l_a parameters depend on the section type, as well as the loading condition, through the different categories showed in tables in EN 1993-1-3 [2] (Category 1 for end loading and Category 2 for interior loading). So, assuming that the angle of the web relative to the flanges is 90 degrees the local transverse resistance $R_{w,Rd}$ per web of each cross section are:

For interior loading in RHS and SHS

$$R_{w,Rd} = 0,51 t^2 \sqrt{f_{yb} E} \cdot (1 - 0,1\sqrt{r/t}) (0,5 + \sqrt{0,02 l_a / t}) / \gamma_{M1} \quad (\text{Eq. 6})$$

For exterior loading in RHS and SHS

$$R_{w,Rd} = 0,255 t^2 \sqrt{f_{yb} E} \cdot (1 - 0,1\sqrt{r/t}) (0,5 + \sqrt{0,02 l_a / t}) / \gamma_{M1} \quad (\text{Eq. 7})$$

For interior loading in top hat sections

$$R_{w,Rd} = 0,39 t^2 \sqrt{f_{yb} E} \cdot (1 - 0,1\sqrt{r/t}) (0,5 + \sqrt{0,02 l_a / t}) / \gamma_{M1} \quad (\text{Eq. 8})$$

For end loading in top hat sections

$$R_{w,Rd} = 0,194 t^2 \sqrt{f_{yb} E} \cdot (1 - 0,1\sqrt{r/t}) (0,5 + \sqrt{0,02 l_a / t}) / \gamma_{M1} \quad (\text{Eq. 9})$$

Cold-formed members subjected to interior loading are more vulnerable because of the combined bending and concentrated load. Hence, interaction must be taken into account by means of (Eq. 10) as specified in 6.1.11 article of Eurocode 3, Part 1-3. It must be point out that assessing interaction in one profile requires results from the IOF test and the 4-point bending test.

$$\frac{R_{Ed}}{R_{w,Rd}} + \frac{M_{Ed}}{M_{c,Rd}} \leq 1.25$$

(Eq. 10)

$$\frac{R_{Ed}}{R_{w,Rd}} \leq 1$$

$$\frac{M_{Ed}}{M_{c,Rd}} \leq 1$$

Where F_{Ed} and M_{Ed} are the IOF ultimate resistance and the produced added bending moment respectively, $R_{w,Rd}$ is the web crippling resistance according to (Eq.6 and 7) and $M_{c,Rd}$ is the bending resistance that corresponds to the ultimate bending moment in the 4-point bending test ($M_{BD,exp}$) of the same profile. Substituting the value of the added bending moment in the IOF test as a function of the applied load ($M_{Ed}=F_{Ed} \cdot l_{IOF}/4$), the reduced ultimate web crippling resistance is set as (Eq. 11) shows.

$$F_{WC-BD} = F_{Ed} = \frac{1,25}{\frac{1}{R_{w,Rd}} + \frac{l_{IOF}}{4 \cdot M_{c,Rd}}} \quad (\text{Eq. 11})$$

Members subjected to an end loading condition do not need to satisfy this interaction condition, but some considerations need to be taken into account before comparing the experimental data obtained from [41] and the load values given in the numerical analysis. Measured forces in the FE calibration tests are reactions, while plug-in outputs are ultimate applied loads, so a simple transformation needs to be done to compare these two results. Remembering the EOF test configuration shown in Figure 1, and imposing moment equilibrium, the relation between the applied load, P , and the reaction, F_R , can be obtained:

$$L \cdot F_R = P \cdot (L - e) \Rightarrow F_R = \frac{P \cdot (L - e)}{L} = P \cdot (1 - e / L) \quad (\text{Eq. 12})$$

3.7.3 FE assessment and results

Tables 3 and 4 and Figures 7 and 8 summarize experimental, analytical and numerical results. Both abridgements $R_{WC,exp}$ and $M_{BD,exp}$ corresponds to experimental results from Gardner et al. [40] and Talja [41]. The former is the ultimate resistant load measured in the web crippling test while the latter is the ultimate bending resistance in the 4-point bending test. $R_{w,Rd}$ is the web crippling resistance obtained from applying (Eq.6-9) whereas F_{WC-BD} is the web crippling strength considering interaction with bending moment according to (Eq. 10). Finally, numerical results, $F_{u,num}$, are presented by considering three different amplitudes of the initial imperfection as specified in 3.5.

Specimen	$R_{WC,exp}$ (kN)	$M_{BD,exp}$ (kNm)	$R_{w,Rd}$ (kN)	F_{WC-BD} (kN)	$F_{u,num}$ (kN)		
					t/10	w_0	t/100
SHS_ES	26.76	-	13.97	-	68,5	68,52	68,52
TH_10_ES	7.18	-	2.78	-	8.62	8.61	8.59
TH_15_ES	15.04	-	5.69	-	19.25	19.1	19.07
TH_20_ES	25.92	-	9.95	-	33.32	32.93	32.9
TH_30_ES	42.07	-	17.12	-	49.22	48.64	48.66
SHS_IS	43.92	8.09	34.28	33.18	37.74	37.33	37.02
TH_10_IS	10	1.57	7.16	6.81	8.42	8.42	8.43
TH_15_IS	20.73	3.07	14.28	13.52	17.87	18.02	18.04
TH_20_IS	34.84	5.03	24.59	23.01	29.19	29.49	29.51
TH_30_IS	55.01	6.44	41.42	35.90	42.07	42.41	42.44
SHS 100x100x3	107.1	23.3	91.26	65.77	99.96	101.23	101.35
RHS 120x80x3	108.3	29.8	93.08	73.78	96.6	96.21	96.42
RHS 140x60x3	107.5	34.6	92.85	77.21	94.95	95.47	95.69

Table 3. Experimental, numerical and predicted results

Specimen	$R_{WC,exp}/R_{w,Rd}$	$R_{WC,exp}/F_{WC-BD}$	$F_{u,num}/R_{WC,exp}$	$t/10$	w_0	$t/100$
SHS_ES	1.92	-	1,82	1,82	1,82	
TH_10_ES	2.58	-	0.852	0.851	0.849	
TH_15_ES	2.64	-	0.909	0.902	0.900	
TH_20_ES	2.6	-	0.913	0.902	0.901	
TH_30_ES	2.46	-	0.831	0.821	0.821	
SHS_IS	1.28	1.033	0.859	0.850	0.843	
TH_10_IS	1.37	1.051	0.842	0.842	0.843	
TH_15_IS	1.45	1.056	0.862	0.869	0.870	
TH_20_IS	1.42	1.069	0.838	0.846	0.847	
TH_30_IS	1.33	1.154	0.765	0.771	0.771	
SHS 100x100x3	1.17	1.388	0.933	0.945	0.946	
RHS 120x80x3	1.16	1.262	0.891	0.888	0.890	
RHS 140x60x3	1.16	1.203	0.883	0.888	0.890	

Table 4. Experimental, numerical and predicted results

FEM calibration. Gardner internal support specimens

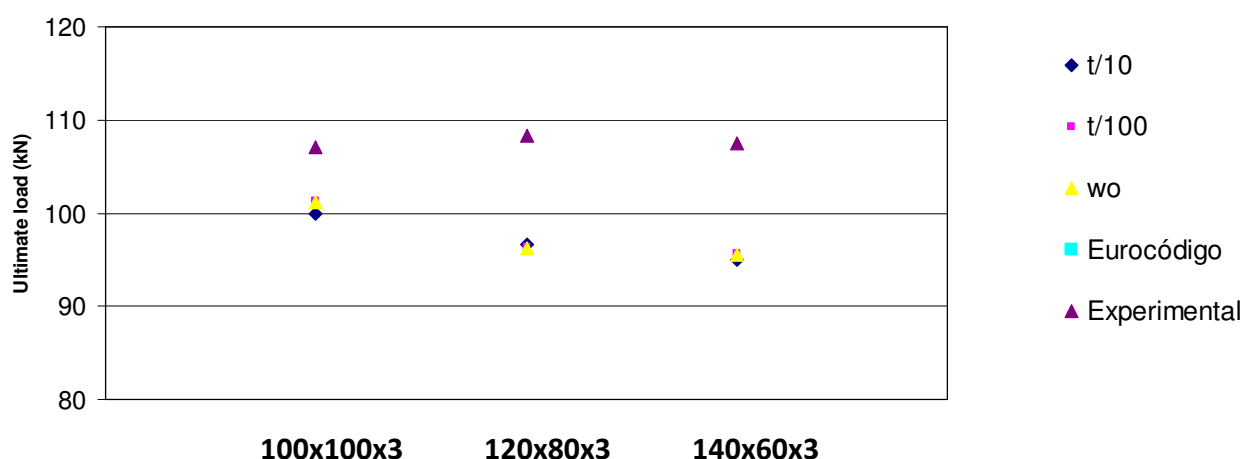


Figure 7. Local transverse resistances $R_{w,Rd}$ for SHS and RHS, internal support test

FEM calibration. VTT internal support specimens

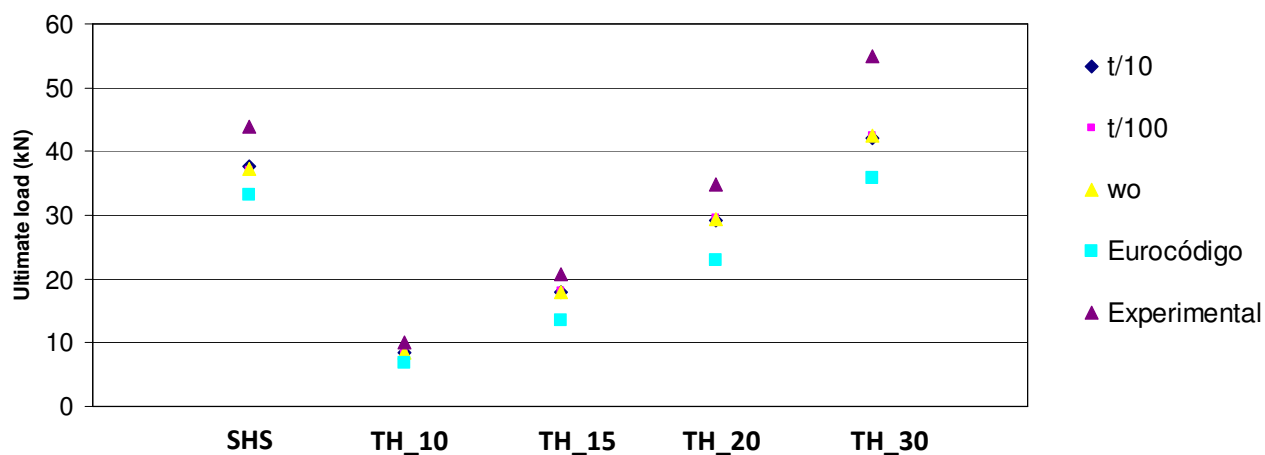


Figure 8. Ultimate loads for SHS and top hat sections, internal support test

FEM calibration. VTT end support specimens

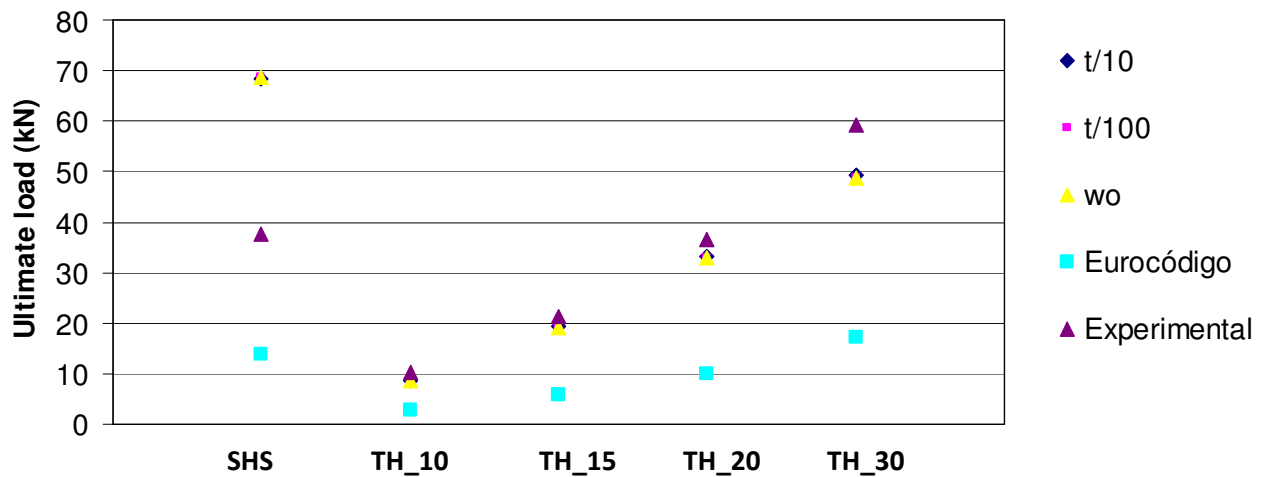


Figure 9. Ultimate loads for SHS and top hat sections, end support test.

The numerical results are similar to the experimentally obtained measurements and to the original numerical simulations in Gardner et al. [40]. The difference between predicted and test results are due to the lack of the information provided in the different papers, so it was no possible to reproduce the tests exactly. The results obtained using the Eurocode proposal are different from experimental and numerical results, so a new analysis is needed.

Figures 10 and 11 show examples of a top hat section model subjected to an internal loading condition and a model of a SHS section under end loading condition.

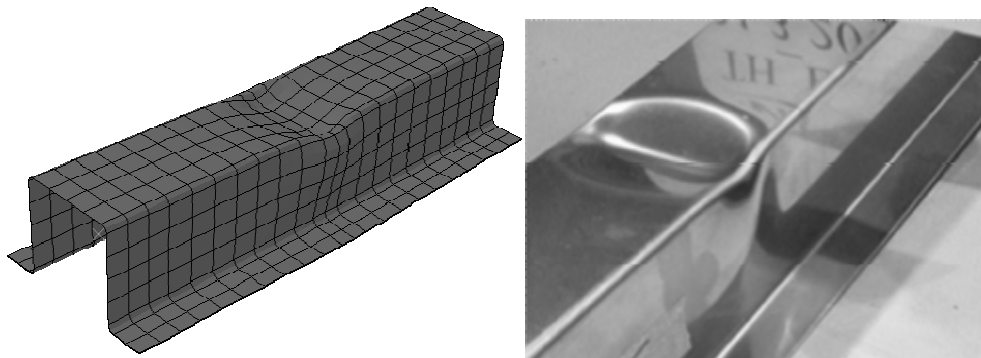


Figure 10. Deformed shape for a top hat section under internal loading condition.

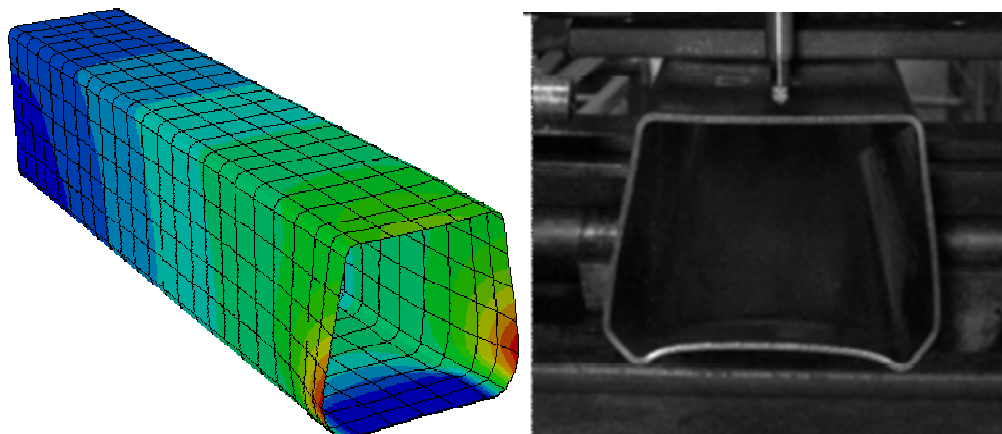


Figure 11. Deformed shape for a SHS section under end loading condition.

4. Parametric study

Once validated the numerical model, the effect of different parameters will be analyzed in the determination of the local transverse resistance $R_{w,Rd}$. This parametric study has been performed for the two defined loading conditions, internal loading and external loading. For each loading condition 3 different types of cross sections will be studied (rectangular and square hollow sections, and top hat sections).

The influence of the stainless steel grade and the different parameters defining the local transverse resistance in EN 1993-1-3 [2] will be analyzed: cross sectional thickness, the internal corner radii, the length over which the concentrated load is applied and the considered amplitude of the local geometrical imperfections.

4.1. Cross sections

The studied sections are the ones defined in Figure 6, but with different geometrical dimensions, and with thicknesses of 3 mm and 1.5 mm each. Table 3 shows the values defining the analyzed geometries.

Section	Designation	a (mm)	b (mm)	c (mm)	r (mm)
RHS 100x80xt	S1	80	100	-	6
SHS 80x80xt	S2	80	80	-	5
SHS 100x100xt	S3	100	100	-	2.5
Hat 80x80x30xt	S4	80	80	30	5

Table 3. Geometrical characteristics of the cross-sections used in the parametric study.

The member length, the bearing length, the support length and the eccentricity of the applied load of both IOF and EOF are summarized in Table 6 following according to Figure 1 nomenclature.

	IOF	EOF
L (mm)	350	350
s _{sa} (mm)	50	25
s _{sb} (mm)	50	50
s _{sL} (mm)	25	50
e (mm)	-	75

Table 6. Web crippling test configuration

For the fundamental case of IOF test, interaction with bending moment must be taken into account, therefore the four considered sections were also subjected to a 4-point bending test in order to obtain the ultimate bending moment strength. Loads were applied at 1/3 and 2/3 of the total member length which was fixed at 1000mm as Figure 4 shows. Simulations were carried out according to Hradil [44] using S4R shell elements with a distance between nodes equal to 5mm along flat section parts. Rounded corners were modeled with 3 segments.

4.2. Materials

The parametric study will analyze 6 different types of ferritic stainless steels, whose main characteristics are summarized in Table 7. These are the same materials used by Hradil et al. [43] analyzing the global stability of thin-walled ferritic stainless steel members. The first group of materials, group N, represents the ferritic grades similar to grade 430 (Figure 12). The difference in non-linear parameter n was studied in this group, where N1 is close to austenitic steels with low n values while N3 represents materials similar to carbon steel with high n values. The second group, F materials, studies the effect of increased strength due to cold-working typical for grade 3Cr12.

	E_0 (GPa)	$\sigma_{0.2}$ (MPa)	n	σ_u (MPa)	m	ϵ_u
N1	200	300	5	600	2.75	0.50
N2	200	300	10	600	2.75	0.50
N3	200	300	25	600	2.75	0.50
F1	200	300	10	420	3.50	0.29
F2	200	400	10	560	3.50	0.29
F3	200	500	10	700	3.50	0.29

Table 7. Material properties for the parametric study.

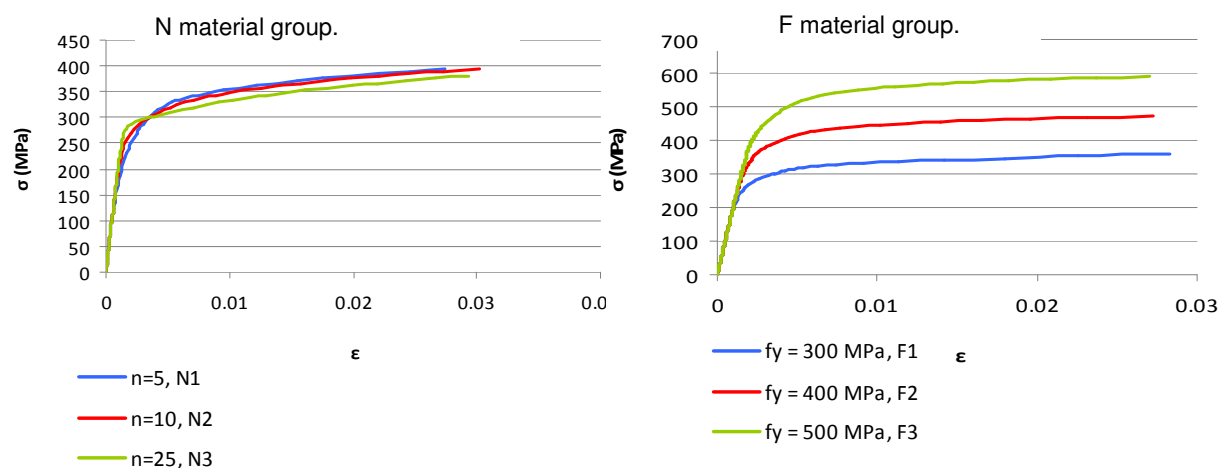


Figure 12. Different types of stainless steel studied.

4.3. Initial geometrical imperfections

Imperfections have been introduced as the first buckling modes, with two different amplitudes (w_0 and $t/10$) to study its effect on the determination of the ultimate loads. Amplitude $t/100$ presents the same order as w_0 , and then it has been eliminated from the analysis.

4.4. Numerical results

More than 200 web crippling models have been conducted in the parametric study. The applicability of the expression for determining the local transverse resistance proposed in EN 1993-1-3 [2] for cold formed ferritic stainless steel members will be corroborated from these results.

4.4.1 Internal support test

Tables 8-12 shows the results for the internal support tests simulation in sections S1, S2, S3 and S4. These results are also plotted in next figures 13 to 22.

Local transverse resistances $R_{w,Rd}$ (kN) S1							
Thickness and amplitude (mm)		N1	N2	N3	F1	F2	F3
t=3 mm	w_0	55.47	55.00	53.70	49.13	64.40	79.24
	$t/10$	55.29	54.82	53.52	48.98	64.22	79.04
	EN 1993-1-3	56.67	56.67	56.67	56.67	65.44	73.16
t=1.5 mm	w_0	16.07	15.94	15.57	14.54	18.91	23.13
	$t/10$	16.06	15.93	15.56	14.54	18.90	23.13
	EN 1993-1-3	15.57	15.57	15.57	15.57	17.98	20.10

Table 8. Local transverse resistances $R_{w,Rd}$ for internal support test, section S1

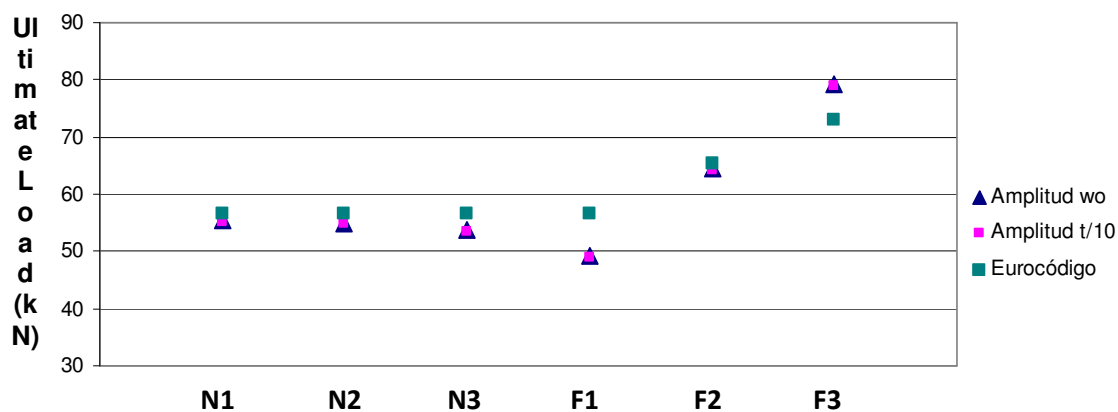


Figure 13. Local transverse resistances $R_{w,Rd}$ for internal support test, section S1, $t=3\text{mm}$

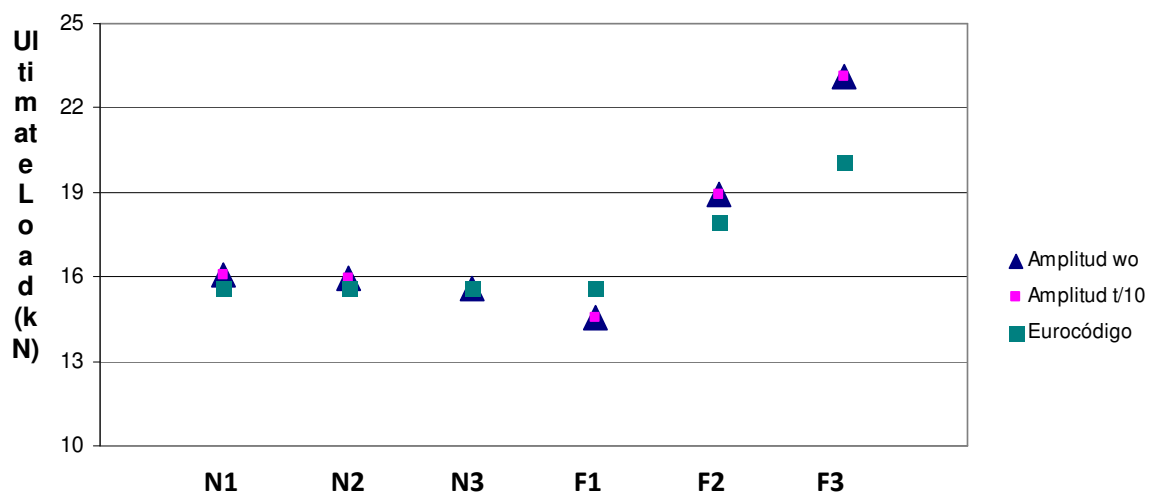


Figure 14. Local transverse resistances $R_{w,Rd}$ for internal support test, section S1, $t=1.5\text{mm}$

Local transverse resistances $R_{w,Rd}$ (kN) S2							
Thickness and amplitude (mm)		N1	N2	N3	F1	F2	F3
$t=3$ mm	w_0	50.45	50.62	49.88	47.30	61.20	74.32
	$t/10$	50.05	50.20	49.45	46.89	60.43	73.76
	EN 1993-1-3	57.60	57.60	57.6	57.6	66.52	74.37
$t=1.5$ mm	w_0	14.39	14.34	14.10	13.32	17.17	20.86
	$t/10$	14.38	14.34	14.08	13.30	17.15	20.85
	EN 1993-1-3	15.93	15.93	15.93	15.93	18.39	20.56

Table 9. Local transverse resistances $R_{w,Rd}$ for internal support test, section S2

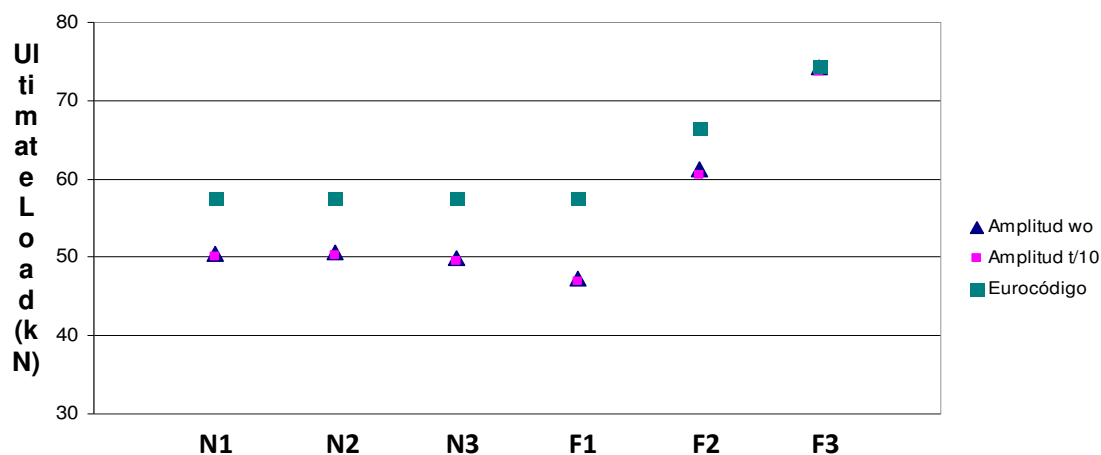


Figure 15. Local transverse resistances $R_{w,Rd}$ for internal support test, section S2, $t=3\text{mm}$

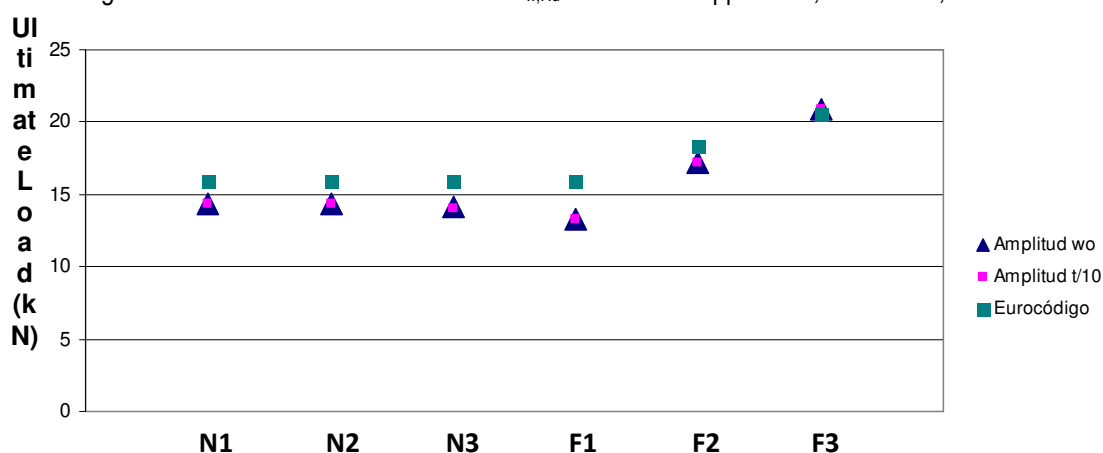


Figure 16. Local transverse resistances $R_{w,Rd}$ for internal support test, section S2, $t=1.5\text{mm}$

It is important to note that S3 internal members were modelled before the calibration tests were carried out, so they were tested using the general internal test provided by the plug-in. Those calibration tests led to the definition of new model-tests for top hat sections, so the model could reproduce the real load configuration.

As in this report it is only shown the preliminary FEM study, results obtained by the old version of the plug-in were kept, but the need of obtaining more accurate results is also highlighted for further research work, also for the calibration of the definitive version of the proposed new expression.

Local transverse resistances $R_{w,Rd}$ (kN) S3							
Thickness and amplitude (mm)		N1	N2	N3	F1	F2	F3
$t=3$ mm	w_0	49.85	49.99	49.22	42.59	55.27	73.16
	$t/10$	49.47	49.61	48.87	42.23	60.04	72.67
	EN 1993-1-3	44.16	44.16	44.16	44.16	50.99	57.01
$t=1.5$ mm	w_0	14.37	14.32	14.06	13.28	17.16	20.80
	$t/10$	14.36	14.30	14.05	13.75	17.15	20.79
	EN 1993-1-3	12.21	12.21	12.21	12.21	14.10	15.76

Table 10. Local transverse resistances $R_{w,Rd}$ for internal support test, section S3

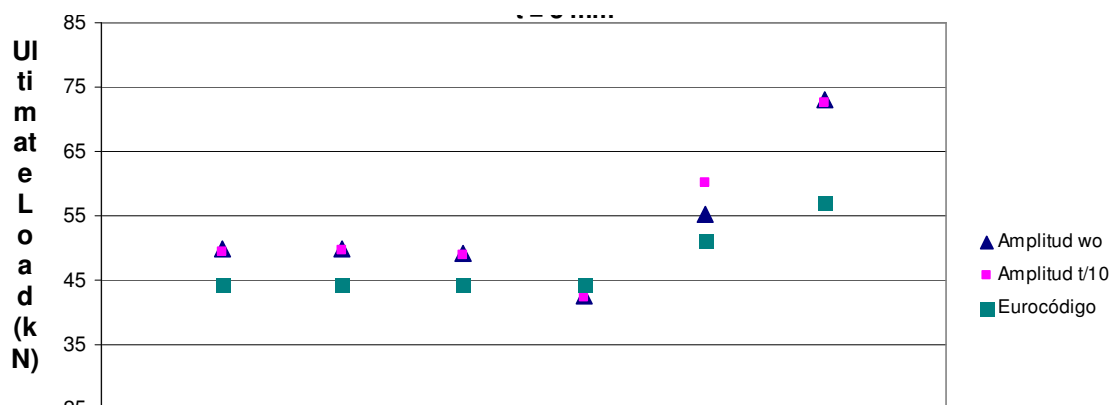


Figure 17. Local transverse resistances $R_{w,Rd}$ for internal support test, section S3, $t=3\text{mm}$

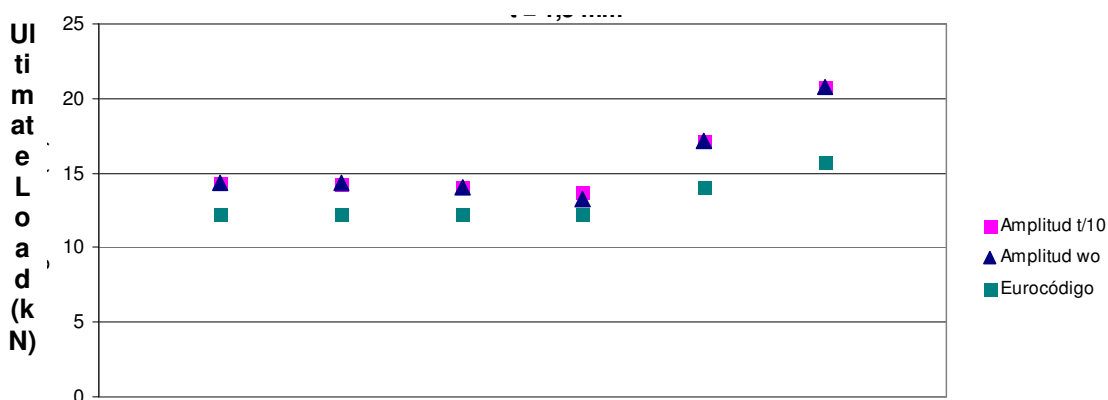


Figure 18. Local transverse resistances $R_{w,Rd}$ for internal support test, section S3, $t=1.5\text{mm}$

New numerical models have been carried out using the new test configuration for top hat sections subjected to internal loading condition. Both calibration and parametric studies have shown that the imperfection amplitude used in the models has no influence on the estimated ultimate load so the new models were conducted for a single imperfection amplitude. New results are shown below.

Local transverse resistances $R_{w,Rd}$ (kN) S3							
Thickness and amplitude (mm)		N1	N2	N3	F1	F2	F3
$t=3$ mm	W_0	47.31	46.92	45.85	41.75	54.77	67.61
	EN 1993-1-3	37.56	37.43	36.74	36.99	44.38	51.04
$t=1.5$ mm	W_0	13.35	13.26	12.97	12.09	15.73	19.29
	EN 1993-1-3	11.24	11.18	11.15	11.14	13.17	15.06

Table 11. Local transverse resistances $R_{w,Rd}$ for internal support test, section S3 under the new test configuration.

Local transverse resistances $R_{w,Rd}$ (kN) S4							
Thickness and amplitude (mm)		N1	N2	N3	F1	F2	F3
$t=3$ mm	W_0	71.63	69.89	69.97	68.90	86.40	104.64
	EN 1993-1-3	42.07	41.71	41.08	41.45	50.27	58.17
$t=1.5$ mm	W_0	17.49	17.68	17.76	17.42	21.80	25.19
	EN 1993-1-3	12.81	12.98	13.14	12.95	15.35	17.55

Table 12. Local transverse resistances $R_{w,Rd}$ for internal support test, section S4

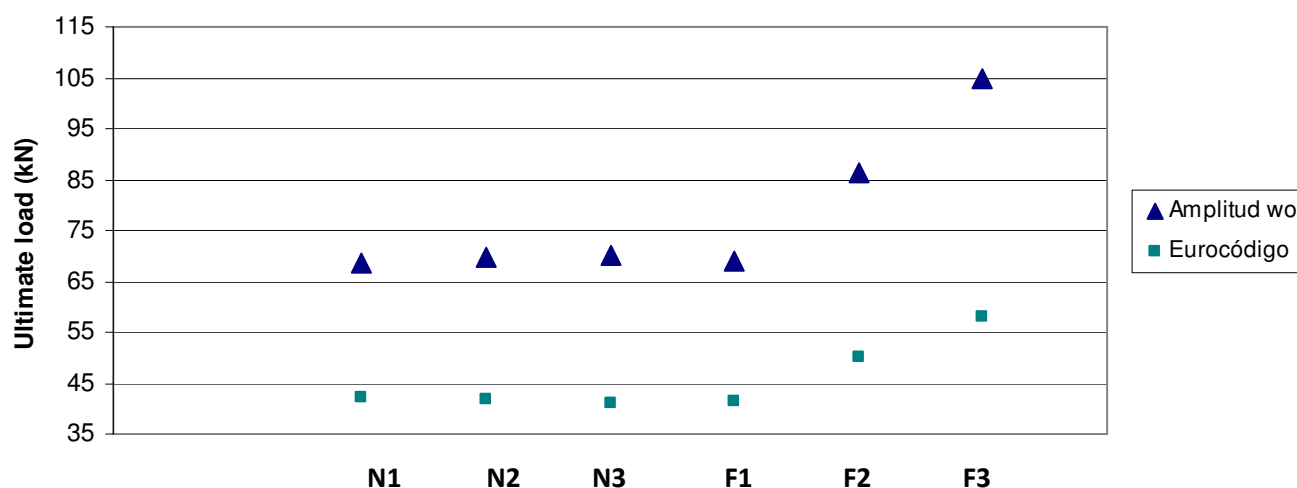


Figure 19. Local transverse resistances $R_{w,Rd}$ for internal support test, section S4, $t=3\text{mm}$

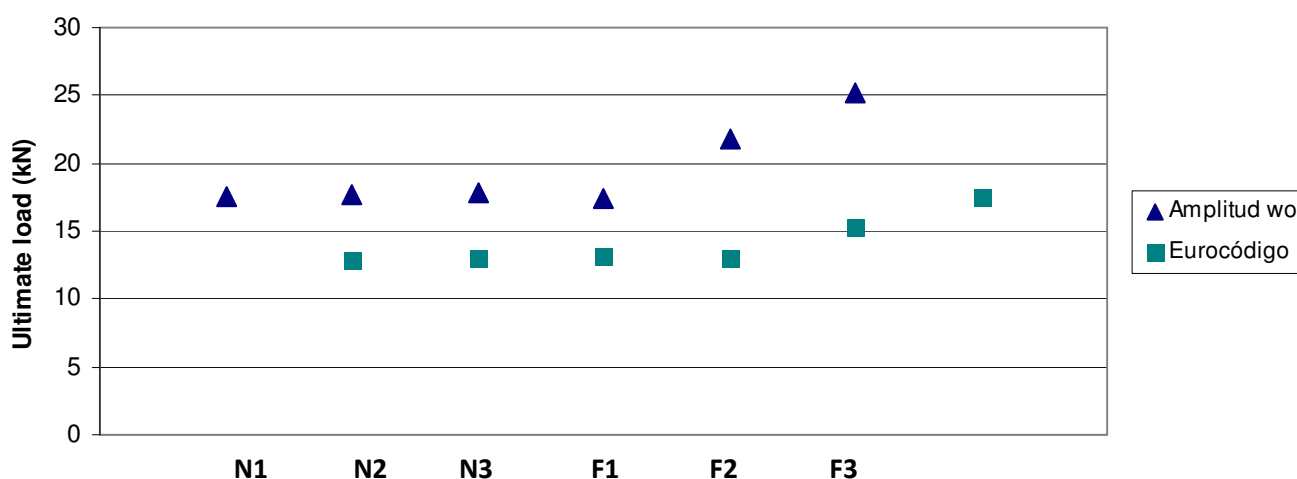


Figure 20. Local transverse resistances $R_{w,Rd}$ for internal support test, section S4, $t=1.5\text{mm}$

During the parametric analysis, a great influence of the internal corner radii in the local transverse resistance of the cross sections has been noticed. Then, an exhaustive analysis has been performed in a section S2 (80x80x3) with N1 and F1 stainless steels. Results are presented in table 9.

Radii (mm)	Local transverse resistances $R_{w,Rd}$ (kN)		
	N1	F1	EN 1993-1-3
2.5	66.89	64.52	58.68
3.5	57.70	55.03	57.60
5	50.45	47.30	56.25
6	49.04	44.04	55.45

Table 13. Radii influence for local transverse resistances $R_{w,Rd}$ in internal support tests

A similar procedure has been used for the analysis of the nominal length of stiff bearing, S_s influence. In this case, the studied section has been the S4 (SHS 100x100xt), and F1 stainless steel. Results are presented in table 14 and figure 21.

		Local transverse resistances (kN) for different Ss (mm)			
		25	50	75	100
t = 3 mm	Numerical	69.70	85.11	96.82	105.57
	EN 1993-1-3	53.35	69.61	70.91	77.33
t = 1,5 mm	Numerical	17.27	20.80	23.31	25.36
	EN 1993-1-3	15.16	18.53	21.11	23.29

Table 14. Nominal length of stiff bearing influence for local transverse resistances $R_{w,Rd}$ in internal support tests, S4 section

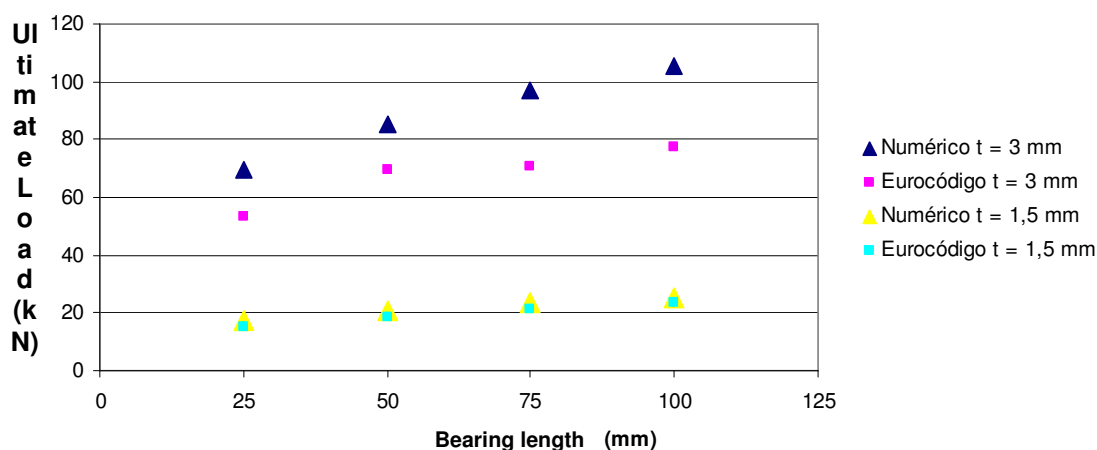


Figure 21. Nominal length of stiff bearing influence for local transverse resistances $R_{w,Rd}$ in internal support tests, S4 section

4.4.2 End support test

The results derived from the analysis for the end support tests simulations are presented, in a similar form as for the internal support tests, in Tables 15 to 18 and figures 22 to 29.

		Local transverse resistances $R_{w,Rd}$ (kN) S1					
Thickness and amplitude (mm)		N1	N2	N3	F1	F2	F3
t=3 mm	w_0	52.45	52.74	51.99	48.83	63.02	76.52
	t/10	52.28	52.57	51.82	48.70	62.85	76.32
	EN 1993-1-3	33.12	33.12	33.12	33.12	38.24	42.75
t=1.5 mm	w_0	12.70	12.72	12.47	12.06	15.46	18.65
	t/10	12.70	12.72	12.47	12.06	15.46	18.65
	EN 1993-1-3	8.75	8.75	8.75	8.75	10.11	11.30

Table 15. Local transverse resistances $R_{w,Rd}$ for end support test, section S1

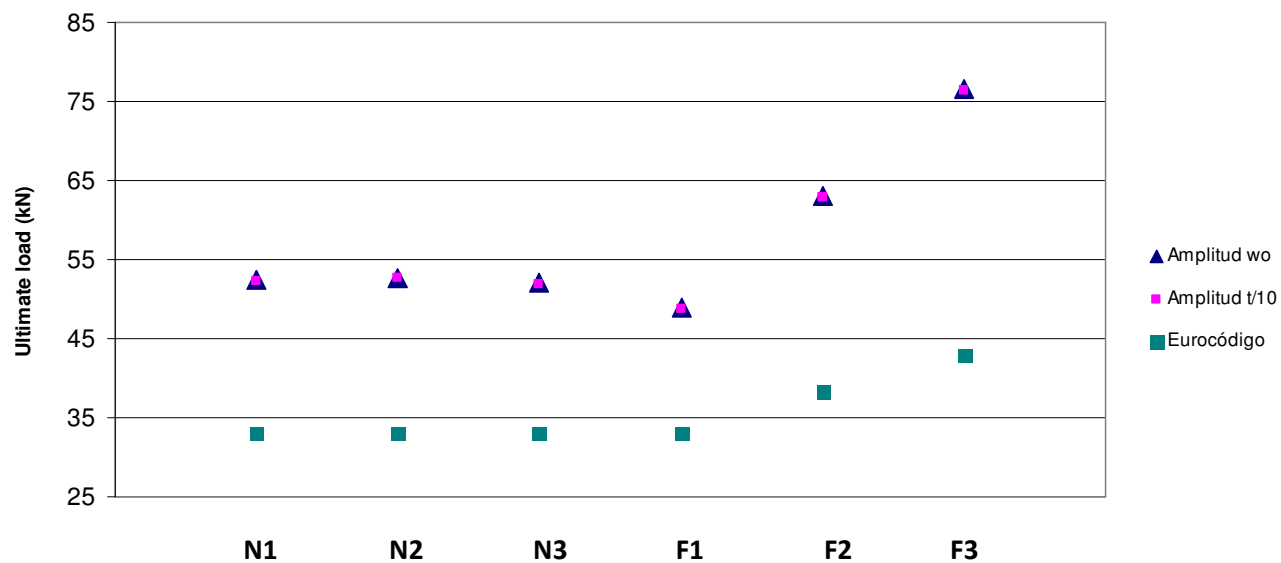


Figure 22. Local transverse resistances $R_{w,Rd}$ for end support test, section S1, $t=3\text{mm}$

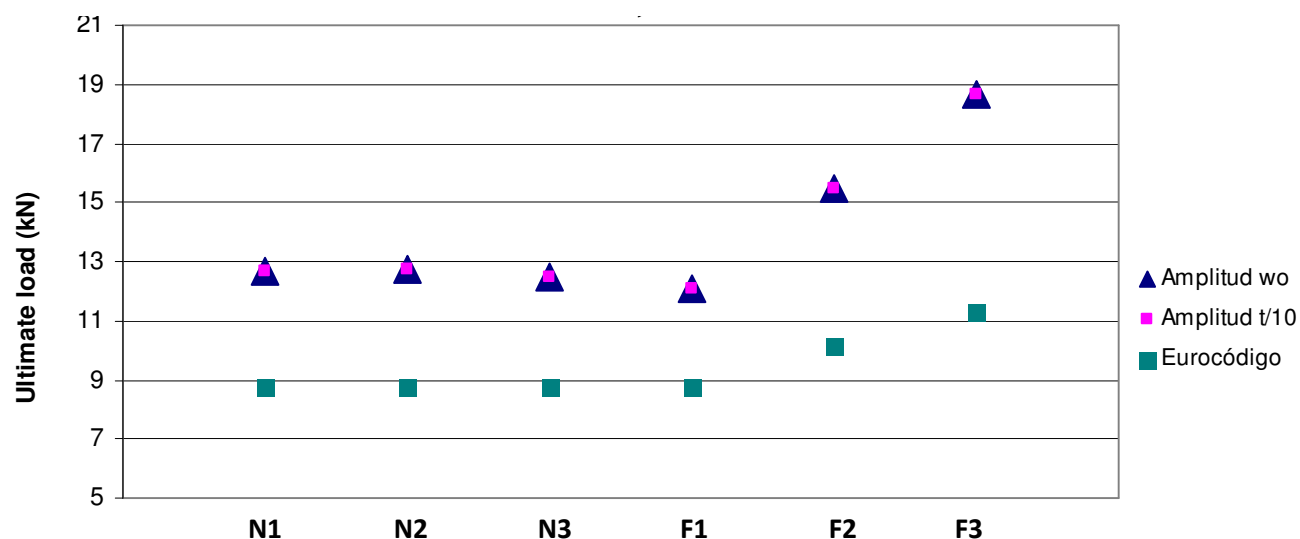


Figure 23. Local transverse resistances $R_{w,Rd}$ for end support test, section S1, $t=1.5\text{mm}$

Local transverse resistances $R_{w,Rd}$ (kN) S2							
Thickness and amplitude (mm)		N1	N2	N3	F1	F2	F3
t=3 mm	w_0	59.20	59.44	58.59	54.97	71.17	86.74
	t/10	58.82	59.03	58.20	54.70	70.84	86.27
	EN 1993-1-3	33.66	33.66	33.66	33.66	38.87	43.46
t=1.5 mm	w_0	14.22	14.27	14.00	13.54	17.32	20.89
	t/10	14.21	14.25	13.99	13.53	17.31	20.88
	EN 1993-1-3	8.95	8.95	8.95	8.95	10.34	11.56

Table 16. Local transverse resistances $R_{w,Rd}$ for end support test, section S2

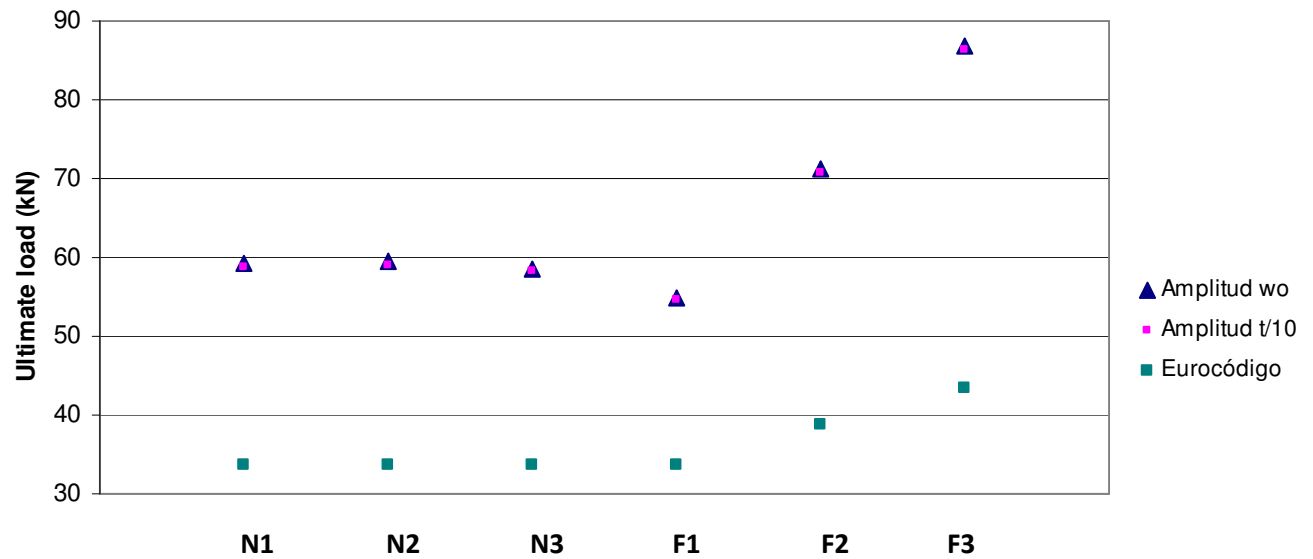


Figure 24. Local transverse resistances $R_{w,Rd}$ for end support test, section S2, $t=3\text{mm}$

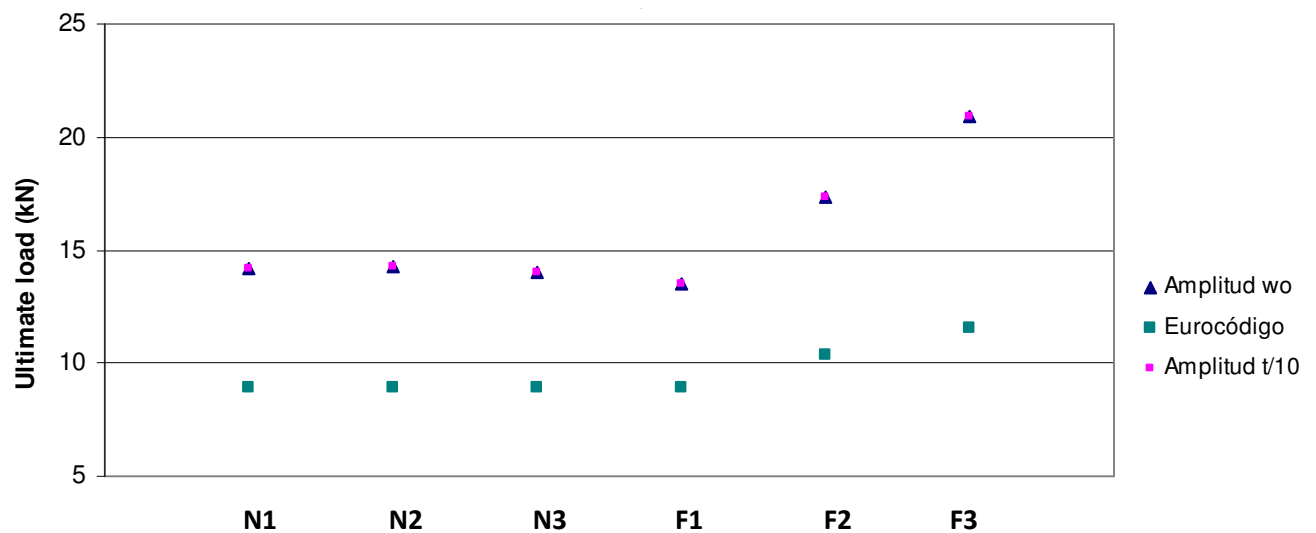


Figure 25. Local transverse resistances $R_{w,Rd}$ for end support test, section S2, $t=1.5\text{mm}$

Local transverse resistances $R_{w,Rd}$ (kN) S3							
Thickness and amplitude (mm)		N1	N2	N3	F1	F2	F3
$t=3$ mm	w_0	18.90	19.04	18.77	18.23	23.34	28.16
	$t/10$	18.66	18.79	18.53	18.01	23.05	28.16
	EN 1993-1-3	9.14	9.14	9.14	9.14	10.55	11.79
$t=1.5$ mm	w_0	4.11	4.12	4.05	3.97	5.06	6.09
	$t/10$	4.11	4.13	4.05	3.96	5.06	6.07
	EN 1993-1-3	2.43	2.43	2.43	2.43	2.8	3.13

Table 17. Local transverse resistances $R_{w,Rd}$ for end support test, section S3

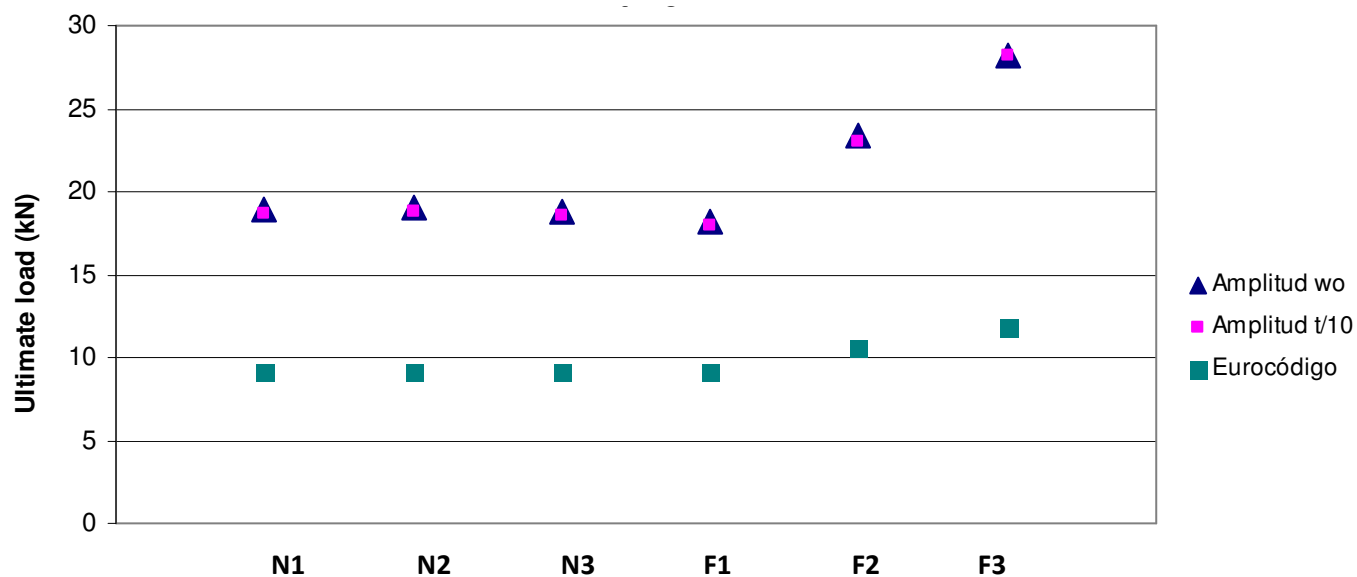


Figure 26. Local transverse resistances $R_{w,Rd}$ for end support test, section S3, $t=3\text{mm}$

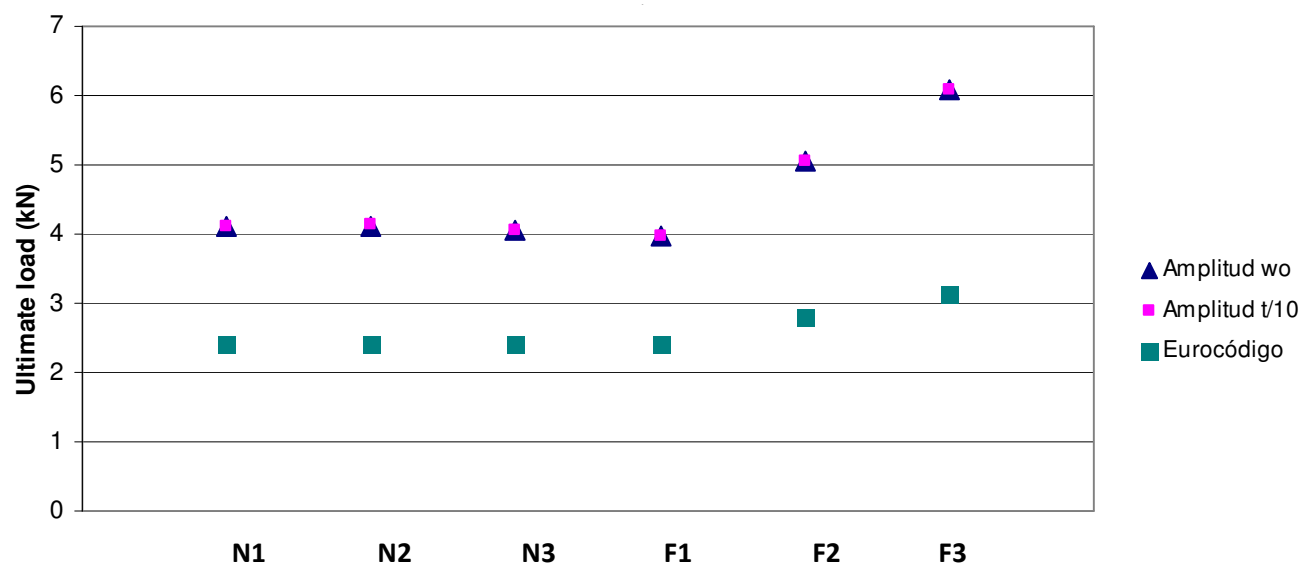


Figure 27. Local transverse resistances $R_{w,Rd}$ for end support test, section S3, $t=1.5\text{mm}$

Local transverse resistances $R_{w,Rd}$ (kN) S4							
Thickness and amplitude (mm)		N1	N2	N3	F1	F2	F3
t=3 mm	w_0	82.09	82.29	81.31	77.15	98.9	119.52
	t/10	82.68	83.16	82.30	77.75	99.92	120.75
	EN 1993-1-3	35.56	35.56	35.56	35.56	41.06	45.91
t=1.5 mm	w_0	19.96	20.17	20.01	19.30	24.2	28.58
	t/10	19.95	20.15	20.00	19.29	24.18	28.57
	EN 1993-1-3	9.60	9.60	9.60	9.60	10.11	11.30

Table 18. Local transverse resistances $R_{w,Rd}$ for end support test, section S4

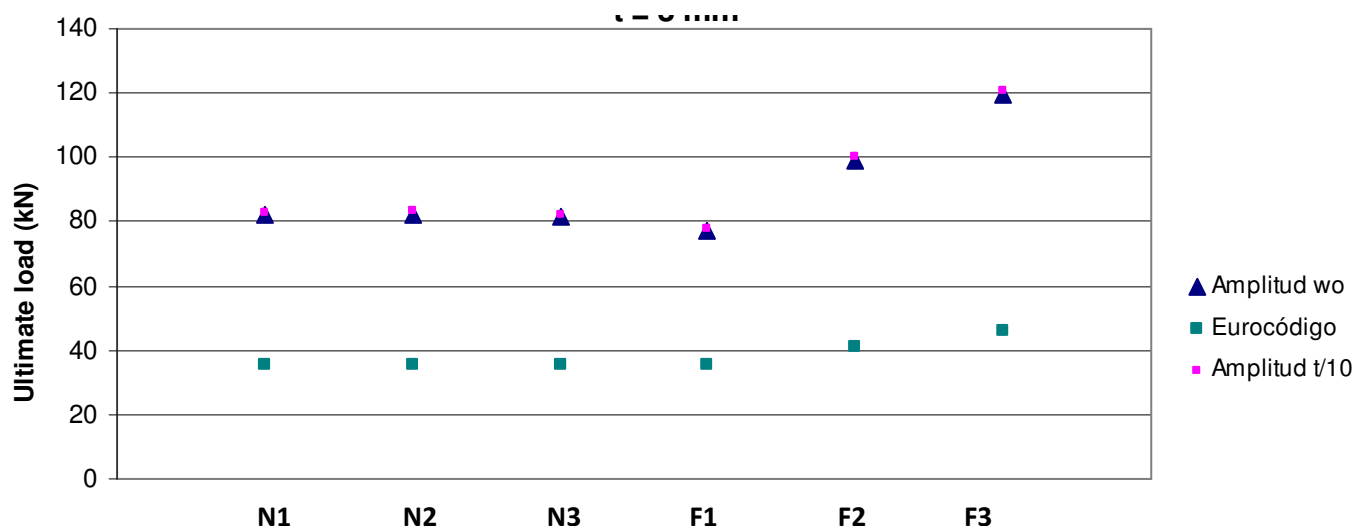


Figure 28. Local transverse resistances $R_{w,Rd}$ for end support test, section S4, $t=3\text{mm}$

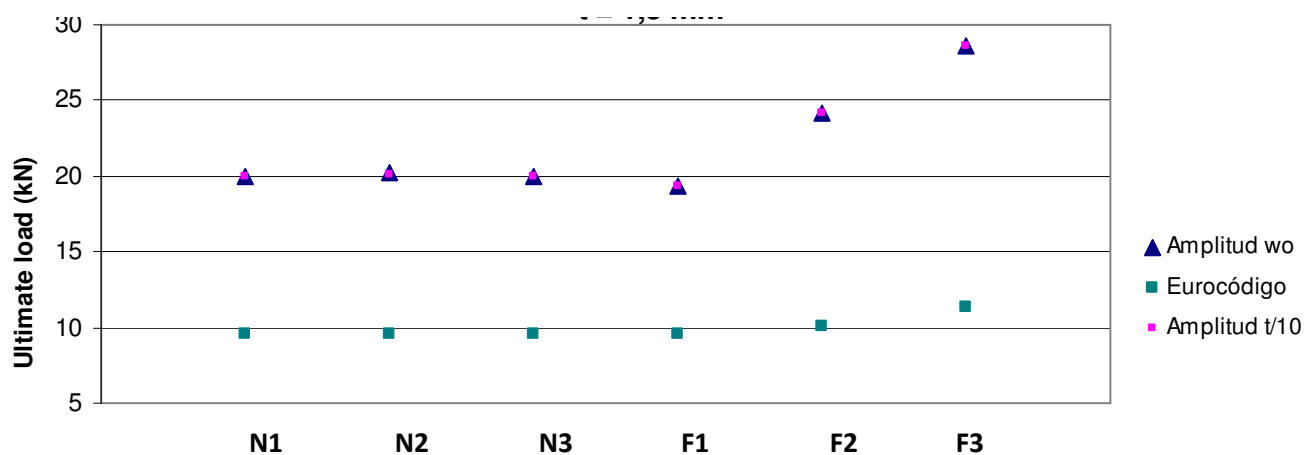


Figure 29. Local transverse resistances $R_{w,Rd}$ for end support test, section S4, $t=1.5\text{mm}$

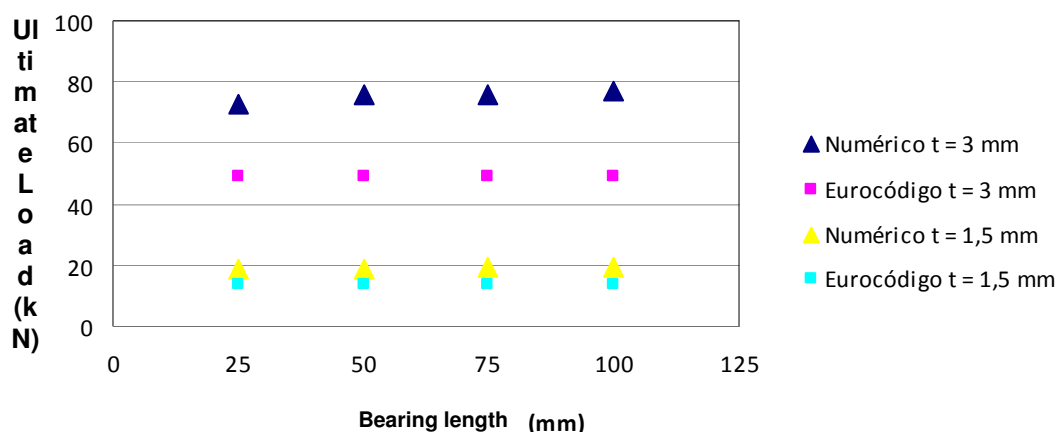
The influence of the internal corner radii in the local transverse resistance of the cross sections under end support test have been analyzed in the same way as for internal support tests. An exhaustive analysis has been performed in a section S2 (80x80x3) with N1 and F1 stainless steels. Results are presented in table 19.

Radii (mm)	Local transverse resistances $R_{w,Rd}$ (kN)		
	N1	F1	EN 1993-1-3
2.5	84.59	79.03	48.99
3.5	71.48	66.73	48.09
5	59.20	54.97	46.95
6	53.58	49.74	46.29

Table 19. Radii influence for local transverse resistances $R_{w,Rd}$ in end support tests

A similar procedure has been used for the analysis of the nominal length of stiff bearing, S_s influence. In this case, the studied section has been the S4 (SHS 100x100x3), and F1 stainless steel. Results are presented in Table 20 and Figure 30.

		Local transverse resistances (kN) for different Ss (mm)			
		25	50	75	100
t = 3 mm	Numerical	72.68	75.61	76.06	77.07
	EN 1993-1-3	49.00	49.00	49.00	49.00
t = 1.5 mm	Numerical	18.39	18.56	18.97	19.38
	EN 1993-1-3	13.39	13.39	13.39	13.39

Table 20. Nominal length of stiff bearing influence for local transverse resistances $R_{w,Rd}$ in end support tests, S4 section

Figure 30. Nominal length of stiff bearing influence for local transverse resistances $R_{w,Rd}$ in end support tests, S4 section

5. Comparative analysis

The results obtained in the parametric study will be analyzed in this chapter, by comparing the ultimate loads provided by the numerical simulation with the values predicted by EN 1993-1-3 [2], to study the applicability of the existing expressions to ferritic stainless steels, as well as help on the understanding of the behavior of cross sections under local transverse loads.

5.1. Initial imperfection magnitude analysis

Table 21 and 22 show the relation between the ultimate numerical loads obtained by Abaqus for the two imperfection amplitudes analyzed for different material groups, for internal support test and end support test respectively.

$R_{w,Rd}(w_0)/R_{w,Rd}(t/10)$ ratios						
	S1		S2		S3	
	t = 3 mm	t = 1,5 mm	t = 3 mm	t = 1,5 mm	t = 3 mm	t = 1,5 mm
N1	1.0032	1.0006	1.008	1.0007	1.007	1.0007
N2	1.0033	1.0006	1.008	1.0	1.007	1.0014
N3	1.0033	1.0006	1.008	1.001	1.007	1.0007
F1	1.0030	1.0	1.008	1.001	1.008	0.966
F2	1.0028	1.0005	1.012	1.001	0.920	1.0006
F3	1.0025	1.0	1.007	1.0005	1.007	1.0005

Table 21. Ratios between ultimate loads for w_0 and $t/10$ imperfection magnitudes for internal support tests

The influence of the used imperfection amplitude is negligible for both loading conditions, so they obtained ultimate loads are similar for amplitudes, w_0 and $t/10$. Accordingly, and for simplicity, the rest of the analysis will be done with one of the values of geometrical imperfection amplitude, w_0 .

$R_{w,Rd(w0)}/R_{w,Rd(t/10)}$ ratios)						
	S1		S2		S3	
	t = 3 mm	t = 1,5 mm	t = 3 mm	t = 1,5 mm	t = 3 mm	t = 1,5 mm
N1	1.0032	1.0	1.006	1.000	0.987	0.988
N2	1.0032	1.0	1.006	1.001	0.987	1.000
N3	1.0033	1.0	1.006	1.001	0.987	0.988
F1	1.0026	1.0	1.004	1.001	0.988	0.999
F2	1.0027	1.0	1.004	1.001	0.988	0.999
F3	1.0026	1.0	1.005	1.001	1.000	0.998

Table 22. Ratios between ultimate loads for w_0 and $t/10$ imperfection magnitudes for end support tests

5.2. Stainless-steel: material analysis

Relations between the numerical load and the one proportioned by EN 1993-1-3 [2] are shown on Tables 23 to 25 for the studied cases for internal support tests (considering interaction with bending moment and without considering it) and end support tests. In this analysis it has been considered just one value of the local imperfection amplitude (w_0), due to the conclusions obtained in 5.1.

In the following tables, each specimen has been labeled to identify it easily. The two first characters indicates the material type of the specimens according to Table 7, the following two characters correspond to the section type as described in Table 5 and finally, the next symbols are the nominal thickness.

Specimen	$F_{u,num}/R_{w,Rd}$	Specimen	$F_{u,num}/R_{w,Rd}$	Specimen	$F_{u,num}/R_{w,Rd}$	Specimen	$F_{u,num}/R_{w,Rd}$
N1S115	1.0322	F1S115	0.9339	N1S130	0.9788	F1S130	0.8669
N1S215	0.9034	F1S215	0.8362	N1S230	0.8757	F1S230	0.8211
N1S315	1.1767	F1S315	1.0875	N1S330	1.1287	F1S330	0.9643
N1S415	1.0238	F1S415	1.0197	N1S430	1.1771	F1S430	1.1322
N2S115	1.0238	F2S115	1.0519	N2S130	0.9705	F2S130	0.9841
N2S215	0.9003	F2S215	0.9335	N2S230	0.8787	F2S230	0.9200
N2S315	1.1726	F2S315	1.2169	N2S330	1.1319	F2S330	1.0838
N2S415	1.0349	F2S415	1.1051	N2S430	1.1485	F2S430	1.2296
N3S115	1.0001	F3S115	1.1508	N3S130	0.9475	F3S130	1.0830
N3S215	0.8852	F3S215	1.0144	N3S230	0.8659	F3S230	0.9993
N3S315	1.1514	F3S315	1.3194	N3S330	1.1144	F3S330	1.2831
N3S415	1.0396	F3S415	1.1422	N3S430	1.1498	F3S430	1.3319

Table 23. Ratios between numerical ultimate loads and EN 1993-1-3 predicted ones for internal loading condition without considering interaction with bending moment

Specimen	$F_{u,num}/F_{WC-BD}$	Specimen	$F_{u,num}/F_{WC-BD}$	Specimen	$F_{u,num}/F_{WC-BD}$	Specimen	$F_{u,num}/F_{WC-BD}$
N1S115	1.064	F1S115	0.961	N1S130	1.070	F1S130	0.956
N1S215	0.996	F1S215	0.922	N1S230	1.050	F1S230	0.999
N1S315	1.093	F1S315	0.990	N1S330	1.071	F1S330	0.945
N1S415	1.058	F1S415	1.047	N1S430	1.275	F1S430	1.237
N2S115	1.052	F2S115	1.063	N2S130	1.066	F2S130	1.051
N2S215	0.994	F2S215	1.004	N2S230	1.059	F2S230	1.078
N2S315	1.086	F2S315	1.115	N2S330	1.062	F2S330	1.074
N2S415	1.062	F2S415	1.119	N2S430	1.250	F2S430	1.305
N3S115	1.023	F3S115	1.153	N3S130	1.050	F3S130	1.132
N3S215	0.974	F3S215	1.081	N3S230	1.057	F3S230	1.136
N3S315	1.062	F3S315	1.224	N3S330	1.038	F3S330	1.186
N3S415	1.059	F3S415	1.142	N3S430	1.263	F3S430	1.386

Table 24. Ratios between numerical ultimate loads and EN 1993-1-3 predicted ones for internal

loading condition considering interaction with bending moment

Specimen	$F_{u,num}/R_{w,Rd}$	Specimen	$F_{u,num}/R_{w,Rd}$	Specimen	$F_{u,num}/R_{w,Rd}$	Specimen	$F_{u,num}/R_{w,Rd}$
N1S115	1.451	F1S115	1.378	N1S130	1.584	F1S130	1.474
N1S215	1.588	F1S215	1.512	N1S230	1.759	F1S230	1.633
N1S315	1.693	F1S315	1.632	N1S330	2.068	F1S330	1.994
N1S415	2.079	F1S415	2.010	N1S430	2.308	F1S430	2.170
N2S115	1.453	F2S115	1.530	N2S130	1.593	F2S130	1.648
N2S215	1.594	F2S215	1.675	N2S230	1.766	F2S230	1.831
N2S315	1.699	F2S315	1.809	N2S330	2.083	F2S330	2.212
N2S415	2.100	F2S415	2.182	N2S430	2.314	F2S430	2.409
N3S115	1.425	F3S115	1.651	N3S130	1.570	F3S130	1.790
N3S215	1.564	F3S215	1.807	N3S230	1.740	F3S230	1.996
N3S315	1.668	F3S315	1.946	N3S330	2.053	F3S330	2.388
N3S415	2.084	F3S415	2.305	N3S430	2.287	F3S430	2.603

Table 25. Ratios between numerical ultimate loads and EN 1993-1-3 predicted ones for end loading condition

Comparing the numerical results with the resistances predicted by EN 1993-1-3 [2], and as can be seen in Tables 23 to 25, Eurocode results are unsafe in 20% of the tests under internal loading condition, including all the cross sectional types (RHS, SHS and top hat sections). Although values for the end loading condition are safe for all the cases, results are too conservative. Therefore, some changes must be done in the EN 1993-1-3 [2] expression for the new stainless steel grades.

Analyzing the numerical values obtained for the N material group and different types of cross sections, the effect of the nonlinearity parameter "n" is shown. It can be noted that the ultimate loads are almost equal for the three N materials, so the "n" parameter has no influence on the ultimate resistance under web crippling.

By comparing the results for N2 and F1 materials, the influence of the ultimate strength of the material, f_u , can be studied. Although the loads predicted by EN 1993-1-3 [2] are the same, the values provided by Abaqus are not, so it is evident that the value of f_u should be taken into account when predicting the web resistance to "web crippling" for all cross sections and loading conditions.

As web crippling is a high localized phenomenon, the instability failure occurs at very high strengths, so it requires a large deformations development for the element collapse, and the ultimate strength f_u of the material influences on the behavior.

Therefore, the need to include the effect of the ultimate strength f_u in the expression that predicts the web crippling resistance under transverse loads is highlighted.

5.3. Internal bend radius analysis

The parametric study conducted shows that the internal bend radius has a great influence on the web crippling resistance. The relation between the ultimate loads for elements whose only different parameter is the bend radius for N1 and F1 has been studied for S2 (SHS section). The ultimate load according to a radius of 2.5 mm has been defined as reference (being the highest load), and it can be concluded that this relation between ultimate loads for different bend radius is very similar to the square root of the ratio between the two radii, as shown in the following table, where $R_{w,Rd}(i)$ represents the ultimate load obtained for a bend radius i .

	Internal loading condition		End loading condition		$\sqrt{2.5 / r_i}$
	N1	F1	N1	F1	
$R_{w,Rd} (2.5) / R_{w,Rd} (3.5)$	1.16	1.17	1.18	1.18	1.183
$R_{w,Rd} (2.5) / R_{w,Rd} (5)$	1.33	1.36	1.43	1.44	1.41
$R_{w,Rd} (2.5) / R_{w,Rd} (6)$	1.36	1.47	1.58	1.59	1.549

Table 26. Ratios between numerical ultimate loads for different bend radius and different materials

5.4. Effective bearing length analysis

Results highlight the importance of the length of load application in the determination of the web crippling resistance. Studying the increase in resistance when increasing the bearing length S_s for section S4 (SHS section) and for material F1, values listed in Table 27 are obtained. Also in this case the highest ultimate load has been taken as reference, which corresponds to a bearing length of 100mm. In Table 27, $R_{w,Rd} (i)$ represents the ultimate load obtained for a load application length i .

Table 27 shows that the increasing proportions are similar for the numerical values and for those predicted by EN 1993-1-3 [2], so the term that involves the bearing length in the EN 1993-1-3 [2] expression appears to be correct, and there is no need to correct it.

			$R_{w,Rd} (100) / R_{w,Rd} (i)$ ratios			
			25 mm	50 mm	75 mm	100 mm
Interior loading condition	t = 3	Numerical	1.51	1.24	1.09	1.0
		Eurocode	1.45	1.11	1.09	1.0
	t = 1.5	Numerical	1.47	1.22	1.09	1.0
		Eurocode	1.54	1.26	1.10	1.0
End loading condition	t = 3	Numerical	1.06	1.02	1.01	1.0
		Eurocode	1.00	1.00	1.00	1.0
	t = 1.5	Numerical	1.05	1.04	1.02	1.0
		Eurocode	1.00	1.00	1.00	1.0

Table 22. Ratios between numerical ultimate loads for different effective bearing lengths

The results show that there is a need to develop a more accurately expression to determine the web crippling resistance of stainless steel cold formed elements.

6. Conclusions

Web crippling is a local instability complex phenomenon in which many parameters are involved, and although several studies have been published, future analysis is essential. The existing rules are statistically adjusted expressions from carbon steel tests, so its application to other cold formed sections must be justified. The same happens for stainless steel, standards and design guidelines for steel specifications do not allow themselves to cold-formed profiles and lightweight structures, referring to those for carbon steels. However, the stainless steel non-linear behavior requires the development of new expressions to determine the web crippling resistance for both types of steel.

Numerical models of cold-formed ferritic stainless steel members under web crippling has shown some aspects to be taken into account when defining future design guidelines for ferritic stainless steels: results provided by the expression in EN 1993-1-3 [2] are sometimes unsafe when applied to ferritic stainless steel, so a new expression has been proposed, based on the existing one, and incorporating all aspects observed for this new material.

The local imperfection amplitude used in the development of the nonlinear analysis of web crippling, as well as the non-linearity parameter "n" have little influence in determining the ultimate load. Furthermore, as web crippling is a local phenomenon which develops great deformations before the element fails, the effect of the ultimate strength of the material, f_u , must be taken into account in the final expression for the prediction of web resistance under local transverse loads.

Although the effect of the bearing length S_s is well represented in the expression given by EN 1993-1-3 [2], the factor involving the bend radius of the sections must be corrected in the new proposal.

7. References

- [1] European Committee for Standardization Eurocode 3. Design of steel structures. Part 1-4: General rules. Supplementary rules for stainless steels. Brussels, Belgium: 2006.
- [2] European Committee for Standardization Eurocode 3. Design of steel structures. Part 1-3: General rules. Supplementary rules for cold-formed members and sheeting. Brussels, Belgium: 2006.
- [3] American Society of Civil Engineers & Structural Engineering Institute Specification for the Design of Cold-Formed Stainless Steel Structural Members. Reston, Virginia: 2002. ISBN 0-7844-0556-5.
- [4] Standards Australia & Standards New Zeland Australian/New Zeland Standard: Cold-formed stainless steel structures. Sydney Australia: 2001. ISBN 0 7337 3979 2.
- [5] Bakker, M.C.M. Web crippling of cold-formed steel members. The Netherlands: Eindhoven University of Technology, 1992.
- [6] Hofmeyer, H. Combined Web Crippling and Bending Moment Failure of First-Generation Trapezoidal Steel Sheeting: Experiment, Finite Element Models, Mechanical models. The Netherlands: Eindhoven University of Technology, 2000.
- [7] Kaitila, O. Web crippling of cold-formed thin-walled steel cassettes. Espoo, Finland: Helsinki University of Technology, 2004.
- [8] Rhodes, J. & Nash, D. An investigation of web crushing behaviour in thin-walled beams. Thin-Walled Structures 1998, 9, Vol. 32, No. 1-3, pp. 207-230. ISSN 0263-8231. doi: DOI: 10.1016/S0263-8231(98)00035-4.
- [9] Final report, civil engineering study, 784. Hetrakul, N. & Yu, W.W. Structural behaviour of beam webs subjected to web crippling and a combination of web crippling and bending. Rolla (MO): University of Missouri-Rolla, 1978.
- [10] Civil engineering study 81-2, structural series. Yu, W.W. Web crippling and combined web crippling and bending of steel decks. Rolla (MO): University of Missouri-Rolla, 1981.
- [11] Studnicka, J. Web crippling of wide deck sections. In: Anonymous Recent research and developments in cold-formed steel design and construction. Rolla (MO): Department of Civil Engineering. University of Missouri-Rolla., 1991. Pp. 317-334.
- [12] Gerges, R.R. Web crippling of single web cold formed steel members subjected to End One-Flange loading. Waterloo (ON, Canada): University of Waterloo, 1997.
- [13] Wing, B.A. Web crippling and the interaction of bending and web crippling of unreinforced multi-web cold-formed steel sections. Waterloo (ON, Canada): University of Waterloo, 1981.
- [14] Santaputra, C., Parks, M.B. & Yu, W.W. Web crippling strength of high strength steel beams. 8th International Specialty Conference on Cold-Formed Steel Structures. 1986. St. Louis, Missouri, USA: .
- [15] Zhao, X. & Hancock, G.J. Square and Rectangular Hollow Sections under Transverse End-Bearing Force. Journal of Structural Engineering 1995, 09, Vol. 121, No. 9, pp. 1323. ISSN 07339445.

- [16] Hofmeyer, H., Kerstens, J.G.M., Snijder, H.H. & Bakker, M.C.M. New prediction model for failure of steel sheeting subject to concentrated load (web crippling) and bending. *Thin-Walled Structures* 2001, 9, Vol. 39, No. 9, pp. 773-796. ISSN 0263-8231. doi: DOI: 10.1016/S0263-8231(01)00032-5.
- [17] Hofmeyer, H. Cross-section crushing behaviour of hat-sections (Part I: Numerical modelling). *Thin-Walled Structures* 2005, 8, Vol. 43, No. 8, pp. 1143-1154. ISSN 0263-8231. doi: DOI: 10.1016/j.tws.2005.03.009.
- [18] Korvink, S.A., van den Berg, G.J. & van der Merwe, P. Web crippling of stainless steel cold-formed beams. *Journal of Constructional Steel Research* 1995, Vol. 34, No. 2-3, pp. 225-248. ISSN 0143-974X. doi: DOI: 10.1016/0143-974X(94)00026-E.
- [19] Talja, A. & Salmi, P. Design of stainless steel RHS beams, columns and beam-columns. VTT Research Notes 1619. Espoo, Finland: VTT Technical Research Centre of Finland, 1995.
- [20] Baddoo, N., Chinen, V.L., Gozzi, J., Clarin, M., Conrad, F., Talja, A., Ala-Outinen, T., Viherma, R., Nilimaa, H., Gardner, L., Zili, G., Riscifuli, S., Fattorini, F., Kasper, R., Stangenberg, H., Blanguernon, A. & Zhao, B. Structural design of cold worked austenitic stainless steel. Brussels: European Commission, 2004.
- [21] Zhou, F. & Young, B. Cold-Formed Stainless Steel Sections Subjected to Web Crippling. *Journal of Structural Engineering* 2006, 01, Vol. 132, No. 1, pp. 134-144. ISSN 07339445. doi: 10.1061/(ASCE)0733-9445(2006)132:1(134).
- [22] Zhou, F. & Young, B. Experimental and numerical investigations of cold-formed stainless steel tubular sections subjected to concentrated bearing load. *Journal of Constructional Steel Research* 2007, 11, Vol. 63, No. 11, pp. 1452-1466. ISSN 0143-974X. doi: DOI: 10.1016/j.jcsr.2006.12.007.
- [23] Zhou, F. & Young, B. Experimental Investigation of Cold-Formed High-Strength Stainless Steel Tubular Members Subjected to Combined Bending and Web Crippling. *Journal of Structural Engineering* 2007, 07, Vol. 133, No. 7, pp. 1027-1034. ISSN 07339445. doi: 10.1061/(ASCE)0733-9445(2007)133:7(1027).
- [24] Zhou, F. & Young, B. Cold-Formed High-Strength Stainless Steel Tubular Sections Subjected to Web Crippling. *Journal of Structural Engineering* 2007, 03, Vol. 133, No. 3, pp. 368-377. ISSN 07339445. doi: 10.1061/(ASCE)0733-9445(2007)133:3(368).
- [25] Zhou, F. & Young, B. Yield line mechanism analysis on web crippling of cold-formed stainless steel tubular sections under two-flange loading. *Engineering Structures* 2006, 5, Vol. 28, No. 6, pp. 880-892. ISSN 0141-0296. doi: DOI: 10.1016/j.engstruct.2005.10.021.
- [26] Zhou, F. & Young, B. Web Crippling of Cold-Formed Stainless Steel Tubular Sections. *Advances in Structural Engineering* 2008, 12, Vol. 11, No. 6, pp. 679-691. ISSN 13694332.
- [27] Abaqus
- [28] Technical Note No. 902. Ramberg, W. & Osgood, W.R. Description of stress-strain curves by three parameters. Washington, D.C., USA: National Advisory Committee for Aeronautics, 1943.
- [29] Mirambell, E. & Real, E. On the calculation of deflections in structural stainless steel beams: an experimental and numerical investigation. *Journal of Constructional Steel Research* 2000, 4, Vol. 54, No. 1, pp. 109-133. ISSN 0143-974X. doi: DOI: 10.1016/S0143-974X(99)00051-6.
- [30] Rasmussen, K.J.R. Full-range stress-strain curves for stainless steel alloys. *Journal of Constructional Steel Research* 2003, 1, Vol. 59, No. 1, pp. 47-61. ISSN 0143-974X. doi: DOI: 10.1016/S0143-974X(02)00018-4.
- [31] Gardner, L. & Ashraf, M. Structural design for non-linear metallic materials. *Engineering Structures* 2006, 5, Vol. 28, No. 6, pp. 926-934. ISSN 0141-0296. doi: DOI: 10.1016/j.engstruct.2005.11.001.
- [32] Rasmussen, K.J.R., Burns, T., Bezkorovainy, P. & Bambach, M.R. Numerical modelling of stainless steel plates in compression. *Journal of Constructional Steel Research* 2003; 59(11): 1345-1362.
- [33] Ellobody, E. & Young, B. Structural performance of cold-formed high strength stainless steel columns. *Journal of Constructional Steel Research* 2005; 61(12): 1631-1649.

- [34] Jandera, M., Gardner, L. & Machacek, J. Residual stresses in cold-rolled stainless steel hollow sections. *Journal of Constructional Steel Research* 2008; 64(11): 1255-1263.
- [35] Rossi, B., Jaspart, J. & Rasmussen, K.J.R. Combined Distortional and Overall Flexural-Torsional Buckling of Cold-Formed Stainless Steel Sections: Design. *Journal of Structural Engineering* 2010; 136(4): 361-369
- [36] Ashraf, M., Gardner, L. & Nethercot, D.A. Finite element modelling of structural stainless steel cross-sections. *Thin-Walled Structures* 2006; 44(10): 1048-1062.
- [37] Gardner, L. & Theofanous, M. Experimental and Numerical Studies of Lean Duplex Stainless Steel Beams. *Journal of Constructional Steel Research* 66 (2010) 816-825.
- [38] Dawson RG, Walker AC. Post-buckling of geometrically imperfect plates. *Journal of the Structural Division, ASCE* 1972;98:ST1:75_94.
- [39] Gardner, L. & Nethercot, D.A. Numerical Modeling of Stainless Steel Structural Components - A Consistent Approach. *Journal of Structural Engineering, ASCE* 2004; 130(10); 1586-601.
- [40] Gardner, L., Talja, A., Baddoo, N. R. Structural design of high-strength austenitic stainless steel. *Thin Walled Structures* 44 (2006), 517-528.
- [41] SAFSS Project. Work Package 2, Model calibration tests. VTT (2011).
- [42] Talja A, and Salmi P. (1995). Design of stainless steel RHS beams, columns and beam-columns. Research Note 1619, VTT Building Technology, Finland.
- [43] Hradil P, Fülöp L and Talja A (2011). Global stability of thin-walled ferritic stainless steel members. ICTWS2011



Research Fund for Coal & Steel

Structural Applications of Ferritic Stainless Steels (SAFSS)

Technical note: Abaqus plugin user manual

Project name: Structural Applications of Ferritic Stainless Steels
Project's short name: SAFSS
Project number: 39594

Change log:

Version	Date	Status	Author(s)	Remarks
0.07	14.09.10	pre-alpha	Petr Hradil	First draft of manual
0.08	27.10.10	alpha	Petr Hradil	Model and Analysis separated
0.09	20.12.10	alpha	Petr Hradil	Improved plug-in functionality
0.10	21.12.10	alpha	Petr Hradil	Added tutorial
0.11	01.03.11	alpha	Petr Hradil	Enhanced material properties and Residual stresses
0.14	22.03.11	closed beta	Petr Hradil	Installer added
0.17	26.05.11	closed beta	Petr Hradil	Possibility of multiple buckling modes
0.18	24.11.11	closed beta	Petr Hradil	Contact loading
0.19	12.12.11	closed beta	Petr Hradil	Minor debugging
0.20	30.01.12	closed beta	Petr Hradil	Option to specify amplitude manually after LEA
0.24	01.03.12	closed beta	Petr Hradil	Option to specify material enhancement manually
0.25	15.06.12	closed beta	Petr Hradil	Denser mesh in specified regions

Distribution: Project group

SAFSS Profiler



Contents

1	Introduction.....	4
2	Development plan	4
3	Installation/Uninstallation.....	4
4	Analysis name	6
5	Section tab.....	6
5.1	Profile selection and parameters.....	6
5.2	Length of the member	7
6	Material tab	8
6.1	Ramberg & Osgood model with Hill's modification.....	8
6.2	Mirambell & Real model.....	9
6.3	Rasmussen's modification.....	9
6.4	Gardner's modification	10
6.5	Transformation for Abaqus solver.....	10
6.6	Enhanced material properties	11
6.7	Residual stresses	12
7	Model tab.....	14
7.1	Experimental layout of pre-defined and user-defined tests.....	14
7.1.1	Stub column tests.....	15
7.1.2	Plate buckling tests	15
7.1.3	Member buckling test.....	15
7.1.4	Bending test.....	16
7.1.5	Web-crippling tests	16
7.2	Element selection.....	16
7.2.1	General purpose shell elements	17
7.2.2	Thin shell elements	17
7.3	Mesh size.....	17
8	Analysis tab.....	18
8.1	Imperfections	18
8.2	GMNIA settings.....	19
9	Calculation report.....	20
10	User-defined profiles	20
10.1	Editing "profiles.cfg" file	20
10.2	Keywords.....	21
10.3	Compiling the configuration file	22
11	User-defined experimental set-ups.....	22
11.1	General keywords.....	22
11.2	Keywords applicable to particular profile	25
12	Example calculation: Plate buckling	27
12.1	Experimental set-up configuration	27
12.2	Profile definition	28
12.3	Material definition.....	29

12.4	Model definition	31
12.5	Analysis settings.....	31
12.6	Simulation outputs.....	32
13	Example calculation: Web crippling	35
13.1	Creating the test set-up	36
13.1.1	Dividing member into segments.....	36
13.1.2	Definition of special-purpose faces	37
13.1.3	Creating supports.....	37
13.1.4	Creating loads	37
13.1.5	Definition of measuring points	38
13.1.6	Saving the experimental setup.....	38
13.2	Running the analysis.....	39
13.2.1	Basic settings	39
13.2.2	Caluclation.....	39
13.2.3	Report file.....	40
	References	41

1 Introduction

The following documentation describes the Abaqus plug-in developed in VTT, Technical Research Centre of Finland for SAFSS project.

2 Development plan

Pre-alpha phase (July 2010 – September 2010)

This stage covers all activities performed during the software project prior to testing. These activities include requirements analysis, software design, software development and unit testing.

Alpha phase and White box testing (October 2010 – December 2010)

The alpha phase of the release life cycle is the first phase to begin software testing. Alpha software can be unstable and could cause crashes or data loss. White box testing refers to testing of internal structure opposed to software functionality (black box testing)

Alpha release and Black box testing (January 2011 – March 2011)

Moving to black box testing within the project group is known as alpha release. The software functionality is tested preferably by another team. During WP 2.2 of SAFSS project the plug-in will be tested by VTT and UPC. The alpha phase ends with a feature freeze, indicating that no more features will be added to the software. At this time, the software is said to be feature complete.

Beta phase (April 2011 – June 2011)

The focus of beta testing is reducing impacts to users, often incorporating usability testing. Plug-in will be tested according to WP 2.3 of SAFSS project plan.

Release candidate (July 2011)

The first stable version of the software ready to be used for WP 2.4 of SAFSS project is called release candidate.

3 Installation/Uninstallation

- a) Run ProfilerSetup.exe.
- b) Select the installation folder. The folder has to be a subdirectory of abaqus_plugins in order to be recognized in Abaqus.



Figure 1 Instalation folder

c) Select the Abaqus working directory where “experiments.cfg” will be copied.

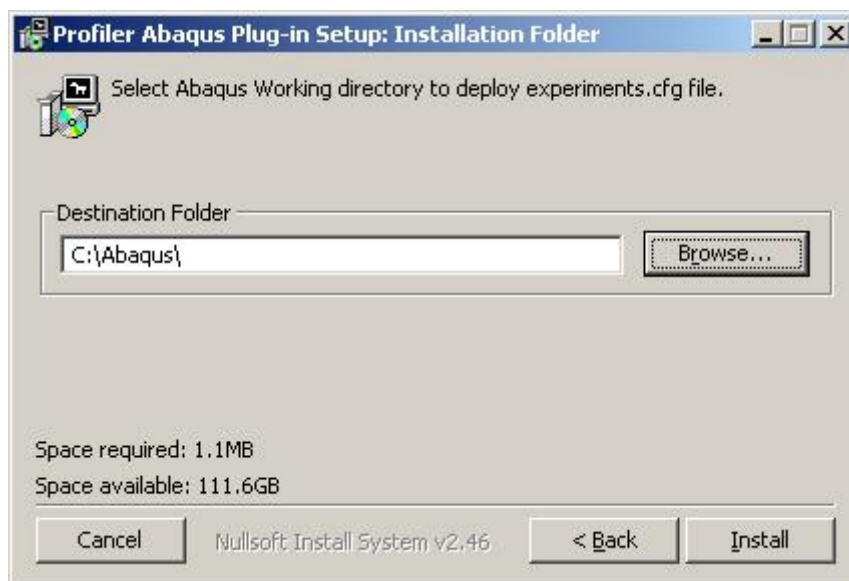


Figure 2 Abaqus working directory

d) Press “Install” button

The plug-in can be uninstalled either by executing “uninstall.exe” in the plug-in folder or from the Windows control panel.

4 Analysis name

The default name of analysis is 'SAFSS' and it can be changed by user. This name will be the name of job files (e.g. 'SAFSS.odb', 'SAFSS.dat') and a folder with the same name will be created in working directory containing the report files.

5 Section tab

The first tab allows user to specify geometry of the member.

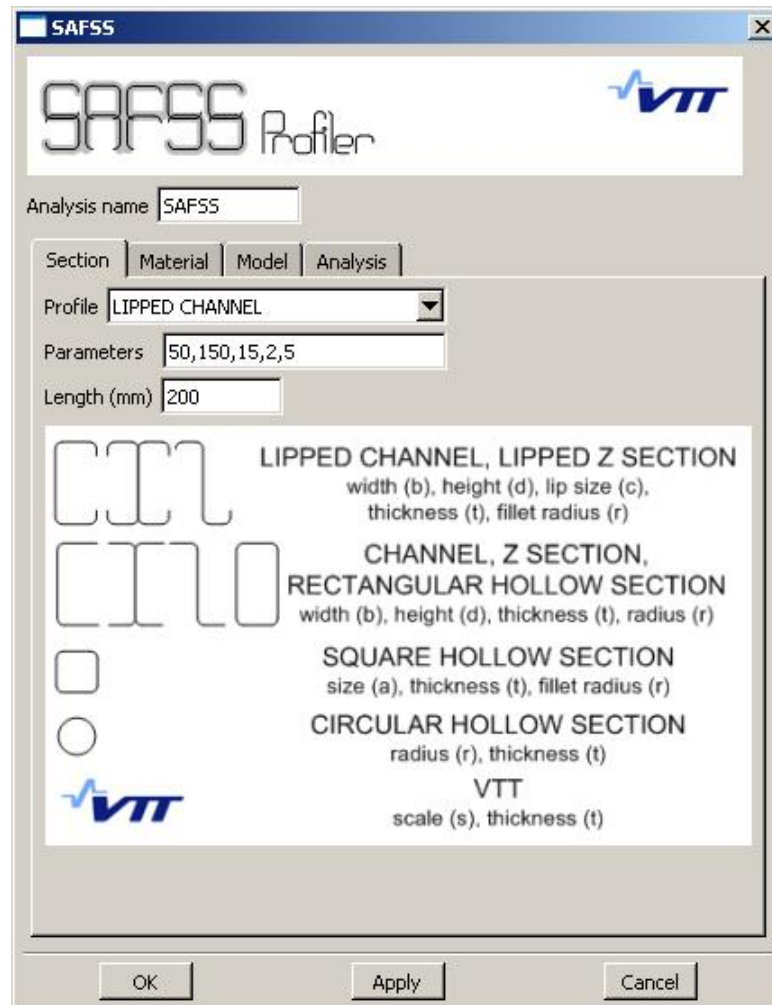


Figure 3 Section tab

5.1 Profile selection and parameters

In the "Profile" drop-down menu, user selects pre-defined profiles and user-defined profiles included in the database file "profiledef.py". Each profile usually has a set of different number of parameters that has to be entered in the following row. In case of pre-defined profiles, the number and ordering of parameters is indicated on the picture.

If the wrong number of parameters is specified, the program shows the following message:

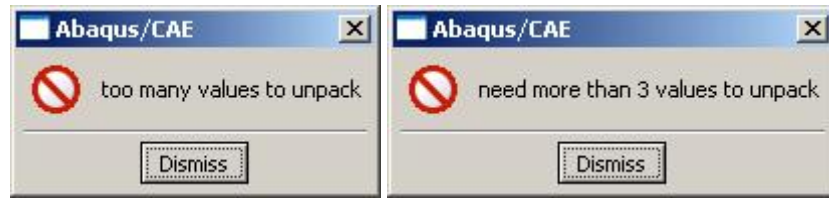


Figure 4 Too many or too few parameters specified

User-defined profiles are selected by choosing “USER DEFINED” option in “Profile” menu and specifying all parameters including the profile identification in the beginning.

Examples of user-defined profiles:

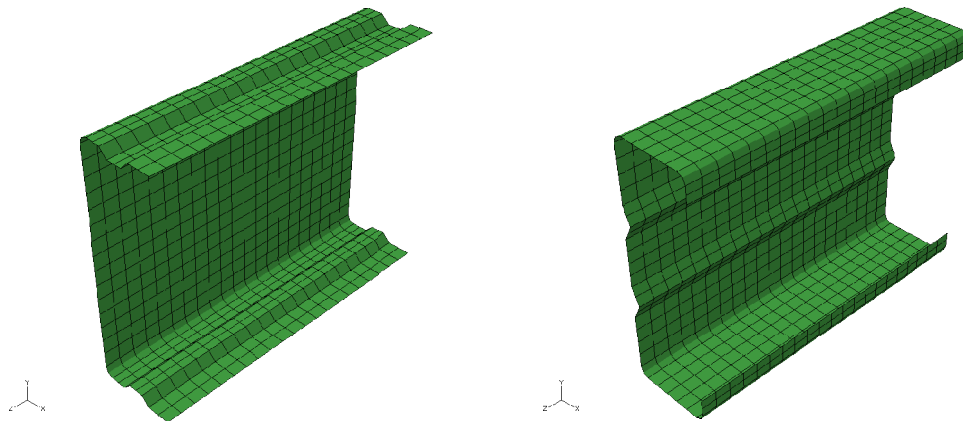


Figure 5 Stiffened track section (SC,50,150,20,2,5) and modified lipped C-section (MLC,50,150,15,20,5,50,2,5)

5.2 Length of the member

Length is indicating the effective length of the member in the same units as section parameters are specified (recommended mm). The real length, however, can be different according to the experiment settings.

For example in 4-point bending test it can be specified (in “experiments.cfg”) that the first support is from -0,01 to 0,01 (x L) and the last one is from 0,99 to 1,01 (x L) which means that the real length of the member is from -0,01 to 1,01 (x L) and the member is 2% longer, while the theoretical span remains 100% because it is from 0,00 to 1,00 (x L).

6 Material tab

Material properties can be entered in the material tab. Selection of material model and its parameters follows the same rules as selection of profiles. Only pre-defined material models can be used. The first line indicates the material model and the type of enhanced material properties and residual stresses distribution.

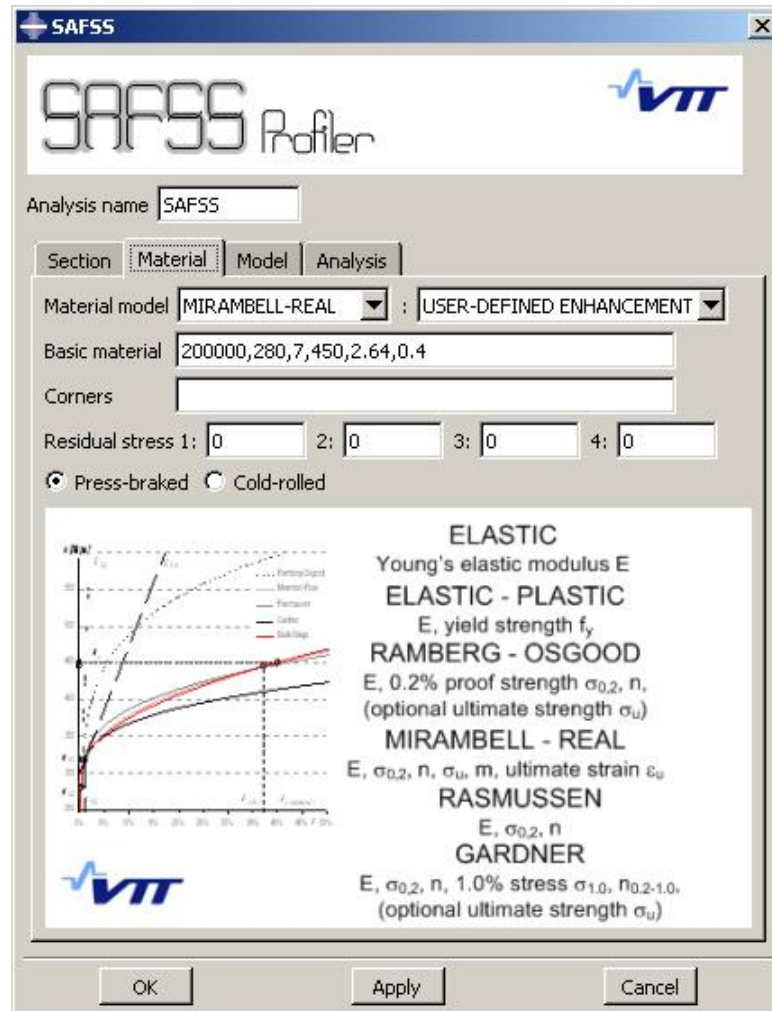


Figure 6 Material tab

6.1 Ramberg & Osgood model with Hill's modification

The original non-linear model developed for aluminium alloys proved to be suitable also for stainless steel and other metallic materials. The offset yield stress was suggested to be 0,2% proof stress for stainless steel.

$$\varepsilon = \frac{\sigma}{E_0} + 0,002 \left(\frac{\sigma}{\sigma_{0,2}} \right)^n,$$

This model is included in AS/NZS 4373:2001, Eurocode 3, Part 1-4 (calculation of deflections) and SEI/ASCE.

If the ultimate strength is not specified, it is automatically calculated as 2 times 0,2% proof stress.

6.2 Mirambell & Real model

A new model developed from Ramberg-Osgood formulation includes also strain hardening effect and is able to describe the material behaviour more precisely for strains larger than 0,2%. It introduces a new Ramberg & Osgood curve originating from 0,2% stress and continuing with the same tangent modulus but with different parameter of non-linearity (called “m” in this case).

$$\varepsilon = \begin{cases} \frac{\sigma}{E_0} + 0,002 \left(\frac{\sigma}{\sigma_{0,2}} \right)^n & \text{for } \sigma \leq \sigma_{0,2} \\ \frac{\sigma - \sigma_{0,2}}{E_{0,2}} + \varepsilon^* \left(\frac{\sigma - \sigma_{0,2}}{\sigma_u - \sigma_{0,2}} \right)^m + \varepsilon_{0,2} & \text{for } \sigma > \sigma_{0,2} \end{cases},$$

$$\text{where } \varepsilon^* = \varepsilon_u - \varepsilon_{0,2} - \frac{\sigma_u - \sigma_{0,2}}{E_{0,2}}, \text{ 0,2\% strain is } \varepsilon_{0,2} = \frac{\sigma_{0,2}}{E_0} + 0,002$$

$$\text{and tangent modulus was derived as } E_{0,2} = \frac{E_0}{1 + 0,002n(E_0/\sigma_{0,2})}$$

6.3 Rasmussen's modification

Rasmussen's study extends Mirambell & Real model reducing its original six parameters to three.

$$\varepsilon = \begin{cases} \frac{\sigma}{E_0} + 0,002 \left(\frac{\sigma}{\sigma_{0,2}} \right)^n & \text{for } \sigma \leq \sigma_{0,2} \\ \frac{\sigma - \sigma_{0,2}}{E_{0,2}} + \varepsilon^* \left(\frac{\sigma - \sigma_{0,2}}{\sigma_u - \sigma_{0,2}} \right)^m + \varepsilon_{0,2} & \text{for } \sigma > \sigma_{0,2} \end{cases}, \text{ where } \varepsilon^* = 1 - \frac{\sigma_{0,2}}{\sigma_u}, m = 1 + 3,5 \frac{\sigma_{0,2}}{\sigma_u}$$

The model is based on assumption that plastic ultimate strain can be approximated with total ultimate strain with a very small error and it is a function of the 0,2% and ultimate stresses ratio. Also the second non-linear parameter “m” is expressed as the function of the same ratio and both equations originate from the experimental data collected by Rasmussen. The third parameter reduced in Rasmussen's modification of Mirambell & Real model is the ultimate stress that can be calculated from the following relations:

$$\frac{\sigma_{0,2}}{\sigma_u} = \begin{cases} 0,2 + 185(\sigma_{0,2}/E_0) & \text{for austenitic and duplex alloys} \\ 0,2 + 185(\sigma_{0,2}/E_0) \\ \frac{1 - 0,0375(n-5)}{1 - 0,0375(n-5)} & \text{for all alloys} \end{cases}$$

Rasmussen's model is included in informative Annex C of Eurocode 3, Part 1-4.

6.4 Gardner's modification

Gardner proposed another interesting modification of Mirambell & Real material model, where the second part of Ramberg-Osgood curve passes through 1,0% proof stress instead of ultimate stress. This approach is said to be more convenient because it can include also compressive behaviour (with a good agreement up to 10% strain) where there is no ultimate value and finally, the 1,0% stress is closer to the mostly used area of application of the material model.

$$\varepsilon = \begin{cases} \frac{\sigma}{E_0} + 0,002 \left(\frac{\sigma}{\sigma_{0,2}} \right)^n & \text{for } \sigma \leq \sigma_{0,2} \\ \frac{\sigma - \sigma_{0,2}}{E_{0,2}} + \left[0,008 - (\sigma_{1,0} - \sigma_{0,2}) \left(\frac{1}{E_{0,2}} - \frac{1}{E_0} \right) \right] \left(\frac{\sigma - \sigma_{0,2}}{\sigma_{1,0} - \sigma_{0,2}} \right)^{n_{0,2}-1,0} + \varepsilon_{0,2} & \text{for } \sigma > \sigma_{0,2} \end{cases}$$

If the ultimate strength is not specified, it is automatically calculated as 2 times 0,2% proof stress.

6.5 Transformation for Abaqus solver

According to the Abaqus documentation, nominal (engineering) stress is recalculated to true stress and nominal (engineering) strain to logarithmic (true) strain using following equations:

$$\sigma_{true} = \sigma_{nom} (1 + \varepsilon_{nom})$$

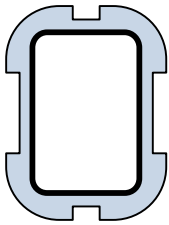
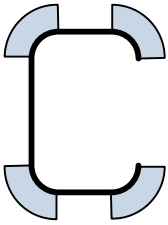
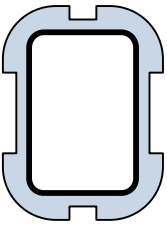
$$\varepsilon_{true} = \ln(1 + \varepsilon_{nom}) - \frac{\sigma_{true}}{E}$$

The equations proposed by Abaqus user documentation can produce small negative values in the first few points which are automatically changed to zeroes.

6.6 Enhanced material properties

The enhanced material properties are calculated separately in the flat parts (f) and corners (c) using virgin material (mill certificate) values (v). If any of the following options are selected, the basic material model is treated as virgin material and both areas (flats and corners) can have different properties in the model. In case of press-braked sections, it is also possible to get all necessary values for 1,0% proof stress and therefore Gardner's material model can be used. Otherwise only Mirambell&Real, Rasmussen and Ramberg&Osgood models are applicable.

Table 1 Enhanced material properties

	Cruise: Cold-rolled	Cruise: Press-Braked	Rossi: Cold-rolled
	 (corner extension 2t)	 (only corners)	 (corner extension 2t)
$\sigma_{02,f}$	$\frac{0,85 \sigma_{02,v}}{-0,19 + \frac{1}{12,42[\pi t/2(b+d)] + 0,83}}$ (Cruise 2008)	no change	$\sigma_{02,v} + \frac{\sigma_{u,v}}{C_1 \left[\frac{(b+d)/\pi}{t/2} \right] + C_2 \left[\frac{(b+d)/\pi}{t/2} \right]^\alpha}$ (Rossi 2010)
$\sigma_{u,f}$	$\sigma_{u,v} \left[0,19 \left(\frac{\sigma_{02,f}}{\sigma_{02,v}} \right) + 0,85 \right]$ (Cruise 2008)	no change	$\sigma_{u,v} \left[0,19 \left(\frac{\sigma_{02,f}}{\sigma_{02,v}} \right) + 0,85 \right]$ (Cruise 2008)
$\sigma_{02,c}$	$0,83 \sigma_{u,f}$ (Cruise 2008)	$\frac{1,673 \sigma_{02,v}}{(r_i/t)^{0,126}}$ (Cruise 2008)	$\sigma_{02,v} + \frac{\sigma_{u,v}}{C_1 \left(\frac{r_i}{t/2} \right) + C_2 \left(\frac{r_i}{t/2} \right)^\alpha}$ (Rossi 2010)
$\sigma_{u,c}$	$0,75 \sigma_{02,c} \left(\frac{\sigma_{u,v}}{\sigma_{02,v}} \right)$ (Ashraf and Nethercot, 2005)	$0,75 \sigma_{02,c} \left(\frac{\sigma_{u,v}}{\sigma_{02,v}} \right)$ (Ashraf and Nethercot, 2005)	$0,75 \sigma_{02,c} \left(\frac{\sigma_{u,v}}{\sigma_{02,v}} \right)$ (Ashraf and Nethercot, 2005)
$\sigma_{10,c}$	n/a	$1,21 \sigma_{02,c}$ (Ashraf and Nethercot, 2005)	n/a

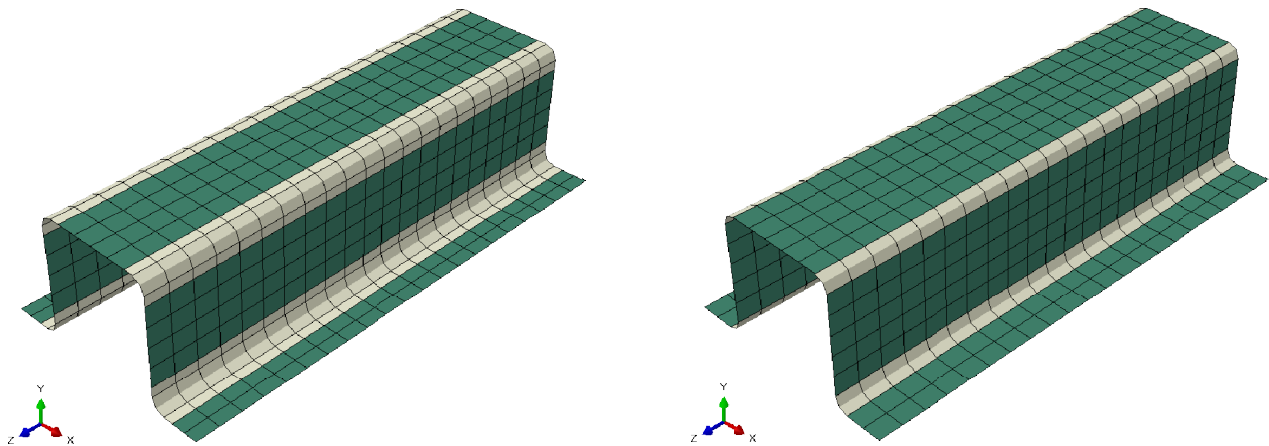


Figure 7 Material distribution pattern for cold-rolled profiles (left) and press-braked profiles (right)

If none of the predictive models is used (the default option of user-defined enhancement is selected), user have an option to define flat parts (basic) material and optionally the enhanced material in corners. If no corner enhancement is used, the inserted values should represent the average properties in the cross-section.

6.7 Residual stresses

For the magnitude of bending residual stresses surface values, we are using Gardner's and Cruise's model that was tested for hollow sections made by circle-to-rectangle forming (CRF) process and for press-braked sections. For the cold-formed sections directly from sheet metal, we don't have enough data, however, the results published by Shafer and Peköz indicate that similar flat part stresses could be observed between two corners with the same orientations but at the end of open-section centre line, the residual stresses are smaller in flat parts than in the corners. Therefore we suggest using 15% of yield strength like in case of press-braked sections.

The residual stresses are inserted as initial model conditions using Abaqus keyword

***INITIAL CONDITIONS, TYPE=STRESS, SECTION POINTS, UNBALANCED
STRESS=STEP**

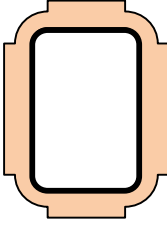
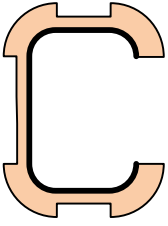
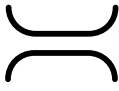


with the through-thickness fully plastic distribution.

Supplementary residual strains are inserted as

***INITIAL CONDITIONS, TYPE=HARDENING, SECTION POINTS**

with the through-thickness linear distribution (assumes that cross-section remains planar after deformation).

Table 2 Residual stresses

	Cold-formed	Press-braked	User-defined
			?
corners	$0,37 f_y$ (Gardner et al., 2009)	$0,36 f_y$ (Gardner et al., 2009)	Option 1 (fraction of f_y)
flats between two corners with the same orientation 	$0,63 f_y$ (Gardner et al., 2009)	$0,15 f_y$ (Gardner et al., 2009)	Option 2 (fraction of f_y)
flats between one corner and one free end 	$0,15 f_y$	$0,15 f_y$ (Gardner et al., 2009)	Option 3 (fraction of f_y)
flats between two opposite corners or two free ends 	0,0 ($0,63 f_y$ in case of two free ends*)	0,0 ($0,15 f_y$ in case of two free ends*)	Option 4 (fraction of f_y)
* a flat part without corners is considered as a special case of coupon test if user selects enhanced properties/residual stresses model and therefore it contains residual stress pattern as if cut from the cold-formed specimen.			

The user-defined stresses are active in combination with the default selection of predictive models (user-defined enhancement).

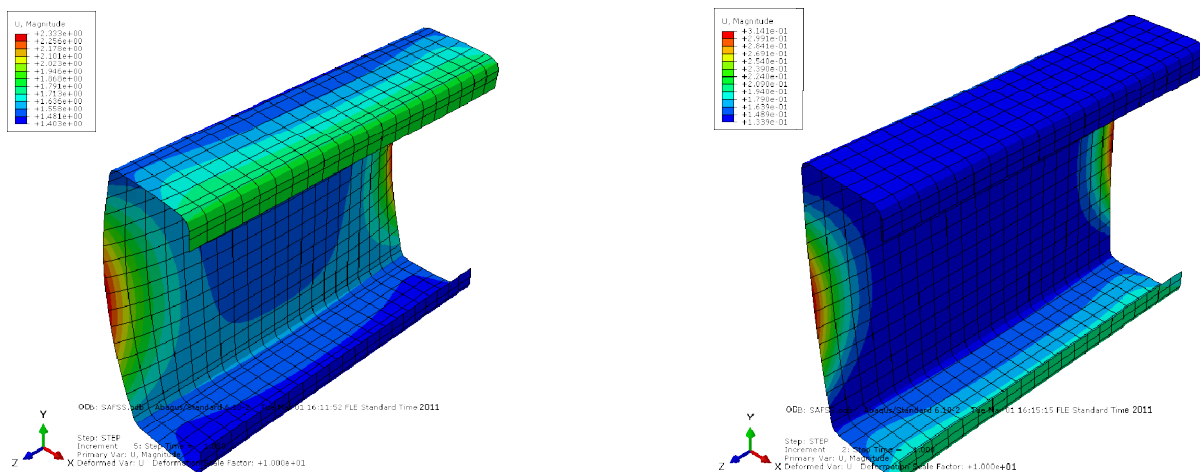


Figure 8 Cold-rolled C section with higher residual stresses in the flat parts (left) and press-braked C section with lower residual stresses in the flat parts (right) – deformation after stress release (10x scaled)

7 Model tab

In the model tab, user can define the test to be performed as well as others information needed for creating FE models.

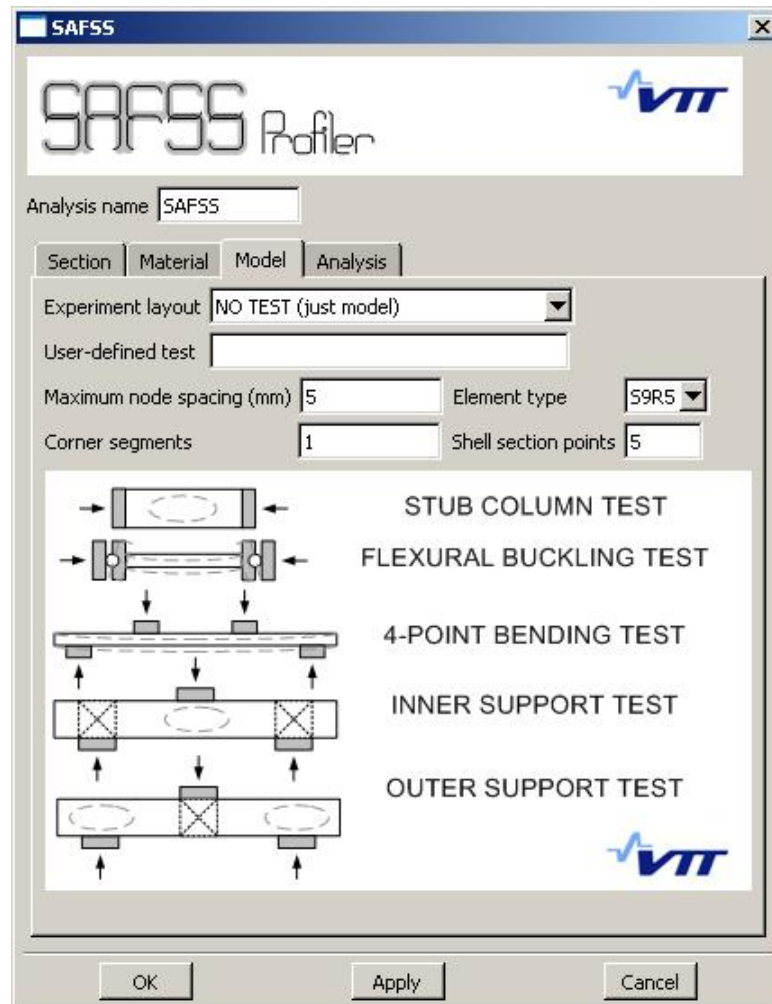


Figure 9 Model tab

7.1 Experimental layout of pre-defined and user-defined tests

Experimental layout drop-down menu offers several pre-defined possibilities of experimental testing. All of them can be modified by user; however, adding a new one requires writing its full name in the textbox below.

Selecting the first option “NO TEST (just model)” will create only geometrical model of member without any supports and loads. Other options will try to execute the buckling and Riks analyses as required.

In the “user-defined test” textbox the custom name of the experimental set-up can be entered and it will override the settings above.

7.1.1 Stub column tests

In order to keep longitudinal deformation of the loaded cross-section equal in all nodes and at the same time release (or restrain) nodal rotation, stub column tests are loaded with deformation and therefore few special rules apply for them.

“Stub column test (free)” simulates rotation-free support condition at the end-supports, while “Stub column test (fixed)” simulates fixed boundary conditions. They produce different imperfection distribution as is demonstrated in the following picture:

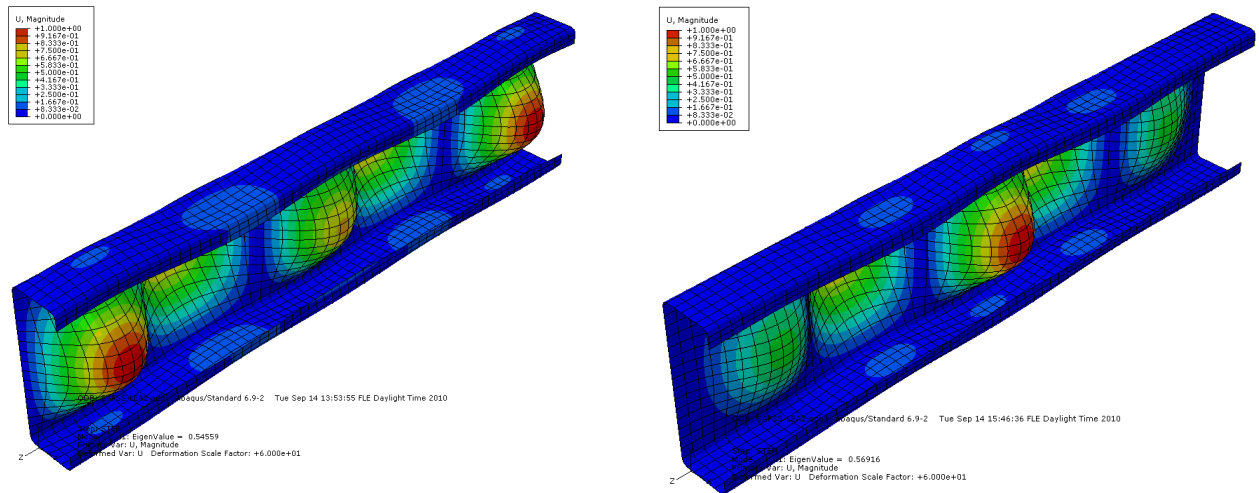


Figure 10 Stub column tests local buckling modes (test 1 – left, test 2 – right)

The simulation is terminated when longitudinal deformation reaches specified fraction of the length (default is 1%).

7.1.2 Plate buckling tests

Plate buckling tests are basically the same as stub column tests but additionally longitudinal edges are supported in the profile on the “top”, “bottom”, “left” and “right” faces. Although the primary purpose of this experimental set-up is to use it in combination with “Plate” profile, it is able to replace stub column tests of longer specimen where the first buckling mode would be normally global buckling.

7.1.3 Member buckling test

Standard member buckling compression test simulates pinned conditions at both ends by making end-sections rigid and by supporting and loading them in their centres of gravity. Because the member is loaded with force, its load level can be directly controlled during the virtual experiment and the calculation is usually terminated when 3 consequent decreasing loads are reported.

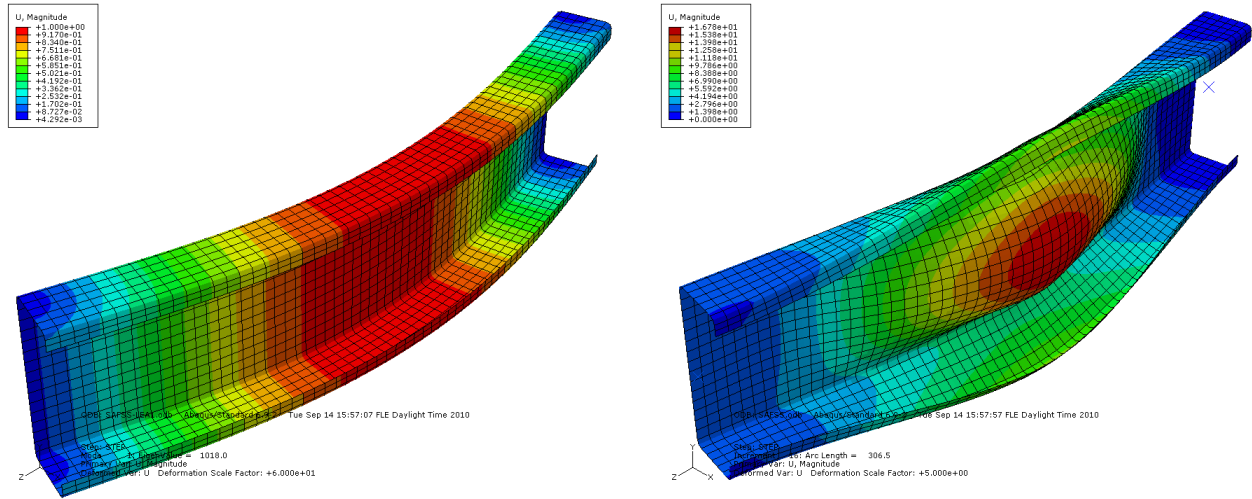


Figure 11 Flexural buckling test: first global buckling mode (left) and GMNIA deformed shape (right)

7.1.4 Bending test

In case of bending, the most used experimental setup is 4-point bending with loads in 1/3 and 2/3 of the span.

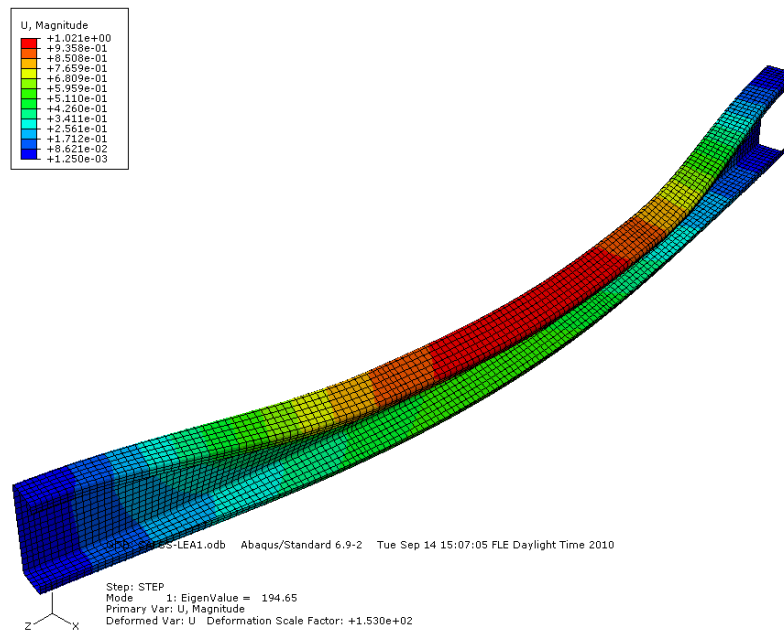


Figure 12 Global buckling mode in bending test

7.1.5 Web-crippling tests

Also several versions of web-crippling test are included in the “experiments.cfg” file. Two versions of internal and two versions of external support tests have different load (in case of internal test) or support (in case of external) conditions.

7.2 Element selection

The typical model sensitivity for element and mesh selection is up to 15% of peak load when considering the following options:

7.2.1 General purpose shell elements

FEM solvers offer usually several types of general purpose linear shell elements with finite strain formulation and 6 degrees of freedom at each node. Basic **S4** shell elements are usually strain-locking in out-of-plane bending situations and user needs at least 5 elements per face to avoid it. On the other hand, **S4R** elements do not have this problem, but may provide inaccurate results due to hourglassing that occurs in linear elements with reduced integration.

7.2.2 Thin shell elements

Thin shells can be modelled also with small strain elements, where the transverse shear deformation is neglected resulting in 5 degrees of freedom per node. Linear **S4R5** elements with 4 nodes suffer the same problems as S4R. There are also two quadratic elements available in Abaqus: **S8R5** and **S9R5** with 8 nodes and 9 nodes respectively, where the hourglassing is not an issue due to their nonlinear nature. According to Abaqus user documentation “S8R5 may give inaccurate results for buckling problems of doubly curved shells due to the fact that the internally defined centre node may not be positioned on the actual shell surface. Element type S9R5 should be used instead.”

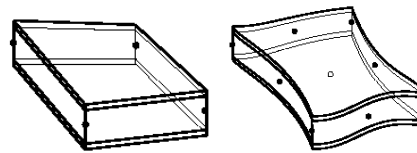


Figure 13 typical linear and quadratic shell elements

7.3 Mesh size

According to the parametric study, there should be more than 5 elements with linear shape function (S4/S4R/S4R5) per buckling half-wave in order to avoid locking. However, elements with quadratic shape function (S8R5/S9R5) provide acceptable results starting with only one element per buckling half-wave. It should be noted that quadratic elements are spanning three nodes which produces less number of bigger elements in the model.

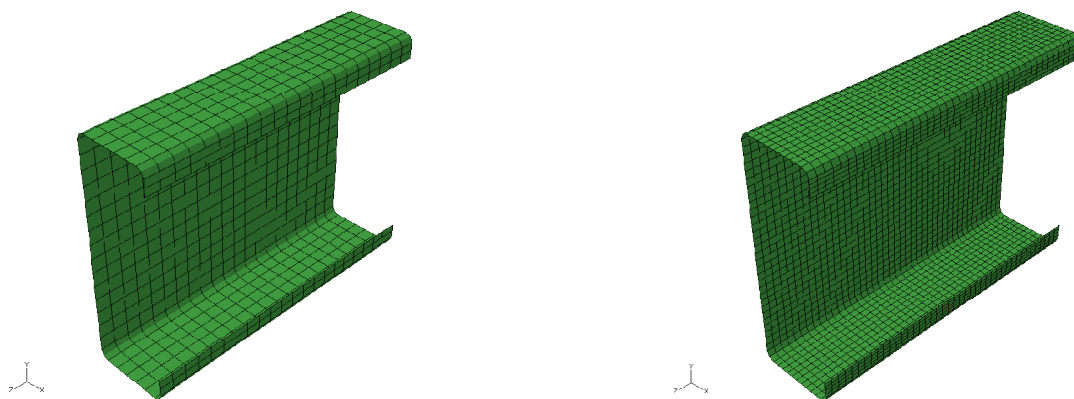
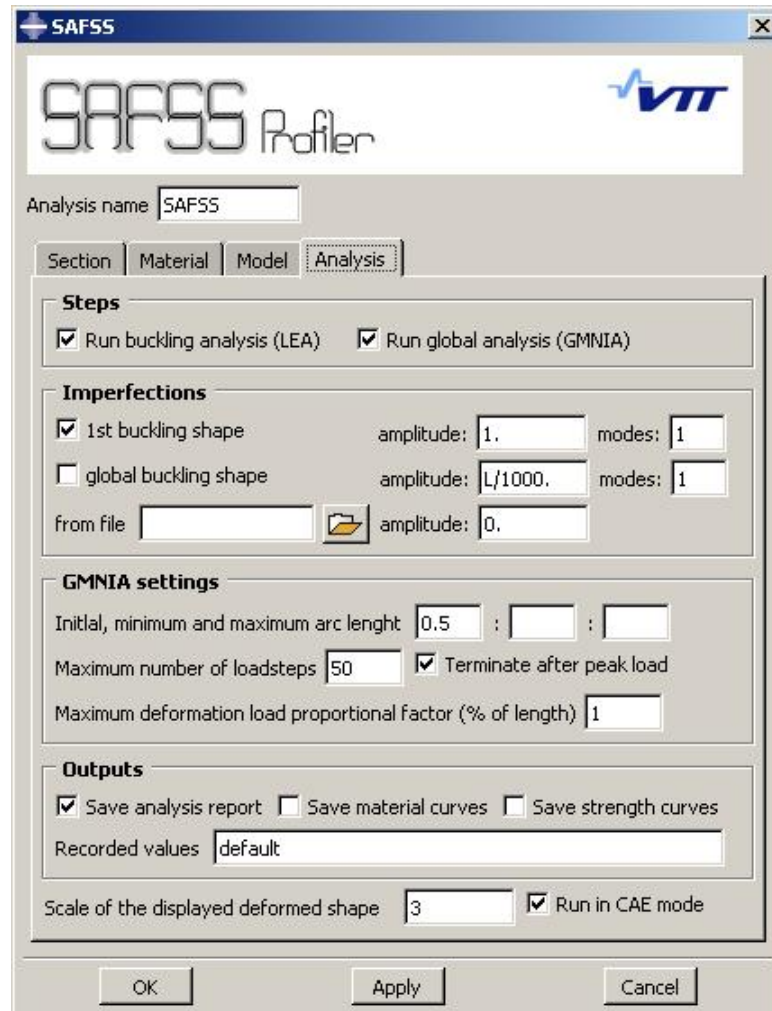


Figure 14 Quadratic elements (S9R5) – left, and linear elements (S4R) – right, with the same node spacing

Corners are meshed differently than flat parts. The governing parameter is ‘Corner segments’ which creates additional nodes along the corner arc if the number is higher than 2. On the Figure 14, one segment is entered in case quadratic elements (left) and two segments were set in case of linear elements (right). The smallest acceptable value is 1. If it is needed to model sharp corners, radius equal to zero has to be entered in the section tab instead of modifying segments number.

8 Analysis tab

In the last tab, user can define the Abaqus settings. Both basic parts of the analysis can be selected or deselected. However, if the LEA step is only deselected and the initial imperfections are still required, program will look for the appropriate .odb database containing the imperfection distribution data.



The screenshot shows the 'SAFSS Profiler' window with the 'Analysis' tab selected. The 'Analysis name' field contains 'SAFSS'. The 'Steps' section has two checked options: 'Run buckling analysis (LEA)' and 'Run global analysis (GMNIA)'. The 'Imperfections' section has three options: '1st buckling shape' (checked) with amplitude '1.' and modes '1'; 'global buckling shape' (unchecked) with amplitude 'L/1000.' and modes '1'; and 'from file' (unchecked) with a file selection icon and amplitude '0.'. The 'GMNIA settings' section has 'Initial, minimum and maximum arc length' set to '0.5', 'Maximum number of loadsteps' set to '50', 'Terminate after peak load' checked, and 'Maximum deformation load proportional factor (% of length)' set to '1'. The 'Outputs' section has 'Save analysis report' checked, 'Save material curves' unchecked, 'Save strength curves' unchecked, and 'Recorded values' set to 'default'. The 'Scale of the displayed deformed shape' is set to '3' and 'Run in CAE mode' is checked. At the bottom are 'OK', 'Apply', and 'Cancel' buttons.

Figure 15 Analysis tab

8.1 Imperfections

There are three possible sources of imperfections that can be freely combined according to the user needs. The first (positive) buckling shape is suitable for the local buckling analysis. The “global” buckling shape will create a special FE model, where all the cross-sections are stiffened with rigid membrane elements and therefore the shape of cross-section is not changing during the analysis. This selection usually produces the first global buckling modes; however, it can fail in very short members. The third option is to use external source (.odb database), where the user is responsible for selecting the proper file with the same mesh as the GMNIA file that is going to inherit the imperfection distribution afterwards.

If user requests more than one buckling modes in global or standard LEA, he will be prompted before GMNIA to select the mode he wishes to use.

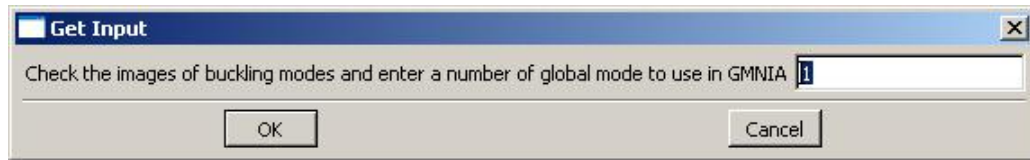


Figure 16 Dialog asking for the buckling mode selection.

Deformed shapes of each calculated mode are saved in the Abaqus working directory in a subfolder named according to the analysis name. It is possible to check those .png pictures before entering the desired number.

If the amplitude of selected analysis is not specified (empty field) or is zero, the user will be prompted to enter a non-zero value after LEA calculation. It is possible to check figure(s) of calculated buckling shape(s) as well.

8.2 GMNIA settings

By default, calculation is terminated when the load proportional factor decreases in three consequent frames indicating that the peak load was already reached. Maximum deformation load proportional factor limit is activated in stub column tests, where it is impossible to have peak load proportional factor and it has to be carefully set in order to record the peak load before the script terminates the calculation.

When the maximum number of loadsteps is reached, job is also terminated and postprocessing tasks are performed automatically.

In the 'recorded values' textbox, users can override default parameters with their own. Values must be separated by commas (e.g. 'FORCES,DISPLACEMENTS'). Acceptable strings are: 'FORCES', 'DISPLACEMENTS', 'MOMENTS', 'STRAINS', 'U1', 'U2', 'U3', 'RF1', 'RF2', 'RF3', 'RM1', 'RM2', 'RM3', 'MISES' and 'E'+3 digits which will produce fraction of nodes with equivalent plastic strain (PEEQ) lower than 1/10000 of the number (e.g. 'E020' will report % of values that are smaller than the 0,2% strain).

9 Calculation report

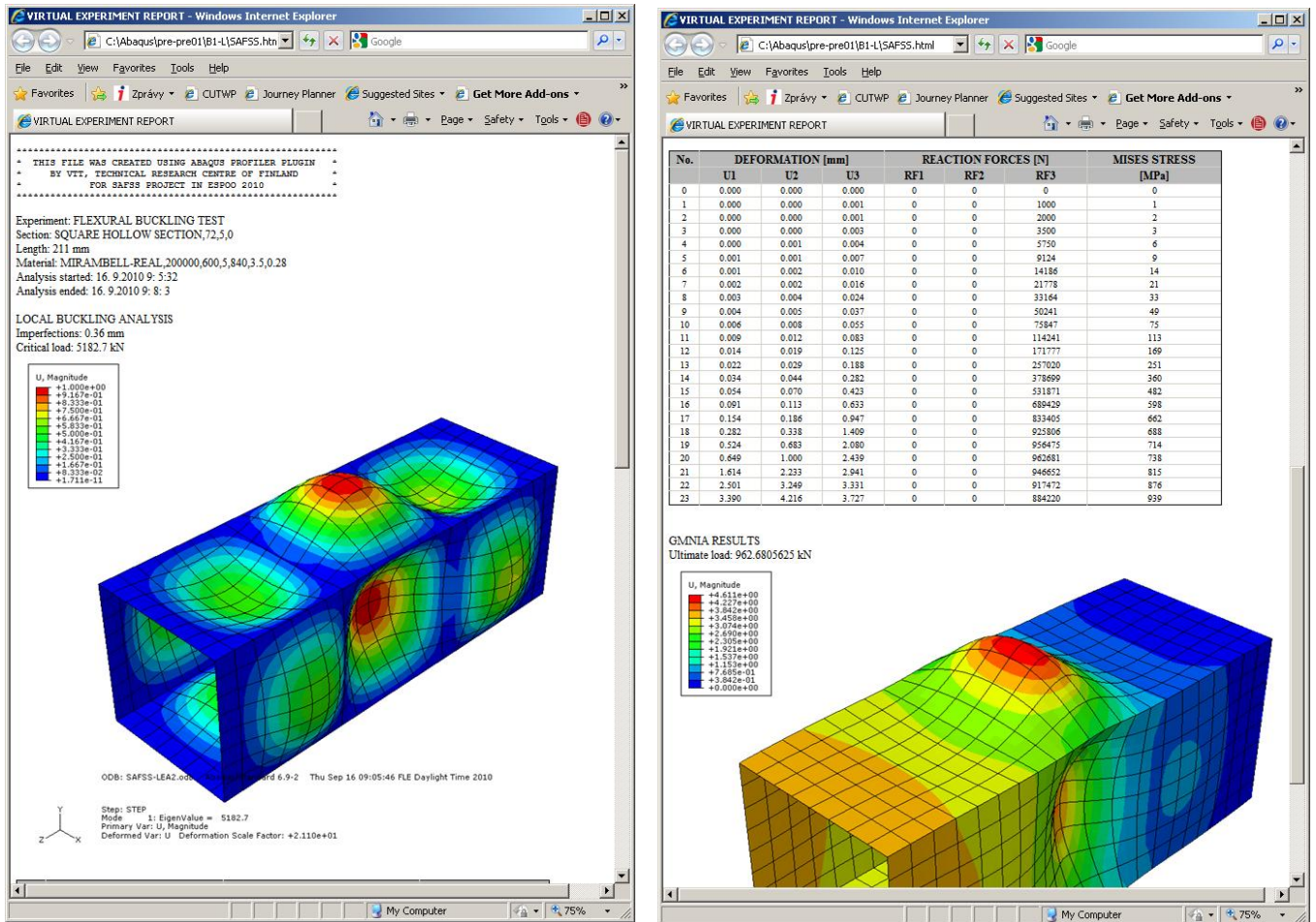


Figure 17 Example of calculation report

The report in HTML format is created automatically after each calculation. It contains:

- Input parameters
- Calculation time (beginning and end)
- Imperfection amplitude (for each LEA calculation)
- Picture of imperfection distribution (for each LEA calculation) in PNG format
- Table of requested output variables.
- Picture of 5x scaled deformed shape (from the last recorded step) in PNG format

At the end of calculation, plug-in attempts to open internet explorer and display the report.

10 User-defined profiles

Users can define the python database file “profiledef.py” directly or use the configuration text file “profiles.cfg” and recompile the database running the “safss.py” script. The former option is recommended only for experienced users skilled in python programming.

10.1 Editing “profiles.cfg” file

Configuration file is a regular text file with the following syntax:

Line starting with “**” indicates the new profile and contains list of possible names of profile.

Line starting with “*” indicates the keyword and it is followed usually by several lines with specific parameters.

Example of profile definition:

```
**SQUARE HOLLOW SECTION,SHS
*VARIABLES
a,t,r
*POINTS
00: a/2,-((a/2)-r)
01: a/2,(a/2)-r
02: (a/2)-r,a/2
03: -((a/2)-r),a/2
04: -(a/2),(a/2)-r
05: -(a/2),-((a/2)-r)
06: -((a/2)-r),-(a/2)
07: (a/2)-r,-(a/2)
*LINES
00: 0,1,t
01: 2,3,t
02: 4,5,t
03: 6,7,t
*FILLETs
00: 1,2,t,r,(a/2)-r,(a/2)-r
01: 3,4,t,r,-((a/2)-r),(a/2)-r
02: 5,6,t,r,-((a/2)-r),-((a/2)-r)
03: 7,0,t,r,(a/2)-r,-((a/2)-r)
```

10.2 Keywords

***VARIABLES**

The next line should contain a list of variables used in profile specification. In our example they are side length (a), thickness (t) and corner radius (r).

***POINTS**

The following lines contain x,y coordinates of points. The first 4 characters are ignored and serve only for the user. It is recommended to use them for numbering (starting from 0) as it is demonstrated in the example.

***LINES**

The following lines contain point1, point2, thickness (starting from the 5th character)

***FILLETs**

The following lines contain point1, point2, thickness, radius, x, y coordinates of the arc centre.

10.3 Compiling the configuration file

Before running the plug-in with new user-defined profiles, the configuration file should be recompiled into the “profiledef.py” python-based module. It is done automatically by executing “safss.py” script by some Python interpreter (e.g. in Abaqus “File” -> “Run script”). Because “safss.py” is the basic module for creating Abaqus input files, it also attempts to find “calculation.cfg” and build new models. Therefore several warnings can be displayed when recompiling the profile database.

11 User-defined experimental set-ups

Similar configuration file “experiments.cfg” is used for experimental definition. It follows the same syntax but uses different keywords. It has to be stored in the Abaqus working directory, where input files are usually created. “experiments.cfg” doesn’t have to be compiled. It is used directly by the plug-in.

Example of experimental test configuration:

```
**4-POINT BENDING TEST
*SECTIONS
00: -0.01
01: 0.01
02: 0.32
03: 0.34
04: 0.66
05: 0.68
06: 0.99
07: 1.01
*SEGMENTS
00: 0
01: 2
02: 4
03: 6
*SEGMENT SUPPORTS
00: 0,111001
01: 3,110001
*SEGMENT LOADS
00: 1,0.,-500.,0.
01: 2,0.,-500.,0.
```

11.1 General keywords

***LOAD UNITS**

Overrides default 'kN' value

***RECORD**

This optional parameter specifies what is going to be reported. Acceptable strings (separated by commas):

DEFORMATIONS,U1,U2,U3,FORCES,RF1,RF2,RF3,MOMENTS,RM1,RM2,RM3,LPF.

Default value is 'DEFORMATIONS,FORCES'.

***ULTIMATE**

Next optional line specifies what is considered to be the ultimate load. Acceptable is one of the following strings:

DEFORMATIONS,U1,U2,U3,FORCES,RF1,RF2,RF3,MOMENTS,RM1,RM2,RM3,LPF.
Default value: 'FORCES'.

***SECTIONS**

Sections, where the loading, support or material conditions change (0. - 1.) in ascending order in points relative to the member length. However, it is possible to insert a fixed-length segment by offsetting the section forward or backward by a specific distance. The offset is recognized by “+” or “-“ sign followed by a number and “mm” (see example). RIGID parameter is optional; it creates rigid lines along the section.

Example:

```
*SECTIONS
00: 0.0
01: 0.0 + 50.0 mm
02: 1.0 - 50.0 mm,RIGID
03: 1.0,RIGID
```

***SEGMENTS**

Special purpose segments (e.g. rigid or with increased mesh density) are specified with 1st section number.

Example:

```
*SEGMENTS
00: 0,RIGID
01: 2,DENSE
```

***FACES**

Definition of faces on deformable segments (1st section number, face name: e.g. TOP, BOTTOM,FRONT,BACK). Note: face will be rigid automatically when FACE SUPPORTS or FACE LOADS are defined on it or when specified by additional parameter RIGID)

Example:

```
*FACES
00: 0,BOTTOM
01: 4,TOP,RIGID
```

***CONTACTS**

Local buckling calculations sometimes need contact rigid body on the surface. This can be defined by CONTACT keyword. The use is similar as FACE, however, the rigid shell (of the same width as selected segment but longer than the member's face in transverse direction) will be created. Then it can be loaded and/or supported using CONTACT LOADS and CONTACT SUPPORTS keywords.

Example:

```
*CONTACTS
00: 3,TOP
```

***SECTION SUPPORTS**

Boundary conditions on sections - section number, 6 characters (1-fixed, 0-free), will apply to all nodes or to the centre of gravity (in case of RIGID section).

Example:

```
*SECTION SUPPORTS
00: 0,111001
01: 1,110000
```

***SEGMENT SUPPORTS**

Boundary conditions on rigid segments (rigid segment number, 6 characters)

***FACE SUPPORTS**

Boundary conditions on rigid faces (rigid face number, 6 characters)

***CONTACT SUPPORTS**

Boundary conditions on previously defined contacts (contact number, 6 characters)

***LINE SUPPORTS**

Boundary conditions on longitudinal lines on deformable face (face number, 6 characters)

***SECTION LOADS**

Loaded sections: section and three numbers separated by commas, will apply to all nodes or to the centre of gravity in case of RIGID sections.

Example:

```
*SECTION LOADS
00: 1,0.,-500.,0.
01: 2,0.,-500.,0.
```

***SEGMENT LOADS**

Loaded rigid segments (rigid segment number, 3 loads)

***FACE LOADS**

Loaded rigid faces (rigid face number, 3 loads)

***CONTACT LOADS**

Loaded contacts (rigid face number, 3 loads)

***LINE LOADS**

Loaded lines on deformable segment face (face number, 3 loads)

***SECTION DEFORMATIONS**

Loaded sections: sections and three numbers separated by commas

Example:

```
*SECTION DEFORMATIONS
00: 1,0.,0.,-1.
```

***CHANNELS**

Definition of measuring points on selected face. Outputs the extreme values of the first and last nodes on lines defined as TOP, BOTTOM, FRONT or BACK in a particular section (recorded value (e.g. U1,RF3,...), section number, face definition (e.g. TOP)). This keyword can be used also on particular profile to measure only one point (see the next chapter)

Example:

```
*CHANNELS
00: U2,2,TOP
01: U2,3,TOP
```

11.2 Keywords applicable to particular profile

Using the general keywords, users have limited options of specifying the position of loads and supports (only TOP, BOTTOM, FRONT and BACK sides that are automatically recognized by plugin). If there is a need of placing loads or supports to a particular point of the selected profile, the following keywords should be used.

***NAMED LINE SUPPORTS**

Creates boundary conditions on particular longitudinal edge of particular cross-section (section name, segment number or ALL, point number, 6 characters), note: in another sections this option will be neglected. The symmetry plane can be also described using this keyword, but it is usually given in the profile definition and thus it is not needed here.

Example:

```
*NAMED LINE SUPPORTS
00: RHSYM,3,2,000100
01: RHSYM,4,2,000100
```

(rotation supports only on RHSYM profile in point number 2 and segments number 3 and 4 of selected experimental setup)

***NAMED LINE LOADS**

Creates load conditions of particular longitudinal edge of particular cross-section (section name, segment number or ALL, point number, 3 loads), note: in another sections this option will be neglected.

Example:

```
*NAMED LINE LOADS
00: RHSYM,3,1,0.,-250.,0.
01: RHSYM,4,1,0.,-250.,0.
```

***CHANNELS**

Definition of measurement specific points and values that will be recorded in the report (recorded value (e.g. U1,RF3,...), section number, cross-section name or face location (e.g.TOP, BOTTOM,..), point number if specific cross-section required)

Example:

*CHANNELS

00: U2,2,TH,0

01: U2,3,TH,0

(vertical displacement at point 0 of TH profile and sections 2 and 3)

12 Example calculation: Plate buckling

Our task is to simulate the experimental test reported by Rasmussen et al. [1] of single 126 mm wide plate cut from 3,2 mm thick Duplex 2205 stainless steel plate 750 mm long. The edges were simply supported (free to rotate).

The measured geometric imperfections were 0,5 mm. The material tests in longitudinal compression show the following results:

$$E_0 = 181650 \text{ MPa}$$

$$\sigma_{0.2} = 527 \text{ MPa}$$

$$n = 4,6$$

12.1 Experimental set-up configuration

NOTE: This example was produced with the plug-in version 0.10 (alpha), therefore the graphic user interface and outputs can be slightly different in the latest version.

For our experiment we can use already pre-defined experimental set-up “Plate buckling (free)” but in this tutorial we will demonstrate how a new experimental set-up can be easily defined. We would like to have faster FE calculation and benefit from the symmetry of the experiment. Therefore we can create a new experimental set-up just by entering new definition in the “experiments.cfg” file stored in the Abaqus working directory.

The name will be “Plate symmetrical test” and like the pre-defined plate test, we will load the plate with deformation, therefore units are set to “mm” and ultimate load is “U3” which refers to the axial deformation

```
**PLATE SYMMETRICAL TEST
*LOAD UNITS
mm
*ULTIMATE
U3
```

Now we have to define the longitudinal geometry of our specimen. We will have only one segment (segment 0) defined by two sections (section 0 and 1) at the beginning (0.0 x length) and the end (1.0 x length) of the specimen.

```
*SECTIONS
00: 0.0
01: 1.0
```

We would like to support all longitudinal edges we can find in this segment. Therefore we will define all possible (top, bottom, front, back) faces as faces 0 to 3 (in fact only one face could be specified if we use only “Plate” profile). And we support lines of those faces vertically (“y” is the vertical axis, therefore the support definition “x,y,z,rx,ry,rz” is “010000”).

```
*FACES
00: 0, TOP
01: 0, BOTTOM
02: 0, FRONT
03: 0, BACK
*LINE SUPPORTS
00: 0,010000
```

```
01: 1,010000
02: 2,010000
03: 3,010000
```

Now we have to support also the cross-sections. Let's say that section 0 is going to be in the symmetry plane (supported longitudinal translation "z" and out-of-plane rotations "rx" and "ry"). The second section will be the loaded edge (supported in-plane translations "x" and "y", and in-plane rotation "rz"). Additionally, we have to create the load on this edge entering the number of section (1) and three initial deformations (ux=0.0, uy=0.0 and uz=1.0).

```
*SECTION SUPPORTS
00: 0,001110
01: 1,110001
*SECTION DEFORMATIONS
00: 1,0.,0.,-1.
```

Now, the file is ready to be saved. We have to make sure that we used all the keyword parameters properly and we don't have duplicate names in the file.

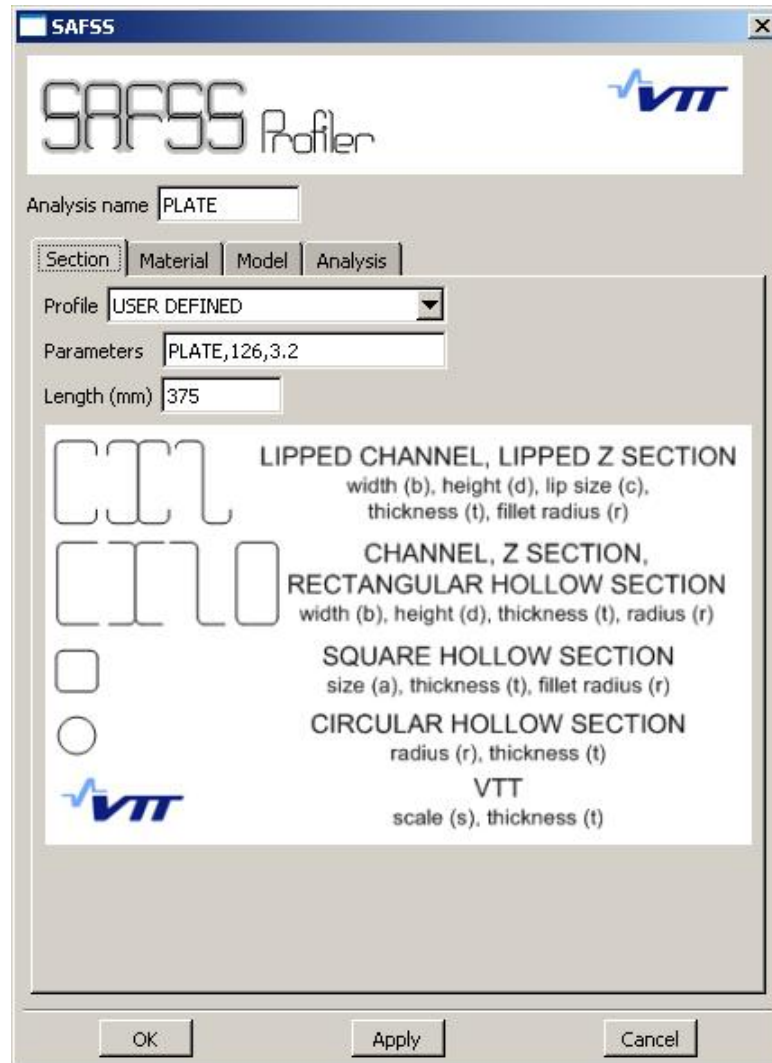
12.2 Profile definition

Because the "Plate" profile is not in the basic group of profiles available in drop-down menu in the profile tab, we have to check if it is available in "profiles.cfg" as a user profile and add it there if it is necessary.

In the configuration file, we found that following lines are describing "Plate" profile:

```
**PLATE
*VARIABLES
b,t
*POINTS
00: -(b/2),0.
01: b/2,0.
*LINES
00: 0,1,t
```

This simple definition (2 points and 1 line between those points) is sufficient for our purposes and the *VARIABLES keyword indicates that we have to enter the width "b" and thickness "t" respectively as profile parameters. Then the table can be filled based on the geometric dimensions of the plate (Figure 18). The length will be 375 mm in our symmetrical case.



The image shows a software window titled "SAFSS" with a sub-header "SAFSS Profiler" and the VTT logo. It contains several input fields and a list of profile types. The "Analysis name" field is set to "PLATE". Below it are tabs for "Section", "Material", "Model", and "Analysis", with "Section" currently selected. The "Profile" dropdown menu is set to "USER DEFINED". The "Parameters" field contains "PLATE,126,3.2". The "Length (mm)" field is set to "375". A list of profile types is shown with corresponding diagrams: "LIPPED CHANNEL, LIPPED Z SECTION" (width (b), height (d), lip size (c), thickness (t), fillet radius (r)), "CHANNEL, Z SECTION, RECTANGULAR HOLLOW SECTION" (width (b), height (d), thickness (t), radius (r)), "SQUARE HOLLOW SECTION" (size (a), thickness (t), fillet radius (r)), "CIRCULAR HOLLOW SECTION" (radius (r), thickness (t)), and "VTT" (scale (s), thickness (t)). At the bottom are "OK", "Apply", and "Cancel" buttons.

Figure 18 Profile definition table

12.3 Material definition

As a stress-strain relationship, we can use two stage model (Figure 19) corresponding to the reported material test curve in longitudinal compression

Additional parameters were used to fit the measured longitudinal compression (LC) data (Figure 20).:

$$\sigma_u = 640 \text{ MPa}$$

$$\varepsilon_u = 0,012$$

$$m = 2,5$$

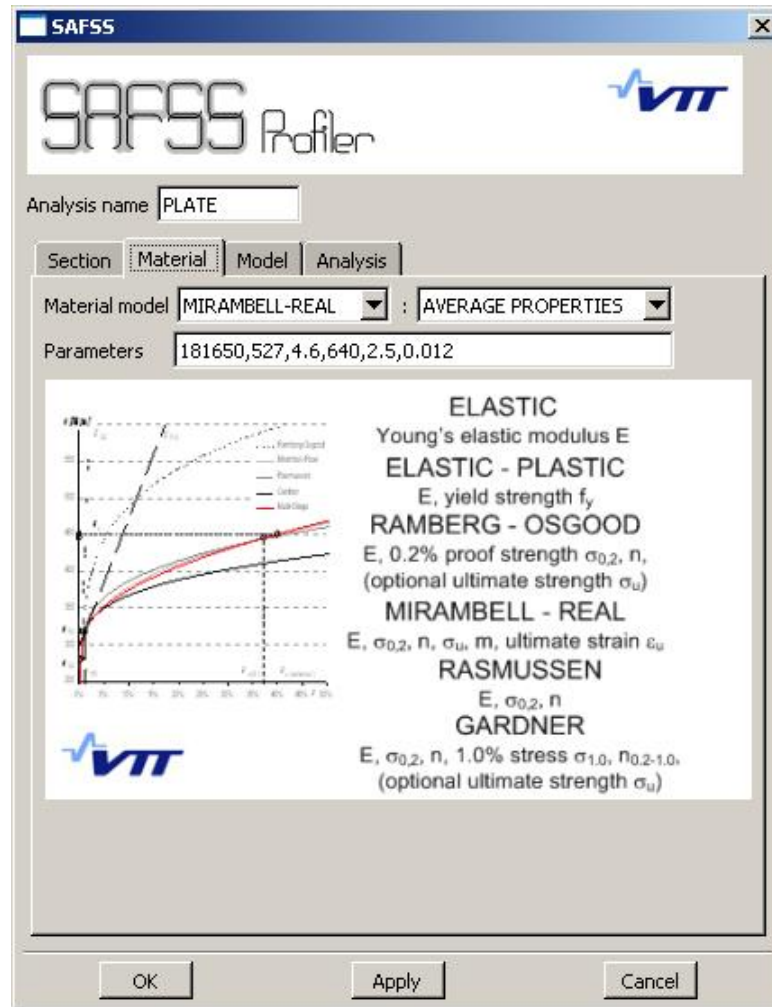


Figure 19 Material definition

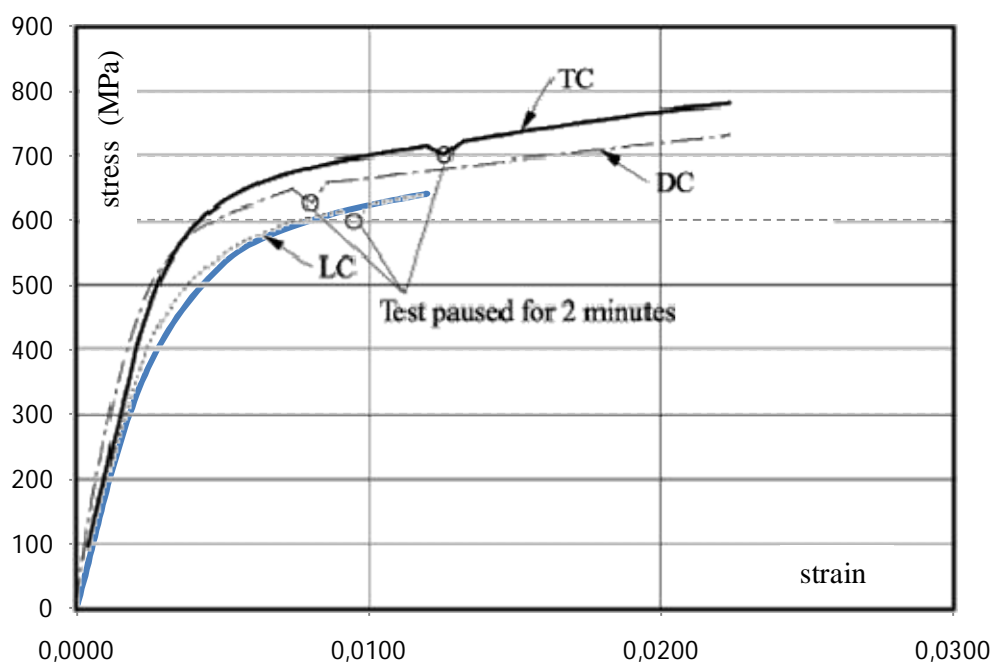


Figure 20 proposed stress-strain model (blue) in comparison with the test data

12.4 Model definition

If we want to use the user-defined experimental set-up, we have to enter its name in the blank text box under the drop-down menu. The selected element is S9R5 with 5 mm node spacing (it means that the maximum element size will be 5x5 mm). We will also need geometrical imperfections which would hopefully be generated as the 1st imperfect shape with the amplitude 0,5 mm (Figure 21).

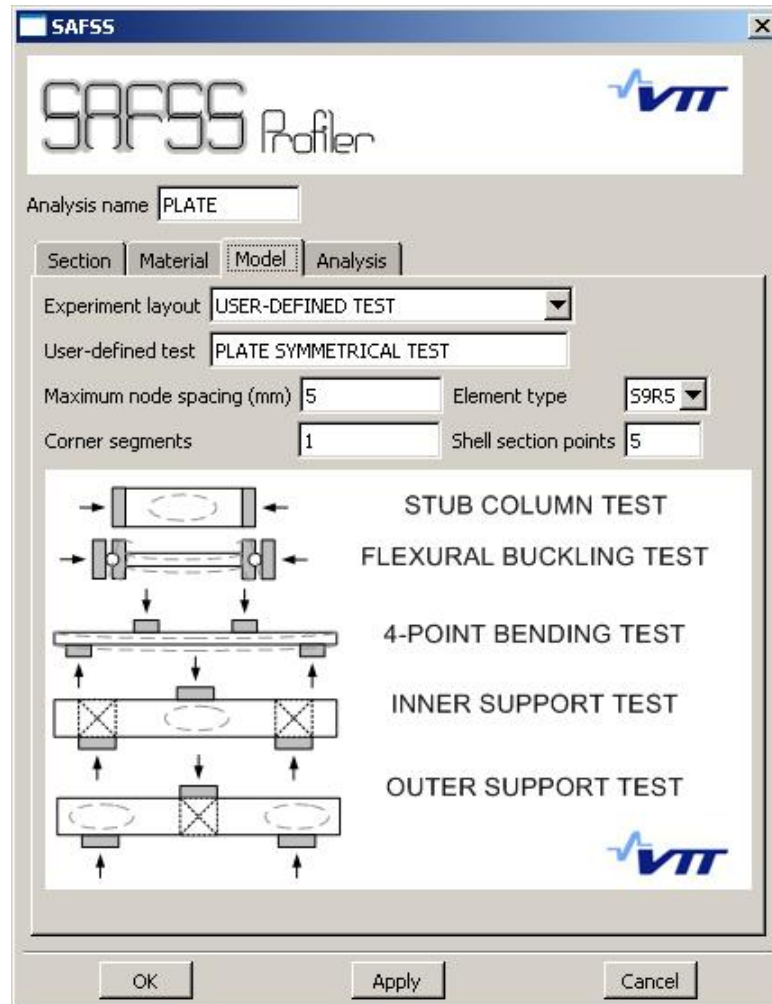


Figure 21 Model definition

12.5 Analysis settings

Finally, we check that “Run analysis” is on and the report will be saved. In the stub column and plate buckling tests where the deformation is controlled instead of the loading force, we have to set the analysis end-criteria as the maximum longitudinal deformation. In Rasmussen’s study, experiments reported results up to 4 mm which is slightly over 0,5% of the length. Therefore 1,0% settings should be enough in our case.

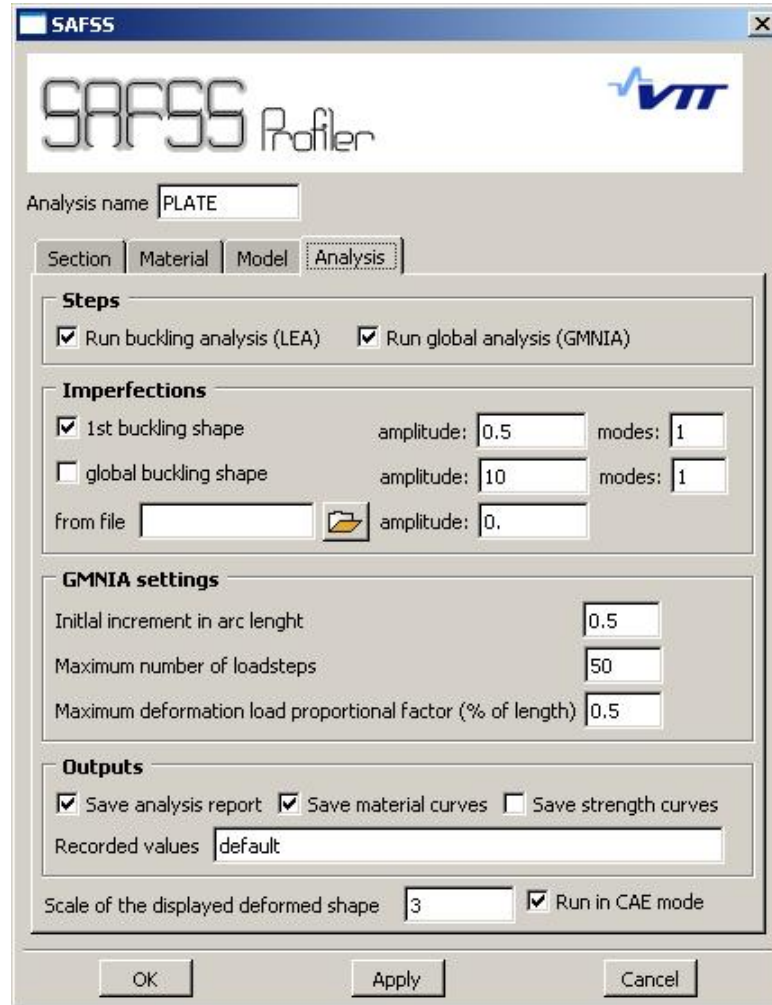


Figure 22 Analysis settings

Now, the calculation is ready to start. Pressing “Apply” button starts the calculation as well as “OK” button and additionally keeps the settings for further use.

12.6 Simulation outputs

In the first steps, model input files are created and imported into Abaqus CAE. We selected to use imperfections from the 1st buckling shape (it is called LEA2 in the plug-in) and the successful import of the file will produce following output:

```
Input file PLATE-LEA2.inp successfully created.
The model "PLATE-LEA2" has been created.
The part "PART" has been imported from the input file.
The model "PLATE-LEA2" has been imported from an input file.
Please scroll up to check for error and warning messages.
```

Similarly, basic input file is created and displayed on screen.

```
Input file PLATE.inp successfully created.
The model "PLATE" has been created.
The part "PART" has been imported from the input file.
The model "PLATE" has been imported from an input file.
Please scroll up to check for error and warning messages.
```

Now, the local buckling analysis has started. It may take a while to get all of the following messages:

LOCAL BUCKLING ANALYSIS

Job PLATE-LEA2: Analysis Input File Processor completed successfully.

Job PLATE-LEA2: Abaqus/Standard completed successfully.

Job PLATE-LEA2 completed successfully.

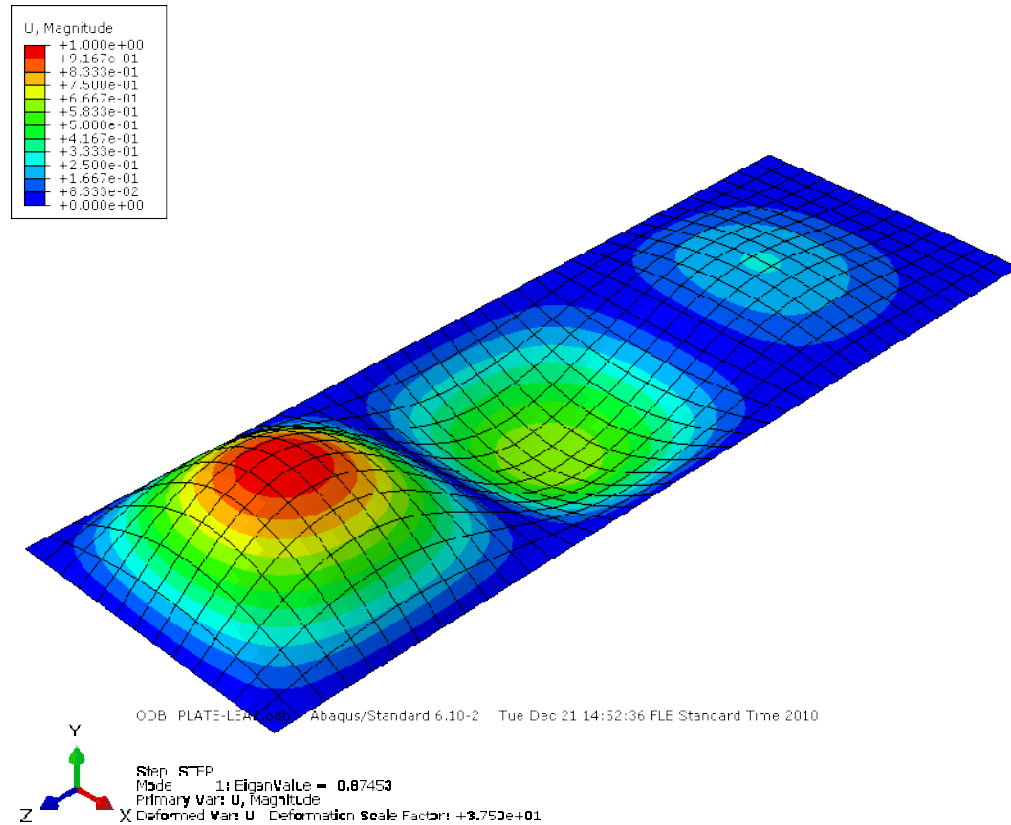


Figure 23 The first buckling mode of the plate

In the next step, the basic model is created again, this time with perturbed shape. However, it is not imported into the CAE but it is still used for the calculation.

GMNIA

Input file PLATE.inp successfully created.

Job PLATE: Analysis Input File Processor completed successfully.

When the GMNIA calculation starts, user has already the full control of the CAE environment and can rotate, pan and zoom the model. The calculation is running in the background updating the deformed shape after each step and producing following outputs:

```
Frame : 0, Load: 0.00 mm
Frame : 1, Load: 0.00 mm
Frame : 1, Load: 0.24 mm
Frame : 2, Load: 0.45 mm
Frame : 3, Load: 0.65 mm
...
Frame : 12, Load: 3.19 mm
Frame : 13, Load: 3.62 mm
Frame : 14, Load: 4.40 mm
```

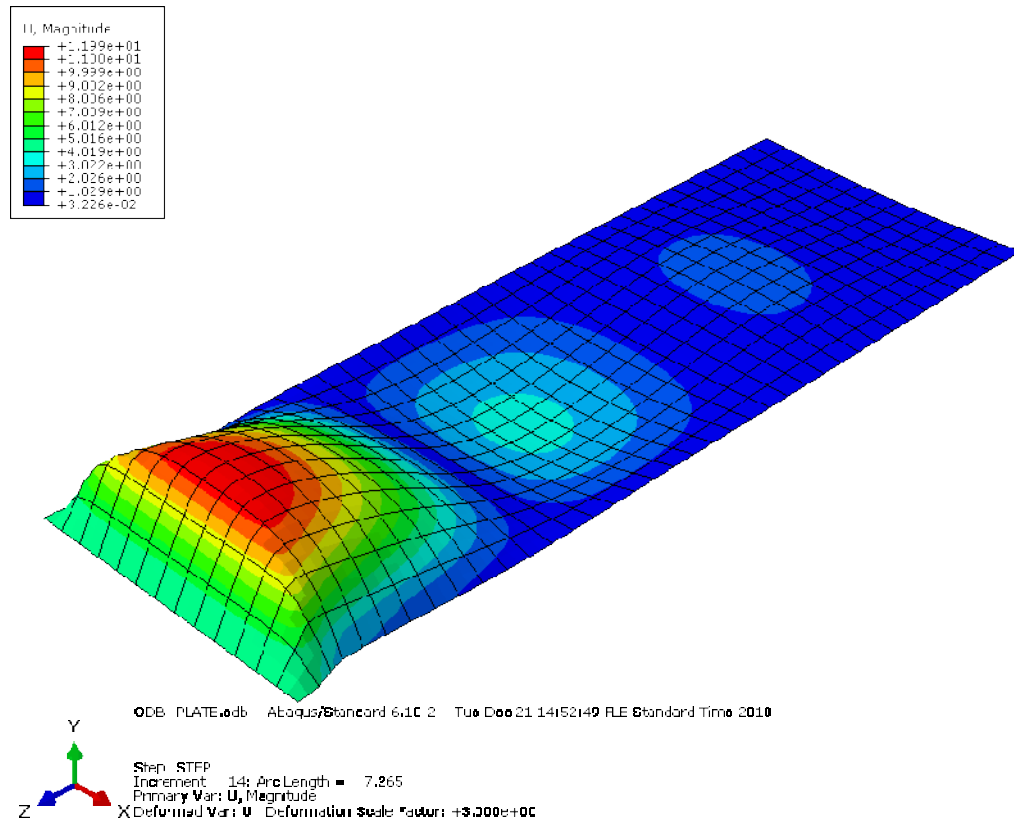


Figure 24 Deformed shape of the plate in the last time increment (scale 3x)

Calculation usually stops when

- Job is completed.
- Job is aborted.
- Monitored values (number of steps or the load proportional factor) reaches given criteria. In this case the calculation is terminated showing NOTE message. When the member is loaded with forces/moments, the peak load can be usually observed and the termination occurs when the load proportional factor decreases 3 times in a row. When the member is loaded with deformations, the load proportional factor has to be limited directly as % of length. Additionally, user can specify the maximum allowed number of load steps.

In our case the job was terminated by plug-in settings of 1% axial deformation limit..

NOTE: JOB TERMINATED BY PLUGIN REQUEST. (1% DEFORMATION REACHED)

HTML report was automatically created and displayed.

ANALYZING ODB DATABASE ... DONE
WRITING HTML REPORT ... DONE.

The most important table in the report represents data requested in the analysis tab. These data requests can be alternatively specified in “experiments.cfg” for each experimental set-up.

No.	DEFORMATIONS [mm]			REACTION FORCES [kN]		
	U1	U2	U3	RF1	RF2	RF3
1	0.000	0.000	0.000	0.0	0.0	0.0
2	0.012	0.183	0.242	2.5	0.8	46.7
3	0.022	0.474	0.447	4.2	2.1	83.4
4	0.032	1.051	0.654	4.8	4.8	112.2
5	0.039	1.939	0.867	4.2	9.2	128.5
6	0.050	3.089	1.186	4.9	15.8	136.7
7	0.184	4.965	1.798	7.2	24.8	138.4
8	0.242	5.572	1.949	7.7	26.3	137.3
9	0.311	6.181	2.098	8.1	27.8	135.2
10	0.433	7.041	2.314	7.8	29.5	128.6
11	0.577	7.850	2.546	6.7	30.8	118.8
12	0.741	8.702	2.836	5.5	31.7	108.9
13	0.953	9.570	3.195	4.4	32.6	100.1
14	1.196	10.484	3.622	3.8	33.6	92.4
15	1.653	11.850	4.405	3.7	35.2	82.4

Figure 25 Results table

From this table we can easily plot charts. Axial deformation is $2 \times U3$ and the load is RF3. As it is demonstrated in Figure 26 our results are very close to the numerical simulation reported by Rasmussen using isotropic strain hardening model with 3 half-waves initial deformation “Iso_sh_3hw”.

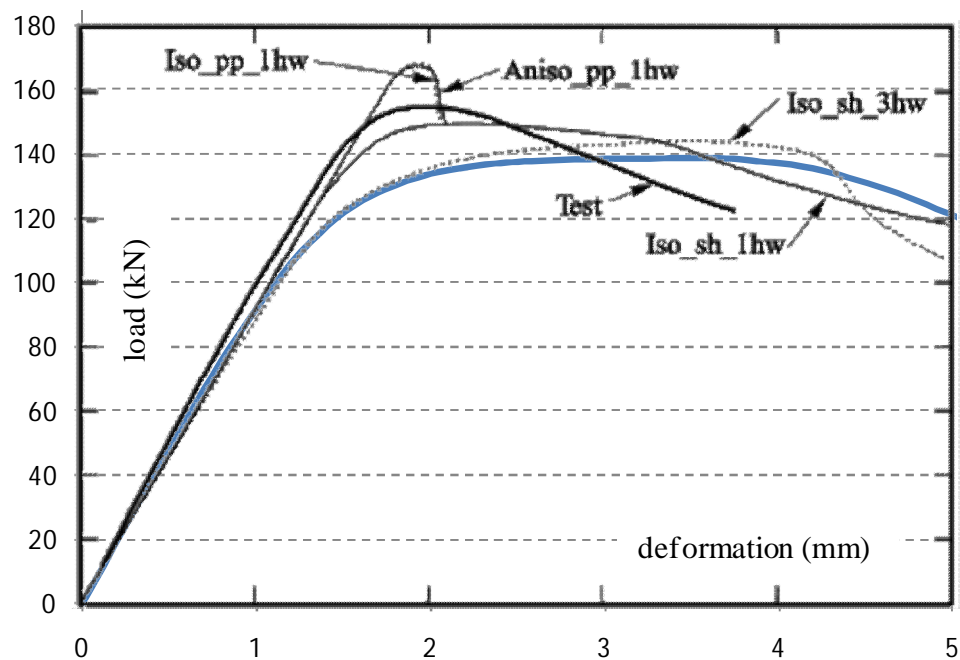


Figure 26 Comparison of Experimental tests and numerical models.
The plugin output is plotted with a blue line.

13 Example calculation: Web crippling

This example explains the Abaqus plug-in configuration of new experiment and the calculation of selected case.

13.1 Creating the test set-up

All the experimental set-ups are stored in the experiments.cfg file that is by default located in Abaqus working directory. User can add new definitions and they are accessed by plug-in as “user-defined test”.

- Open the file and write “**” and the name of new test on an empty line

```
**UPC-CHANNEL
```

Since the load will be introduced by displacement, it is necessary to change default load units (kN) to mm. The ultimate load will be the maximum vertical displacement (y axis is U2 in Abaqus) and this has to be also specified.

- Write the keywords “*LOAD UNITS” and “*ULTIMATE” as follows

```
*LOAD UNITS  
mm  
*ULTIMATE  
U2
```

13.1.1 Dividing member into segments

All functional segments with different load or support conditions are divided by so called sections. Since the length of the member is variable, the position of each section is a fraction of the member length (usually between 0.0 and 1.0). However, it is possible to define fixed length of the segment by setting offset value in mm from the relative position (e.g. 0.0 + 25 mm will create section 25 mm from the member end regardless its length).

- Using “*SECTIONS” keyword define sections for the beginning and end of the member (0.0 and 1.0), 40 mm long support aread (0.0 + 40 mm and 1.0 – 40 mm), 100 mm long loading area (0.5 -50 mm and 0.5 + 50 mm) and 200 mm long area that will have denser mesh (0.5 -100 mm and 0.5 + 100 mm). For the monitoring purposes create also the middle section (0.5). Each section has its own line and the first four characters are just for the numbering purposes (usually “00: “, “01: “, ...).

```
*SECTIONS  
00: 0.0  
01: 0.0 + 40.0 mm  
02: 0.5 - 100.0 mm  
03: 0.5 - 50.0 mm  
04: 0.5  
05: 0.5 + 50.0 mm  
06: 0.5 + 100.0 mm  
07: 1.0 - 40.0 mm  
08: 1.0
```

Note that the section order has to be ascending (here from 0.0 to 1.0) and the length of the member has to be bigger than 280 mm due to fixed length of several segments.

If the whole segment is affected by some modification (at the moment it can be either rigid body or it can have denser mesh), it has to be specified using keyword “*SEGMENTS”

- Indicate segments with denser mesh in the loading area (200 mm wide). The number before “DENSE” parameter indicates the starting section of each segment.

```
*SEGMENTS
00: 2,DENSE
01: 3,DENSE
02: 4,DENSE
03: 5,DENSE
```

13.1.2 Definition of special-purpose faces

Since the loads and supports will be applied only at the top or bottom faces of the member, we will have to indicate the faces location using the keyword “*FACES”. Faces are defined the same way as segments with the parameter “TOP”, “BOTTOM”, “FRONT” or “BACK” at the end. Plugin automatically recognize the proper face (or more faces if necessary). It is also possible to specify a certain face of a certain profile, but this requires another keyword.

- Specify two faces at support location and two faces in the middle of the member for the loading. Stiffen the web at the support area using parameter “RIGID” to suppress web-crippling there.

```
*FACES
00: 0,BOTTOM
01: 0,FRONT,RIGID
02: 3, TOP
03: 4, TOP
04: 7,FRONT,RIGID
05: 7,BOTTOM
```

13.1.3 Creating supports

We will create supports on rigid faces at the bottom of the first and the last segments. These faces can be loaded or supported only at their reference points that are automatically created at their centre of gravity. Even though the support point is not exactly the same as in experiment, it will have minor effect in web-crippling simulations.

- With the “*FACE SUPPORTS” keyword specify simple support at both ends (faces 0 and 5). The 6-digits number refers to the 6 degrees of freedom (x,y,z,rx,ry,rz) where 0 and 1 stands for free and fixed support respectively.

```
*FACE SUPPORTS
00: 0,111111
01: 5,110011
```

13.1.4 Creating loads

The member will be loaded in the middle segments (segment 1 and 2) only in upper corners because of local buckling of the flange.

Loads can be inserted on faces (keyword “*FACE LOADS” or “*FACE DEFORMATIONS”) or on their longitudinal edges (keyword “*LINE LOADS” or “*LINE DEFORMATIONS”).

- Create vertical deformation load on both faces (face 2 and 3). Three numbers separated by comma will define loadstep in x,y and z direction that refers to the load unit.

*LINE DEFORMATIONS

00: 2,0.,-1.,0.

01: 3,0.,-1.,0.

We would like to prevent the loaded face moving sideways, and therefore it is necessary to support the same lines in horizontal direction

- Create horizontal support of the loaded area

*LINE SUPPORTS

00: 2,100000

01: 3,100000

13.1.5 Definition of measuring points

Even though the report usually contains general information about the extreme stress and deformation at each step, these values are measured only at specific points in real experiments. We will create one measuring point at the bottom of the middle section.

- Use the keyword “*CHANNELS” to define measurement of vertical deflections in the middle of the member

*CHANNELS

00: U2,4,BOTTOM

13.1.6 Saving the experimental setup

- Save the “experiment.cfg” in your working folder of Abaqus. It is not required that Abaqus/CAE is closed during the changes or restarted afterwards.

**UPC-CHANNEL

*LOAD UNITS

mm

*ULTIMATE

U2

*SECTIONS

00: 0.0

01: 0.0 + 40.0 mm

02: 0.5 - 100.0 mm

03: 0.5 - 50.0 mm

04: 0.5

05: 0.5 + 50.0 mm

06: 0.5 + 100.0 mm

07: 1.0 - 40.0 mm

08: 1.0

*SEGMENTS

00: 2,DENSE

01: 3,DENSE

02: 4,DENSE

03: 5,DENSE

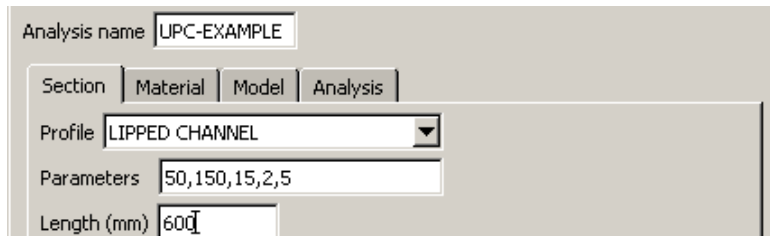

```
*FACES
00: 0,BOTTOM
01: 3, TOP
02: 4, TOP
03: 7, BOTTOM
*FACE SUPPORTS
00: 0,111111
01: 3,110011
*LINE DEFORMATIONS
00: 1,0.,-1.,0.
01: 2,0.,-1.,0.
*LINE SUPPORTS
00: 1,100000
01: 2,100000
*CHANNELS
00: U2,4,BOTTOM
```

13.2 Running the analysis

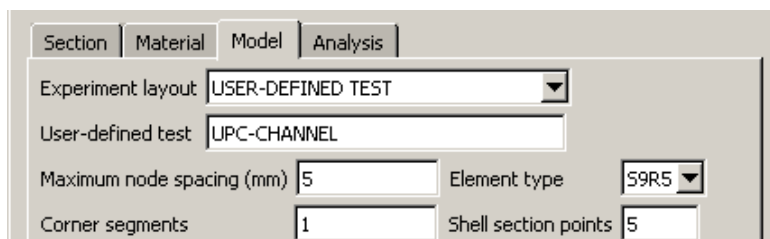
- Open Abaqus/CAE and start “SAFSS” plugin in program menu.

13.2.1 Basic settings

- Name your analysis (e.g. UPC-EXAMPLE)
- Insert the geometry of the cross-section in the first tab. Here we changed only the default length 200 mm to 600 mm.



- In the “Model” tab, indicate the user-defined test name.



- Change the other settings according to your preference and click “OK” or “Apply”.

13.2.2 Calculation

From this moment the plugin is controlling the Abaqus environment until the end of the calculation. In the beginning there is usually one or two buckling steps and then the arc-length analysis where user can interact with the environment (e.g. rotate and scale the deformed model or prepare parameters for another analysis).

13.2.3 Report file

After the end of calculation, report file is usually displayed (if running on Windows with Internet Explorer installed) in form of HTML file.

```
*****
*   THIS FILE WAS CREATED USING ABAQUS PROFILER PLUGIN   *
*   BY VTT, TECHNICAL RESEARCH CENTRE OF FINLAND       *
*   FOR SAFSS PROJECT IN ESPOO 2011                     *
*****
```

Experiment: UPC-EXAMPLE

Set-up: UPC-CHANNEL

Section: LIPPED CHANNEL,50.0,150.0,15.0,2.0,5.0

Length: 600.0 mm

Material: MIRAMBELL-REAL,200000,280,7,450,2.64,0.4

Analysis started: 14. 6.2012 10:20:47

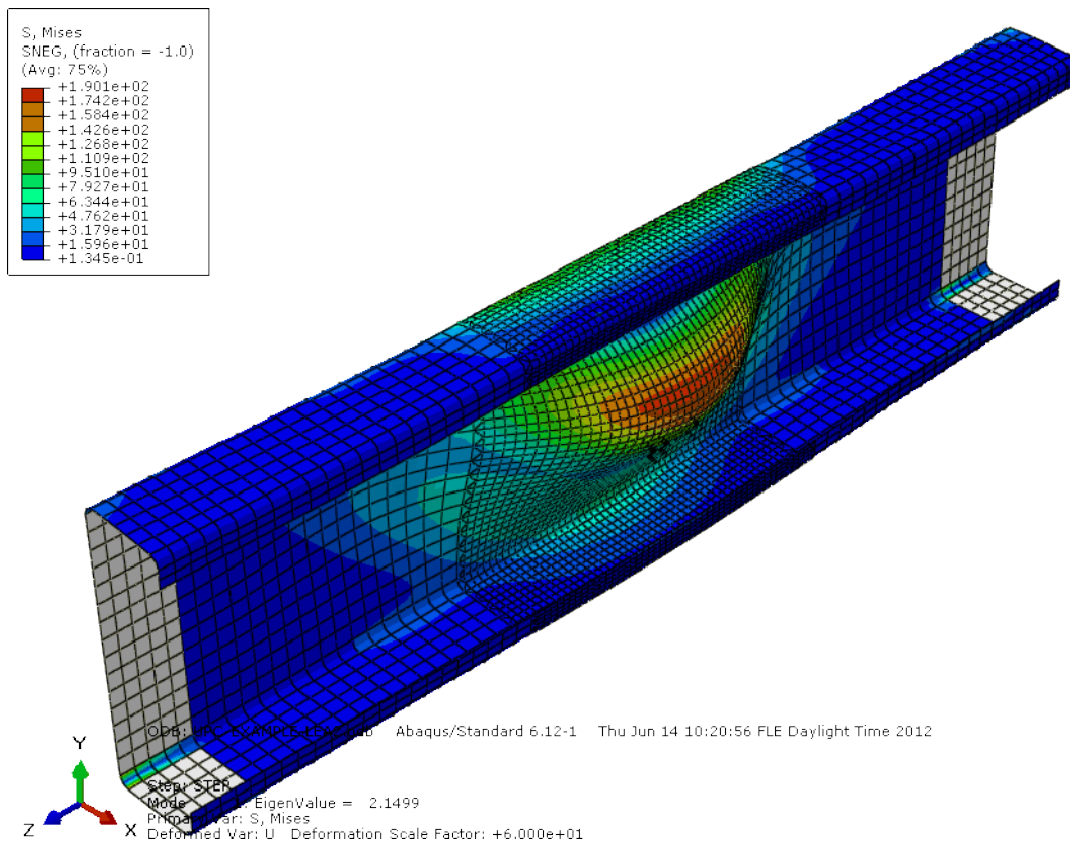
Analysis ended: 14. 6.2012 10:27: 2

Analysis end event: terminated by plug-in

LOCAL BUCKLING ANALYSIS

Imperfections: 1.0 mm

Critical deformation: 2.1499 mm



No.	DEFORMATIONS [mm]			REACTION FORCES [kN]			LPF	CH0-U2
No.	U1	U2	U3	RF1	RF2	RF3	LPF	CH0
1	0.000	0.000	0.000	0.0	0.0	0.0	0.000	0.000
2	1.000	0.141	0.019	0.9	2.1	0.0	0.000	-0.086
No.	DEFORMATIONS [mm]			REACTION FORCES [kN]			LPF	CH0-U2
No.	U1	U2	U3	RF1	RF2	RF3	LPF	CH0
1	0.000	0.000	0.000	0.0	0.0	0.0	0.000	0.000
2	0.946	0.707	0.119	4.4	13.7	0.0	0.478	-0.184
3	2.285	1.324	0.171	6.7	19.1	0.0	0.947	-0.252
4	2.628	1.479	0.180	7.4	19.8	0.0	1.073	0.262
5	2.967	1.643	0.189	8.2	20.5	0.0	1.206	0.295
6	3.464	1.904	0.203	9.5	21.2	0.0	1.421	0.341
7	4.178	2.329	0.226	11.6	22.1	0.0	1.776	0.404
8	4.857	2.784	0.251	13.6	22.9	0.0	2.165	0.460
9	5.506	3.264	0.281	15.6	23.6	0.0	2.581	0.513
10	6.127	3.758	0.321	17.4	24.2	0.0	3.020	0.562
11	6.723	4.262	0.363	19.1	24.9	0.0	3.477	0.609
12	7.294	4.775	0.407	20.6	25.5	0.0	3.949	0.655
13	7.847	5.294	0.453	21.9	26.1	0.0	4.435	0.699
14	8.377	5.819	0.499	23.1	26.6	0.0	4.931	0.741
15	8.886	6.348	0.548	24.2	27.0	0.0	5.438	0.782
16	9.384	6.882	0.598	25.1	27.3	0.0	5.952	0.821
17	9.864	7.419	0.650	26.0	27.5	0.0	6.473	0.859

GMNIA RESULTS

Ultimate load: 7.41946 mm

References

- [1] Rasmussen, K.J.R., Burns, T., Bezkorovainy, P. & Bambach, M.R. Numerical modelling of stainless steel plates in compression. Journal of Constructional Steel Research 2003, 11, Vol. 59, No. 11, pp. 1345-1362. ISSN 0143-974X. doi: DOI: 10.1016/S0143-974X(03)00086-5.